Peptidoglycan architecture and dynamics in *Bacillus subtilis*

By

Ashley Davies BSc (Hons) MSc (Hons)

(University of Manchester)

September 2014

A thesis submitted for the degree of Doctor of Philosophy

Department of Molecular Biology and Biotechnology, University of Sheffield,

Firth Court, Western Bank, Sheffield, S10 2TN

Summary

Peptidoglycan (PG) is the main structural component of Gram-positive bacterial cell walls; a macromolecule comprising glycan strands cross-linked by peptide side chains. PG provides the framework for bacterial cell shape, as well as being required for growth and division. However, the relationship between PG chemistry, PG architecture and the dynamic nature of their roles are poorly understood.

Bacillus subtilis is a Gram-positive rod-shaped bacterium that is able to differentiate. Growth, division and differentiation all involve morphological change, dependant on PG dynamics and architecture. Here, I have studied three different processes, combined with a range of imaging techniques; protoplast regeneration, loss of PG hydrolase activity and sporulation/germination. This allowed a model to be developed detailing the stepwise regeneration of spherical protoplasts to vegetative rod-shaped cells, through morphological intermediates. The role of two redundant essential PG hydrolases was examined, leading to a new hypothesis as to their role in cell growth and PG architecture. The study of *B. subtilis* PG architecture during sporulation lead to confirmation of the recently postulated PG architecture model; the 'coiled-coil' hypothesis. Finally, my study gave the first utilization of Stochastic Optical Resolution Microscopy (STORM) in the study of *B. subtilis* PG structure, revealing it to be a potent future tool for the study of the relationship between PG chemistry and architecture.

Acknowledgements

Firstly, I would like to thank my supervisor Prof. Simon Foster for giving me the opportunity to carry out my PhD and for his constant guidance and support throughout the project. I am also grateful to the BBSRC for funding my PhD.

I would like to thank all past and present members of the Foster lab, particularly Alex and Azhar. Special thanks to Dr Bob Turner and Victoria Lund for their contributions and advice concerning microscopy. I also would like to thank Prof. Jamie Hobbs at the AFM facility and Chris Hill at the EM facility for their technical assistance.

To all my friends in Sheffield - Nikki, Tom, Arthur, Serina, Laura, Ellie, Kai, Rob, Dave and Jack; the last four years would have been truly rubbish without you all. Massive love and thanks for all the drinks, jokes and dancing.

To Mum, Dad and Fiona (Bear) – you are the roots to my branches. I would never have been able to do this without your never-ending love, sustenance and encouragement. I am eternally grateful and I love you all. Love and thanks also go to my extended family, particularly the Boswells and Chisnells.

Finally, I would like to express my utmost gratitude to Calum. Thank you for your unwavering love and support, for your advice, for proofreading, for doing all the housework, for drying my tears, for making me laugh, for making me safe and warm, and finally for your resolute belief that I could do it. Without you, this thesis would not exist. I love you more than words can express and I dedicate this thesis to you.

Abbreviations

3D	Three dimensional
°	Degree
°C	Degree Celsius
AFM	Atomic force microscopy
Amp	Ampicillin
AZA*	Azido-D-Alanine
BODIPY-FL	Boron-dipyrromethene
C6	Carbon six
cfu	Colony forming units
Cm	Chloramphenicol
CM	Cytoplasmic membrane
Cryo-EM	Cryo-electron microscopy
D-Ala	D-alanine
D-Glu	D-glutamine
DAA	D-Amino acid
DAPI	4',6-diamidino-2-phenylindole
dH2O	Distilled water
DMSO	Dimethyl sulphoxide
DNA	Deoxyribonucleic acid
DPA	Dipicolinic acid
DPX	Distyrene-plasticizer-xylene
DV	DeltaVision
EM	Electron microscopy
Ery	Erythromycin
FDAA	Fluorescent D-Amino acid
FITC	Fluorescein isothiocyanate
FL	Fluorescent
FWHM	Full width half maxima
GlcNAc	N-acetyl glucosamine
GSLE	Germination-specific lytic enzyme
h	hours
H	Height image
HADA	Hydroxycoumerin 3-amino-D-Alanine
HF	Hydrofluoric acid
HMM	High molecular mass
Kan	Kanamycin
l	Litre
L-Ala	L-alanine
LB	Luria-Bertani medium
LMM	Low molecular mass
LPS	Lipopolysaccharide
LTA	Lipoteichoic acid
M	Molar
meso-DAP	meso-diamonopimelic acid
mg	Milligrams
min	Minutes
ml	Millilitres

mM	Millimolar
mRFP	Monomeric red fluorescent protein
MurNAc	N-acetyl muramic acid
NA	Numerical aperture
NADA	Nitrobenzofurazan 3-amino-D-Alanine
*N*AG	N-acetyl glucosamine
*N*AM	N-acetyl muramic acid
Neo	Neomycin
nm	Nanometre
nM	Nanomolar
No.	Number
ODx	Optical density at indicated wavelength x (nm)
OM	Outer membrane
P	Phase image
PBP	Penicillin-binding protein
PBS	Phosphate buffered saline
PCM	Phase contrast microscopy
PG	Peptidoglycan
PGT	Peptidoglycan transferase
psi	Pounds per square inch
P_{xyl}	Xylose-inducible promoter
rpm	Revolutions per min
RT	Room temperature
s	Seconds
SIM	Structured illumination microscopy
SDS	Sodium dodecyl sulphate
Spc	Spectinomycin
Spp.	Species
STED	Stimulated emission depletion microscopy
STORM	Stochastic optical reconstruction microscopy
t	Time
TA	Teichoic acid
TCS	Two component signal transduction system
Tet	Tetracycline
TEM	Transmission Electron Microscopy
Tris	Tris (hydroxymethyl) aminomethane
µg	Microgram
µl	Microlitre
µm	Micrometre
µM	Micromolar
UDP	Undecaprenylphosphate
Van	Vancomycin
WT	Wild-type
WTA	Wall teichoic acid
(w/v)	Weight for volume
×	Times
×g	Times gravity
YFP	Yellow fluorescent protein
~	Approximately

Table of Contents

Page Number:

List of Figures

List of Tables

Chapter 1

Introduction

1.1 *Bacillus subtilis*

Bacillus subtilis (*B. subtilis*) is a Gram-positive rod-shaped bacterium, which functions as a facultative anaerobe (Hoffmann et al., 1995). *B. subtilis* is able to differentiate into spores in response to undesirable changes to its external environment. For this reason, *B. subtilis* is utilised as a model system in the study of bacterial morphological differentiation, division machinery and the cell cycle (Errington, 2010). It is also for this reason that *B. subtilis* has been considered a useful target for investigation into cell wall architecture (Atrih et al., 1999)

1.2 The bacterial cell wall

The bacterial cell wall is a dynamic, multi-functional and essential structural component of a bacterial cell. The cell wall acts as a key determinant in the maintenance of a defined bacterial shape and formation of new daughter cells during the cell division process. The cell wall also has a central role of protecting the cell against distress by resisting changes to extracellular conditions e.g. osmotic or internal turgor pressure, and/or mechanical disruption (Matteï et al., 2010). The cell wall also provides a scaffold for anchoring other cell envelope components such as proteins and teichoic acids (Vollmer et al., 2008a). Furthermore, inhibition of the cell wall

biosynthesis e.g. by mutation or antibiotic activity, or by direct degradation e.g. enzyme, will result in a direct lysis of the cell (Vollmer et al., 2008a).

1.2.1 Cell wall structure

The structure of the bacterial cell wall differs markedly between Gram-positive and Gram-negative bacteria, so named because of their differences in appearance following a Gram stain for light microscopy. This difference in structure is related to the number of lipid membranes and the organisation of peptidoglycan (PG), the key component of bacterial cell walls. The difference in amount and organisation of the PG contained by bacterial cell walls forms the basis of the Gram stain and therefore the differentiating taxonomic factor between Gram-positives and Gram-negatives. A schematic providing a rough visual representation of the two structures is shown in **Figure 1.1**. (Madigan and Martinko, 2006)

1.2.1.1 Gram-negative cell wall organisation

The Gram-negative cell wall consists of several separate layers (**Figure 1.1A**). The outermost layer, the outer membrane (OM) is a phospholipid bi-layer comprising mainly negatively-charged lipopolysaccharide (LPS) on the external phospholipid leaflet (Silhavy et al., 2010). The innermost layer of the Gram-negative cell wall is the cytoplasmic membrane (CM). Between the CM and OM, there exists a protein-rich periplasmic space in which a thin (approximately 2-6 nm) layer of PG is sandwiched (Vollmer et al., 2008a).

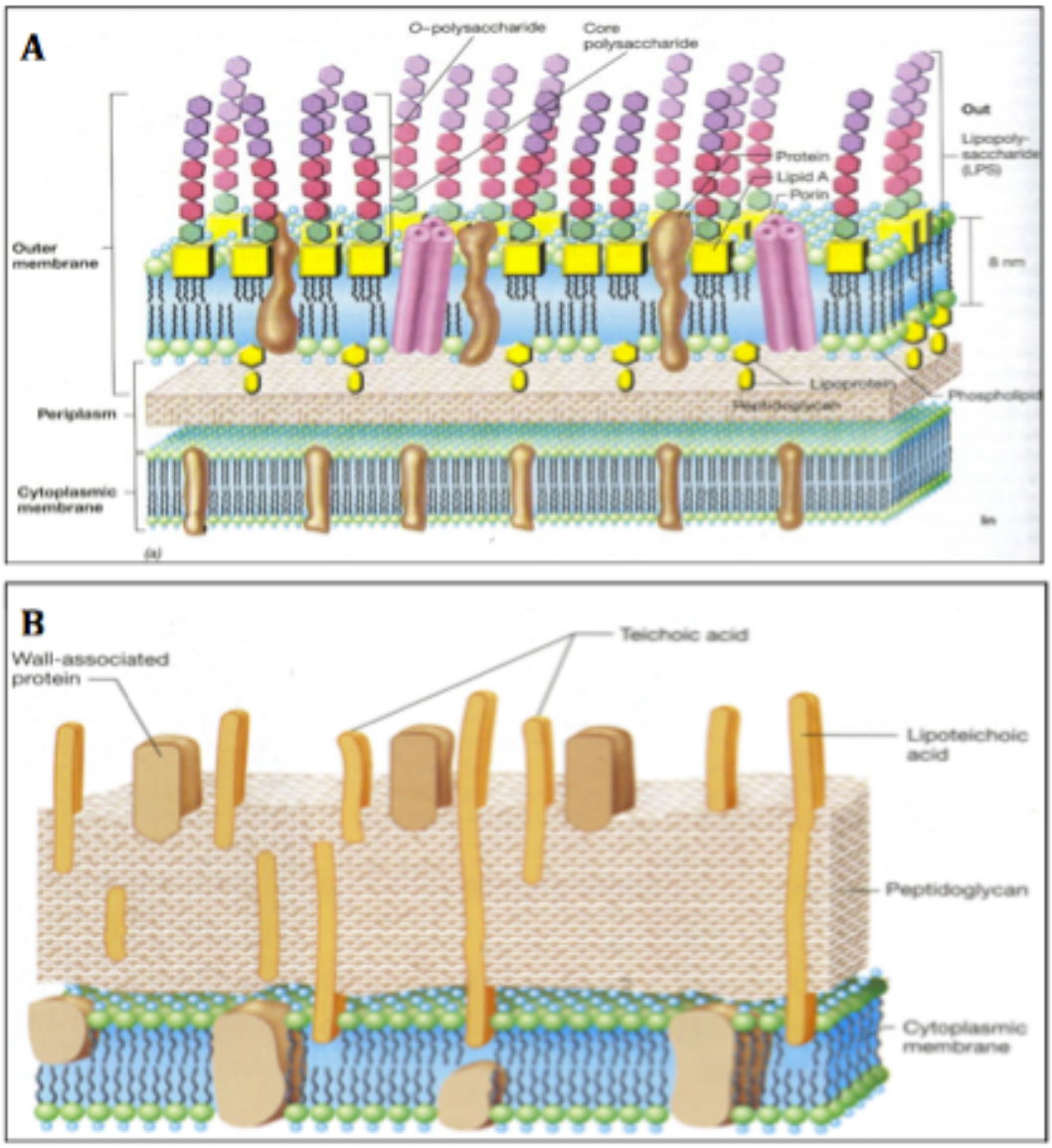

Figure 1.1. **Bacterial cell wall organisation. A**, **The Gram-negative envelope**. The major structural features of the cytoplasmic membrane, periplasm and outer membrane are indicated. **B**, **The Gram-positive envelope**, showing the major structural components of the cytoplasmic membrane and thick peptidoglycan layer. Adapted from Madigan and Martinko (2006).

1.2.1.2 Gram-positive cell wall organisation

The cell envelope of Gram-positive bacteria (**Figure 1.1B**) is organised into a cytoplasmic membrane, (CM) and and a thick outermost layer made up of PG. In several strains, a proteinaceous S-layer also coats the bacterial cell, on top of the PG layer (Beveridge and Graham, 1991).

Gram-positive bacterial cell wall organisation differs from that of Gram-negative bacteria. Most obviously, the OM is absent in Gram-positive bacterial species. In place of an OM, PG layers in Gram-positive species are many times thicker than in Gram-negatives. Gram-positive PG is approximately 20-35nm thick, which accounts for 30-70% of the total cell wall mass, compared with just 5-10% in Gram-negatives (Matias and Beveridge, 2005; Schleifer and Kandler, 1972; Vollmer and Seligman, 2010). PG in Gram-positive bacteria accounts for half of the total dry weight of the wall and the remaining component is mainly made up of polyanionic accessory polymers and proteins (Archibald et al., 1993). Anionic polymers are comprised of the wall teichoic acids (WTAs) and the structurally related lipoteichoic acids (LTAs) that are anchored to the cytoplasmic membrane (Matias and Beveridge, 2008; Swoboda et al., 2010).

1.3 Peptidoglycan structure

Peptidoglycan (also known in older literature as murein) is the major structural component of bacterial cell walls, particularly Gram-positive cell walls. Bacterial cell shape is largely determined by the structure and

architecture of PG. Proof of this is provided following the isolation of the PG sacculus, which retains a cell's original shape after treatment with SDS (Dworkin, 2010).

The main difference in structure and architecture of Gram-positive and Gram-negative PG sacculi is thickness; AFM analysis revealed the thickness of *E. coli* sacculi to be 2 nm (Turner et al., 2013) whereas the thickness of *B. subtilis* sacculi is 8 nm (Hayhurst et al., 2008). However, there are some similarities between the sacculi of Gram-positive and Gram-negative bacterial species. Within the PG network, pores were of similar average sizes in Gram-negative and Gram-positive species and they were relatively homogenous in size: the mean radius of the pores was 2.06 nm for *E. coli* peptidoglycan and 2.12 nm for *B. subtilis* peptidoglycan (Vollmer et al., 2008a).

PG structure and architecture contributes to the preservation of cell shape and integrity against internal turgor or osmotic pressure. The details of how and why PG architecture contributes to these viability factors is currently unknown (Hayhurst et al., 2008) and thus demands further investigation. Furthermore, knowledge of the PG structure and architecture is required for understanding the mechanism of sacculus enlargement during cell growth and division (Vollmer and Seligman, 2010).

1.3.1 Peptidoglycan biochemistry

PG is a single macromolecule made up of glycan strands cross-linked via peptide side-chains (Vollmer et al., 2008a). The crosslinking of both

carbohydrate and peptide components allows the formation of two and three-dimensional structures. In general, the basic unit structure of PG is highly conserved between all eubacteria except *Mycoplasma spp.* and a few other species that lack a cell wall (Scheffers and Pinho, 2005).

The basic unit of PG is a disaccharide pentapeptide; glycan strands are cross-linked by peptide side chains (**Figure 1.2**). The glycan strands are made up of alternating disaccharide residues of *N*-acetylglucosamine (*N*AG or Glc*N*Ac) and *N*-acetylmuramic acid (*N*AM or Mur*N*Ac). The alternating NAG and *N*AM disaccharide residues are held together by β-1,4 glycosidic linkages (Archibald et al., 1993). The D-lactoyl group of each Mur*N*Ac residue is substituted by a peptide stem whose composition is most often L-Ala-γ-D-Glu-*meso*-A2pm(or L-Lys)-D-Ala-D-Ala(A2pm, 2,6-diaminopimelic acid) in nascent PG, the last D-Ala residue being mostly lost in the mature macromolecule (Vollmer et al., 2008a). Crosslinking of the glycan strands generally occurs between the carboxyl group of D-Ala at position 4 and the amino group of the diamino acid at position 3, either directly or through a short peptide bridge (Vollmer et al., 2008a).

1.3.1.1 PG glycan chains

The PG glycan chains are synthesized by peptidoglycan glycosyltransferases (PGTs). The glycan strand lengths vary depending on the type of PGT synthesized by a bacterial species (Wang et al., 2008).

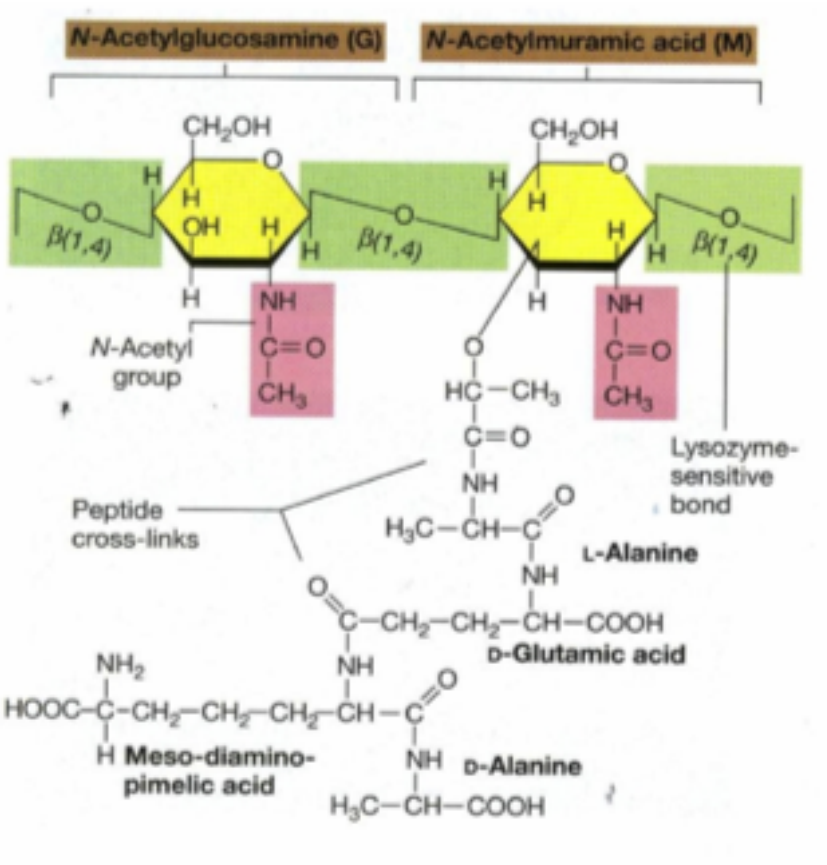

Figure 1.2. PG building blocks. The basic unit of PG is a disaccharide pentapeptide composed of alternating *N*-acetylglucosamine and *N*-acetylmuramic acid, linked together by glycosidic bonds. The pentapeptide is covalently linked to the lactoyl group of the muramic acid, and its composition can vary between different bacteria. Adapted from Madigan and Martinko (2006).

Remarkably, the average chain length of the glycan strands is not directly proportional to the thickness of the PG layer, as there are Gram-positive species with a thick cell wall with either short (*S. aureus*) or long (*B. subtilis*) glycan strands (Wang et al., 2008). Similarly, there are Gram-negative species with either short (*H. pylori*) or long (*P. morganii*) glycan strands (Vollmer et al., 2008a).

The glycan strands of *B. subtilis* were previously thought to have an average chain length of between 50 and 250 disaccharide units (Ward, 1973). However, Hayhurst et al. (2008) showed that *B. subtilis* has glycan strands up to 5μm long, corresponding to 5000 disaccharides, 50 times longer than previously reported. Chain length was determined using a combination of High Pressure Liquid Chromatography (HPLC) and Atomic Form Microscopy (AFM) (Hayhurst et al., 2008). In species with high activity of strand-cleaving enzymes (glucosaminidases and muramidases), the PG may contain glycan strands with all possible combinations of *N*AG and *N*AM residues at their ends . However, there are no bacterial species known to have such unmodified, poly(*N*AG-*N*AM) glycan strands in their mature PG, as glycan strands invariably become modified or linked to other cell wall polymers shortly after their synthesis (Vollmer et al., 2008a). An example of this was shown by Boneca et al. (2000) who showed that many chains in *S. aureus* were found to have been processed *in vivo* by glucosaminidase activity, demonstrating that hydrolysis may be important in the PG reaching its final architecture.

1.3.1.2 PG peptide cross-linkage

Variations of the peptide moiety of PG occur during the cross-linkage of the interpeptide bridge (Vollmer et al., 2008a). Penicillin-binding proteins (PBPs) catalyse the cross-linking reactions (Sauvage et al., 2008). These will be discussed later in this chapter.

As with glycan chain length, the degree of cross-linkage varies between bacterial species and is not correlated with being a Gram-positive or Gram-negative. For example, dimeric peptide cross-links are found in *B. subtilis*, whereas multimeric peptides with approximately 20 connected peptides exist in *S. aureus* (Snowden and Perkins, 1990). The peptide cross-link increases the length of the peptides and potentially, the distance between glycan strands (Vollmer et al., 2008a).

It is not yet known how the variability of cross-linking contributes to overall PG architecture and this phenomenon thus requires further investigation.

1.4 PG synthesis

The biosynthesis of PG can be divided into three separate stages; 1) synthesis in the cytoplasm of a monosaccharide pentapeptide; (2) assembly of the disaccharide-pentapeptide monomer unit on the inner surface of the cytoplasmic membrane, and translocation of the monomer to the periplasm; (3) transglycosylation of the monomer unit into a glycan polymer, and transpeptidation into the sacculus (Scheffers and Pinho, 2005; Typas et al., 2012). PG biosynthesis is shown in a schematic in **Figure 1.3**.

1.4.1 Monosaccharide pentapeptide synthesis

The first stage of PG biosynthesis occurs in the cell cytoplasm. In this stage, the sugar-linked precursors, UDP-Mur*N*Ac-pentapeptide and UDP-Glc*N*Ac i.e. the disaccharide pentapeptide units, are synthesized (Scheffers and Pinho, 2005).

Initially, glucose is converted to Glc*N*Ac and attached to an undecaprenylphosphate (UDP) lipid anchor. In addition, phosphenolpyruvate is ligated to the 3' hydroxyl group of UDP-Glc*N*Ac producing UDP-Glc*N*Ac-enolpyruvate. Finally, The pentapeptide stem is then synthesised by sequential attachment of each amino acid, beginning with the linkage of L-alanine to D-lactate of the UDP-Mur*N*Ac anchor (Typas et al., 2012).

1.4.2 Assembly and translocation of the disaccharide pentapeptide

In the second stage of PG biosynthesis, which takes place at the cytoplasmic membrane, precursor lipid intermediates are synthesized. The phospho--Mur*N*Ac-pentapeptide moiety of UDP-Mur*N*Ac-pentapeptide is transferred to the membrane acceptor, bactoprenol, yielding Lipid I [Mur*N*Ac-(pentapeptide)-pyrophosphoryl-undecaprenol]. Following this, Glc*N*Ac from UDP-Glc*N*Ac is added to Lipid I, yielding Lipid II [Glc*N*Ac-ß-(1,4)-Mur*N*Ac-(pentapeptide)-pyrophosphoryl-undecaprenol], which is the substrate for the polymerization reactions in bacteria that have directly cross-linked PG (Scheffers and Pinho, 2005). Lipid II is flipped across the cytoplasmic membrane for polymerisation to the peptidoglycan layer (Typas et al., 2012).

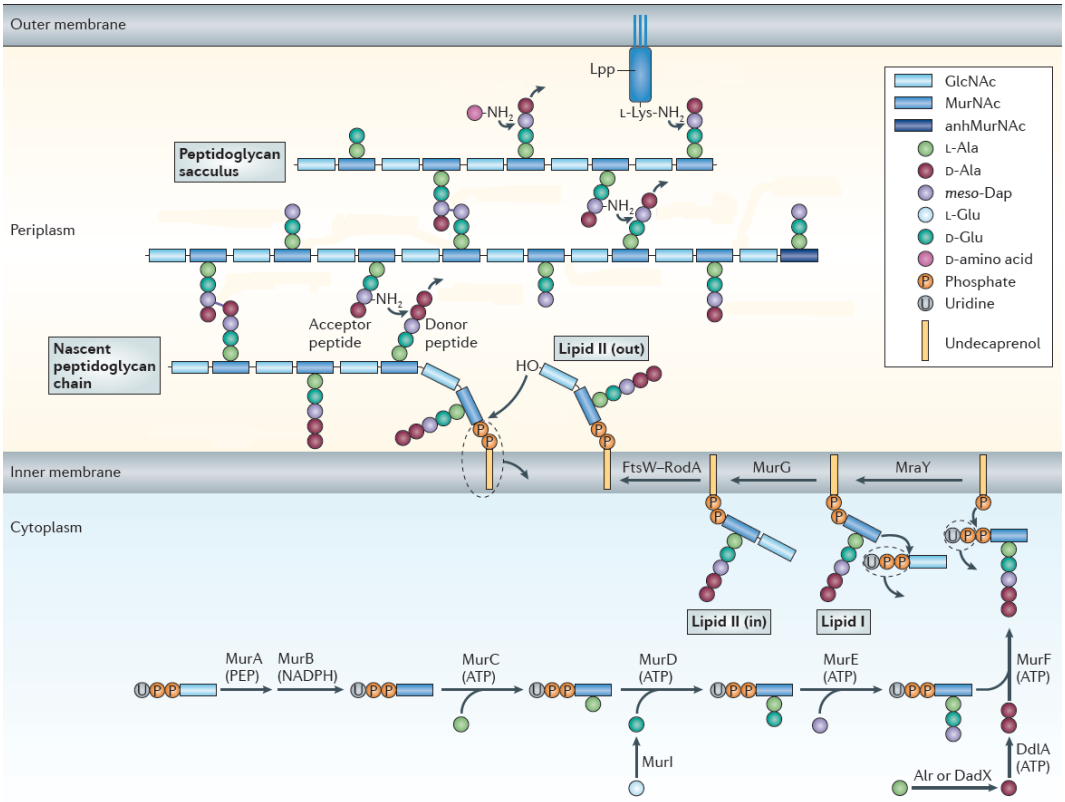

Figure 1.3. The peptidoglycan biosynthesis pathway. The peptidoglycan disaccharide pentapeptide precursor is synthesised in the cytoplasmic membrane, transported across the cytoplasmic membrane to the periplasm, and polymerised into the existing sacculus. This schematic shows peptidoglycan assembly in a Gram-negative organism, however the process is essentially the same for Gram-positive bacteria, except that the sacculus is not anchored to an outer membrane lipoprotein.

Adapted from (Typas et al., 2012).

1.4.3 Incorporation of nascent PG into the cell wall

The third and final stage of PG biosynthesis, which takes place at the outer leaflet of the cytoplasmic membrane, involves the polymerization of the newly synthesized disaccharide-peptide units and their incorporation into the growing PG sacculus.

Glycan strands are polymerised by the formation of a glycosidic bond between the non-reducing *N*AG terminus of lipid-linked disaccharide-pentapeptide and the lipid-anchored *N*AM residue at the reducing end of the growing glycan strand (Ward and Perkins, 1973). UDP is released from the terminal reducing *N*AM during formation of the glycosidic bond, and is subsequently dephosphorylated, releasing the lipid anchor (which is reused in subsequent synthesis cycles) (Typas et al., 2012).

In order to cross-link the disaccharide pentapeptides, the transpeptidation reaction takes place. Transpeptidation occurs by hydrolysis of the terminal D-alanine of the pentapeptide. The donor tetrapeptide D-alanine is then cross-linked to an acceptor peptide (Typas et al., 2012).

The polymerization of glycan chains and cross-linking of peptides i.e. the transglycosylation and transpeptidation reactions respectively, are catalysed by Penicillin-binding proteins (Sauvage et al., 2008).

1.5 Penicillin-binding proteins in *B. subtilis*

Penicillin-binding proteins (PBPs) catalyse the polymerization of the glycan strand (transglycosylation) and the cross-linking of the peptides between

glycan chains (transpeptidation) during PG biosynthesis (Sauvage et al., 2008). Some PBPs can hydrolyse either the peptide bond connecting two glycan strands (endopeptidation) or the last D-alanine of pentapeptides (DD-carboxypeptidation) (Sauvage et al., 2008)

PBPs as classed as high molecular mass (HMM) PBPs and low molecular mass (LMM) PBPs. *B. subtilis* has 16 PBPs, most of which have been extensively studied for their role in vegetative peptidoglycan synthesis and in sporulation (Sauvage et al., 2008).

The 16 *B. subtilis* PBPs can often be associated with a specific mode of cell wall synthesis, where mutants may not be able to elongate or septate. However, the precise physiological role of PBPs is often hard to deduce, due to functional redundancy and complex relationship between PBP activities *in vivo* (Sauvage et al., 2008).

The class and function (if known) of these 16 PBPs found in *B. subtilis* are summarized in **Table 1.1** (Daniel et al., 2000; Lawrence and Strominger, 1970; McPherson et al., 2001; Murray et al., 1998, 1996; Popham et al., 1999, 1995; D. L. Popham and Setlow, 1993; Scheffers et al., 2004; Scheffers and Errington, 2004; Wei et al., 2004, 2003).

1.5.1 HMM PBPs

HMM PBPs are multimodular PBPs responsible for peptidoglycan polymerization and insertion into pre-existing cell wall (Goffin and Ghuysen, 1998). HMM PBPs are subdivided into Classes A and B, depending on the

structure and catalytic activity of the N-terminal domain (Goffin and Ghuysen, 1998).

Class A HMM PBPs are bifunctional enzymes: the N-terminal domain has transglycosylase activity, whilst the C-terminal domain has transpeptidase activity (Sauvage et al., 2008). In class A HMM PBPs, the N-terminal domain is responsible for their glycosyltransferase activity, catalyzing the elongation of uncross-linked glycan chains (Höltje, 1998). *Bacillus subtilis* has four class A PBPs. PBP1 is part of the cell division machinery and is required for the efficient formation of the asymmetric sporulation septum (Scheffers and Errington, 2004). PBP2c and PBP2d catalyse the synthesis of spore PG (McPherson et al., 2001; Murray et al., 1998).

In class B, the N-terminal domain is believed to play a role in cell morphogenesis by interacting with other proteins involved in the cell cycle (Höltje, 1998). *Bacillus subtilis* PBP2a is required for normal outgrowth of spores (Murray et al., 1998). PBP2a and PBPH play redundant roles in determining the rod cell shape and the activity of one of these proteins is required for viability (Wei et al., 2003). PBP3 and PBP4b are Class B PBPs with transpeptidase activity but their role is unknown (Murray et al., 1996; Wei et al., 2004).

Name	Class	Gene	Enzymatic Function
PBP1	A	*ponA*	Cell division and diameter control during cell elongation
PBP2a	B	*pbpA*	Synthesis of lateral wall PG
PBP2c	A	*pbpF*	Synthesis of spore PG
PBP2d	A	*pbpG*	Synthesis of spore PG
PBP4	A	*pbpD*	Unknown
PBP2b	B	*pbpB*	Septum formation during cell division
PBP3	B	*pbpC*	Unknown transpeptidase activity
PBP4b	B	*pbpI*	Unknown transpeptidase activity
PBPH	B	*pbpH*	Synthesis of lateral wall PG
SpoVD	B	*spoVD*	Synthesis of spore PG
PBP4a	C	*dacC*	Unknown carboxypeptidase activity
PBP4*	C	*pbpE*	Unknown endopeptidase activity
PBP5	C	*dacA*	Unknown carboxypeptidase activity
PBP5*	C	*dacB*	Peptide cross-linking in spore PG
PbpX	C	*pbpX*	Unknown endopeptidase activity
DacF	C	*dacF*	Peptide cross-linking in spore PG

Table 1.1 A summary of the 16 PBPs found in *B. subtilis*. The name, class, encoding gene and enzymatic function of each PBP are listed (Daniel et al., 2000; Lawrence and Strominger, 1970; McPherson et al., 2001; Murray et al., 1998, 1996; Popham and Setlow, 1993; Popham et al., 1999, 1995; Scheffers and Errington, 2004; Scheffers et al., 2004; Wei et al., 2004, 2003).

1.5.2 LMM PBPs

LMM-PBPs are monofunctional DD-peptidases generally known as Class C PBPs (Sauvage et al., 2008). In *B. subtilis*, PBP5 (*dacA*) is the major carboxypeptidase found in vegetative cells (Lawrence and Strominger, 1970). PBP5 has no role in spore peptidoglycan synthesis but PBP5* (*dacB*) and DacF (*dacF*) both function in regulating the degree of cross-linking of spore peptidoglycan (Popham et al., 1999). PBP5* is required for proper spore cortex synthesis (Popham et al., 1995) and DacF regulates the degree of cross-linking of spore peptidoglycan (Popham et al., 1999). PBP5* is expressed only in the mother cell compartment of the developing sporangium whereas *dacF* is expressed in the forespore compartment and they can act differently on the nascent spore peptidoglycan (Popham et al., 1999). Studies have shown that *B. subtilis* PBP4a, another carboxypeptidase, is recruited to the lateral wall and is absent from the septum (Scheffers et al., 2004).

1.6 PG dynamics in *B. subtilis*

In order to reproduce, *B. subtilis* cells elongate and then divide by binary fission to produce two identical daughter cells. To grow and divide, *B. subtilis* needs to not only synthesise new PG but also to break the covalent bonds of the existing PG sacculus to enable the insertion of new material (Scheffers and Pinho, 2005).

1.6.1 Enlargement of the sacculus

It has been proposed that growth of the sacculus requires hydrolysis of existing covalent bonds to accommodate insertion of nascent peptidoglycan (**Figure 1.4**). However, such a mechanism could potentially compromise the cell wall integrity (Dmitriev et al., 2005). A "three-for-one" mechanism was proposed for safe incorporation of nascent material into a monolayered peptidoglycan network such as *Escherichia coli* (*E. coli*) (**Figure 1.4A**; (Höltje, 1998). In this model, one glycan strand in the sacculus (the docking strand) is displaced by a nascent triplet of cross-linked glycan strands and pulled into the plane of the sacculus under turgor stress (Höltje, 1998). A three-for-one growth mechanism of 'inside-to-outside' growth, compatible with growth of the multilayered Gram-positive sacculus was later proposed (**Figure 1.4B**; Höltje and Heidrich, 2001). In this model, it was hypothesized that packs of newly synthesized PG are inserted pack by pack and passed on from layer to layer by the activity of transferases until the first PG triplet reaches the outermost layer (Höltje and Heidrich, 2001; Koch and Doyle, 1985). The mechanism not only explains maintenance of the thickness of the PG shell but also in addition explains the rate of PG turnover if one assumes that only every second PG strand can function as docking strand. However, it is not known whether this model of sacculus enlargement occurs *in vivo* (Höltje and Heidrich, 2001). These models also imply that the region where new PG is

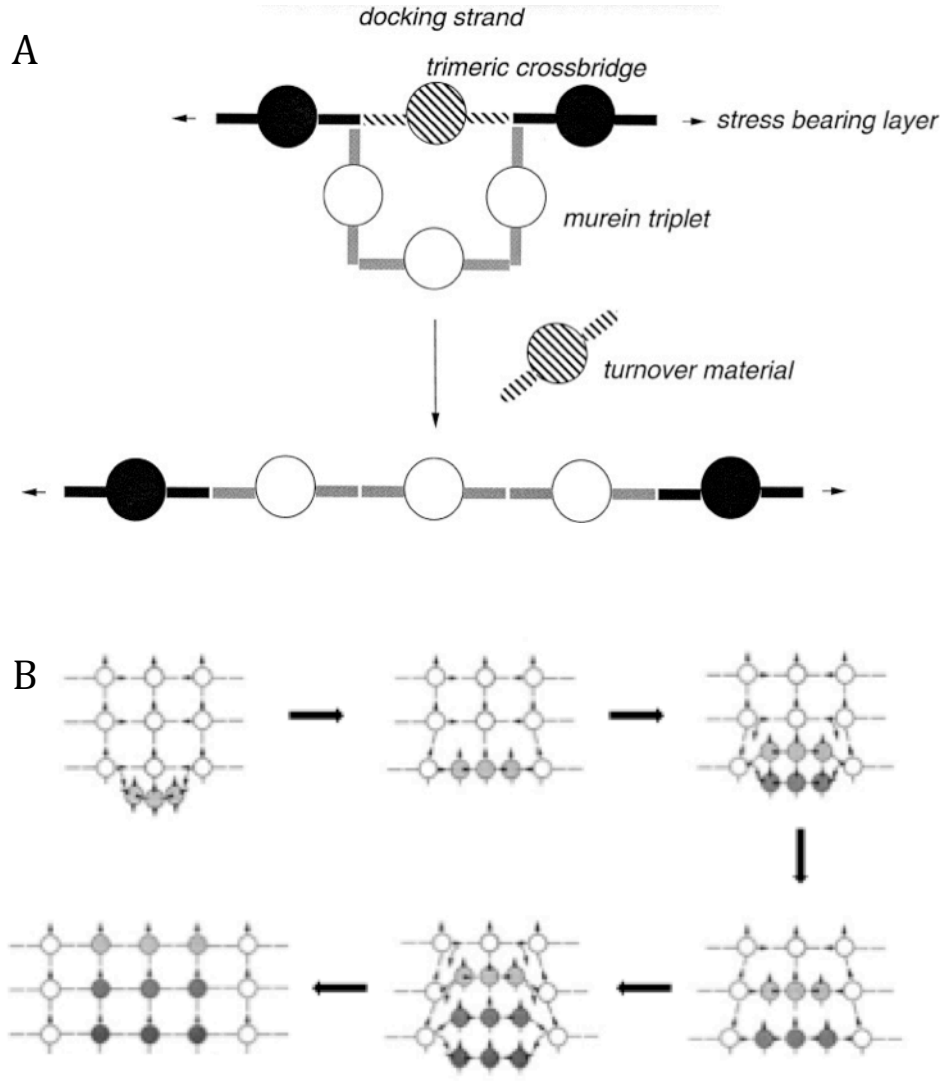

Figure 1.4. Enlargement of the PG sacculus in Gram-positive rods.

A: The three-for-one model. A cross-linked triplet of nascent peptidoglycan forms a trimeric crossbridge beneath a single glycan strand (the docking strand) in the sacculus. The docking strand is selectively excised, drawing the nascent material into the stress bearing plane of the sacculus.

B: Multilayered peptidoglycan wall grows by the addition of new layers of PG underneath the existing ones. Removal of the outermost layers allows the newly added ones to become part of the stress-bearing wall structure. Therefore, the cell grows from "inside to outside".

Adapted from Höltje and Heidrich (2001).

added cannot be load-bearing. However, data produced by Misra et al. (2013) suggested that cells can vary their growth rate without changing wall thickness or strain by maintaining a constant ratio of synthesis and hydrolysis rates.

1.6.2 Cell Elongation

During cell division, the pre-existing glycan chain is elongated by incorporation of Lipid II in the glycosyltransferase domain of PBP1 (Class A PBP). Transpeptidation between the glycan chain and the pre-exisiting PG occurs in both the transpeptidase domain of PBP1 and the transpeptidase domain of PBP2a (Class B). The new glycan chain is incorporated into PG after endopeptidation of Class C PBPs (Sauvage et al., 2008).

Maintenance of sacculus shape is essential during PG biosynthesis and is thus tightly co-ordinated. Cytoskeletal elements, MreB and FtsZ which are structural homologues of eukaryotic actin and tubulin respectively, act as scaffolds to coordinate the peptidoglycan biosynthetic apparatus (Daniel and Errington, 2003; Errington et al., 2003). The MreBCD proteins have been identified as crucial to directing the incorporation of nascent PG during cell division. MreB has been identified in many bacterial species, including paralogues in *B. subtilis,* where it guides the longitudinal cell wall synthesis (Kruse et al., 2005; Matteï et al., 2010). *B. subtilis* possesses three MreB paralogues, MreB, Mbl (MreB-*l*ike) and MreBH (Daniel and Errington, 2003). MreB and Mbl coordinate the peptidoglycan synthesis machinery, whilst MreBH may coordinate peptidoglycan hydrolase activity, as has been suggested for *B. subtilis* LytE (Carballido-López et al., 2006). *B. subtilis*

depends on the coordination of cell wall synthesis and hydrolysis in helical tracts defined by MreB proteins (Carballido-López et al., 2006). The MreB ATPase is highly dynamic and polymerises in localised patches which move rapidly around the cell cylinder in a helical manner (Domínguez-Escobar et al., 2011). Furthermore, MreB filaments associate directly with the peptidoglycan biosynthetic machinery in *B. subtilis* as part of the mechanism that brings about controlled cell elongation (Kawai et al., 2009).

The function of the MreC and MreD proteins is less well understood. MreC and MreD act in a morphogenic pathway in *B. subtilis* that couples the helical cytosolic Mbl cables to the extracellular cell wall synthetic machinery, which is critical for cylindrical elongation of the rod-shaped cells.

1.6.3 Cell division

For a *B. subtilis* cell to bisect and divide into two daughter cells, a septum must be synthesized in the centre of the cell to mark the position of cell division. This septal cross-wall formation precedes the splitting of the mother cell and is modulated by several proteins in *B. subtilis*.

Bacterial cell division is initiated by the tubulin homologue protein FtsZ (Adams and Errington, 2009). The FtsZ GTPase polymerises at the bacterial division ring and is required for division in almost all bacteria (Adams and Errington, 2009; Erickson et al., 2010). Prior to septum formation, FtsZ polymerises to form a ring-like structure, known as a Z-ring, which acts as a scaffold for the bacterial cytokinetic machinery (Adams and Errington, 2009). This Z-ring appears to subsequently contract while maintaining a position at the leading edge of the developing septum (Harry, 2001a). The Z-ring at the

septal site then acts as a scaffold to which all other members of the division machinery are recruited. Recruitment of FtsZ and correct subsequent placement of Z-rings in *B. subtilis*, i.e. centrally to halve the mother cell during division, is controlled by the MinCDE gene complex (Harry, 2001a). A conserved division inhibitor MinCD, which prevents aberrant division at the cell poles, controls division site selection (Marston et al., 1998). The *B. subtilis* DivIVA protein controls the topological specificity of MinCD action. DivIVA is targeted to division sites late in their assembly, after a MinCD-sensitive step requiring FtsZ has occurred (Marston et al., 1998). DivIVA then recruits MinD to the division sites preventing another division from taking place near the newly formed cell poles (Marston et al., 1998).

Following Z-ring contraction, several additional division proteins are recruited to form a complex known as the 'divisome'. This complex connects the Z-ring and associated proteins to the PG synthesis machinery (Daniel et al., 2006). DivIC, DivIB, and PBP2b are interdependent for assembly of the division complex. Finally, PG hydrolysis is required for septation of daughter cells. Multiple PG hydrolases participate in the splitting of the septum in *B. subtilis* cell division (discussed in next section).

1.7 PG hydrolases in *B. subtilis*

PG hydrolases form a diverse group of bacterial enzymes that cleave specific bonds within the PG network (Ghuysen, 1968). For every type of amide or glycosidic bond found in the PG, there is a PG hydrolase capable of cleaving it

(Vollmer et al., 2008a). *B. subtilis* has an even larger complement of 35 known putative PG hydrolases (Smith et al., 2000). The major activity of PG hydrolases occurs during vegetative growth and division. However many are required for more specialised functions.

1.7.1 Types of PG hydrolases

Enzymes that hydrolyse the amide bonds between amino acids in the peptide stems are peptidases. Endopeptidases cleave between the alternating L- and D-isoform amino acids in the peptide stem or between *meso*-DAP – *meso*-DAP crosslinks. DD-Endopeptidases hydrolyse between D-Ala-*meso*-DAP. Carboxypeptidases remove the C-terminal amino acid from the peptide stem. Removal of the terminal D-Alanine from the D-Ala-D-Ala moiety by DD-carboxypeptidases is an important activity as it permits formation of D-Ala-*meso*-DAP crosslinks (Höltje, 1995)

N-acetylmutamyl-L-alanine amidases (amidases) are enzymes that cleave the amide bond between the lactyl group of *N*AM and the α-amino group of L-alanine at the *N*-terminus of the peptide stems, essentially separating the peptide and glycan components (Höltje, 1995).

Glycosidases cleave the glycosidic bonds in the glycan backbone of PG, and fall into two major groups, *N*-acetyl-β-D-muramidases, which cleave the bond between *N*AM and *N*AG, and *N*-acetyl-β-D-glucosaminidases, which cleave the bond between *N*AG and *N*AM. *N*-acetyl-β-D-muramidases are further classed as lysozymes or lytic transglycosylases. Lysozymes hydrolyse the glycan strand to produce a reducing Mur*N*Ac terminus.

Lytic transglycosylases hydrolyse the glycosidic bond with concomitant transglycosylation of the Mur*N*Ac residue, forming a 1,6-anhydro ring at the glycan strand terminus (Höltje et al., 1975). In *B. subtilis*, lytic transglycosylases make a minor contribution processing of glycan strands, <0.5% of muropeptide material (Atrih et al., 1999).

1.7.2 PG hydrolysis during growth and division

During vegetative growth, muropeptides are shed from the cell wall in a growth rate-dependant manner, a process termed cell wall turnover. In *B. subtilis*, the rate of turnover is as high as 40-50% per generation, and is diminished in hydrolase-defective mutants (Reith and Mayer, 2011). Most models of cell wall growth envisage a system of tightly coordinated synthesis and hydrolysis (Höltje and Heidrich, 2001; Höltje, 1998). According to these models, cell growth should stop when PG hydrolase activity is inhibited. However, as individidual PG synthases and hydrolases can be lost without altering growth, it is difficult to ascertiain the potentially complementary activities of each single hydrolases (Nelson and Young, 2001).

Carboxypeptidase activity regulates the balance of penta- and tetrapeptide stems available for transpeptidation during cell wall synthesis (Atrih et al., 1999). Pentapeptides participate as donor or acceptor peptide stems in cross-linking reactions, whilst tetrapeptides (the product of carboxypeptidase activity) can participate only as acceptor peptides (Atrih et al., 1999).

PG hydrolases are utilised during separation of *B. subtilis* daughter cells. Two main PG hydrolases participate in splitting of the septum; LytF and CwlF

(LytE). *B. subtilis* LytF and CwlF (LytE) mutants were unable to separate following cell division, thus forming chains (Ohnishi et al., 1999). These proteins are localized at cell separation sites and cell poles in the vegetative phase (Yamamoto et al., 2003). LytC and LytD were shown to have roles in cell separation, cell wall turnover, antibiotic-induced lysis and motility (Blackman et al., 1998). Another hydrolase, an endopeptidase gene product, YojL (renamed CwlS), also plays a putative role in cell separation with LytE and LytF (Fukushima et al., 2006).

1.7.3 Role of PG hydrolases during sporulation and germination

PG hydrolases play an integral role throughout sporulation and germination (Errington, 2003; Smith et al., 2000). They are required for hydrolysis of the asymmetric septum (SpoIID and SpoIIP), maturation of the spore cortex (CwlD and LytH) and endospore release by lysis of the mother cell wall (CwlC, LytC and CwlH) (Smith et al., 2000).

The germination specific cortex-lytic enzymes (GSLEs) SleB and CwlJ catalyse germination-like changes in permeabilized spores. During germination, hydrolysis of the endospore cortex initiates influx of water and nutrient uptake for regeneration of vegetative cells (Smith et al., 2000). Both SleB and CwlJ have roles in the later stages of germination, during cortex hydrolysis (Ishikawa et al., 1998).

1.7.4 Regulation of *B. subtilis* PG hydrolases.

PG hydrolases are potentially lethal for the producing bacterial cell, therefore the activity of these enzymes is tightly controlled. Regulation occurs during

transcription or post-translationally, via protein-protein interactions, proteolytic processing and regulation by secondary wall polymers.

Regulation by sigma factors facilitates differential expression of PG hydrolases. The late mother-cell specific sigma factor of *B. subtilis*, SigK, regulates transcription of sporulation specific hydrolases including LytH, CwlC and CwlH (Horsburgh et al., 2003). Dual regulation of *B. subtilis* endopeptidase *lytE* by SigA and SigI facilitates differential coordination of a single enzyme. SigA mediates LytE activity during vegetative growth, but expression of *lytE* is rapidly upregulated by SigI as an emergency response (Tseng et al., 2011).

Two-component signal transduction systems (TCS) provide a mechanism for regulating PG hydrolases expression in response to environmental signals. TCSs are phosphotransfer schemes involving two conserved components, a histidine protein kinase and a response regulator protein (Stock et al., 2000). The histidine protein kinase, which is regulated by environmental stimuli, autophosphorylates; this creates a high-energy phosphoryl group that is subsequently transferred to the response regulator protein (Stock et al., 2000). Phosphorylation induces a conformational change in the regulatory domain that results in activation of an associated domain that effects the response (Stock et al., 2000). In *B. subtilis*, WalKR localises to the septum, possibly acting as a sensor for initiation of cell division (Fukushima et al., 2008). The WalKR regulon in *B. subtilis* includes four PG hydrolases, LytE, YocH, YvcE and YkvT (Bisicchia et al., 2010, 2007).

Protein-protein interactions may also coordinate PG hydrolase localization. Cylinder wall localisation of *B. subtilis* LytE is MreBH dependent. Yeast two-hybrid analysis suggested a direct interaction between LytE and MreBH (Carballido-López et al., 2006).

Proteases may also regulate the activity of PG hydrolases by maintaining the balance between synthesis and degradation. *B. subtilis* LytF localises to one cell pole in wild type cells, but is present at both poles in a mutant lacking the extracellular proteases WprA and Epr (Yamamoto et al., 2003).

1.8 Models of PG architecture

Although PG is biochemically well characterised, the three-dimensional architecture of the PG layer *in vivo* is poorly understood (Vollmer and Seligman, 2010). Many architectural models have been proposed, but two models have received the most focus - the classical planar model and the vertical scaffold model. A schematic and of these models is shown in **Figure 1.5**.

1.8.1 Orientation of the glycan strands – planar vs. scaffold model

In the planar model of PG architecture, glycan chains are oriented parallel to the lipid membrane (Koch, 1998). The thick wall of Gram-positive organisms would comprise multiple planar layers. In a cylindrical system, (such as a rod-shaped cell), the lateral forces acting on the cylinder wall are twice that

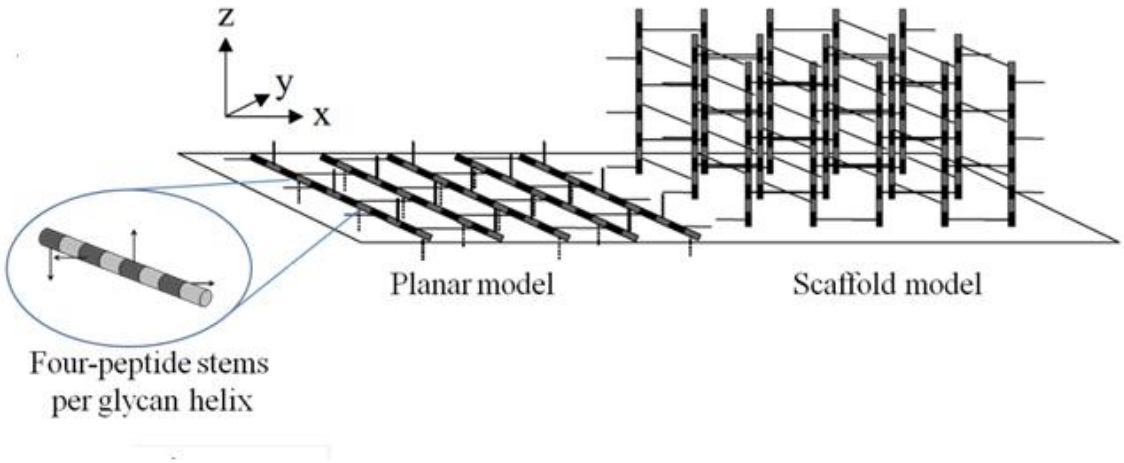

Figure 1.5. Planar and scaffold models of peptidoglycan architecture. In the planar model, glycan strands (striped cylinders) are parallel to the plasma membrane. The scaffold model suggests glycan strands are oriented perpendicular to the plasma membrane. Adapted from Vollmer and Höltje, (2004).

of the longitudinal direction (Koch, 1998). Therefore the rather inelastic glycan strands would be oriented circumferentially, perpendicular to the cell long axis. This would provide the biomechanical strength to maintain a rod shape under turgor pressure, such as in *B. subtilis*. An alternative vertical model of PG architecture was proposed, the 'scaffold' model (Dmitriev et al., 2003). In this model, the glycan chains are oriented perpendicular to the plasma membrane, along the axes of tensile stress. The PG would be maximally cross-linked close to the cytoplasmic membrane, and less cross-linked toward the outer membrane. This refutes the planar model of PG orientation, which was presumed by the authors to be inherently unstable under turgor pressures.

1.8.2 Rod-shaped PG architecture

1.8.2.1 Maintenance of rod-shaped architecture

A concern raised regarding PG architecture, is a rod shape is maintained under turgor pressure. Using *E. coli* as a model, Koch described three possible mechanisms for maintenance of rod-shape, (1) the belt model, (2) surface stress theory and (3) the contractile elements model (Koch, 1998). These models are summarized in **Figure 1.6**.

In the belt model the cylinder wall is constrained by inflexible glycan hoops (perpendicular to the cylinder's longitudinal axis) that act as a template for cylinder growth. Peptide stems bear none of the hoop stress, as their higher elasticity would cause the belts to stretch, resulting in successively wider cells with each new generation (Koch, 1998). However, whilst purified sacculi are more elastic in the direction of the long axis, they are not

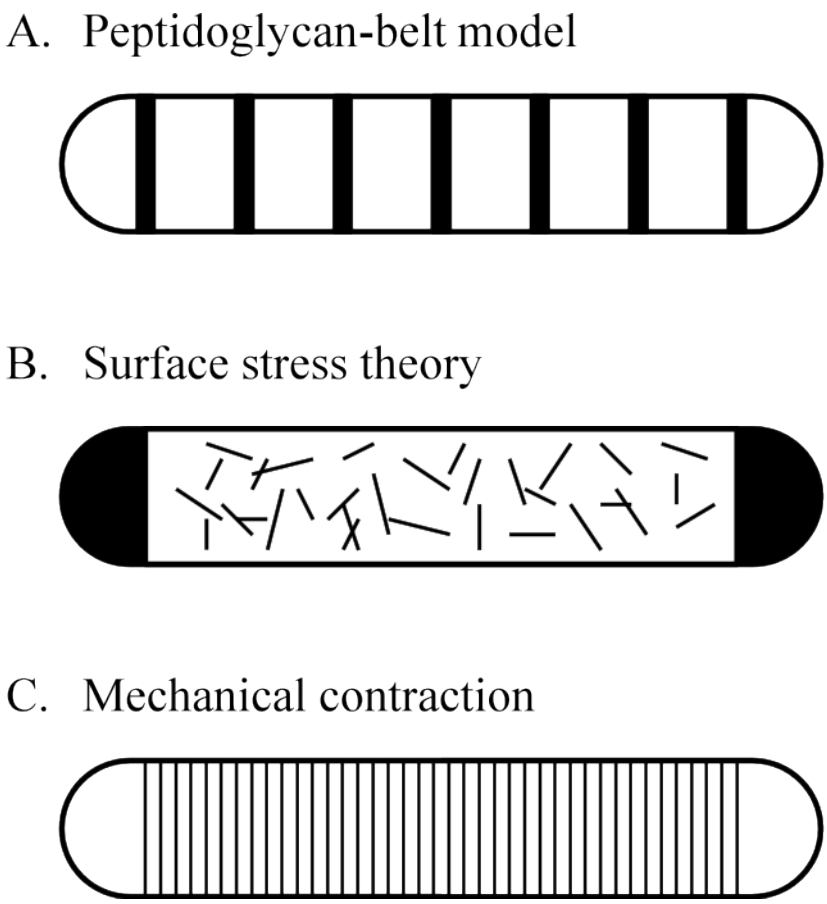

Figure 1.6. Three models for maintenance of rod shape. A, The belt model. Inflexible belts of peptidoglycan (black bands) constrain the cylinder circumference. **B**, The Surface stress model. Inert cell poles act as a framework for cylinder shape. A strict orientation is not required for the incorporation of nascent material in the cylinder wall. **C,** The mechanical contraction model. Cytoskeletal elements either pushes the poles apart, or apply a circumferentially constricting force to generate the cylinder shape. Adapted from (Koch, 1998)

completely inelastic across the short axis, and belts of PG were not observed by Atomic Force Microscopy (AFM) or cryo-Electron Microscopy (cryo-EM) of purified sacculi, therefore this model is unlikely to be correct (Gan et al., 2008; Yao et al., 1999).The surface stress theory suggests that poles are metabolically inert and act as a framework for cylinder growth. Rod shape is maintained by elongation rather than deformation of the cylinder under stress. Bonds stretched under turgor pressure are favoured for autolysis. Cleavage of these bonds pulls pre-attached nascent material into the stress-bearing plane, resulting in cylinder elongation. This does not require a strict arrangement of the PG network, nor does it preclude such a possibility (Koch, 1998).

The contractile elements model suggests that the cylinder circumference is constrained by a cytoskeletal system that pulls the wall inward, or pushes the poles apart (Koch, 1998). In *B. subtilis,* MreB, Mbl and MreBH form a self-organizing and dynamic filamentous scaffold underneath the membrane (Dempwolff et al., 2011). However, it is not known whether the forces generated by the action of MreB polymerization play a structural role in rod-shape maintenance.

1.8.2.2 *B. subtilis* PG architecture

Long fibres of cell wall material have been observed during cell wall regeneration of *Bacillus lichenformis* protoplasts (Elliott et al., 1975b). A study of the peptidoglycan architecture in *Bacillus subtilis*, utilising AFM of purified peptidoglycan sacculi, revealed similar features (Hayhurst et al., 2008). The inner surface of purified sacculi contained approximately 50 nm

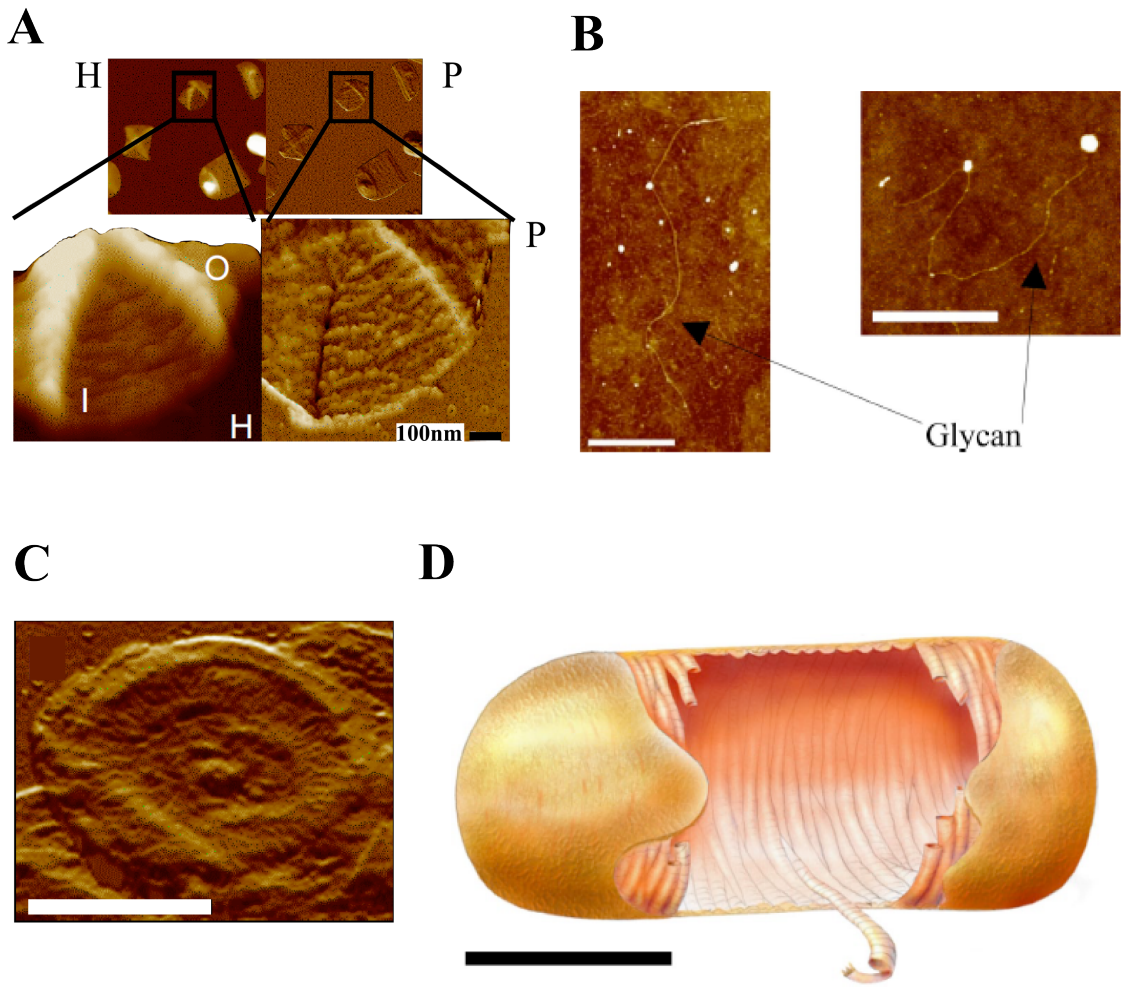

Figure 1.7. Proposed peptidoglycan architecture of *B. subtilis*. (A) AFM height (H) and phase (P) images showing cabled architecture on the inner cylinder surface of *B. subtilis* sacculi. I, inner surface; O, outer surface. (B) AFM height image showing long glycan strands. (C) AFM phase image showing a completed septum with spiral architecture and cross striations. (D) Model of proposed *B. subtilis* peptidoglycan architecture. The cylinder wall comprises coiled cables of peptidoglycan running around the circumference of the cell in the plane of the cell membrane. Scale bars: (B) 1µm; (C) 500 nm; (D) 1µm. Adapted from (Hayhurst *et al.*, 2008)

wide cables running perpendicular to the long axis of the cell (**Figure 1.7A**). Cross striations with an average periodicity of ~25 nm were observed throughout the cables, suggesting twists or coils of material. Size exclusion chromatography of purified glycan strands indicated that *B. subtilis* have extremely long glycan strands, as approximately 25% of glycan material was over 500 disaccharides in length (Hayhurst et al., 2008). AFM analysis of this purified material revealed the presence of strands up to 5 μm in length (**Figure 1.7B**). The architecture of the septa was different, comprising ~135 nm wide cables (**Figure 1.7C**). A model was proposed in which the cylinder contains cables of PG, comprising coiled-coils of long glycan strands, looped circumferentially around the cell cylinder, providing the mechanical strength for the cell to maintain a rod shape under turgor pressure (**Figure 1.7D**).

1.9 Use of microscopy to study PG dynamics and architecture

Previous studies have demonstrated that various microscopy approaches are an incredibly useful tool to study PG architecture and dynamics (Hayhurst et al., 2008; Turner et al., 2013, 2010; Wheeler et al., 2011). Such microscopy approaches have included epifluorescence microscopy, transmission electron microscopy (TEM), atomic force microscopy (AFM) and Stochastic Optical Resolution Microscopy (STORM). These techniques allow the imaging of PG dynamics within a cell *in vivo* (Epifluorescence, STORM), direct observation of isolated PG sacculi and architecture (AFM), and reveal structural details about cell envelope arrangement (TEM). Therefore, these approaches were deemed important for use in this study.

1.10 Project Aims and Objectives

Previous work in this lab has characterised the PG architecture of the Gram-positive rod-shaped bacterium *B. subtilis* (Hayhurst et al., 2008). The aim of this study was to further characterise PG dynamics and architecture of *B. subtilis* during differentiation of the vegetative rod-shaped morphology.

To analyse PG dynamics during growth and differentiation, three approaches were used:

a) A model of cell wall regeneration was developed for *B. subtilis*, produced from the image-based analysis of protoplast generation and subsequent regeneration.
b) The roles of the PG hydrolases LytE and YvcE were investigated during vegetative growth.
c) PG dynamics were studied during differentiation to map changes during sporulation.

Chapter 2

Materials and Methods

2.1 Growth media

Unless otherwise stated, all media were prepared using distilled water (dH_2O) and were sterilised by autoclaving for 20 min at 121°C (15 pounds per square inch).

2.1.1 Nutrient broth (NB)

Nutrient broth (Oxoid)	13 g l^{-1}

Oxoid Agar No. 1 (1.5% (w/v)) was added for Nutrient agar (NA).

2.1.2 Nutrient agar (NA)

Nutrient agar (Oxoid)	28 g l^{-1}

2.1.3 Luria-Bertani (LB)

Tryptone (Oxoid)	10 g l^{-1}
NaCl	10 g l^{-1}
Yeast extract (Oxoid)	5 g l^{-1}

Oxoid Agar No. 1 (1% (w/v)) was added for LB agar.

2.1.4 Penassay Broth (PAB)

Penassay Broth (PAB)	17.5 g l^{-1}
4x PAB	70 g l^{-1}

2.1.5 DM3

Solutions were autoclaved separately (except for Bovine Serum Albumin [BSA] which was filter-sterilised) and combined in the following volumes.

2.1.5.1 DM3 Protoplast Regeneration Agar

1M Sodium Succinate pH7.3 (adjusted with HCl)	250ml
5% ((w/v)) Casamino acids	50ml
10% ((w/v)) Yeast Extract	25ml
3.5% ((w/v)) K_2HPO_4 + 1.5% ((w/v)) KH_2PO_4	50ml
20% ((w/v)) Glucose	12.5ml
1M $MgCl_2$	10ml
2%((w/v)) BSA	2.5ml
4% ((w/v)) Bacto agar	100ml
TOTAL	500ml

2.1.5.2 DM3 Protoplast Regeneration Liquid

DM3 liquid was combined in the same volume ratio as described for DM3 agar except in 50ml quantities. In addition, the 4% ((w/v)) Bacto agar was omitted and 10ml dH_20 used instead. Furthermore, the final volume of DM3 liquid was subject to one final filter sterilisation. Liquid DM3 was kept at 4°C for up to one week until use before discarding.

2.1.6 2xSG

The following components were added and autoclaved together:

Difco Nutrient Broth	16.0 g l^{-1}
KCl	2.0 g l^{-1}
$MgSO_4.7H_2O$	0.5 g l^{-1}
Bacto agar (omitted if used liquid culture)	17.0 g l^{-1}

To the cooling (~55°C) liquid, the following sterile solutions were added:

1.0M $Ca(NO_3)_2$	1.0ml
0.1M $MnCl_2$	1.0ml
1.0mM $FeSO_4$	1.0ml
50% ((w/v)) glucose	2.0ml

2.2 Antibiotics

Antibiotics used in this study are listed in Table 2.1. For stock solutions, antibiotics were dissolved in the appropriate solvent, filter sterilised (0.2 μm pore size) and aliquots stored at -20°C. For agar plates, media was cooled to approximately 50°C prior to addition of antibiotic stock solution. For liquid media, antibiotic stock solutions were added just before use. Concentrations for antibiotic selection were as shown in Table 2.1, unless otherwise stated.

Table 2.1. Antibiotic Stock Solutions and Concentrations

Antibiotic	Stock concentration (mg ml^{-1})	Working concentration (µg ml^{-1})	Solvent
Erythromycin (Erm)	5	5	95% (v/v) ethanol
Chloramphenicol (Cm)	30	30	95% (v/v) ethanol

2.3 Buffers and stock solutions

Stock solutions were prepared using dH_2O unless otherwise stated, and stored at room temperature (15-25°C). Solutions used for microbiological work were sterilised by autoclaving.

2.3.1 Osmotically stable solutions

The following solutions allowed osmotically stable maintenance of protoplasts (Chang and Cohen, 1979). All components were autoclaved separately and filter-sterilised once combined.

2.3.1.1 2x SMM

1M Sucrose	46ml
0.04M Maleic acid	2ml
0.04M $MgCl_2$	2ml

TOTAL	50ml

2.3.1.2 SMMP

4x PAB	25ml
2x SMM	25ml
TOTAL	50ml

2.3.2 Phosphate buffered saline (PBS)

NaCl	8.0 g l^{-1}
KCl	0.2 g l^{-1}
Na_2HPO_4	1.4 g l^{-1}
KH_2PO_4	0.2 g l^{-1}

The pH was adjusted to 7.4 using a dilute solution of Na_2HPO_4 or KH_2PO_4 as appropriate.

2.3.3 Fixative preparation

2.3.3.1 Preparation of 16% ((w/v)) paraformaldehyde

100 mM sodium phosphate buffer (pH 7.0) was prepared as follows:

Na_2HPO_4 (1M)	57.7ml
NaH_2PO_4 (1M)	42.3ml

The final volume was adjusted to 1 l.

For 16% ((w/v)) paraformaldehyde:

100 mM sodium phosphate buffer (pH 7)	50ml
Paraformaldehyde (reagent grade, crystalline)	8.0g

The solution was heated to 60°C in a water bath and mixed vigorously. NaOH (≥5M) solution was added drop wise, with heating and vigorous mixing, until the solution cleared. Solution was stored at 4 °C for no longer than 8 weeks.

2.3.9.2 Fixative

Paraformaldehyde, 16 % ((w/v))	1.68ml
Glutaraldehyde, 25 % ((w/v))	2µl
100 mM sodium phosphate buffer (pH 7)	8.32ml

2.4 Bacterial strains and plasmids

2.4.1 *B. subtilis* strains

The *B. subtilis* strains used in this study are listed in **Table 2.2**. Routine culture of *B. subtilis* was on NA plates for solid media, or NB for liquid culture at 37 °C with aeration. *B. subtilis* BP115 was maintained on LB agar for solid media and LB for liquid media with the appropriate antibiotics and xylose concentrations, as described by Bisicchia et al., (2007).

Liquid cultures were typically inoculated to a known OD_{600} from an overnight starter culture. For short-term storage, plate cultures were stored at room temperature for up to 48 hr. For long term storage 20% (v/v) glycerol was

combined with an overnight culture, snap frozen in liquid N_2 and stored at -70 C.

2.5 Chemicals and enzymes

All chemicals used in this study were purchased from Fisher Scientific or Sigma-Aldrich unless otherwise stated. Concentrations and storage of stock solutions are shown in **Table 2.3**.

Table 2.2. *B. subtilis* strains used in this study

B. subtilis strain	***Relevant Genotype***	***Source***
HR168	Wild-type (WT)	Lab strain
BP115	*trpC2*Δ*lytE*::*cm*^{r}, Δ*yvcE*::pBP092(P_{xyl}*yvcE*) *erm*^{r}	Bisicchia et al. (2007)

Abbreviations: Cm^R, chloramphenicol resistance; Erm^R, erythromycin resistance.

Table 2.3. Stock Solutions and Concentrations

Stock solution	*Solvent*	*Concentration*	*Storage*
Glutaraldehyde	dH_2O	25% (v/v)	-20 °C
Lysozyme	dH_2O	20 mg ml^{-1}	-20 °C
Pronase	TES pH 8.0	10 mg ml^{-1}	-20 °C
Xylose	dH_2O	5% ((w/v))	-20°C
Vancomycin, BODIPY®Fl conjugate (Invitrogen)	dH_2O	100 µg ml^{-1}	-20 °C in dark
Vancomycin, AlexaFluor 532 conjugate (Molecular Probes)	DMSO	100 µg ml^{-1}	-20 °C in dark
Azido-D-Alanine (Iris Biotech)	DMSO	100mM	-20°C
Tetramethylrhodamine Alkyne (Molecular Probes)	DMSO	Unknown	-20 °C in dark
FM1-43 (Invitrogen)	dH_2O	1 mg ml^{-1}	-20 °C in dark
NADA (Nitrobenzofurazan 3-amino-D-Alanine) (Chemistry Dept, University of Sheffield)	DMSO	100mM	-20°C in dark
HADA (Hydroxycoumerin 3-amino-D-Alanine) (Chemistry Dept, University of Sheffield)	DMSO	100mM	-20°C in dark

2.6 Centrifugation

Details of centrifuges used to harvest samples throughout this study are given below. Centrifugation was carried out at room temperature unless otherwise stated:

i. Eppendorf microfuge 5415D.

   Max. load, 24 × 2.0ml; Max. speed, 13,200rpm (16,110 ×g)

ii. Sigma centrifuge 4K15C

   Max. load, 16 × 50ml; Max speed, 5,100 rpm (5525 ×g)

iii. Jouan centrifuge JAC50.10

   Max. load, 6 × 50ml; Max. speed, 13,000 rpm (10,000 ×g)

iv. Avanti™ J25I (Beckman)

   JA-20: Max. load, 6 × 50ml; Max. speed, 20,000 rpm (48,384 ×g)

   JA-10.5: Max. load, 6 × 400ml; Max. speed, 10,000 rpm (18,480 ×g)

2.7 Determination of bacterial cell density

2.7.1 Measurement by spectrophotometry (OD_{600})

Spectrophotometric measurement at 600nm wavelength (OD_{600}) was conducted for quantification of the bacterial yield of a liquid culture. Measurements were taken using a Jenway 6100 spectrophotometer. Culture samples were diluted in sterile culture medium or buffer as appropriate, to provide readings within the optimum accuracy range (below 0.6).

2.7.2 Measurement by direct cell counts (cfu ml^{-1})

Viable cell numbers of liquid cultures were quantified by plate counts. Bacterial samples were serial diluted 1:10 in PBS. 20µl of each dilution was spotted onto agar plates containing appropriate antibiotics or supplements as necessary. The number of colony forming units (cfu) was determined once individual colonies could easily be visualised for quantification (between 12 and 48 h growth).

2.8 *B. subtilis* protoplast generation and regeneration

2.8.1 Generation of bacterial protoplasts in *B. subtilis*

B. subtilis was grown to a mid-exponential phase (OD_{600} = 0.5-0.7) in 20ml 1XPAB, taken from a 5ml overnight starter culture in NB. The *B. subtilis* cells were then harvested by centrifugation at 12,000g for 10 min. Following this, the cells were resuspended in 2ml SMMP. Lysozyme was added to the resuspended cells to reach a working concentration of 2mg ml^{-1}. The cells were incubated with the lysozyme for 2h at 37°C, while being gently swirled at 50rpm.

Following incubation, the protoplasts were harvested by centrifugation at 2500g for 15min. The protoplast pellet was then gently resuspended in 2ml SMMP.

The resulting protoplast suspension was used straight away in regeneration and imaging experiments. Alternatively, the protoplast suspension was flash frozen using liquid nitrogen and stored at 80°C for future use.

2.8.2 Regeneration of bacterial protoplasts in *B. subtilis*

If previously frozen, the protoplasts were gently defrosted on ice. The 2ml of protoplast suspension in SMMP was added to 20ml of liquid DM3 media to allow the protoplasts to regenerate.

The regeneration assay was incubated at 37°C with gentle agitation (50rpm) over a period of 12h. Samples were taken at pre-determined time points for use in cell quantification.

2.8.1.1 Storage of protoplast regeneration samples

Samples were flash frozen in liquid nitrogen and stored at -80°C for up to two weeks. For use in subsequent imaging experiments, the samples were slowly defrosted on ice.

2.8.3 Quantification of protoplasts and regenerating cells

During the 12 hr regeneration assay, samples were taken at set time points over the course of the experiment and plated to generate viable counts. These time points were; vegetative cells (pre-lysozyme treatment), protoplasts (upon removal of lysozyme) and regenerated protoplasts (following 12hrs incubation in liquid DM3).

Two viable counts were generated for each time point using two different plate agars and dilution media: one to test for protoplast regeneration and one to act as a negative control (**Table 2.4**).

Table 2.4 Protoplast regeneration assay plates and corresponding dilution media

	Plate Media	***Dilution Media***
Regeneration test	DM3	SMMP
Negative control	NA	1xPBS

2.9 *B. subtilis* growth experiments

2.9.1 *B. subtilis* WT growth in NB

For growth in liquid media *B. subtilis* WT was grown aerobically at 37°C. A single colony was used to inoculate 10ml of NB in a sterile 25ml universal tube and grown overnight at 37°C and at 250rpm on a rotary shaker. This culture was used to inoculate fresh NB in a sterile conical flask at an OD_{600} of 0.05. Cells were then grown at 37°C and 250rpm to required growth phase.

2.9.2 *B. subtilis* BP115 growth with and without xylose induction

For growth in liquid media *B. subtilis* WT was grown aerobically at 37°C. A single colony was used to inoculate 10ml of LB with 1% (w/v) xylose in a sterile 25ml universal tube and grown overnight at 37°C and at 250rpm on a rotary shaker. This culture was used to inoculate fresh LB with 1% (w/v) xylose in a sterile conical flask at an OD_{600} of 0.05 as a starter culture for 2 hours. This BP115 starter culture was then divided in two, harvested and each half resuspended to an OD of 0.05 in fresh NB and incubated for a further 2 hours; one with 1% (w/v) xylose and one without.

2.10 Sporulation in *B. subtilis*

This method was adapted from Leighton and Doi (1971). For sporulation in liquid media *B. subtilis* WT was grown aerobically at 37°C. A single colony was used to inoculate 10ml of 2xSG in a sterile 25ml universal tube and grown overnight at 37°C and at 250rpm on a rotary shaker. This culture was used to inoculate fresh pre-warmed 2xSG in a sterile conical flask at an OD_{600} of 0.05 as a starter culture. This starter culture was then grown at 37°C and shaken at 250rpm to mid-exponential phase (OD_{600} 0.4-0.7). A 10ml aliquot of thisculture was taken and used to inoculate 200ml of pre-warmed 2xSG in a sterile conical flask. This sporulation culture was either a) sampled for imaging experimentation or b) left to incubate for 2 days or until complete

sporulation of the *B. subtilis* cells had occurred. Detection of complete sporulation was judged using phase contrast microscopy.

For further use in germination, spores were harvested by centrifugation at 10,000xg for 10 min at 4°C and resuspended in 25ml dH_2O. These cells were placed in a sonic bath for 30min at room temperature. The spores were harvested and twice washed by centrifugation (10,000xg for 10 min at 4°C) and resuspension in 25ml dH_20, to wash away the extraneous mother cell debris. The final spore pellets were frozen at -20°C.

2.11 Germination in *B. subtilis*

Spore pellets from previous sporulation experiments were gently defrosted on ice. The spore pellets were washed, harvested and resuspended (10,000xg for 10 min at 4°C and resuspension in 25ml dH_2O).

To initiate germination, the spores were then heat-shocked at 70°C for 60 min in a heating block. The heat-shocked spores were then harvested and resuspended in dH_2O as described previously. The heat-shocked spore resuspension was used to inoculate a 50ml NB culture containing 1mM L-alanine in a sterile conical flask. The germination culture was incubated for 3 hours at 37°C and samples were taken for microscopy every 30 min.

2.12 Preparation of purified cell walls and sacculi

2.12.1 Breakage of cell walls for imaging

When broken cell walls were required for imaging purposes, cell breakage was carried out immediately prior to boiling in 5% ((w/v)) SDS during cell wall purification (Chapter 2.14.3). Breakage of *B. subtilis* cells was achieved by passing 20-30ml cell suspensions (OD_{600} 0.4-0.7) through a French press at approximately 1000 psi.

2.12.2 Extraction of cell walls for AFM

An exponential phase culture (OD_{600} ~0.4) was harvested by centrifugation (5000xg for 10 min at room temperature) and supernatant discarded. The pellet was immediately resuspended in ~20ml boiling dH_2O and boiled in a water bath for 10 min to kill the cells and inactivate autolysins. Cells were resuspended in 10ml pre-heated (55°C) 5% ((w/v)) SDS and boiled for 25 min for release of non-covalently bound cell wall components. Cells suspension were transferred as 1ml aliquots to 1.5ml microfuge tubes and harvested by centrifugation at 14,000xg for 10 min at room temperature, then resuspended in pre-heated (55°C) 4% ((w/v)) SDS and boiled for 15 min. Material was then washed six times by centrifugation and resuspension (as above) in dH_2O (60°C) to remove SDS. For hydrolysis of covalently bound proteins, pellets were resuspended in 1ml 50 mM Tris-HCl (pH 7.5) containing 2 mg ml^{-1} pronase and incubated at 60°C for 90 min. The resulting walls were harvested by centrifugation and washed once with water.

2.12.3 Chemical purification of sacculi

Following chemical extraction of cell walls, removal of accessory polymers was achieved by incubation in 250 µl of 48% (v/v) hydrofluoric acid (HF) at 4°C for 48 h. Purified PG sacculi were recovered by centrifugation and washed at least six times with LC-MS CHROMASOLV® grade water (Fluka) at room temperature, until the pH reached at least 5.0. Purified sacculi were stored as pellets at -20°C.

2.12.4 Preparation of cell walls and sacculi for AFM imaging

Purified cell walls were thawed and washed by centrifugation (13,000rpm for 5 min) and resuspension at least six times with LC-MS CHROMASOLV® grade water (Fluka) at room temperature. Sacculi were prepared at their original working concentration for imaging of the cell walls and sonicated gently with a Sanyo Soniprep 150 for 10-20 s to disperse cell wall aggregates. Around 5µl was transferred to a freshly cleaved mica sheet - cleaved using Scotch Magic tape (3M) to peel a new mica layer - attached to a magnetic stub, and dried gently under nitrogen gas.

2.13 Microscopy

2.13.1 Fixing of cells for microscopy

Cell pellets were resuspended in fixative (Chapter 2.3.9) for 30 min at room temperature. Fixed cells were washed at least twice in sterile dH_2O by centrifugation at 13,000 rpm for 2 min at room temperature.

2.13.2 Labelling of cell membranes with FM1-43

A 1ml aliquot of cell culture was transferred to a microcentrifuge tube and FM 1-43 (Invitrogen) was added to make a final concentration of 5µg ml^{-1}. The tube was incubated for 5 min at the appropriate growth temperature on a rotary mixer. Aliquots were washed twice with sterile dH_2O by centrifugation (13,000 rpm for 1 min).

2.13.3 Fluorescent vancomycin labelling of nascent cell wall synthesis.

A 1ml aliquot of cell culture was transferred to a microcentrifuge tube and vancomycin-BODIPY (Invitrogen) was added to make a final concentration of 1µg ml^{-1}. The tube was incubated for 5 min at the appropriate growth temperature on a rotary mixer. Aliquots were washed twice with sterile dH_2O by centrifugation (13,000 rpm for 1 min).

2.13.4 Labelling of cell walls with Fluorescent D-Amino Acids

A 1ml aliquot of cell culture was transferred to a microcentrifuge tube and FDAA was added to make a final concentration of 500µM The tube was incubated for 5 min at 37°C. This was washed once with 1ml PBS at room temperature (4min, 13,400rpm).

2.13.4.1 Pulse-chase using FDAAs in *B. subtilis* WT

A 1ml aliquot of cell culture was transferred to a microcentrifuge tube and FDAA was added to make a final concentration of 500µM The tube was

incubated for 5 min at 37°C. This was washed once with 1ml PBS at room temperature (4min, 13,400rpm).

The HADA-labelled cell pellet was then resuspended in 1ml fresh pre-warmed NB in a sterile 25ml universal tube and incubated at 37°C for 30 min with agitation (250 rpm). This was washed once with 1ml PBS at room temperature (4min, 13,400rpm) and resuspended in PBS containing 500mM NADA (a green FDAA). This was incubated for 5 min at 37°C. The double-labelled cells were then washed and resuspended with 1ml PBS at room temperature (4min, 13,400rpm).

2.13.4.2 Pulse-chase using FDAAs in *B. subtilis* BP115

This technique was also adapted for use with *B. subtilis* BP115, utilising induction then starvation of xylose upon the cells to control *lytE* and *yvcE* expression. An initial 10ml starter culture of LB including 1% (w/v) xylose was grown to mid-exponential phase. The entire 10ml starter culture was labelled with NADA at 50μM and incubated for 5 min at 37°C. The NADA-labelled culture was halved and harvested (5500xg, 10 min). Each pellet was resuspended in 5ml fresh, pre-warmed LB, one with 1% (w/v) xylose, one without, both in sterile universals. The two cultures were incubated at 37°C for 90 min with agitation (250 rpm). Both cultures were washed once with PBS at room temperature (4min, 13,400rpm) and resuspended in PBS containing 50μM HADA. Both were incubated for 5 min at 37°C. The two sets of double-labelled cells were then washed and resuspended with PBS at room temperature (4min, 13,400rpm).

2.13.4.3 Click-iT® reaction

A A 1ml aliquot of cell culture was transferred to a microcentrifuge tube and Azido-D-Alanine(AZA*) in DMSO was added to make a final concentration of 500µM The tube was incubated for 5 min at 37°C. then fixed as described previously (Chapter 2.14.1). The Click-iT® reaction was then carried out according to the instructions provided by Invitrogen to attach the fluorophore. This entailed the incubation of fixed cells with 0.5ml Click-iT® reaction cocktail for 30min at room temperature. The Click-iT® reaction cocktail contains 1x Click-iT® reaction buffer, Click-iT® cell buffer additive, Copper(II) sulphate($CuSO_4$) at 2mM and the alkyne modified fluorophore at 1-5µM.

2.13.5 Fixed cell slide preparation for light microscopy

Glass slides were washed once with dH_2O followed by 70 % (v/v) ethanol. Slides were air-dried, then 10 µl of 0.01 % ((w/v)) poly-L-lysine (Sigma) applied to aid attachment of the sample to the slide surface, and set on a flat surface to air-dry. An appropriate sample dilution was prepared in dH_2O, and 5 µl spread gently onto the poly-L-lysine coated slide and left to air-dry. A coverslip was then mounted with 5 µl SlowFade Gold antifade reagent (Molecular Probes), and sealed by spotting DPX mountant (BDH) at each corner.

2.13.6 Live-cell slide preparation for light microscopy

Glass slides were washed once with dH_2O followed by 70 % (v/v) ethanol. Slides were air-dried, then 50 µl of 0.5 % ((w/v)) molten agarose (Sigma)

applied gently to the glass to form a disc, and set on a flat surface in a fumehood to set. N.B. Usually, PBS was used as the agarose buffer but SMMP was used for protoplast generation and regeneration imaging.

An appropriate sample dilution was prepared in dH_2O, and 5 µl spread gently onto the poly-L-lysine coated slide and left to air-dry. A coverslip was then mounted with 5 µl SlowFade Gold antifade reagent (Molecular Probes), and sealed by spotting DPX mountant (BDH) at each corner.

2.13.7 Preparation of slides for STORM

Prior to the sample being dried onto the slide a layer of gold nanoparticles was first applied as fiducial marks for drift correction. 5µl of 103nm gold nanoparticles (Nanopartz) were added to 95µl HPLC-grade water, 5µl of this suspension was sppled to each poly-L-Lysine slide in a stream of nitrogen gas. An appropriate dilution of fixed cells (typically OD_{600} 0.4-0.7 for *B. subtilis*) was applied to the slide and dried down with nitrogen.

2.13.8 Fluorescence microscopy.

Fluorescence microscopy was carried out using a DeltaVision deconvolution microscope (Applied precision) equipped with appropriate filters for imaging of each fluorophore (**Table 2.5**). Objective lens used was 100x (with immersion oil). Images were deconvolved using SoftWoRx suite v.3.5.1. Deconvolved fluorescence images were processed, and cell measurements carried out, using ImageJ (version 1.47v)

Table 2.5 DeltaVision microscope filter sets.

Filter	*Compatible fluorophore*	*Excitation filter/bandpass (nm)*	*Emission filter/bandpass (nm)*
DAPI	Hydroxycoumerin	360/40	457/50
FITC/YFP	BODIPY-FL, nitrobenzofurazan AlexaFluor-532	490/20	528/38
RD-TR-PE	FM1-43	555/28	617/73
mRFP	Trimethylrhodamine	580/20	630/60

2.13.9 Imaging of purified cell walls by AFM

Sacculi were imaged using a Multimode AFM with and Extended Nanoscope IIIa controller (Veeco Instruments). Imaging was carried out in tapping mode using silicon tips (Olympus) under ambient conditions in air. Post-processing of images was performed using Gwyddion v2.26 software.

2.13.10 Electron microscopy

Cells were grown to exponential phase (final OD_{600} ~ 0.5), washed by centrifugation with dH_2O and fixed with 3% (v/v) glutaraldehyde in 0.1 M sodium cacodylate buffer pH 7.4 overnight at 4°C.

Fixed cells were then prepared for electron microscopy (EM) by Chris Hill at the Electron Microscopy Unit, University of Sheffield, using the method as follows. Fixed cells were washed twice in 0.1 M sodium cacodylate buffer pH 7.4 and post-fixed in 2% ((w/v)) aqueous osmium tetroxide for 2 h at room temperature. Cells were washed once with cacodylate buffer by centrifugation then dehydrated by stepwise incubation at room temperature in 75% (v/v) ethanol (15 min), 95% (v/v) ethanol (15 min), absolute ethanol (2 × 15 min) and dried absolute ethanol (2 × 15 min).

For transmission electron microscopy (TEM) the specimens were equilibrated in propylene oxide (2 × 10 min), and infiltration accomplished using a 1:1 mixture of propylene oxide:araldite resin overnight at room temperature. Pellets were incubated in fresh 100% (v/v) araldite (6-8 h), then embedded in 100% ((w/v)) araldite and polymerised at 60°C for 48 h. 80nm sections were cut using a Reicher Ultracut E ultramicrotome and labelled with a saturated solution of uranyl acetate in 50% (v/v) ethanol for 25 min. Sections were washed in dH_2O and labelled in Reynold's lead citrate (Reynolds, 1963) for 25 min. Sections were viewed using a FEI Tecnai transmission electron microscope operating at 80 kV.

2.13.11 Stochastic Optical Resolution Microscopy (STORM)

To examine samples using STORM, the following protocol was used as described by Turner et al. (2013). A 100mW, 532-nm diode laser (Laser 2000) was focussed onto the back plane of a 60 × numerical aperture 1.4 oil immersion objective mounted in an Olympus IX71 inverted optical microscope. A filter cube containing a 552-nm longpass dichroic filter

(Semrock FF552-DI02) and a 565(24)-nm bandpass emission filter (Semrock Brightline 565/24) was inserted for STORM. A piezoelectric motor (Physik Instrumente) was used to alter focus. An image expander comprising a 35-mm and a 100-mm lens was used to direct the image onto a Hamamatsu ImagEM camera set to acquire at 50 frames $second^{-1}$. A 1m focal length cylindrical lens was inserted between the image expander lenses to compensate for drift perpendicular to the focal plane.

Focus was preserved by repeatedly localising a fiducial particle and adjusting the lens position using the piezo. Laser power was varied using pulse-width modulation to maximize signal without saturating the charge-coupled device. The camera and piezo were controlled using Labview (version 10).

Image processing was conducted using STORM methodology as previously described by others (Betzig et al., 2006; Huang et al., 2008). Data were processed by fitting Gaussian functions to individual molecule fluorescence, identified by very clear intrinsic blinks, using Matlab and ImageJ (version 1.46c).

Chapter 3

Cell wall regeneration in *B. subtilis*

3.1. Introduction

In this chapter, a novel approach was used in the study of *de novo* PG synthesis in *B. subtilis*; the utilisation of bacterial protoplast cell wall regeneration.

3.1.1 General properties of protoplasts

Gram-positive protoplasts (also known as spheroplasts) are bacterial cells, which have had the PG component of their cell walls removed enzymatically. The pre-existing lipid bi-layer cytoplasmic membrane then contains the remaining cellular contents (Heijenoort, 2001). Upon removal of the PG, the cells exhibit a morphological change from their original cell shape to spherical (Elliott et al., 1975b); a sphere being the most physically stable structure the lipid bi-layer can form without the rigidity and support of PG.

Bacterial cell walls are essential for the maintenance of cell viability, providing protection against external turgor and osmotic pressure. As a consequence, protoplasts are extremely susceptible to lysis caused by osmotic, mechanical or temperature-based changes to their extracellular environment. Thus, it is essential to maintain viable protoplasts in osmotically stable media (Chang and Cohen, 1979). Furthermore, protoplasts

must be manipulated gently during experimentation to reduce any unnecessary mechanical stress.

3.1.2 Protoplasts and L-form bacteria

3.1.2.1 Bacterial L-forms

L-form strains are wall-deficient derivatives of common bacteria that are able to proliferate without the need for a cell wall (Allan et al., 2009). Like bacterial protoplasts, they exist without their PG layer, surviving with only a single lipid bi-layer membrane as their protection against their external environment (Allan et al., 2009).

Many bacteria are able to switch to the L-form state (Mercier et al., 2013). In *B. subtilis*, a model system of L-form proliferation was developed using a strain that can quickly and quantitatively convert from the walled to the L-form state (Domínguez-Cuevas et al., 2012). Propagation of these *B. subtilis* L-forms is independent of FtsZ-ring constriction mechanism and is undertaken instead by a range of rather poorly regulated shape perturbations, including blebbing, tabulation, and vesiculation (Domínguez-Cuevas et al., 2012; Leaver et al., 2009; Mercier et al., 2013). Studies suggest that the mode of L-form proliferation in *B. subtilis* is based purely on a biophysical process based on the fluidity of the cells' lipid bilayer membrane (Mercier et al., 2013, 2012).

To create bacterial L-forms, inhibiting cell wall synthesis with appropriate antibiotics or degrading the wall with lysozyme or similar hydrolytic enzymes initiates the process. The cells initially need to be maintained on osmotically supportive medium to prevent lysis of the membrane bound

protoplast. Prolonged incubation under selective conditions is usually required before 'stable' wall deficient variants emerge. These can be maintained indefinitely without reverting to the walled state, suggesting that one or more genetic changes are needed (Domínguez-Cuevas et al., 2012). In *B. subtilis*, a single point mutation in the *ispA* gene that predisposes cells to grow without a wall was identified (Leaver et al., 2009).

3.1.2.2 Differences between *B. subtilis* protoplasts and L-forms

The main difference between *B. subtilis* protoplasts and L-forms is in the origin of their wall-less state. The lack of cell wall found in L-form bacteria comes from a genetic mutation over time rather than manual enzymatic removal, as with protoplasts (Allan et al., 2009; Leaver et al., 2009).

Protoplasts are unable to proliferate by cell division of their own accord. In contrast bacterial L-forms are able to do so (Domínguez-Cuevas et al., 2012; Leaver et al., 2009). *B. subtilis* L-forms can be maintained indefinitely without reversion (Domínguez-Cuevas et al., 2012). It is important to note that little is known about the molecular basis for L-form generation, nor of the specific changes that are needed to generate L-forms and then stabilize them (Domínguez-Cuevas et al., 2012). In contrast, *B. subtilis* protoplasts do not survive long after their enzymatic creation. However, unlike L-forms, the cell walls of *B. subtilis* protoplasts can be regenerated using certain experimental conditions (Elliott et al., 1975a).

3.1.3 Previous experimental uses of protoplasts.

3.1.3.1 Protoplasts as competent cells

In previously published experimental approaches, protoplasts were created and utilised as competent cells for genetic transformation, exploiting their ability to take up foreign DNA and then survive after regenerating their cell wall material. In previous years, bacterial protoplasts were the only viable method of creating chemically competent cells and their use in genetic transformation experiments is well documented in model organisms such as *B. subtilis* (Akamatsu and Taguchi, 2012, 2001; Chang and Cohen, 1979; Elliott et al., 1975a, 1975b; Gabor and Hotchkiss, 1979; Hopwood, 1981).

3.1.3.2 Use of protoplasts in cytoplasmic membrane analysis

More recently, protoplasts have been used to study cytoplasmic membrane components. Protoplasts were used to determine the qualities of the *B. subtilis* periplasm (Merchante et al., 1995). This study showed that the operationally defined periplasm corresponded closely, both quantitatively and qualitatively, to the contents of the periplasm of *E. coli* (Merchante et al., 1995). In addition, another study showed that in protoplasted *B. subtilis* cells, some structures were not preserved in the cell membrane after the loss of the external PG; thus indicating a link between lipid domain formation and PG synthesis (Muchová et al., 2011).

Other studies have utilised protoplasts in the patch-clamp technique to study ion channel activity in *B. subtilis* cell membranes (Nakamura et al., 2011; Szabo et al., 2002). These studies elucidated further details about aerobic

respiration (Nakamura et al., 2011) and transmembrane translocation of the *B. subtilis* genetic material (Szabo et al., 2002).

3.1.4 Protoplast regeneration: studying PG synthesis

Bacillus protoplasts have a unique ability to regenerate their cell walls under certain experimental conditions (Elliott et al., 1975a, 1975b). As discussed previously, this phenomenon was exploited for use in transformation experiments; as protoplasts are able to take up recombinant DNA and survive with their new genetic material after the regeneration of their cell walls.

Early observations of protoplast regeneration in *Bacillus lichenformis* by Elliott et al (1975a) showed that fibres which appeared to be sheared from the protoplasts were similar in composition to the bacillary walls. These 'fibrils' could have possibly been single glycan strands emerging during PG synthesis. This paper indicated that it was possible to utilise protoplast regeneration to examine PG synthesis *in vivo*.

Recently, protoplast regeneration was shown to be successful in the Gram-negative bacterium, *E. coli* (Ranjit and Young, 2013). This study showed that *E. coli* recovered a rod shape from spherical protoplast morphology after four to six generations. Regeneration proceeded via a series of cell divisions that produced misshapen and branched intermediates before later progeny assumed a normal rod shape.

The method of protoplast regeneration used in this study was initially derived from Chang and Cohen, (1979) with significant adaptations made in order to generate liquid samples for subsequent use in cell imaging.

3.1.5 Aims of this chapter

1. Establish the kinetics and morphological dynamics during *B. subtilis* protoplast generation and regeneration.
2. Investigate the dynamics and architecture of peptidoglycan synthesis during cell wall regeneration.
3. Develop a model for protoplast regeneration in *B. subtilis*.

3.2 Results

3.2.1 *B. subtilis* protoplast generation

B. subtilis WT cells were grown to mid-exponential phase. The *B. subtilis* vegetative cells were harvested and converted into protoplasts using lysozyme treatment. The protoplasts were maintained in osmotically stabilised media, thus avoiding their lysis. A sample of the cells was plated twice to obtain separate viable counts for both newly created protoplasts and for any unchanged vegetative cells. The protoplast suspension could then be stored for future use (if necessary). Alternatively, the protoplasts were used straight away in regeneration experiments. Samples were also used for morphological evaluation.

3.2.2 *B. subtilis* protoplast regeneration

A suspension of previously generated protoplasts in osmotically stable media was added to regeneration media (liquid DM3) to allow the protoplasts to regenerate.

The regeneration assay was incubated for 12 hours. A sample of this culture was plated twice to obtain separate viable counts for both regenerated protoplasts and for any unchanged vegetative cells. Furthermore, samples were taken for use in microscopy experiments to evaluate changes in cell morphology. A schematic overview of this process is shown in **Figure 3.1**.

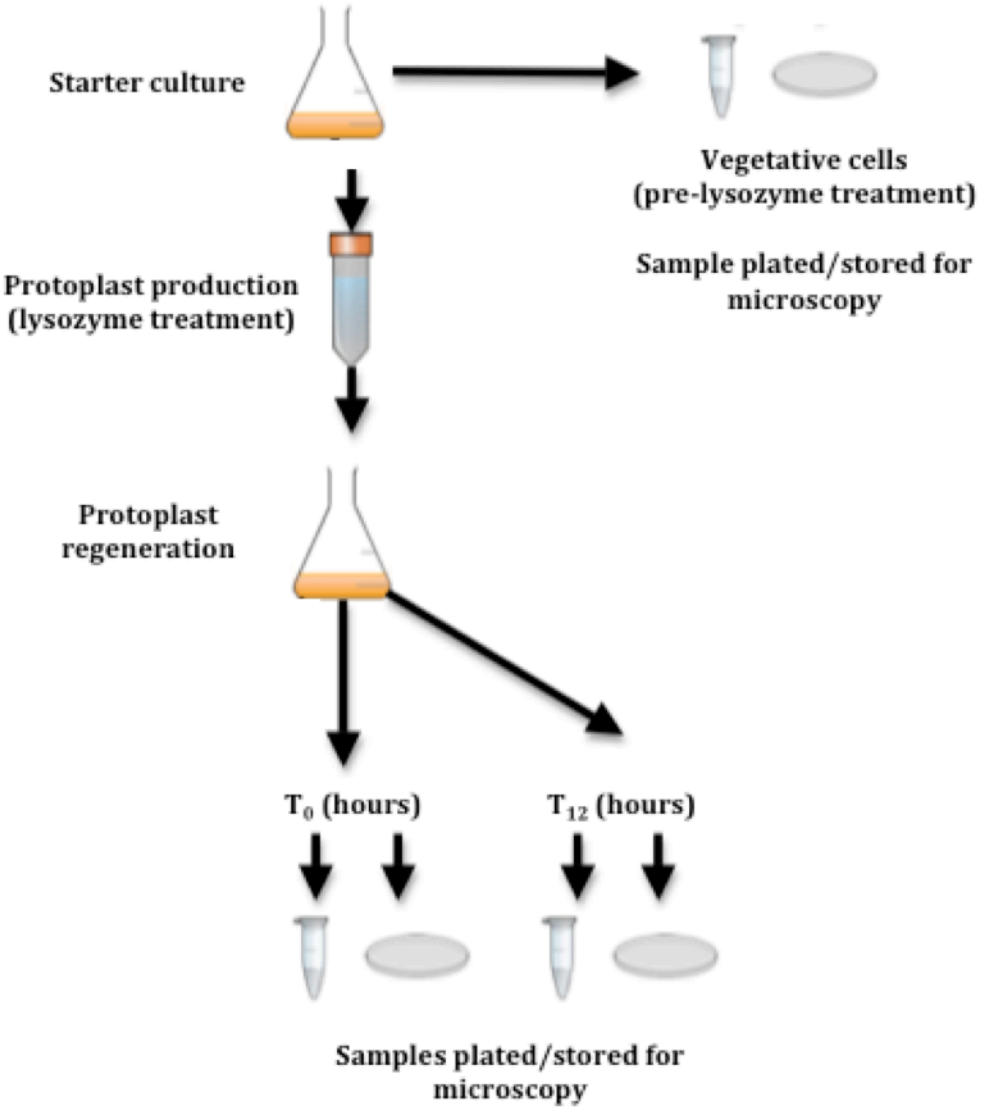

Figure 3.1. Schematic overview of protoplast generation and regeneration in *B. subtilis*.

Initially, the regeneration assay samples were taken over a period of 6 hours. However, microscopic analysis of these samples, using epifluorescence microscopy, showed no detectable morphological changes compared to the data obtained by protoplast examination, i.e. no regeneration had yet occurred.

3.2.2.1 Vegetative cell growth kinetics in regeneration media

Before quantifiably assessing protoplast regeneration, it was necessary to determine whether the remaining vegetative cells (which had not converted to protoplasts) would grow in the regeneration media (liquid DM3). This question was raised to rule out the possibility that any increase in viable count detected during the 12 hours' regeneration time was a result of vegetative cell growth, rather than because of protoplast regeneration. Therefore, *B. subtilis* vegetative cells were grown in liquid DM3 over 12 hours and the optical density measured (**Figure 3.2**).

The results of this experiment showed some growth of *B. subtilis* in protoplast regeneration media (liquid DM3) after 3 hours' incubation. However, the optical density of the culture remained stationary for the remainder of the experiment; after 4 hours' incubation in DM3, *B. subtilis* cell density decreased and then remained stationary for the remainder of the incubation indicating that some cells may have lysed and the remainder did not undergo any further growth. This suggested that while *B. subtilis* cells were able to grow for a small amount of time in liquid DM3 but this growth was not sustained over an 8-hour period, never exceeding an OD_{600} reading of 1.

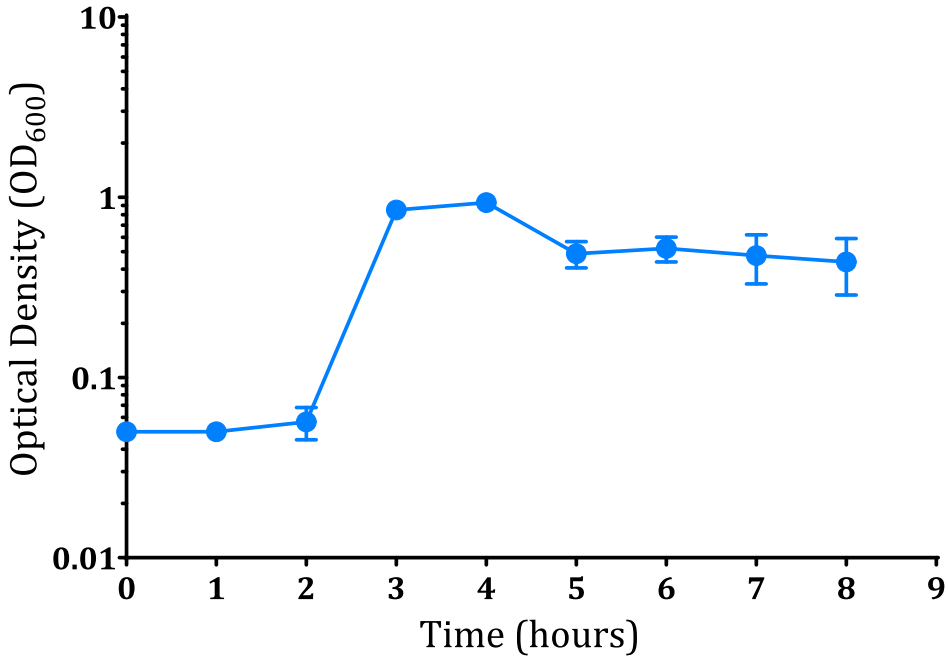

Figure 3.2. Growth kinetics of *B. subtilis* WT vegetative cells in liquid protoplast regeneration media. *B. subtilis* vegetative cells were incubated over 8 hours in liquid DM3 media and sampled every hour. The samples were tested for optical density (OD_{600}) using a spectrophotometer, the results of which are denoted by the blue plot on the graph. The error bars denote Standard Error, for three culture replicates.

Therefore, DM3 was considered to be suitable media for protoplast regeneration, without permitting extended growth of any *B. subtilis* vegetative cells (which had not converted to protoplasts during protoplast generation) during protoplast regeneration.

3.2.3 Quantification of vegetative cells, protoplasts, and regenerating cells.

In order to understand the kinetics of changes to cell morphology during the regeneration assay, it was necessary to quantify the number of vegetative cells, protoplasts and regenerating cells. During (and preceding) the 12-hour regeneration assay, liquid samples were taken at three set time points over the course of the experiment and plated to obtain viable counts. These three key time-points were as follows; vegetative cells (pre-lysozyme treatment), protoplasts (post-lysozyme treatment) and regenerating cells (after 12 hours regeneration, see **Chapter 3.2.2**).

3.2.3.1 Regeneration assay viable counts

The samples were serially diluted using SMMP and plated onto DM3 regeneration agar and NA; one to test for protoplast regeneration and one to act as a negative control respectively. The regeneration test (DM3 agar) measures the total viable cells available as protoplasts/regenerating protoplasts were able to form a colony on this media, as the osmotically stable dilution media protected protoplasts. In contrast, the purpose of the negative control plates was to test the number of viable bacteria remaining in the culture that had not converted to protoplasts during the lysozyme treatment. Therefore, the negative control samples were serially diluted

using 1xPBS, in order to cause osmotic lysis of any protoplasts, thus leaving only vegetative cells remaining. The negative control sample dilutions were plated onto NA. This therefore provided a baseline vegetative cell viable count from which to compare protoplast generation and regeneration. Thus, two separate viable counts were generated per sample.

An example of the results obtained from the protoplast regeneration assay using *B. subtilis* is shown in **Figure 3.3.** Each protoplast regeneration experiment was considered to be an independent event, as each experiment started with a different viable count. Therefore the viable counts from each experiment were qualitatively compared, rather than analysed quantatively. Therefore, no error bars were generated.

The initial viable counts taken pre-lysozyme treatment are of comparable value; approximately $1x10^7$ cfu ml^{-1} for both types of media. The lack of difference between the two counts indicated that each media was measuring the same type of cell, i.e. vegetative cells that had not yet been converted into protoplasts. The immediate 4-log viable count decrease on the NA plot following lysozyme incubation (T_0) indicates that the action of lysozyme was successful in stripping the cells of their walls and thus creating protoplasts. To complement this, the T_0 viable count on DM3 media stayed close to the original pre-lysozyme viable count, indicating the potential of the newly created protoplasts to regenerate under the right conditions. After 12

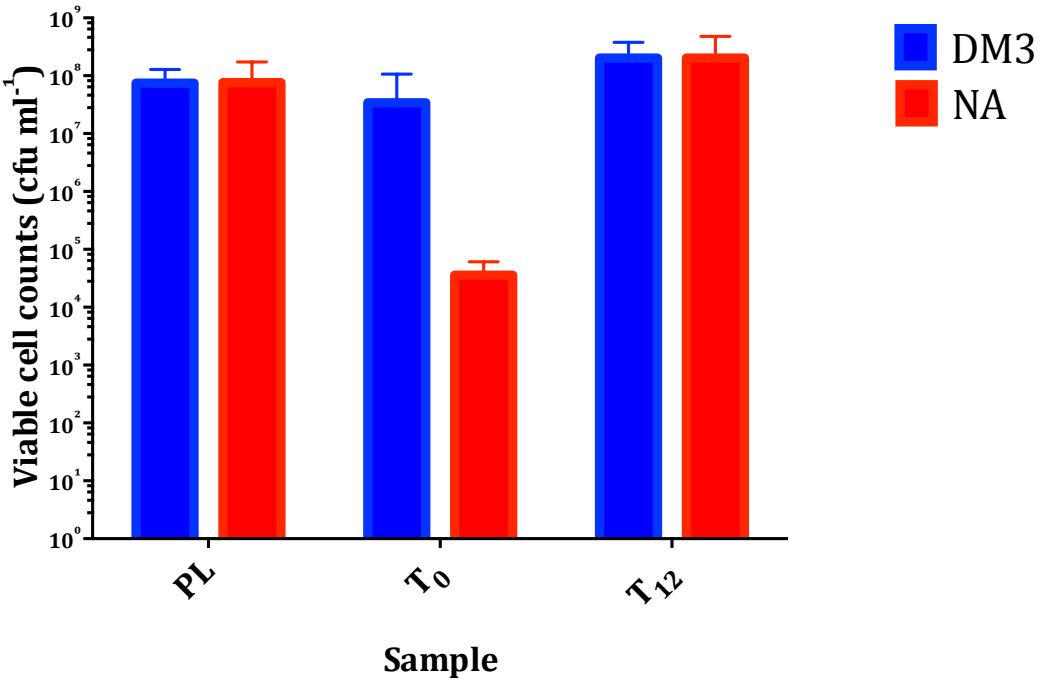

Figure 3.3. Protoplasting and Regeneration Efficiency in *B. subtilis*. Graph showing typical viable counts obtained during a *B. subtilis* protoplast regeneration assay. 'PL' refers to the sample taken pre-lysozyme treatment i.e. vegetative cells. T_0 refers to the sample taken immediately post-lysoyzme treatment i.e. newly made protoplasts. T_{12} refers to the sample taken after 12 hours' incubation in liquid DM3 i.e. regenerating protoplasts. The blue plot denotes the viable counts obtained after dilution in SMMP and plating onto DM3 agar i.e. all viable cells. The red plot denotes viable counts obtained after dilution in 1xPBS and plating onto NA i.e. vegetative cells only. Error bars show Standard Error for 5 experimental replicates.

hours incubation, the viable count on NA increased to match the DM3 viable count (both were approximately $5x10^7$ cfu ml^{-1}). This meant that the number of cells able to form a colony on NA (without the need for osmotically stable dilution) had increased. Vegetative cells do not grow properly in liquid DM3 media (**Chapter 3.2.2.1**). Therefore; this meant that the increase in viable count was a result of protoplast generation. Therefore, the cell walls of the protoplasts were reformed over 12 hours in regeneration media.

3.2.3.2 Calculation of protoplast production efficiency

The viable counts generated by the *B. subtilis* protoplast regeneration assays were used to calculate the average protoplast production efficiency for the experiment repetitions. The protoplast production efficiency was calculated as follows; the number of vegetative cells in the sample taken immediately following protoplast creation was subtracted from the total number of cells in the sample taken immediately following protoplast creation, this value was then divided by the total number of cells measured pre-lysozyme treatment. Protoplast production efficiency ranged between 0.5% and 100% over the course of the assay repetitions.

This showed a large amount of variability in protoplast production efficiencies between experiments. However, the purpose of this study was to visually assess protoplast cell wall regeneration. Nevertheless, calculation of the protoplast production efficiency was useful in itself to merely confirm the presence of protoplasts and therefore confirm their potential to regenerate.

3.2.4 Microscopic analysis of cell morphology during *B. subtilis* protoplast regeneration

The establishment of the kinetics involved in protoplast generation and regeneration set the framework for morphological analysis of these phenomena. Samples generated from the protoplast generation and regeneration assays were subjected to microscopic imaging evaluation in order to evaluate cell morphology at different experimental stages.

3.2.4.1 *B. subtilis* vegetative cell morphology

TEM analysis of *B. subtilis* vegetative cells sampled pre-lysozyme treatment revealed the characteristic rod shape associated with the bacteria (**Figure 3.4**). In the high magnification examples shown in Panel B (**Figure 3.4**), the organism's cylindrical rod-shaped morphology can be clearly observed. It must be noted that any round-shaped objects observed in this sample were cross sections of rod-shaped cells that had been sectioned across their short axes during TEM processing. Characteristically, the organism pictured exhibited a cell length of ~2μm and measured ~0.5μm across its short axis. These measurements were similar to other cells shown in the total field image (Panel A, **Figure 3.4**). Closer inspection of the images in Panel B (**Figure 3.4**) showed both the lateral dividing septum and distinct gram-positive cell wall associated with the species.

Examination of the vegetative cell sample by epifluorescence microscopy also revealed the classic rod-shape of *B. subtilis* wild-type cells (**Figure 3.5**). The vegetative cell sample was stained with FM1-43 and fluorescent Vancomycin before examination. FM1-43 binds phospholipids and was therefore used as a

A

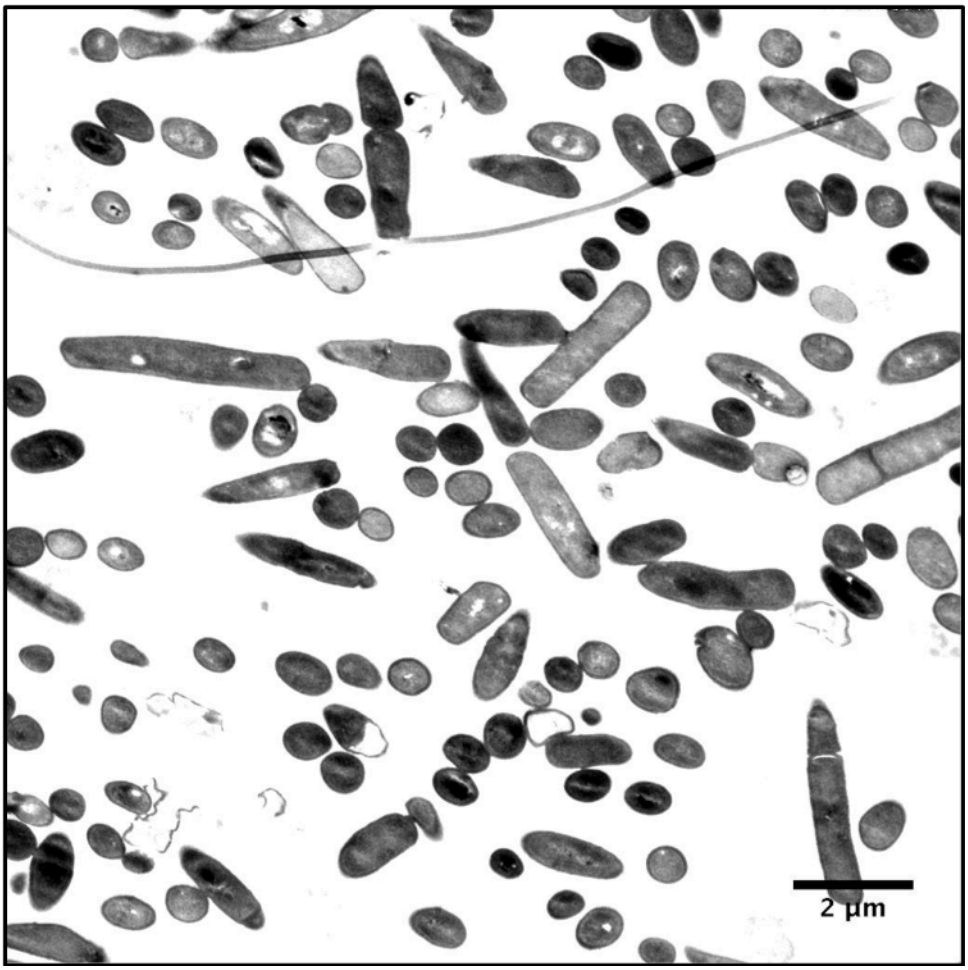

B

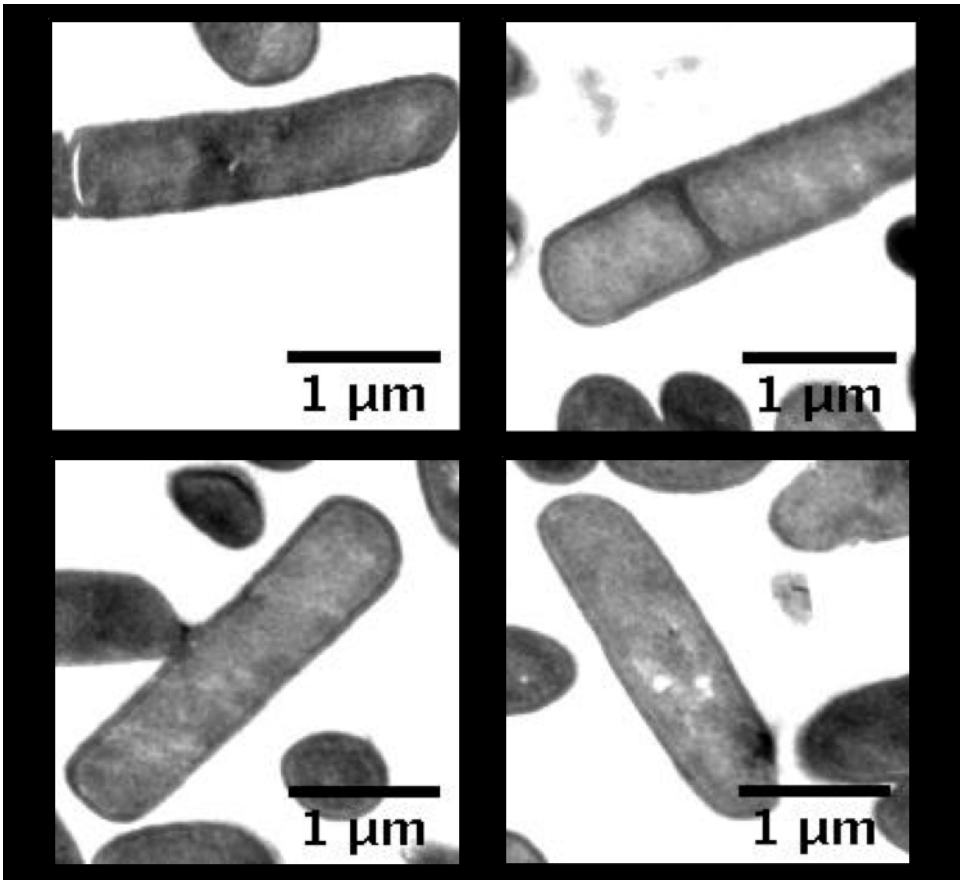

C

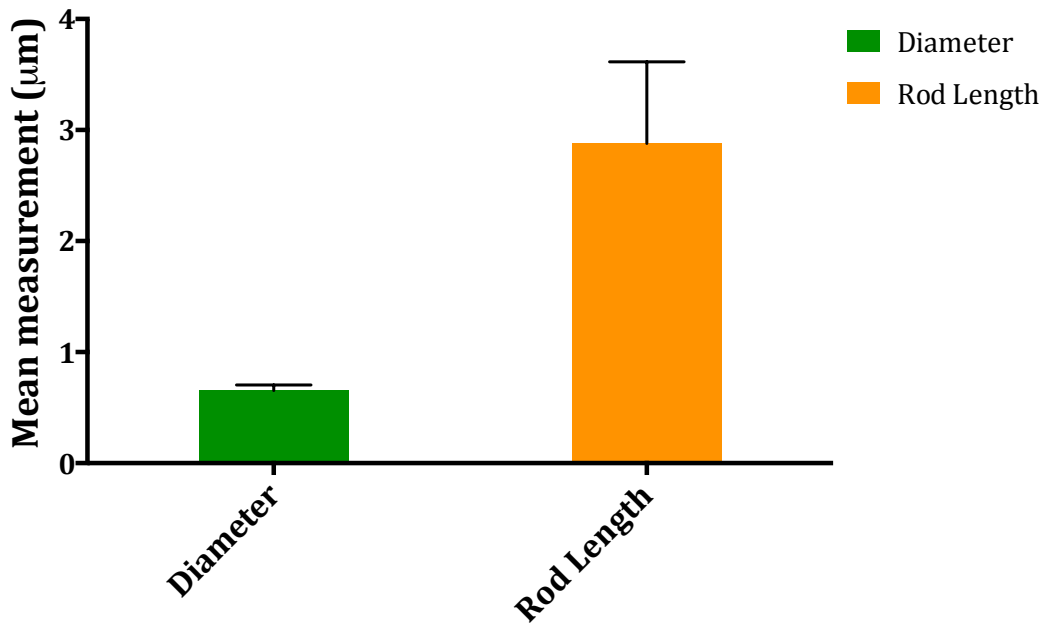

Figure 3.4. Transmission electron microscopy images generated from a *B. subtilis* protoplast regeneration assay sample taken of vegetative cells (pre-lysozyme). Panel A shows a full field and Panel B shows high magnification images of single vegetative *B. subtilis* cells. Panel C shows a histogram giving the mean and standard deviation of *B. subtilis* rod length and diameter.

DIC

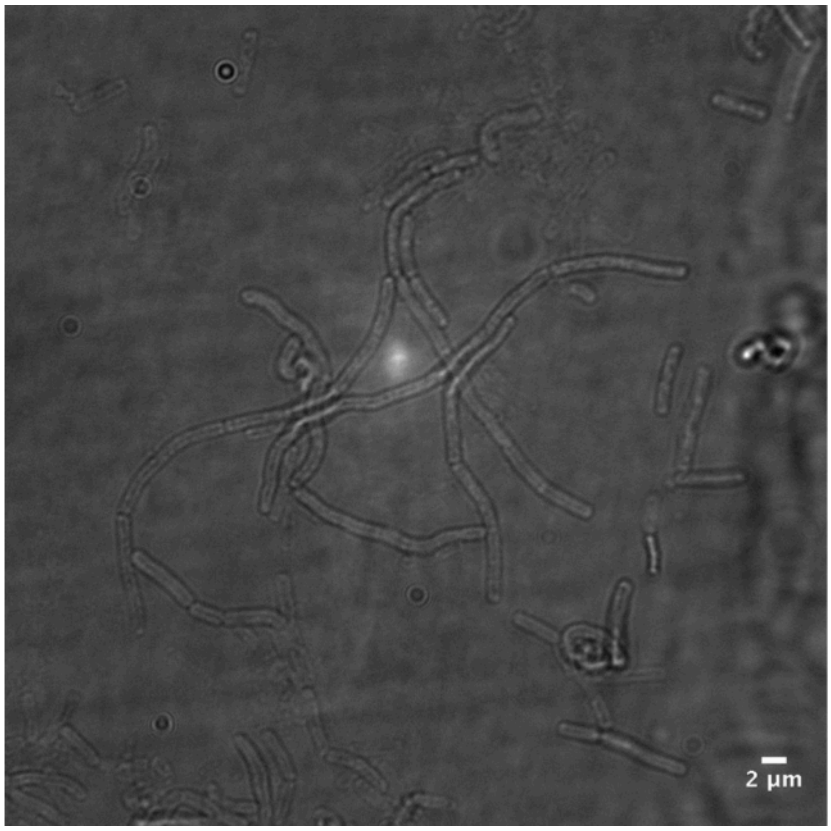

FM1-43

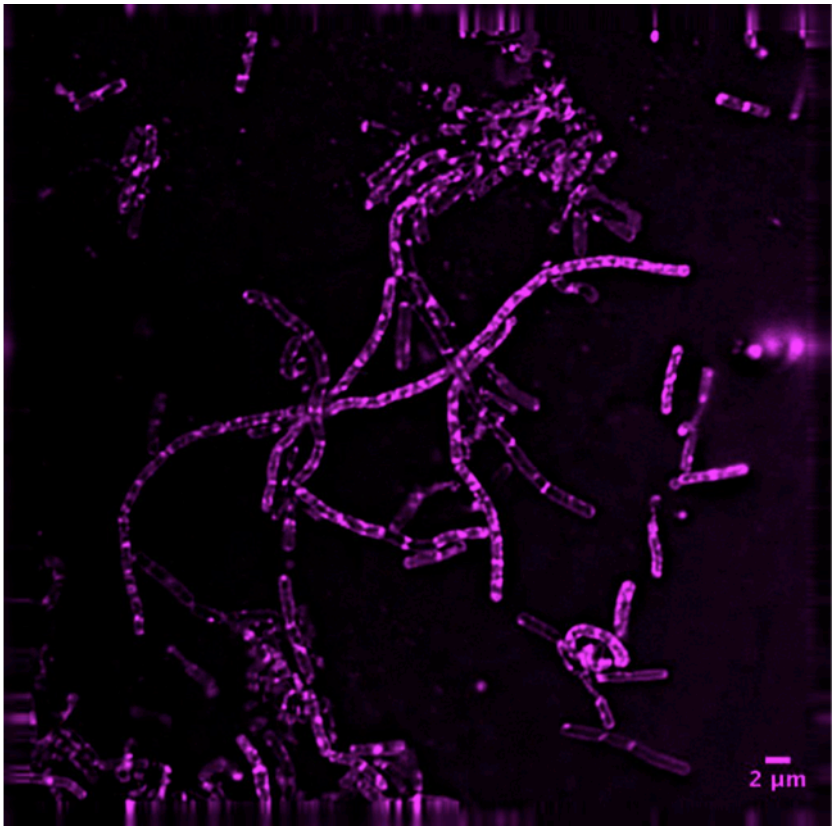

Vanc

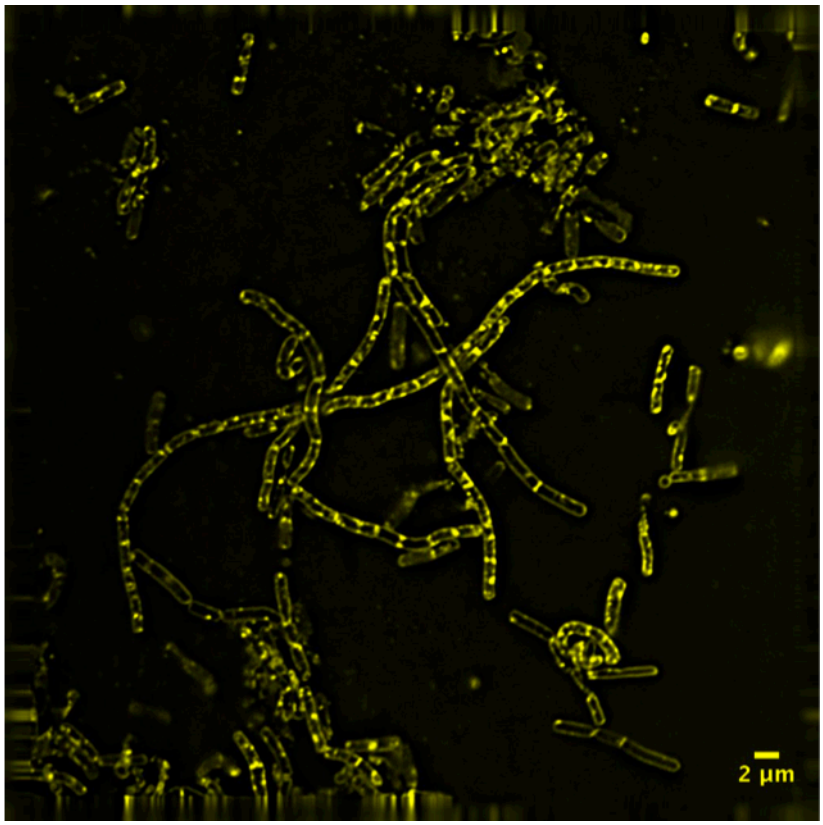

Merge

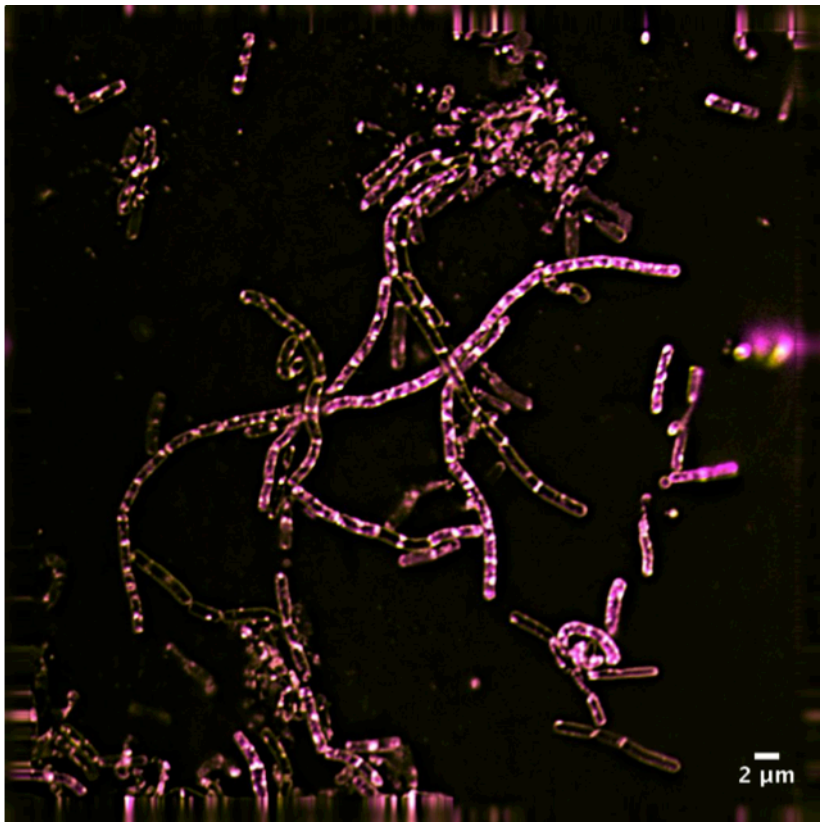

Figure 3.5. *B. subtilis* vegetative cells: sampled prior to protoplast generation and regeneration and examined by epifluorescence microscopy. Each image shows an entire microscopic field of cells. Cell walls are stained pink with Vancomycin BODIPY-FL (Vanc), which binds D-Alanine residues in the PG. Cell membranes are stained yellow with FM1-43, which binds phospholipids in the lipid bi-layer.

cell membrane dye. Fluorescent Vancomycin binds to D-Ala D-Ala residues in the peptide side chain of PG, and was therefore used as a dye for nascent PG. Both dyes bound the vegetative cells throughout the outer cell envelope in a heterogeneous pattern, highlighting the *B. subtilis* rod-shaped morphology, as shown in the high magnification images of the vegetative cells (**Figure 3.6**). Cell features can also be seen in these images; these include cell septa and poles. Some foci of dye 'blobs' can be observed which are not attributed to poles or septa i.e. the dyes have bound more strongly to some areas of the cell cylinders than others. This could have been indicative of varying wall thickness throughout the cell. Furthermore, the cells exhibited different levels of fluorescence and therefore staining between each other. This was possibly due to varying amounts of wall material between individual cells or whether the cell staining technique produces variable results.

The use of both these dyes in combination provided a negative control for examination of subsequent samples. Any instance where only cell membrane could be detected instead of nascent PG (rather than both architectures) therefore may have indicated the absence of complete cell wall in protoplasts or regenerating protoplasts.

In conclusion, the *B. subtilis* vegetative cell morphology results provided a solid basis of comparison for further imaging analysis of subsequent protoplast generation and regeneration samples.

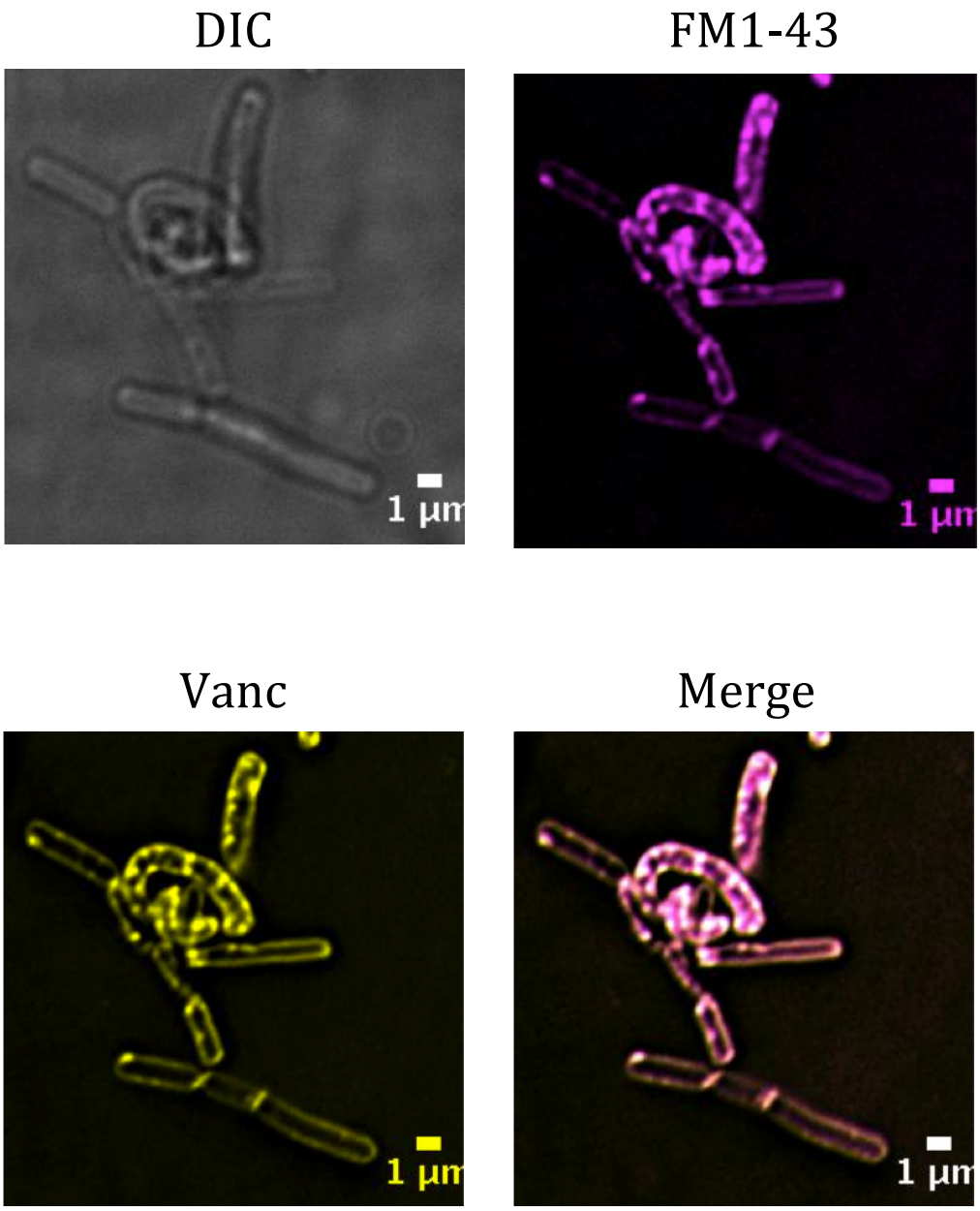

Figure 3.6. High magnification of *B. subtilis* vegetative cells: sampled prior to protoplast generation and regeneration and examined by epifluorescence microscopy. Each image field shows a few vegetative cells. Cell walls are stained pink with Vancomycin BODIPY-FL (Vanc), which binds D-Alanine residues in the PG. Cell membranes are stained yellow with FM1-43, which binds phospholipids in the lipid bi-layer. Cells were not fixed prior to imaging.

3.2.4.2 *B. subtilis* protoplast morphology

Following examination of the sample taken of *B. subtilis* cells immediately after lysozyme treatment, a clear change in morphology was observed compared to images taken of vegetative cells. Transmission electron microscopy and epifluorescence microscopy revealed that the previously rod-shaped vegetative cells had converted to spherical protoplasts, as predicted.

Firstly the protoplasts were studied using TEM, which revealed protoplasts exhibited a uniformly spherical morphology (**Figure 3.7**). The full field image generated (Panel A) showed many spherical protoplasts, all measuring roughly 1μm in diameter, and most being intact i.e. retaining their cytoplasmic content. Some cells were broken and therefore showed the loss of their cytoplasmic content. This was likely due to a combination of the fixative procedure involved in TEM sample processing and the fragile nature of the protoplasts themselves. The high magnification images of single *B. subtilis* protoplasts (Panel B, **Figure 3.7**) showed single intact protoplasts containing cytoplasmic material, measuring 1μm in diameter. These images also provided greater detail with regard to the outermost layer of an intact protoplast. When compared to a TEM image of a vegetative cell wall (**Figure 3.4, Panel A**) it became obvious that the outermost layer of a protoplast was much thinner, thus allowing direct observation of cell wall removal using lysozyme. In addition, this image provided physical evidence that the cell wall (and therefore PG) was reduced in volume by lysozyme in the formation of protoplasts. Finally, the observation of PG reduction and subsequent

A

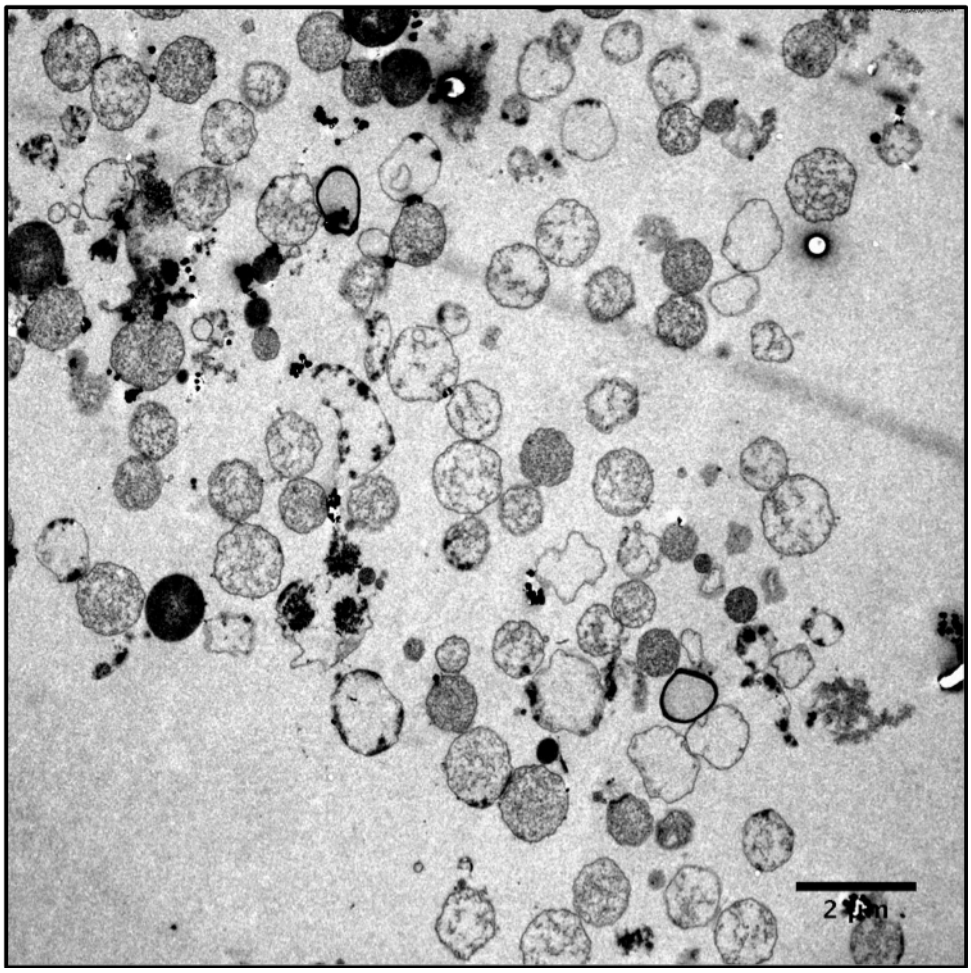

B

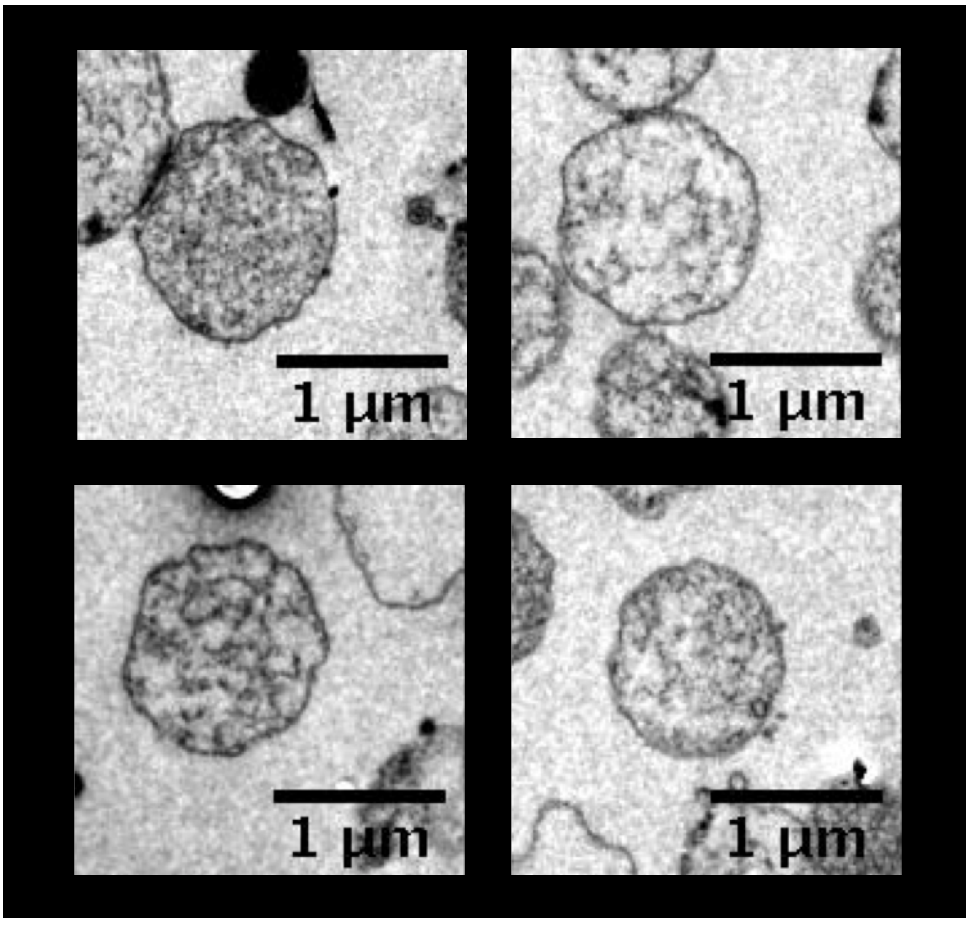

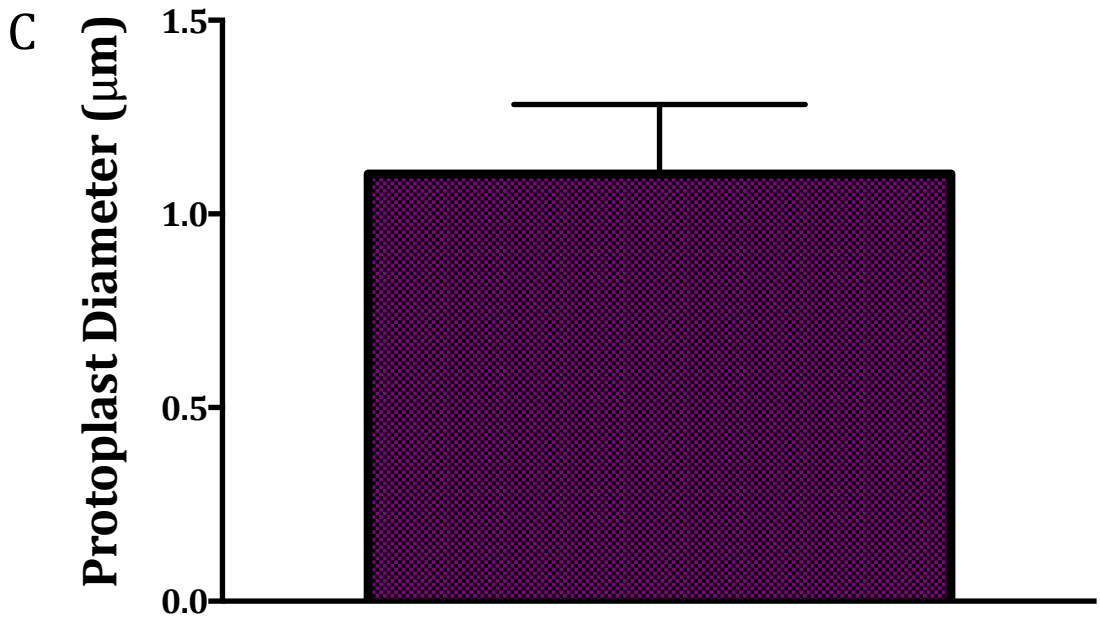

Figure 3.7. *B. subtilis* protoplasts: sampled immediately post-lysozyme treatment and examined by transmission electron microscopy. Panel A shows a full field and Panel B shows high magnification images of single *B. subtilis* protoplasts. Panel C shows a histogram giving the mean and standard deviation of *B. subtilis* protoplast diameter.

change from vegetative rod-shape to spherical protoplast further cemented the common understanding that PG contributes to and maintains cell shape.

A *B. subtilis* protoplast sample taken immediately after lysozyme treatment was then subjected to examination using epifluorescence microscopy. The protoplasts were stained with FM1-43 and fluorescent vancomycin, which bound to cell membrane and PG respectively. The full field of cells showed that rod-shaped vegetative cells had converted to spherically shaped protoplasts, as predicted (**Figure 3.8**). Closer inspection of the protoplasts at higher magnification revealed further details (**Figure 3.9**). Interestingly, while the FM1-43 bound to the membrane as expected, the images showed that vancomycin had also bound to the outermost layer of the protoplasts. This suggested that the action of the lysozyme did not remove the entirety of the cell wall PG. As previously stated, fluorescent vancomycin (Vancomycin BODIPY-FL) binds and stains D-Ala D-Ala residues in the peptide side chain of PG. As a consequence, it appeared that a very thin layer of fragments of PG was retained by the protoplasts. It must be noted that vancomycin can also bind Lipid II in the cell wall, as well as D-Ala D-Ala residues in PG.

It is known that PG provides protection for cells but its rigidity also assists cells in the maintenance of their shape. Therefore, the remaining PG layer or fragments were presumed to be small due to the obvious loss of the vegetative cell cylindrical shape upon cell wall removal. It is tempting to speculate that the leftover PG fragments or layer provided a scaffold for the subsequent synthesis of new PG during protoplast cell wall regeneration.

DIC

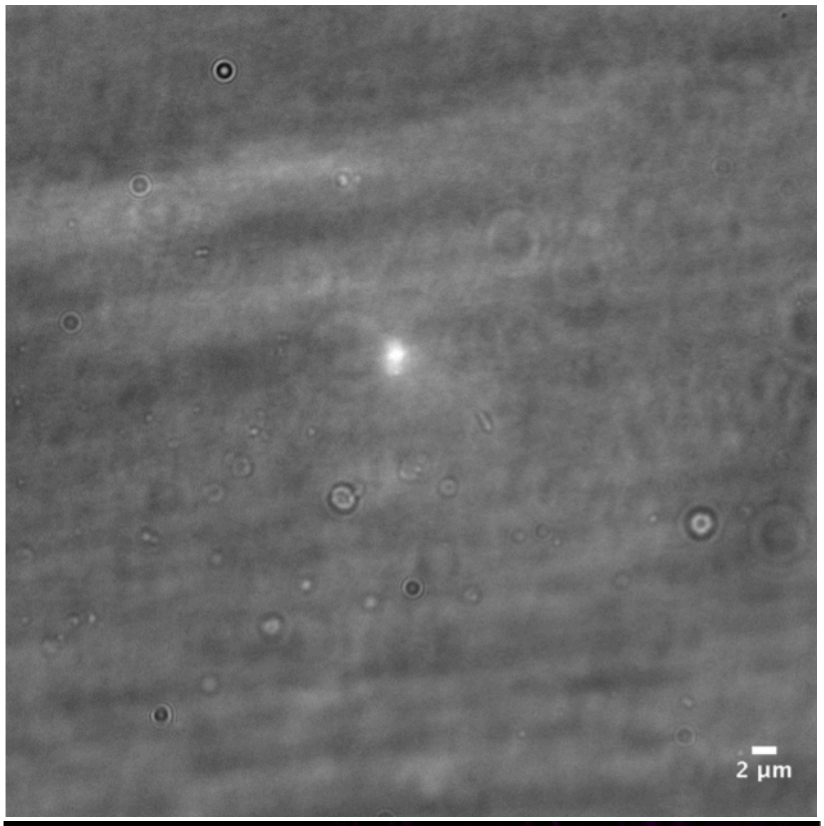

FM1-43

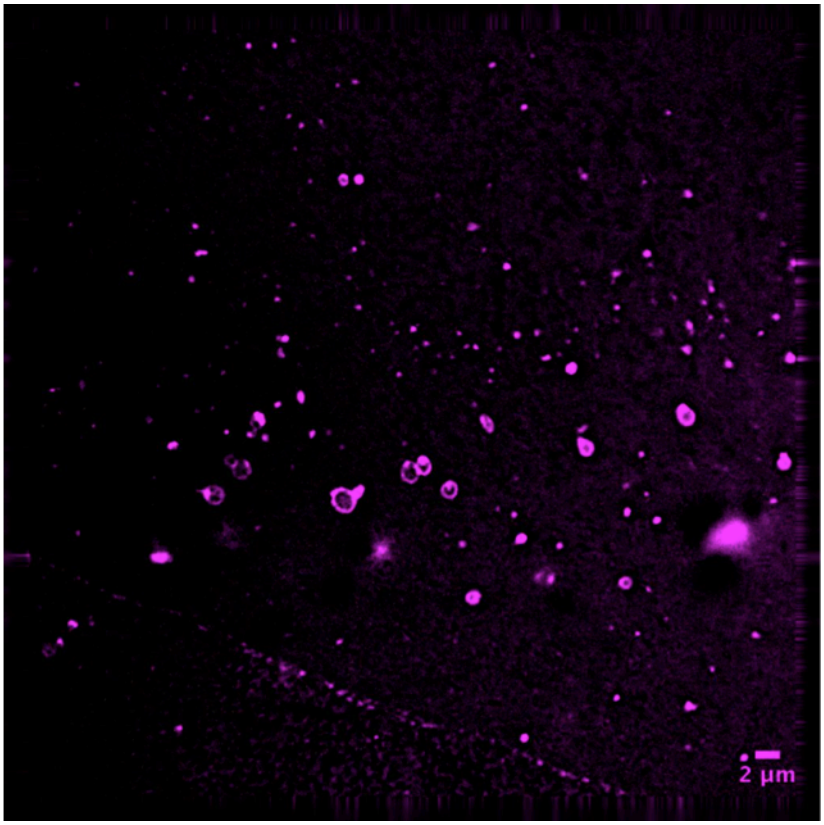

Vanc

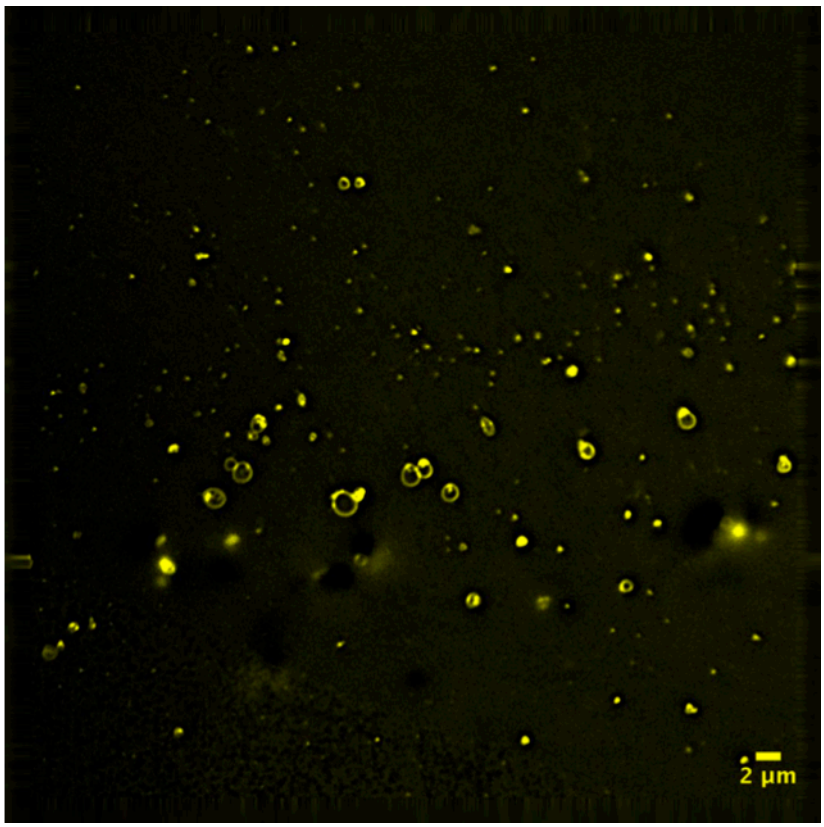

Merge

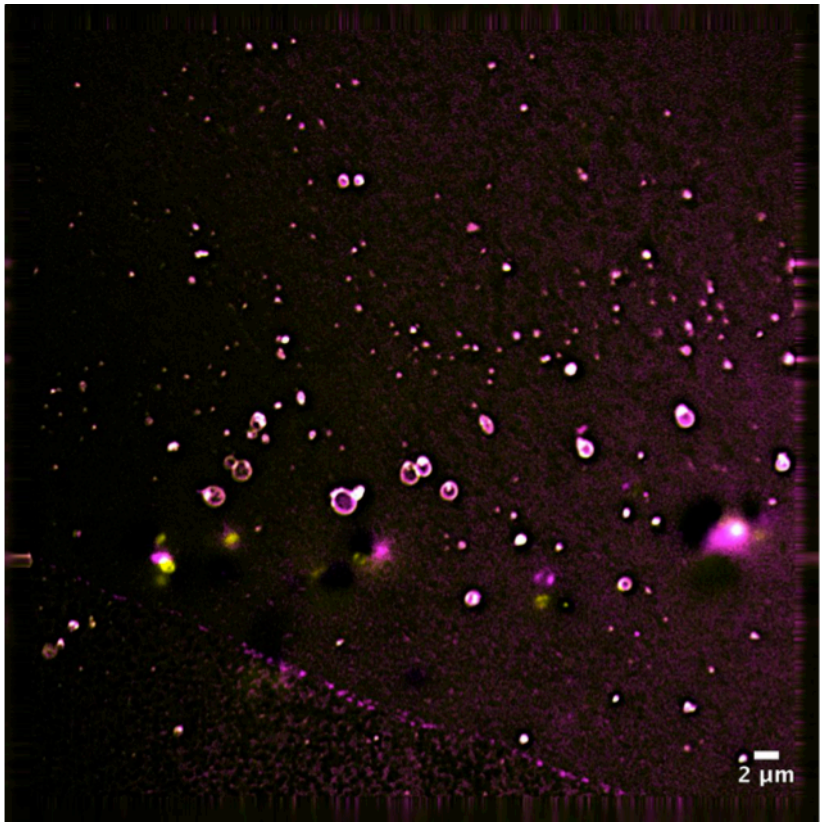

Figure 3.8. *B. subtilis* protoplasts: sampled immediately post-lysozyme treatment and examined by epifluorescence microscopy. Each image shows an entire microscopic field of cells. Cell walls are stained pink with Vancomycin BODIPY-FL (Vanc), which binds D-Alanine residues in the PG. Cell membranes are stained yellow with FM1-43, which binds phospholipids in the lipid bi-layer.

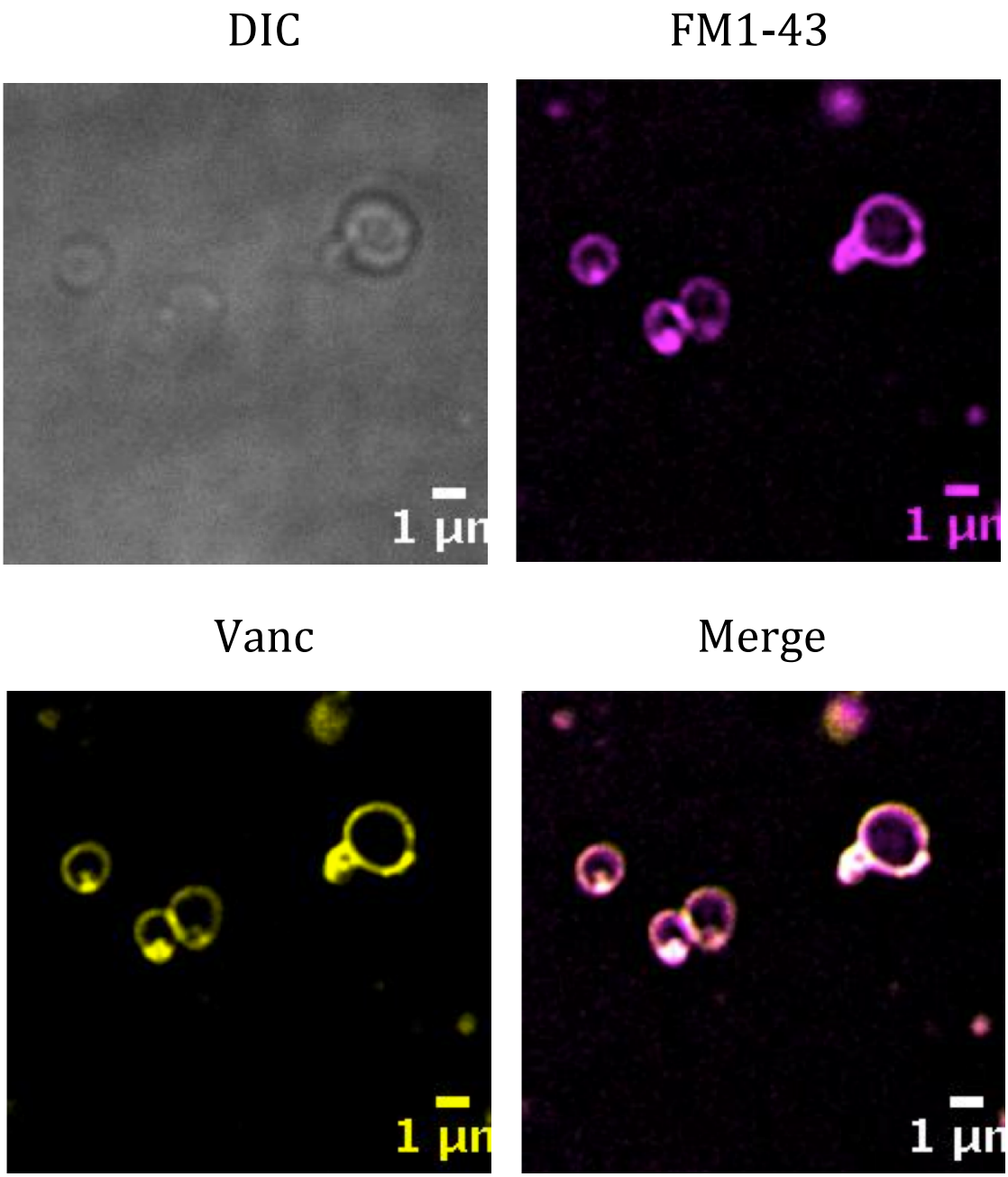

Figure 3.9. High magnification of *B. subtilis* protoplasts: sampled immediately post-lysozyme treatment and examined by epifluorescence microscopy. Each image field shows a few protoplasts. Cell walls are stained pink with Vancomycin BODIPY-FL (Vanc), which binds D-alanine residues in the PG. Cell membranes are stained yellow with FM1-43, which binds phospholipids in the lipid bi-layer.).

In conclusion, the combined electron and epifluorescent microscopic analysis of protoplasts showed that they exhibit a spherical morphology upon creation. Furthermore, while the action of lysozyme is successful in removing most of the outermost PG in the cell wall, some PG is still retained by the protoplasts.

3.2.4.3 Morphological dynamics during protoplast regeneration

As with the previous *B. subtilis* vegetative cell and protoplast samples taken from the regeneration assay, regenerating protoplasts were sampled and examined using transmission electron and epifluorescence microscopy. In contrast to the previous two samples where the cell morphology was known or accurately predicted, the images obtained showed unexpected morphological stages during protoplast regeneration.

TEM analysis of regenerating *B. subtilis* protoplasts revealed extremely unusual cell morphology (**Figure 3.10**). Panel A showed a full field of cells; some of which displayed rod-like morphology, measuring roughly 2μm along their longitudinal axes. The outermost layer of the regenerating protoplasts was thicker in comparison to the TEM image of the outermost layer of newly created protoplasts. In addition, the outermost layer of the regenerating protoplasts appeared to be similar in thickness to the TEM image of vegetative cell walls. Most obviously, however, nearly all of the regenerating protoplasts were completely devoid of cytoplasmic material. This is seen in Panel A (**Figure 3.10**) where only empty 'sacks' or 'cuffs' of cell wall material remain of the regenerating protoplasts. This indicated that the cell wall was weak and possibly not intact due to only partial regeneration of the PG.

Furthermore, most observed regenerating protoplasts were open at either one or both poles of the cell (with no cytoplasmic content remaining). High magnification examples of these single and double open-ended regenerating protoplasts are shown in Panel B and C (**Figure 3.10**). Panel B shows single open-ended regenerating protoplasts i.e. 'sacks'. Panel C shows double open-ended regenerating protoplasts i.e. 'cuffs'. In both sets of images, part of a rod-shaped cylinder was observed in individual cells. Furthermore, at the open cells' ends, a slight outward curling of the two walls can be seen. This was particularly obvious in the double open-ended 'cuff' protoplast (Panel C, **Figure 3.10**), where it seems as if there was once more material joined to the regenerated cell wall at either end. It appeared as if there was once another pre-existing part to either one of both poles of a regenerating protoplast that was not detectable using TEM. It was therefore logical to hypothesise that the suggested missing feature(s) at the cells' pole(s) was/were lost or damaged during TEM processing.

The unusual morphology of regenerating *B. subtilis* protoplasts observed during TEM analysis was echoed when the same sample was examined using epifluorescence microscopy. The regenerating protoplasts were stained with FM1-43 and fluorescent vancomycin, which bound to cell membrane and PG respectively (**Figure 3.11**). Throughout numerous repetitions of this experiment, two distinct morphological stages of protoplast regeneration were observed; 'lollipops' and 'dumbbells', so named for their shapes.

A

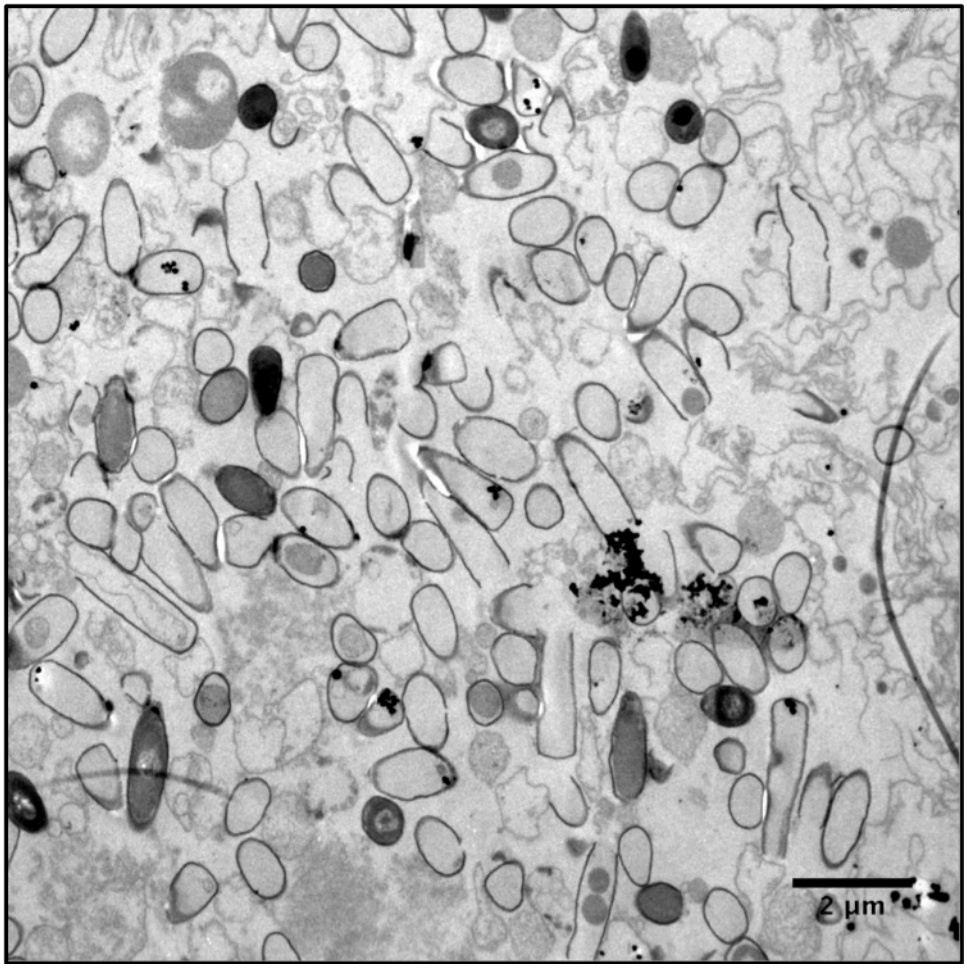

B

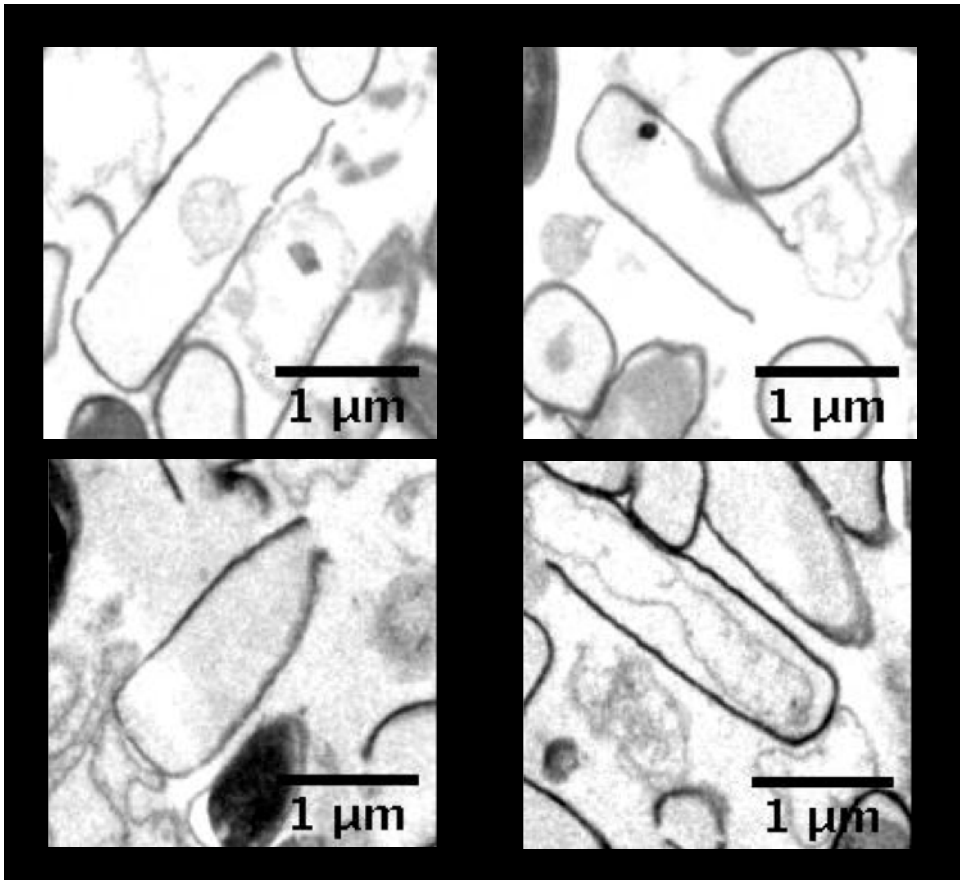

C

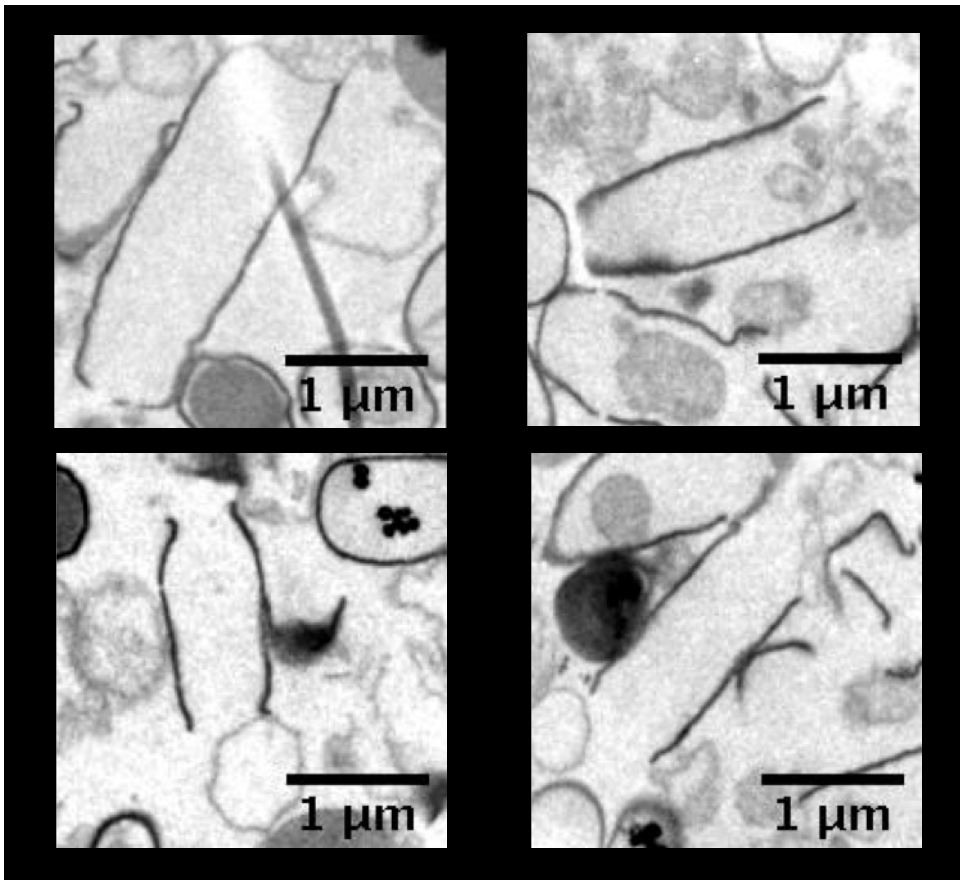
1 µm
1 µm
1 µm
1 µm

D

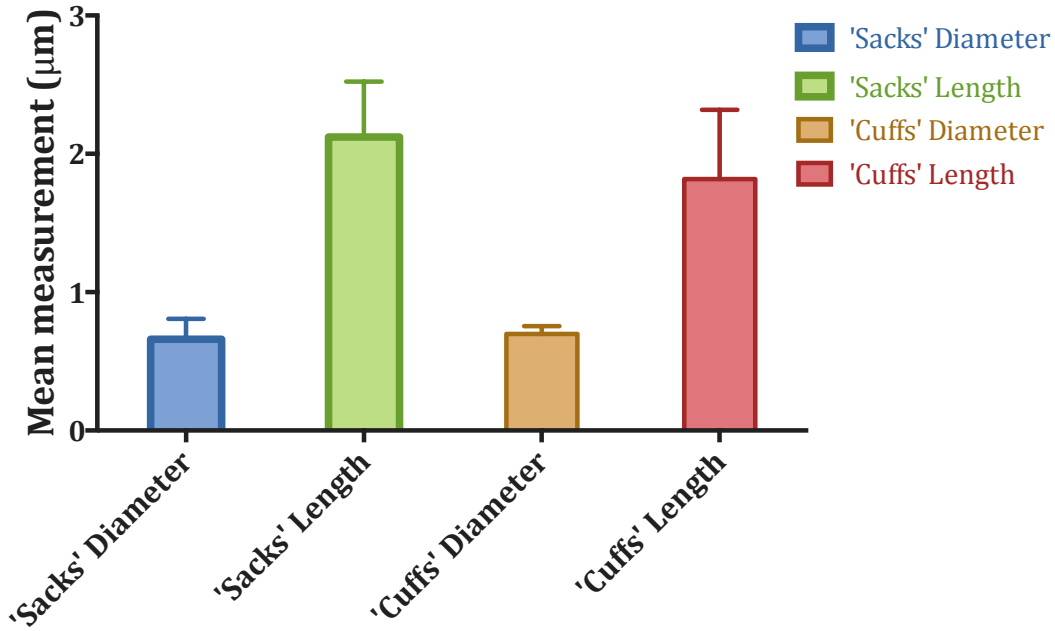
Mean measurement (µm)
0
1
2
3
'Sacks' Diameter
'Sacks' Length
'Cuffs' Diameter
'Cuffs' Length
'Sacks' Diameter
'Sacks' Length
'Cuffs' Diameter
'Cuffs' Length

Figure 3.10. *B. subtilis* regenerated protoplasts: sampled after 12 hours incubation in liquid regeneration media and examined by transmission electron microscopy. Panel A shows a full field of regenerated protoplasts (some non-regenerated protoplasts can be observed). Panels B and C show zoomed-in images of single *B. subtilis* regenerated protoplasts. The cells shown in Panels B and C are grouped by their similar morphologies, 'sacks' and 'cuffs' respectively. Panel D shows the mean and standard deviation of length and diameter of 'sacks' and 'cuffs'.

DIC

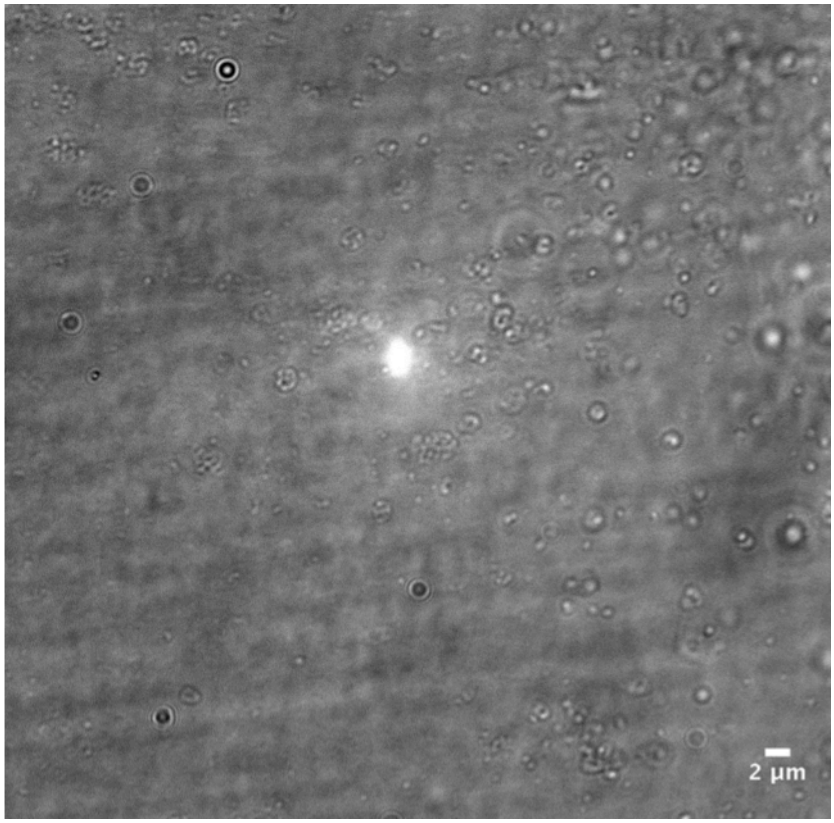

FM1-43

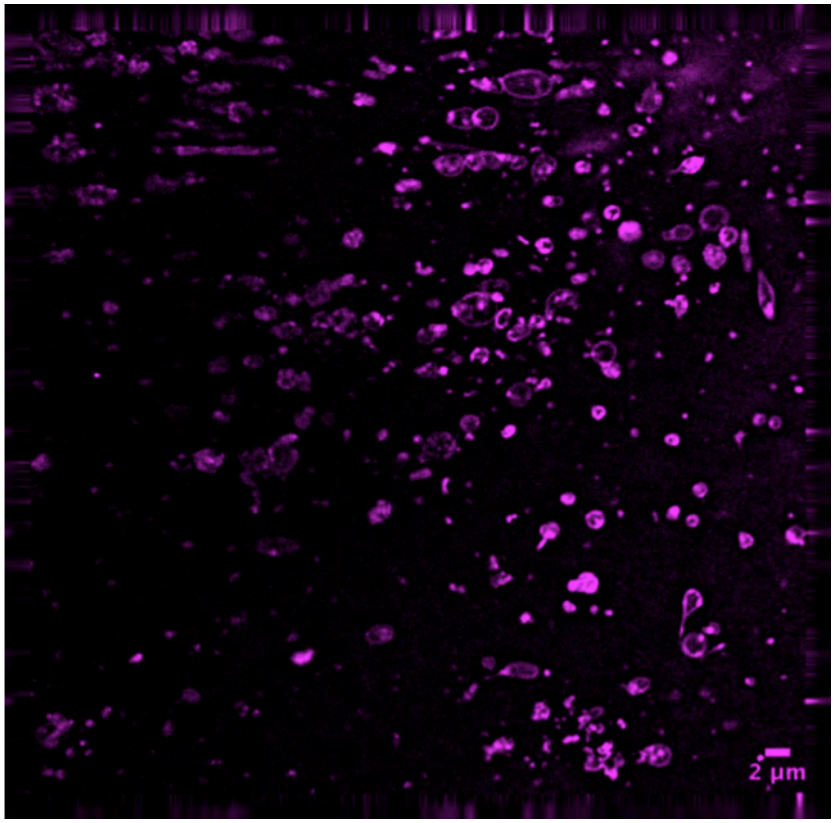

Vanc

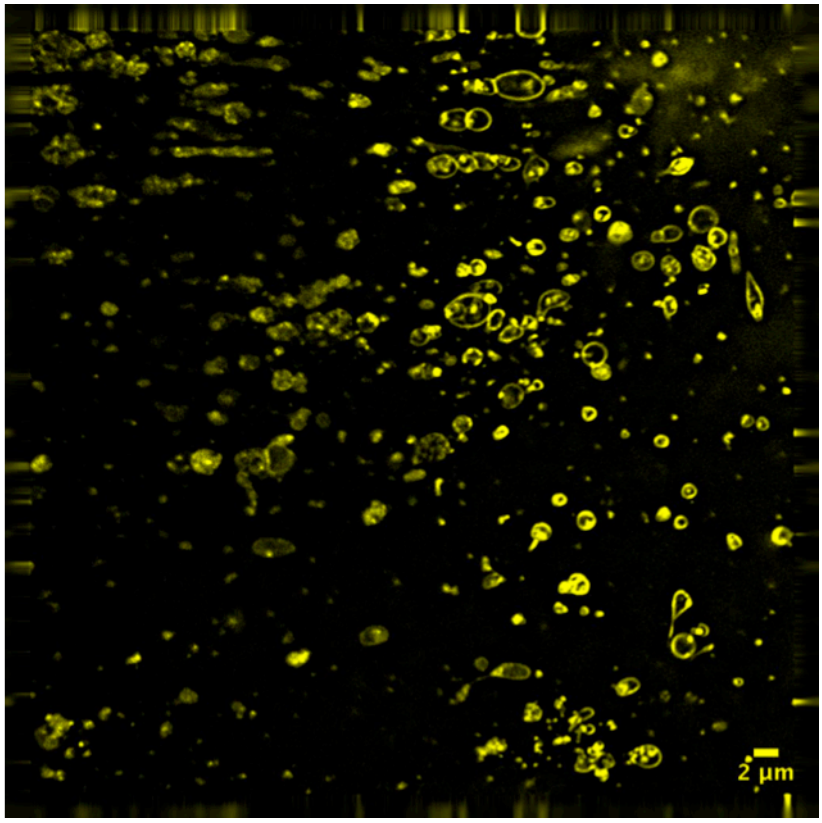

Merge

A

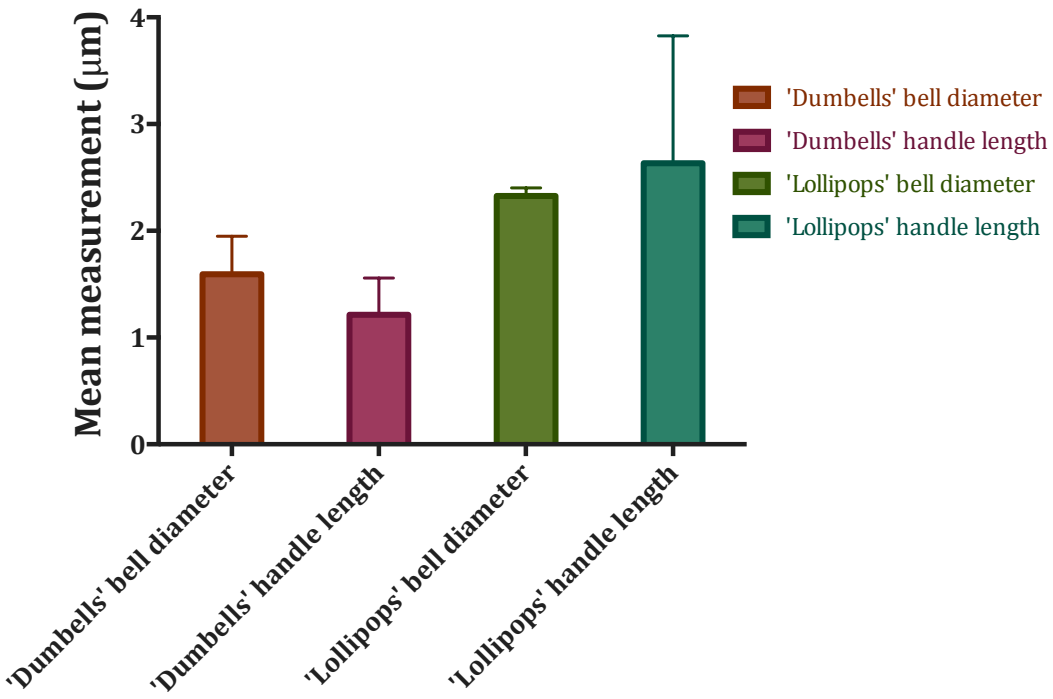

Figure 3.11. *B. subtilis* regenerating protoplasts: sampled after 12 hours incubation in liquid regeneration media, examined by epifluorescence microscopy. Each image shows an entire microscopic field of cells. Cell walls are stained pink with Vancomycin BODIPY-FL (Vanc), which binds D-Alanine residues in the PG. Cell membranes are stained yellow with FM1-43, which binds phospholipids in the lipid bi-layer. Panel A shows the mean and standard deviation of length and diameter of 'sacks' and 'cuffs'.

These two morphologies of regenerating protoplasts can be seen at higher magnification in **Figure 3.12**. Examination of the 'lollipop' cell shape showed a rod attached to a spherical pole at one end, measuring roughly 2μm along the longitudinal axes. The 'dumbbell' cell shape was examined; the cells showed a rod-shape attached to two spherical poles (one at either end). The structure of the spherical poles observed at either one or both ends of the 'lollipops'/'dumbbells' was reminiscent of the epifluorescence images of newly created protoplasts (**Figure 3.9**). Therefore, it was thought that the rod-shaped cylinders attached to these spherical structures were in fact newly synthesised PG produced during protoplast regeneration. This hypothesis was further consolidated when the binding of fluorescent vancomycin to the regenerating protoplasts was examined (**Figure 3.12**). The rod-shaped cylinder parts of the regenerating protoplasts exhibited a stronger fluorescent signal compared to the original protoplast spherical structure, i.e. more vancomycin binding. As vancomycin binds D-Ala D-Ala residues in PG peptide side chains, this implied that there was in fact more PG to bind on the rod-shaped sections of the regenerating protoplasts. This provided observable evidence that the protoplasts were indeed regenerating by synthesising new PG.

Initially, the epifluorescence images taken of the regenerating protoplasts appeared to contradict the equivalent images obtained via TEM analysis, due to the differing morphologies observed. On closer inspection, it emerged that the TEM and epifluorescence data actually complemented each other. It is extremely likely that the missing ends of regenerating protoplasts observed

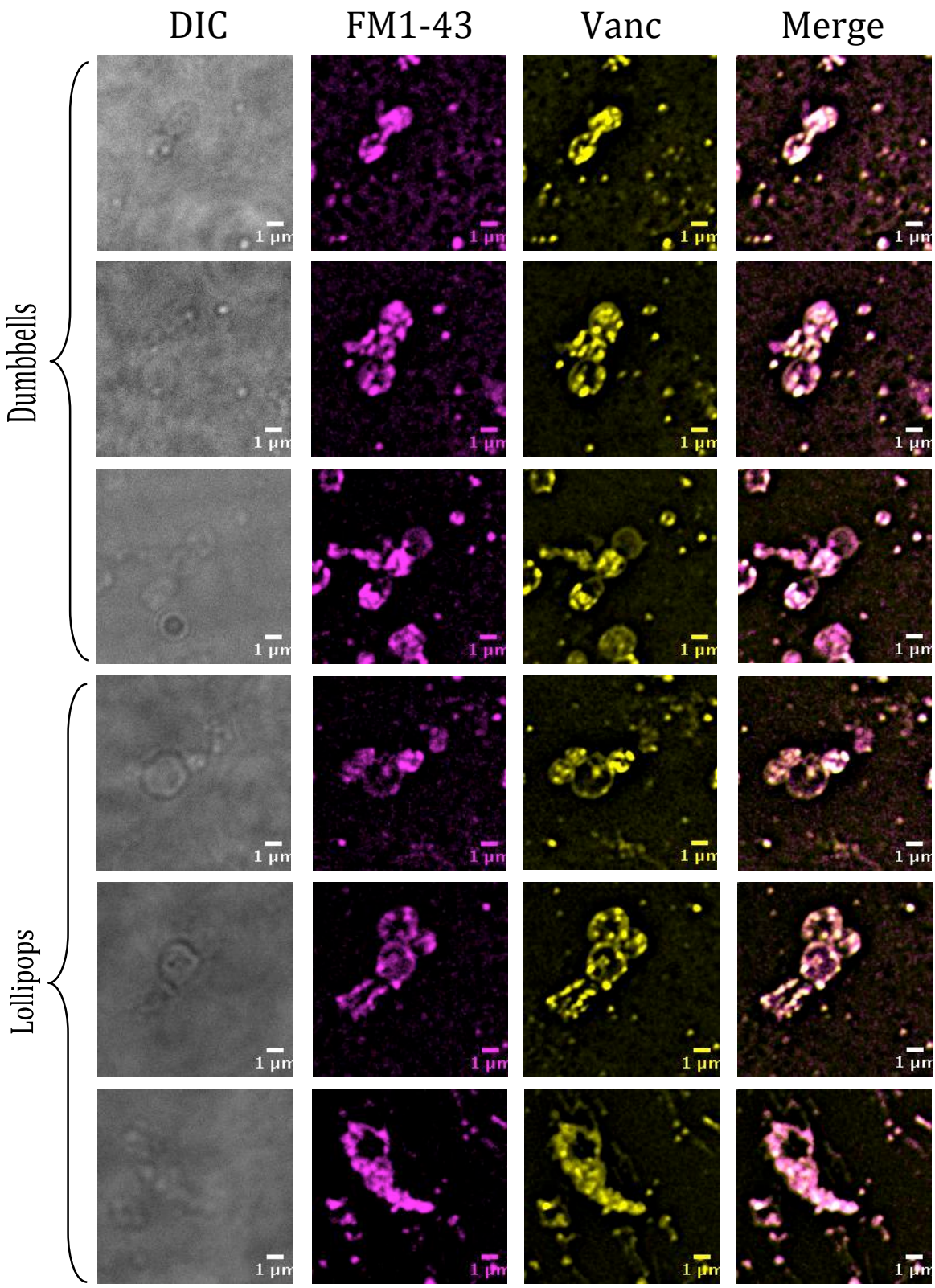

Figure 3.12. High magnification of *B. subtilis* regenerating protoplasts: sampled after 12 hours incubation in liquid regeneration media, examined by epifluorescence microscopy. The differing morphologies are grouped according to label; 'dumbbell' and 'lollipop'. Cell walls are stained pink with Vancomycin BODIPY-FL (Vanc), which binds D-Alanine residues in the PG. Cell membranes are stained yellow with FM1-43, which binds phospholipids in the lipid bi-layer.

by TEM were in fact lost remnants of the original protoplasts. The experimental procedure for preparing cells for epifluorescence microscopy was less harsh for the delicate regenerating protoplasts, which is an explanation for their survival and subsequent observation during this approach.

3.2.5 AFM analysis of regenerating *B. subtilis* cell wall material

AFM was used to examine the regenerating protoplasts. The cells were extracted by boiling in SDS and the resulting sample washed and ultracentrifuged to collect the ensuing insoluble material. The sample was then treated with pronase to remove any proteins from the recovered material before being centrifuged and washed again prior to AFM analysis. This approach differed to purification of vegetative cell PG for AFM. The initial French pressing and final HF treatment were omitted for purification of regenerating protoplast cell walls as these two procedures were hypothesised as being too destructive for the presumed more 'delicate' regenerated protoplast cell wall compared with vegetative cell wall. Therefore, the examined material could not be truly described as PG alone.

The cell wall material was air-dried onto a clean mica-sheet and imaged by AFM in tapping mode under ambient conditions at room temperature (15-30 °C). A typical field of sacculi is shown in **Figure 3.13**. In some cases, the regenerating cell wall material

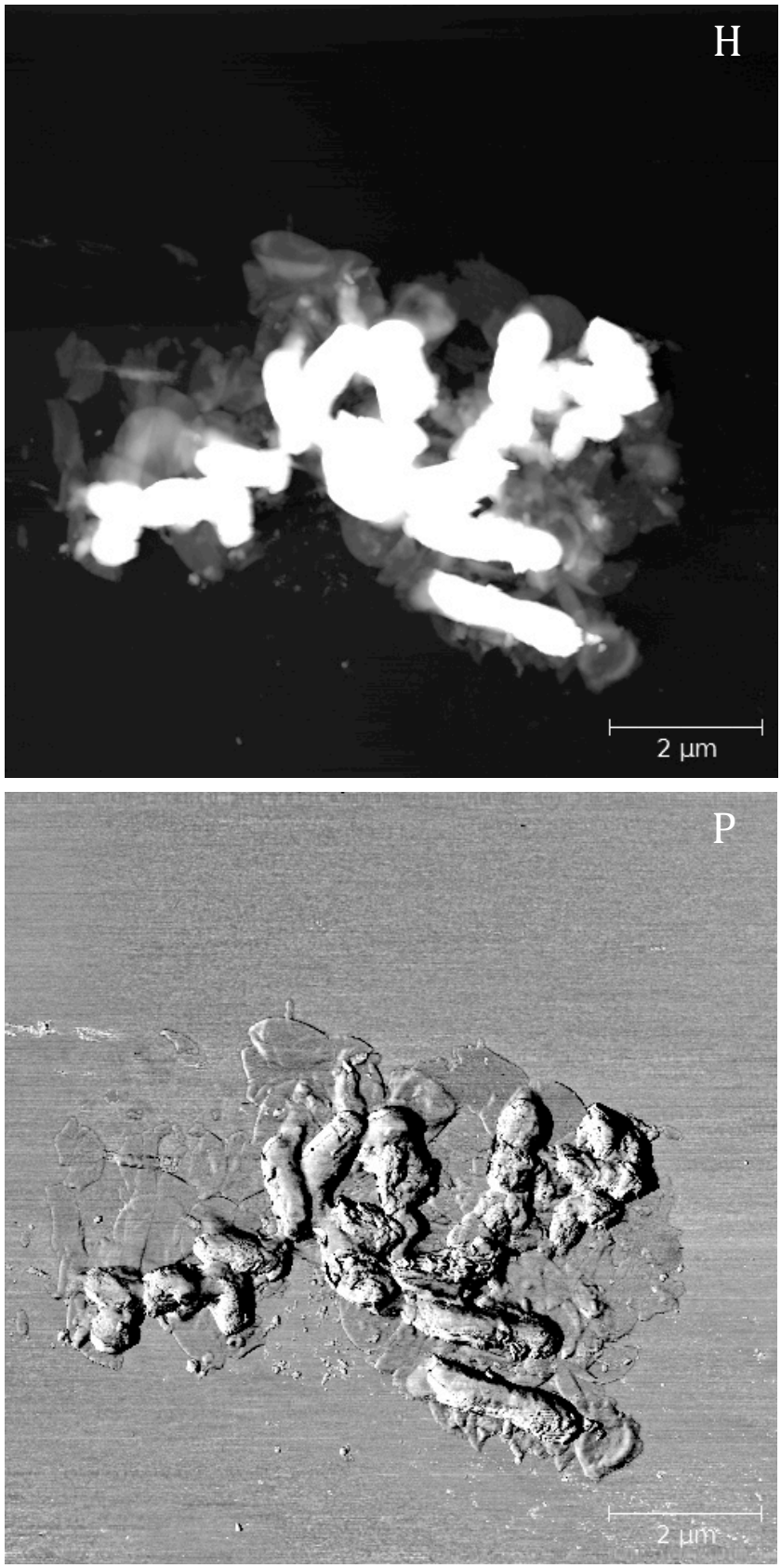

Figure 3.13. AFM analysis of purified *B. subtilis* regenerated protoplast cell wall material. Height (H) and phase (P) images showing a typical field of broken *B, subtilis* regenerated protoplasts dried onto a mica surface. Scales:H 120 nm, P 12°. The Z-axis scales on each image indicate the topographical height of the sample; the height image in nm and the phase image in relative degrees.

remained intact and appeared to retain cytoplasmic content, which only allowed proper examination of the cell wall's gross architectural features.

3.2.5.1 Gross architectural features of regenerating cell wall in *B. subtilis*

AFM images of cell wall material (and therefore, potential peptidoglycan) recovered from regenerating *B. subtilis* cells (**Figure. 3.13**) revealed some similarities to previously published images of *B. subtilis* vegetative cell sacculi (Hayhurst et al., 2008). The height of the material being examined was comparable to published peptidoglycan data, measuring between 50-100 nm. While the image displays mainly heavily broken material, some gross architectural cell features can be observed e.g. curved poles at the end of the cell and some cell cylinders.

However, the observed morphology of the cell wall material of regenerating protoplasts was not as obviously different to equivalent vegetative cell sacculi data (compared with the obvious morphological differences observed during EM and epifluorescence microscopy approaches used in this study). Some cells still retained cytoplasmic material, which distorted the topographical analysis. Furthermore, from the images obtained, it was not possible to observe distinct single morphologies due to the clumping of the cell wall material.

In summation, the images obtained via AFM analysis were inconclusive and did not elucidate any new information regarding the gross architecture of the regenerating protoplast cell wall.

3.3 Discussion

Architectural analysis of *B. subtilis* PG has revealed it to be both complex and elegant. How its architecture is produced and yet remains dynamic is mostly unknown. In this study, protoplast regeneration was used to provide a framework to establish the mechanism of *de novo* PG synthesis in *B. subtilis.*

This study has established a reliable method of *B. subtilis* protoplast regeneration in liquid media, which allows both quantitative and qualitative analysis of morphological changes to the cell during this phenomenon. Visual analyses revealed that PG could be generated to reform vegetative cells under the right assay conditions, as highlighted by the morphological changes observed using fluorescence and electron microscopy. PG has the unique ability to regenerate and be restored under certain conditions, following biochemical damage to its structure.

3.3.1 How does *B. subtilis* PG regenerate?

One of the main questions raised by this study is: how does the *Bacillus* rod-shape re-establish itself during successful protoplast regeneration? At the time of writing, protoplast regeneration in *B. subtilis* had never been investigated in terms of PG dynamics. Therefore, any external insight was provided by investigations into similar systems i.e. *B. subtilis* L-forms and *E .coli.* Furthermore, how the vegetative *B. subtilis* PG growth and division machinery is utilised in protoplast regeneration remains unanswered.

3.3.1.1 Re-establishment of rod-shape in *E. coli*

A recent study showed that *E.coli* protoplasts are able to re-establish their vegetative rod-shape after a series of morphological division intermediates (Ranjit and Young, 2013). As *E. coli* is a Gram-negative organism, its vegetative cell wall is of a different organisation than in *B. subtilis* (Hayhurst et al., 2008; Turner et al., 2013). Therefore, it is sensible to assume that *E.coli* protoplast regeneration may have a differing mechanism to *B. subtilis*, even if only due to the lack of outer membrane and larger PG layer observed in Gram-postive bacteria.

Nevertheless, the gross morphological features of the two species are similar, both in protoplast and vegetative cell states; spherical and rod-shaped, respectively. It is therefore tempting to speculate that the step-wise conversion of a spherical protoplast to a rod-shaped vegetative cell in *E.coli* is echoed in *B. subtilis*.

3.3.1.2 Mode of *B. subtilis* L-form proliferation

The most similar type of cell state to *B. subtilis* protoplasts are *B. subtilis* L-forms. It has even been argued that L-forms are a more differentiated version of a protoplast (Allan et al., 2009). *B. subtilis* L-forms are well documented in their ability to produce new L-form cells through proliferation, a mode of FtsZ-independent cell division/differentiation (Devine, 2012; Domínguez-Cuevas et al., 2012; Leaver et al., 2009; Mercier et al., 2013, 2012).

Newer studies on L-form proliferation in *B. subtilis* suggest that the enlargement and subsequent division of these cells is caused purely biomechanically rather than being cell-directed (Mercier et al., 2013, 2012).

These papers suggest that excess membrane production by the L-forms causes biomechanical blebbing of the cells due to an uneven surface area to volume ratio, thus completing a primitive form of cell proliferation (Mercier et al., 2013).

While *B. subtilis* protoplasts are not able to proliferate in terms of cell multiplication, they do undergo a form of cell differentiation upon completion of cell wall regeneration. However, the results generated by epifluorescent morphological analysis of this study indicated that there were sites of nascent PG synthesis present in regenerating *B. subtilis* protoplasts. This suggested that, rather than being a passive biomechanical process as seen in L-forms (Mercier et al., 2013), protoplast regeneration in *B. subtilis* was a result of some form of active PG biosynthesis.

3.3.1.3 Model of cell wall regeneration in *B. subtilis*

The data obtained from combined microscopic analyses of vegetative cells, protoplasts and regenerating protoplasts in this study led to the formulation of a *B. subtilis* cell wall regeneration model (**Figure 3.14**).

This model provides a hypothesis that accounts for the differing cell morphologies observed in regenerating protoplasts (**Chapter 3.2.4.3**), with reference to the 'dumbell' and 'lollipop' cell shapes. In this study, we hypothesise that these observed cell shapes are intermediate steps in the process *B. subtilis* undergoes during regeneration from a protoplasted state.

The model of cell wall regeneration in *B. subtilis* is as follows; the vegetative cell wall is removed to form a protoplast, the protoplast synthesises a 'cuff' of

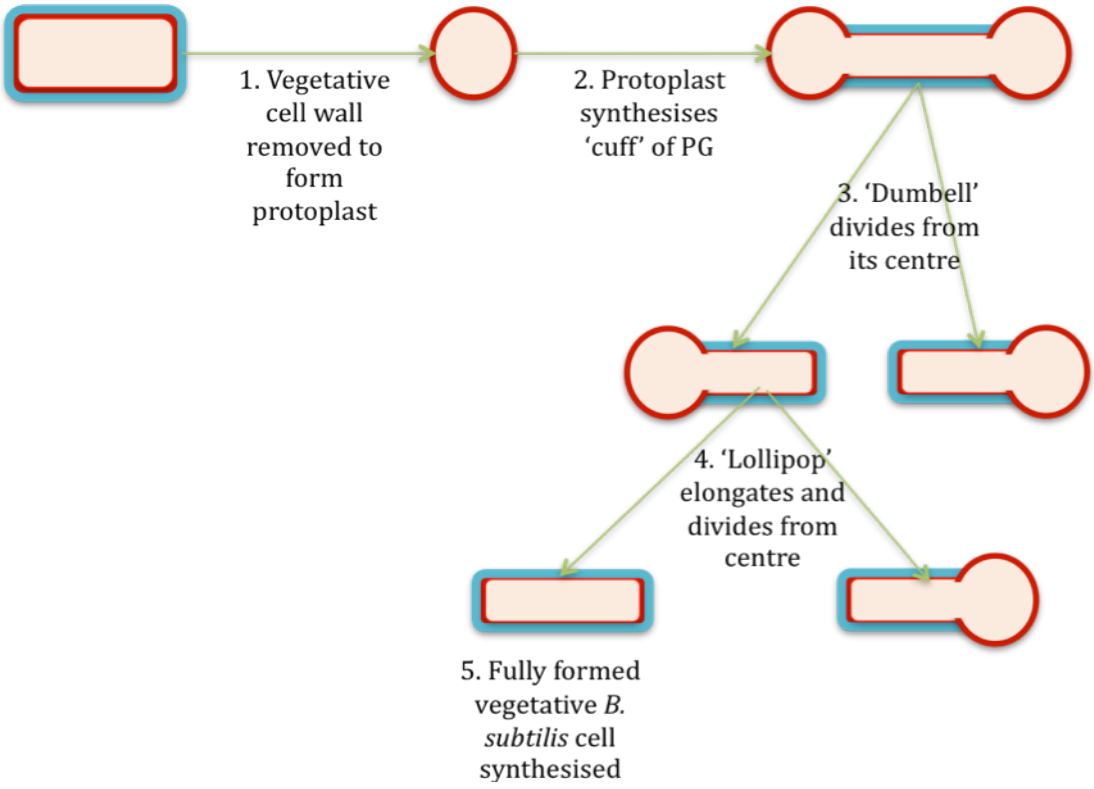

Figure 3.14. Schematic showing the hypothesis for the morphological changes involved in protoplast generation and regeneration in *B. subtilis,* This was derived from evidence obtained by fluorescence and electron microscopy. The diagram shows how a vegetative cell fully regenerates itself from protoplast. The cell membrane is shown in red and the cell wall (PG) is shown in blue.

PG around its centre to form a 'dumbbell', the 'dumbbell' divides from its centre to form a 'lollipop', the 'lollipop' elongates and divides from its centre and thus a fully formed vegetative *B. subtilis* cell is synthesised.

This model was hypothesised based on the visual findings of this study. It is somewhat similar to the observed re-establishment of the rod-shape exhibited by *E .coli* protoplasts. In this Gram-negative system, regeneration proceeds via a series of cell divisions that produced misshapen and branched intermediates (Ranjit and Young, 2013). This 'misshapen' division intermediates are echoed in the 'dumbbell' and 'lollipop' morphologies observed during *B. subtilis* protoplast regeneration.

3.3.1.4 Role of PG division machinery in *B. subtilis* wall regeneration

B. subtilis cell division is an incredibly dynamic process involving the co-ordination and interaction of several types of protein machinery. This machinery includes penicillin binding proteins (PBPs) and the Min system and other cell division proteins. A question raised by the *B. subtilis* cell wall regeneration model is how this division machinery contributes to the morphological intermediates observed?

Bacterial cell division is initiated by the tubulin homologue protein FtsZ (Adams and Errington, 2009). The FtsZ GTPase polymerises at the bacterial division ring and is required for division in almost all bacteria (Adams and Errington, 2009; Erickson et al., 2010). Prior to septum formation, FtsZ polymerises to form a ring-like structure, known as a Z-ring, which acts as a scaffold for the bacterial cytokinetic machinery (Adams and Errington, 2009).

Recruitment of FtsZ and correct subsequent placement of Z-rings in *B. subtilis*, vegetative cells i.e. centrally to halve the mother cell during division, is controlled by the MinCDE gene complex (Harry, 2001a). Furthermore, A conserved division inhibitor MinCD, which prevents aberrant division at the cell poles, controls division site selection (Marston et al., 1998). It is possible the MinCDE system plays a similar role in the placement of a septum to halve a 'dumbbell' into two 'lollipops' during protoplast regeneration.

B. subtilis has 16 PBPs, most of which have been extensively studied for their role in vegetative peptidoglycan synthesis and in sporulation (Sauvage et al., 2008). In *E. coli*, PBP1B mutants were unable to undergo protoplast regeneration (Ranjit and Young, 2013). To give an example in *B. subtilis* vegetative cells; knocking out the PBP1 gene affects the formation of asymmetric septa during sporulation (Scheffers and Errington, 2004). Due to their obvious effect in maintenance of a rod-shape morphology, it is logical to assume that PBPs play a putative role in the re-establishment of a *B. subtilis* rod-shape during cell wall regeneration.

3.3.2 Implications of PG regeneration in *B. subtilis*

B. subtilis is well documented in its ability to undergo sporulation and/or subsequent germination as a response to a changing external environment. It is also known that PG hydrolases play a vital role in the initiation of these cell differentiation processes (Errington, 2003; Smith et al., 2000). It is possible that PG hydrolases also play a similar role in the co-ordination of cell wall regeneration.

It has been suggested that L-form proliferation in *B. subtilis* is a primitive form of cell survival prior to the evolution of the cell wall (Mercier et al., 2013). It is therefore possible that cell wall regeneration from *B. subtilis* protoplasts is another form of an adaptive response to cell wall damage caused by a change in the cells' external environment.

Furthermore, this perpetuates the idea that the PG sacculus in *B. subtilis* is a dynamic, adaptive cell component that contributes to bacterial survival.

3.3.3 Future work

The questions raised by this study can only be answered by further examination and experimentation of *B. subtilis* during protoplast regeneration. Further analysis of this phenomenon could have taken a variety of different experimental approaches. Continuation of AFM analysis of regenerating protoplast cell wall material is desirable; to further examine the gross PG architecture. This procedure was not yet fully optimised during the course of the study. Furthermore, it would be interesting to use fluorescent D-amino acid dyes (FDAAs) such as HADA, to further probe the regenerating cell wall during epifluorescence microscopy. These dyes have been utilised in the imaging of vegetative *B. subtilis* cell walls (Kuru et al., 2012).

The next most obvious next step would be to subject the samples, particularly the regenerating protoplasts, to more high-resolution microscopic analysis using the same dyes, such as STORM. This approach has been demonstrated in *E. coli* and *C. crescentus* by Turner et al. (2013) This would reduce the limitations provided by resolution in epifluorescence

microscopy, by being able to pinpoint precisely where each fluorescent molecule has bound to the cells.

While the steps of cell wall regeneration in *B. subtilis* protoplasts have been examined, the approach of this study did not include any interrogation of how this ability is controlled and managed by the cell. We do not currently have any understanding of how protoplast regeneration in *B. subtilis* is controlled genetically. Further experimentation of this aspect of PG remodelling in protoplasts would provide an even greater understanding of how the macromolecule controls itself in vegetative cells. It would be interesting to use *B. subtilis* mutants deficient in PG biosynthesis in a protoplast generation and regeneration experiment and then observe if and how the cells regenerate themselves. *B. subtilis* strains appropriate for this could include those with genes deleted that are involved in cylinder elongation e.g. PG hydrolases, MreB or Penicillin binding proteins (PBPs) (Bisicchia et al., 2007; Kawai et al., 2009; Sauvage et al., 2008).

Chapter 4

Cell wall synthesis and peptidoglycan remodelling in *B. subtilis*

4.1 Introduction

The rod-shaped *B. subtilis* has long been studied as a gram-positive model organism with regard to bacterial genetics, biochemistry and physiology. The cell wall acts as a key determinant in the maintenance of a defined shape and provides protection from the extracellular environment and internal turgor pressure. It thus is crucial to all aspects of cell biology.

In gram-positive cells, the largest component of the cell wall is its peptidoglycan (PG). PG is a complex polymer, comprised of alternating *N*-acetyl glucosamine and N-acetyl muramic acid residues that are cross-linked by peptide side chains. It is a complex and dynamic macromolecule.

4.1.1 Elucidating peptidoglycan dynamics in *B. subtilis*

As discussed in **Chapter 1**, our current understanding of PG dynamics in *B. subtilis* is relatively limited. Previous experimental approaches have revealed some details about PG composition and architecture in this species (Atrih et al., 1999; Hayhurst et al., 2008).

One of the main objectives of this study was to examine *B. subtilis* WT cell wall growth and dynamics. This entailed the use of a variety of different fluorescent dyes in epifluorescence microscopy. Using fluorescent

vancomycin and fluorescent D-amino acids as *in situ* cell wall probes meant that the sites nascent PG synthesis could be mapped. Also, recently developed super resolution microscopy approaches allow molecular resolution. In particular, Stochastic Optical Reconstruction Microscopy (STORM) has resolution down to 20-30 nm (Rust et al., 2006).

4.1.2 Role of PG hydrolases in PG dynamics

Two PG hydrolases have been identified that are required for both growth and PG synthesis of *B. subtilis*; LytE and YvcE. The *B. subtilis* strain BP115 (P_{xyl}*yvcE*Δ*lytE*::*cm*^{r}) has had the *lytE* gene deleted and *yvcE* expression is inducible by xylose (Bisicchia et al., 2007). The two genes (*lytE* and *yvcE*) encode endopeptidase-type autolysins, one or other of which is essential for growth, and perform an important function in lateral cell wall synthesis and cell elongation (Bisicchia et al., 2007). As discussed previously (**Chapter 1**), endopeptidases in *B. subtilis* hydrolyse the amide bond between two amino acids in PG. This breaking of peptide bonds allows expansion of the sacculus during cell growth (Vollmer et al., 2008b). In BP115 when *yvcE* expression is not induced, a detectable morphological defect occurs in that cells become bowed (Bisicchia et al., 2007). Imaging of BP115 cells under different experimental conditions will reveal the role of the endopeptidases in cell wall dynamics at the molecular level.

4.1.3 Use of Stochastic Optical Resolution Microscopy

One of the main limitations of cell biology using epifluorescence microscopy is its relatively low resolution (approximately 250nm). However, a new

super-resolution fluorescence microscopy technique has been developed in recent years; Stochastical Optical Reconstruction Microscopy (STORM).

STORM utilises high-resolution site-specific targeting of photo-switchable fluorophores (Rust et al., 2006). The imaging process consists of a series of imaging cycles in which only a fraction of the fluorophores in the field of view are switched on. This means that the position of each fluorophore is optically distinguishable and can be determined with high accuracy. The fluorophore locations obtained from a series of imaging cycles are then used to reconstruct the overall image.

For a sample to be detectable using STORM, STORM-compatible dyes or probes must be used during investigation. For a dye or probe to be STORM-compatible, its fluorophores must be photo-switchable, i.e. must alternate between a fluorescent and non-fluorescent state in a controlled and reversible manner (Rust et al., 2006).

This technique was considered to be an excellent new approach for the purposes of cell wall PG visualisation and was therefore undertaken in this study using *B. subtilis* WT.

4.1.4 Aims of this study

The experimental aims and objectives for this chapter are:

1. Characterise PG dynamics and synthesis during growth in *B. subtilis* WT.
2. Determine the role of *lytE* and *yvcE* during PG dynamics in *B. subtilis* BP115.

4.2 Results

4.2.1 *B. subtilis* WT growth in nutrient broth

Prior to image-based experimentation of cell wall synthesis in *B. subtilis* WT (HR168), it was necessary to first understand the kinetics of cell growth of the strain. *B. subtilis* WT was grown over six hours in nutrient broth (NB) at 37°C and a growth curve was established by measuring optical density (**Figure 4.1**).

After inoculation of the culture from a small overnight sample, growth of the *B. subtilis* WT cell growth reached exponential phase after 2 hours with an optimal doubling time of 36 minutes. Post-exponential phase of growth was reached after 4 hours.

Samples were therefore taken for future microscopy experiments 2-4 hours into the culture to ensure *B. subtilis* WT cells were in exponential phase.

4.2.2 Epifluorescence imaging of *B. subtilis* WT cell walls

In order to investigate the dynamics of *B. subtilis* WT cell wall PG synthesis during the cell cycle of growth and division, samples were taken during mid-exponential phase of growth in NB and labelled using a variety of different fluorescent dyes/probes and approaches. These samples were then examined using epifluorescence live cell microscopy. This approach was used with the aim of comparing and contrasting the potentially differing labelling patterns, as all dyes and probes were used with the specific aim of binding to cell walls. In some experiments a combination of fluorescent dyes was used

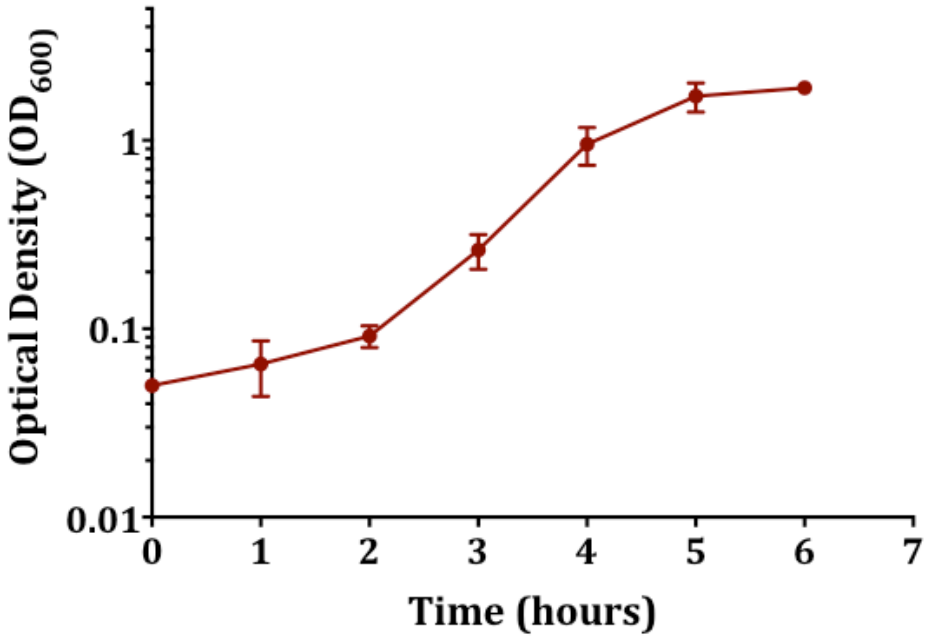

Figure 4.1. **Growth of *B. subtilis* WT in NB.** Change in optical density of the culture was assessed by measuring the OD_{600} every hour over 6 hours, as denoted by the plot in red. Error bars denote Standard Error for 2 culture repeats.

at different time intervals in order to observe changes to cell wall PG during growth and division. Furthermore, all *B. subtilis* WT cells examined during fluorescent imaging experiments were used in live cell microscopy, in order to directly observe PG *in vivo*.

4.2.2.1 Use of a fluorescent vancomycin probe

B. subtilis WT cells were labelled with fluorescent vancomycin for 5 minutes during the mid-exponential phase of growth. Fluorescent vancomycin binds to D-Ala D-Ala residues in the peptide side chain of PG, and was therefore used as a dye for binding sites of nascent PG synthesis. However, it must be noted that vancomycin can also bind Lipid II in the cell wall, as well as D-Ala D-Ala residues in PG. It seems that the pool levels of Lipid II are higher in Gram-positive organisms compared with Gram-negative, in agreement with these organisms' known higher peptidoglycan content (Heijenoort, 2007). In *Bacillus megaterium*, the lipid II pool was estimated at 34,000 molecules per cell (Fuchs-Cleveland and Gilvarg, 1976).

The full field image generated from this experiment showed the characteristic rod-shaped cell morphology, measuring approximately 2-4μm in length and 1μm in width (**Figure 4.2**). In addition, the cells appeared to have divided into chains of rods. The fluorescent vancomycin bound to the outermost layer of *B. subtilis* WT in a heterogeneous pattern i.e. to the cell wall PG. In most cases the cells were imaged during division. Partial and complete cell septum formation can be observed in most cells in the image field. Increased vancomycin binding at the septa occured as this is a site of

nascent PG synthesis. Furthermore, foci of vancomycin binding were observed at some curved cell poles. These cells may well have just completed a cycle of growth and division as a cell pole is formed from the previous septum, thus explaining the presence of nascent PG. Examination of vancomycin binding to *B. subtilis* WT at higher magnification reveals further features of the cell wall (**Figure 4.3**). At higher magnification, the rod-shaped morphology of *B. subtilis* WT was again displayed when fluorescent vancomycin bound to the cell wall PG, particularly at the septa (**Figure 4.3**). In addition, further foci of vancomycin binding were distinguished across the short axes of the cell cylinders. When detected at the centre of the cell, it is possible that these foci indicated the next site of septal placement for cell division. Also, PG is synthesised across the cell cylinder during elongation of the *B. subtilis* rod-shape (prior to division).

4.2.2.2 Labelling *B. subtilis* WT with fluorescent amino acids

Sites of active PG synthesis were labeled using fluorescent D-amino acids (FDAAs) developed by Kuru et al., (2012). FDAAs have small fluorophores attached to D-Amino acid (DAA) backbones. When added during growth, these are incorporated into the peptide side chain of PG. Analysis of FDAA-modified muropeptides in *B. subtilis* indicated that FDAAs were exclusively incorporated in the fifth position of the stem peptide (Kuru et al., 2012). A few different FDAAs were available for use in imaging experimentation,

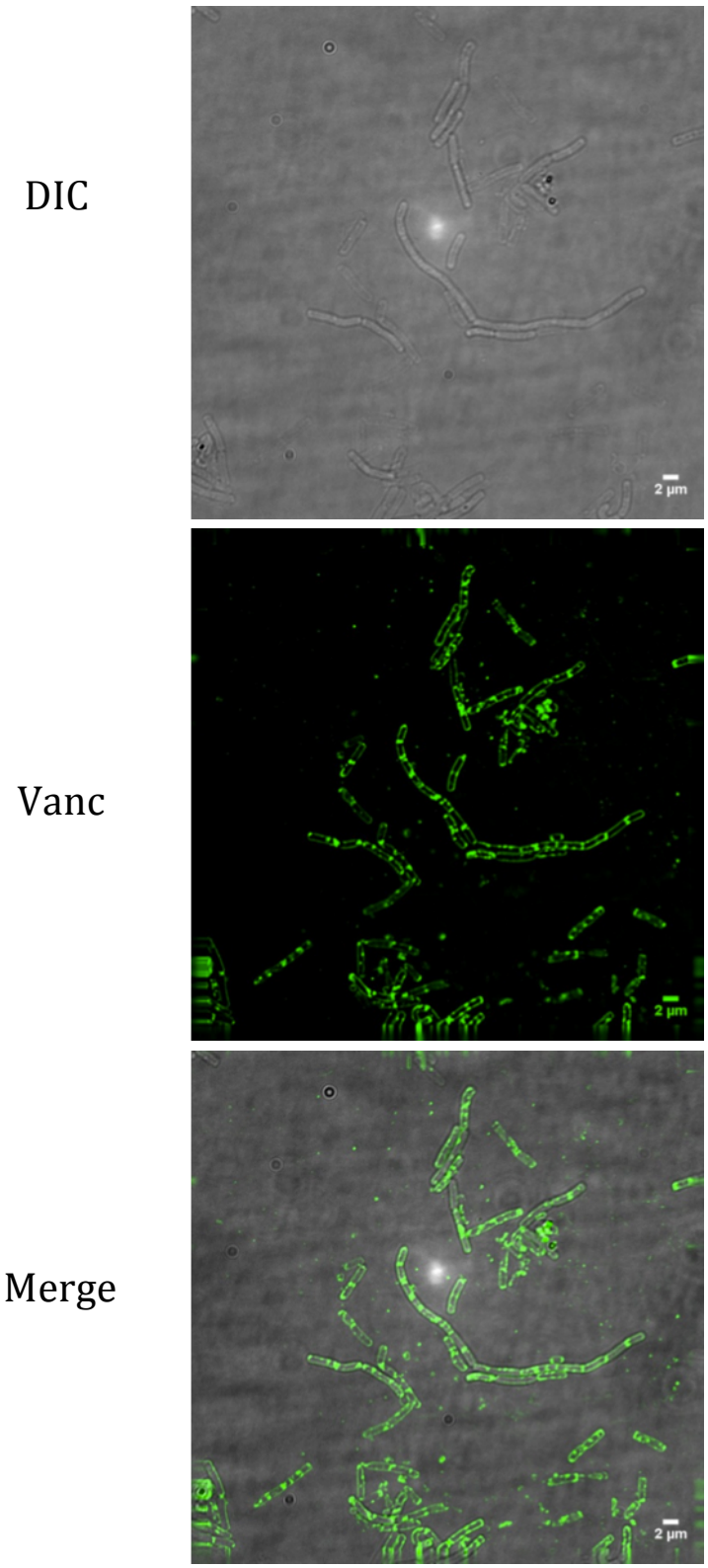

Figure 4.2. WT *B. subtilis* vegetative cells labelled with vancomycin and examined by epifluorescence microscopy. Each image shows an entire microscopic field of cells. Cell walls are labelled green with Vancomycin BODIPY-FL (Vanc), which binds D-Ala D-Ala residues in the PG. Cells were not fixed prior to viewing.

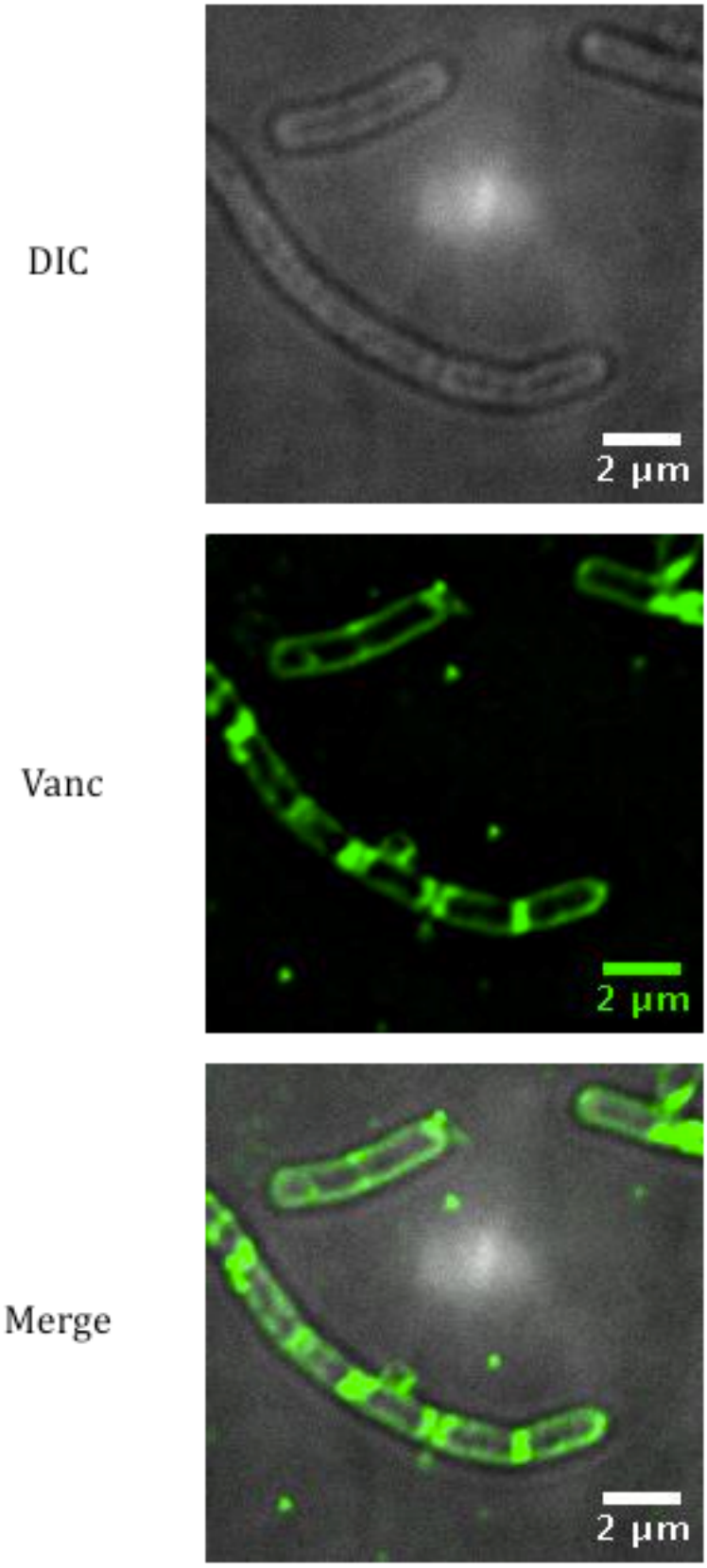

Figure 4.3. High magnification of WT *B. subtilis* vegetative cells labelled with vancomycin and examined by epifluorescence microscopy. Each image field shows a few vegetative cells. Cell walls are labelled green with Vancomycin BODIPY-FL (Vanc), which binds D-Ala D-Ala residues in the PG. Cells were not fixed prior to viewing.

which fluoresced at different wavelengths of light, depending on which fluorophore was attached. FDAA fluorescence was detected using epifluorescence microscopy which when combined with their specificity for nascent PG thus allowed direct imaging of *B. subtilis* WT PG synthesis.

The first experiment utilizing FDAAs involved incubating a sample of mid-exponential phase *B. subtilis* WT with HADA (a blue-fluorescing FDAA; emission maximum 450 nm (Kuru et al., 2012)) for 5 minutes at 37°C and examining these cells using epifluorescence microscopy (**Figure 4.4**).

The full field image generated from this experiment shows a clear and strong incorporation of HADA into the outermost peripheral layer of all cells. As with the vancomycin labelling, the characteristic rod-shaped morphology of *B. subtilis* WT was evident. As the complete cell outline was labelled with HADA, it was possible to view the cells without the need for the merged DIC and fluorescence overlay, as shown in the image showing just the HADA fluorescence emission. Due to the previously published specificity of FDAAs (Kuru et al., 2012), it was assumed that the HADA was therefore directly incorporated into the fifth position of the stem peptide in the cell wall PG. As well as being incorporated into the cell wall PG, the HADA also showed a strong binding specificity for the septa. This was expected, as FDAAs naturally incorporate into areas of nascent PG synthesis. The formation of septa during division is a site where most nascent PG synthesis would occur,

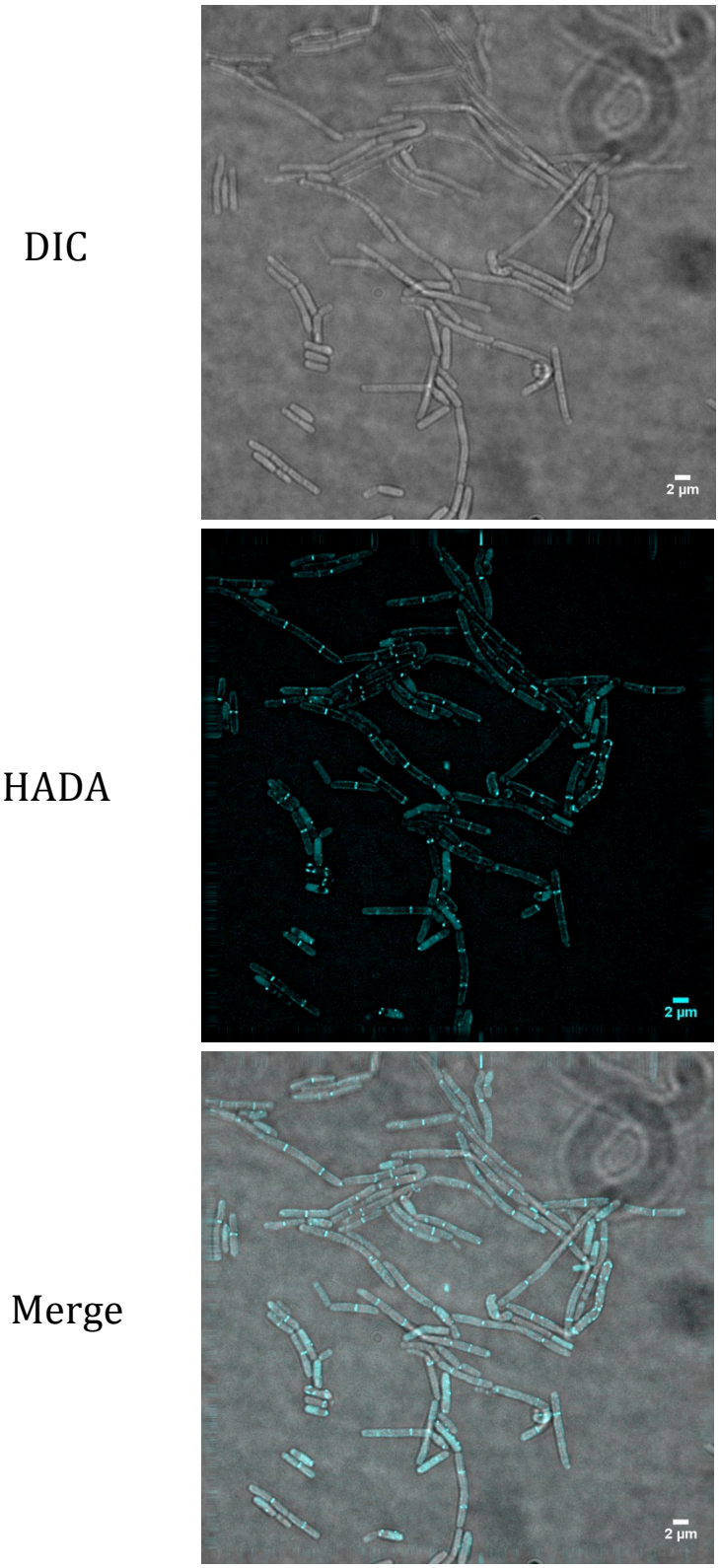

Figure 4.4. WT *B. subtilis* vegetative cells labelled with HADA and examined by epifluorescence microscopy. Each image shows an entire microscopic field of cells. Cell walls are labelled cyan with HADA, an FDAA that is incorporated into cell PG.

hence the increased incorporation of HADA into this area of the cell. Interestingly however, unlike fluorescent vancomycin, the HADA seemingly did not show as much incorporation into the cell poles. This may mean that the poles retain terminal D-Ala D-Ala residues after synthesis, to a greater extent than the rest of the cell.

Examination of a selection of HADA-labelled *B. subtilis* WT cells at higher magnification elucidated further information about nascent PG synthesis. (**Figure 4.5**). The high levels of HADA incorporation into cell septa were even more apparent at high magnification. In addition, the formation of a new septum in a dividing cell, which has incorporated HADA into its nascent PG, can be seen at the centre of the image (indicated by a white arrow, **Figure 4.5**). Bands of HADA incorporation into nascent PG across the short axis of the cells that are not septa were also detected. This was considered to be potential evidence of PG growth across the cell cylinder as part of elongation.

In order to determine how PG synthesis is organised temporally, a range of HADA incorporation times were used. Cell samples were taken from a *B. subtilis* WT culture during mid-exponential phase and labelled with HADA for 5, 10 and 20 minutes at 37°C. These samples were then examined by epifluorescence microscopy (**Figure 4.6**). All the timepoints showed a similar pattern of labeling. This suggested that the position 5 D-amino acid in PG is turned over after synthesis.

In order to further dissect the temporal dynamics of PG synthesis, a pulse-chase experiment was carried out using two FDAAS with different emission

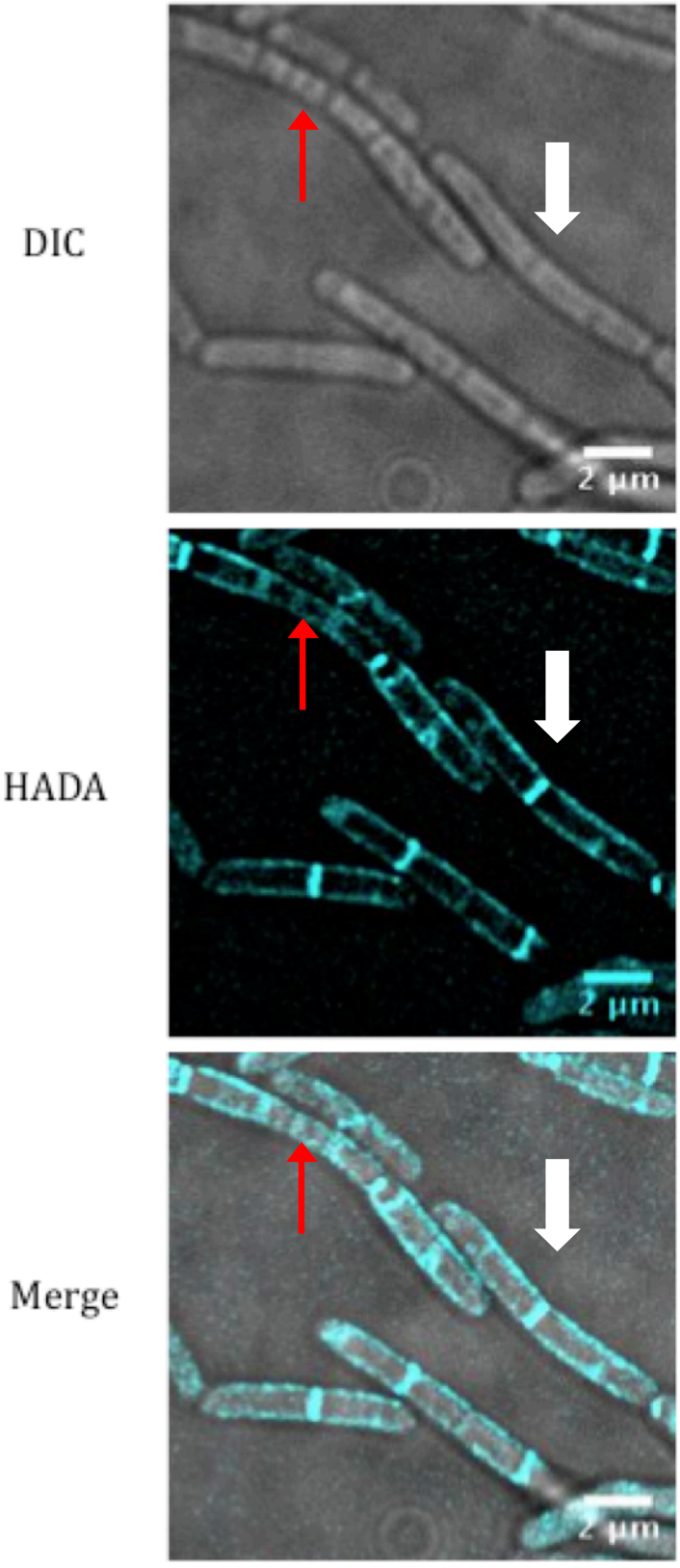

Figure 4.5. High magnification of WT *B. subtilis* vegetative cells labelled with HADA and examined by epifluorescence microscopy. Each image field shows a few vegetative cells. Cell walls are labelled cyan with HADA, an FDAA that incorporates into cell PG. The white arrow indicates the formation of a new septum in a dividing cell and the red arrow shows non-septal bands of HADA incorporation.

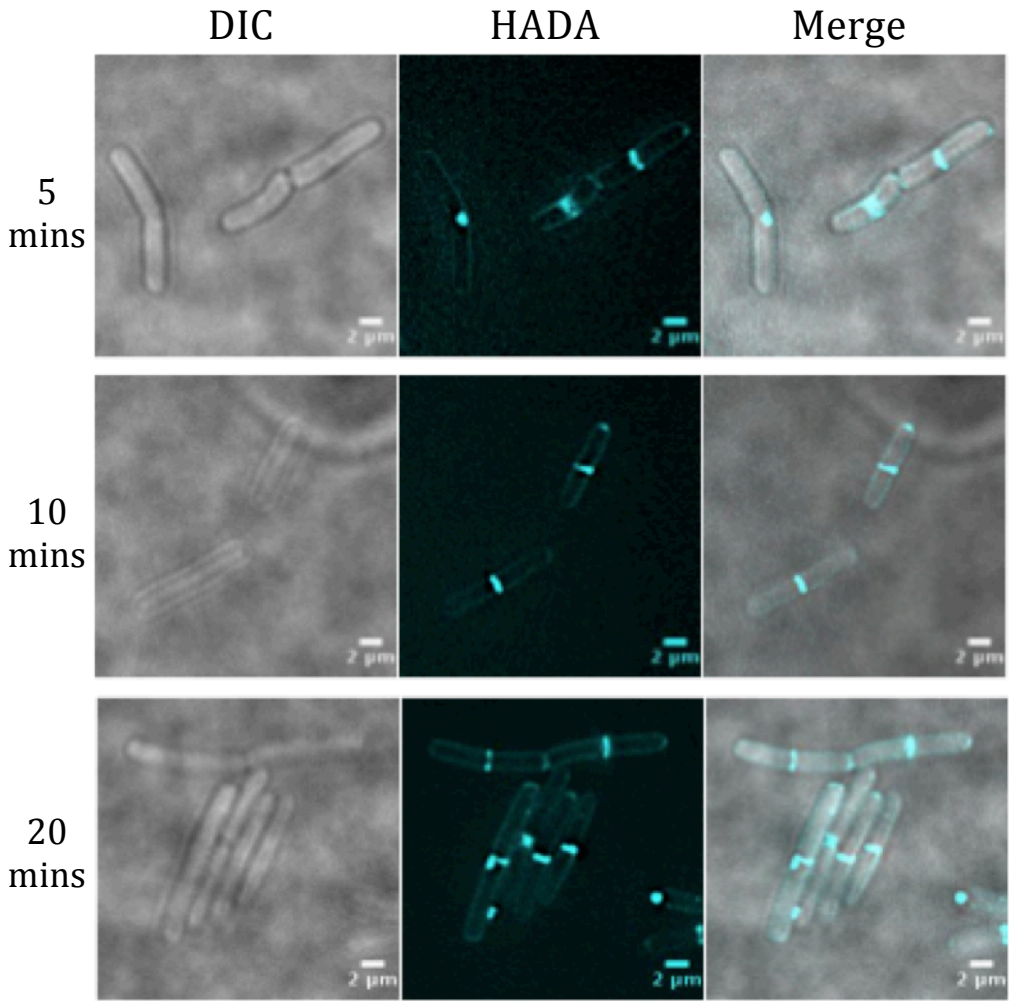

Figure 4.6. High magnification WT *B. subtilis* vegetative cells labelled with HADA for different amounts of time and examined by epifluorescence microscopy. Each image field shows a few vegetative cells. Cell walls were labelled cyan with HADA, an FDAA that incorporates into cell PG. Separate cell samples (grown in NB) were taken and labelled for 5, 10 and 20 minutes.

wavelengths. The use of two differently coloured FDAAs allowed the detection of pre-existing PG and the subsequent differentiation of new PG synthesized during 30 minutes growth. The combination of NADA (green-fluorescing) and HADA (blue-fluorescing) was used to target and dye sites of nascent PG in *B. subtilis* WT during growth in NB. A small sample of this culture was taken during mid-exponential phase of growth and labelled initially with NADA for 5 minutes at 37°C, i.e. pulsing the cells with an initial stain. NADA-incorporated cells were harvested, resuspended in NB and incubated at 37°C for a further 30 minutes. The sample was then labelled with HADA for 5 minutes at 37°C, i.e. the new PG synthesis was chased using a new dye. The final cell sample (initially pulsed with NADA then chased with HADA after 30 minutes' growth) was imaged using epifluorescence microscopy. The image field was photographed using two fluorescence filters to allow detection and differentiation of both dyes. These two emission filter images were then merged to create a final image showing where both FDAAs had been incorporated (**Figure 4.7**). The NADA labelled the sites of nascent PG; the outermost layer of the cell wall and the cell septa. In comparison, the labelling of the HADA-chased cells revealed much brighter fluorescence at the septa. This is likely due to turnover of NADA incorporation and utilisation of new sites of PG synthesis. Wherever the two FDAAs bound to the same site of PG synthesis, the merged image showed purple fluorescence as a combination of the NADA and HADA colour merging (magenta and cyan respectively). The merged image clearly shows HADA incorporation at septal sites. The original NADA binding during the 'pulse' along the cell cylinder

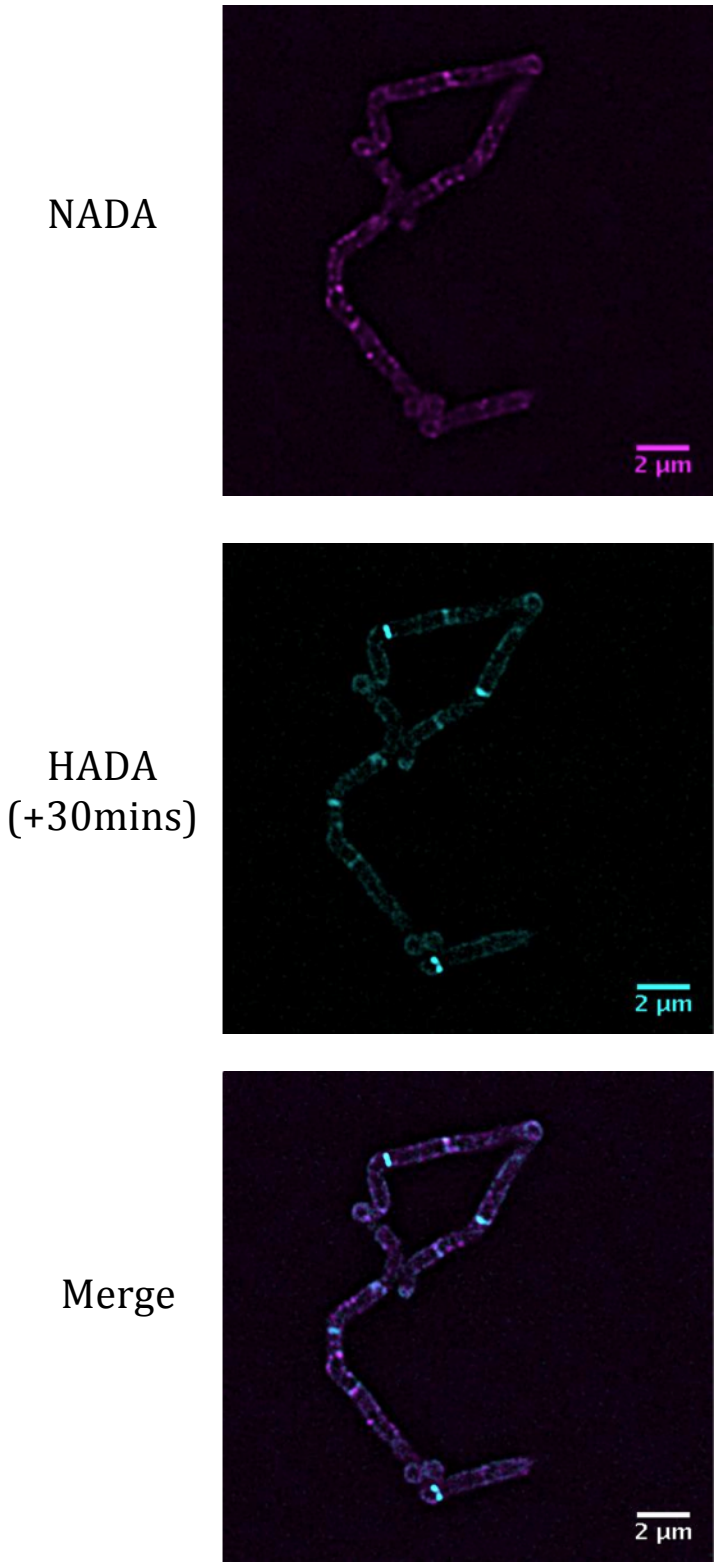

Figure 4.7. WT *B. subtilis* vegetative cells: labelled with NADA, grown for 30 minutes then also labelled with HADA; examined by epifluorescence microscopy. HADA and NADA are FDAAs that incorporate into cell PG. Each image shows a few vegetative cells. Cell walls are labelled magenta with NADA and cyan with HADA. The merged image shows purple areas where both dyes are detected.

shows that this septal material is constructed during the 'chase' period.

4.2.3 Examination of *B. subtilis* WT PG using super-resolution fluorescence microscopy

In order to examine *B. subtilis* cells using STORM, a sample was taken from a mid-exponential phase culture of NB and labelled with STORM-compatible fluorescent Vancomycin 532.

The Vancomycin-labelled cells were then examined using STORM in collaboration with R.D. Turner. The total fluorescence emitted by the bound Vancomycin fluorophores during the imaging cycles was reconstructed to create an image (**Figure 4.8**). The cell walls and septa were labelled due to the binding of Vancomycin to the D-Ala D-Ala residues in the cells' PG. While this information was not technically different to the information provided from studying Vancomycin-labelled *B. subtilis* WT using epifluorescence microscopy, the increased resolution of STORM compared to epifluorescence was immediately obvious in the two dividing cells depicted. This therefore provided an improvement to the Vancomycin labelling of cells by increasing the microscopic resolution.

The next technique adapted for STORM was the utilisation of FDAAs in labelling *B. subtilis* WT cell walls. However, the FDAAs used previously in this study were not compatible with STORM as they do not have photo-switchable fluorophores. Therefore, the cells were labelled using click chemistry fluorophores compatible with the STORM microscope. In this study, the click reaction involved the copper-catalysed cycloaddition of an azide fluorescent probe to D-amino acids. Upon activation of the click

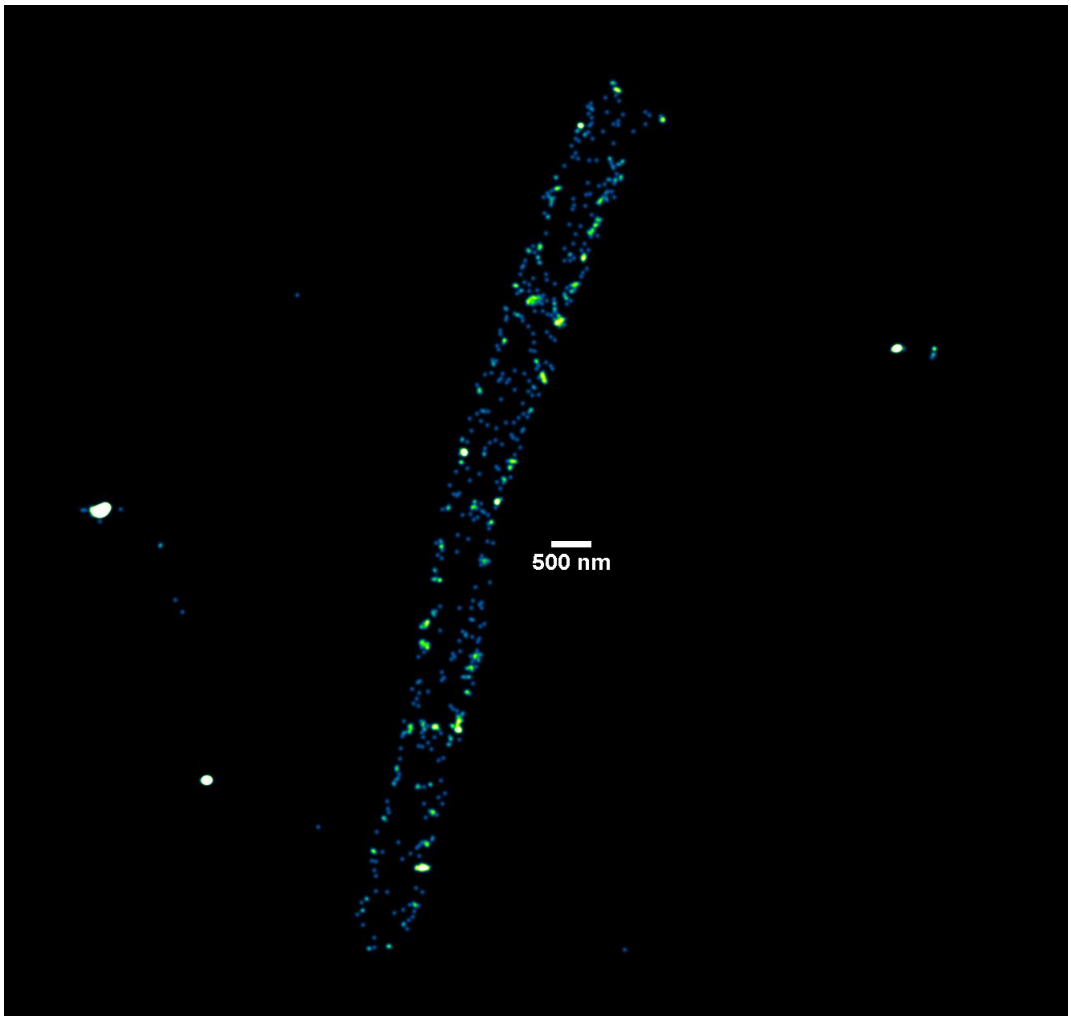

Figure 4.8. WT *B. subtilis* vegetative cell labelled with fluorescent vancomycin and examined by STORM. The 2D image shows two dividing WT *B. subtilis* cells. Cell walls are labelled blue-green with Vancomycin (Vanc-532), which binds D-Ala D-Ala residues in the PG. The colour used indicates density of labelling, i.e. more green rather than blue indicates more bound vancomycin. Image in collaboration with R.D. Turner.

reaction using copper, the D-amino acids then fluoresce (Kuru et al., 2012; Li et al., 2010; Shieh et al., 2014).

B. subtilis WT cells were grown in the presence of a click-compatible D-amino acid in collaboration with V.A. Lund. The click-compatble FDAA was incorporated into the peptide side chains of nascent PG (as with FDAAS). This was followed by the addition of the photoswitchable click fluorophores, which bound these D-amino acids. The fluorophores were then covalently bound using the click reaction and the sample examined by STORM, in collaboration with R.D. Turner. The fluorescence emitted by the amino acid click-labelled cells during the imaging cycles was reconstructed (**Figure 4.9**). As with the STORM images of Vancomycin labelling, the improved microscopic resolution compared with epifluorescence microscopy is obvious. This image showed that the amino acid was incorporated mainly to the peripheral cell wall PG, where the rod shape of the cell is highlighted by the bound fluorophores. Furthermore, the amino acid was also concentrated at the cell septum, where the nascent PG synthesis occurred. Interestingly, the amino acid also incorporated in bands across the short axis of the cell. This was detected during epifluorescence microscopic examination of FDAA labelling and Vancomycin labelling of *B. subtilis* WT but was suggested to be a possible artefact created by the resolution limit of the technique. However, this banding pattern was detected at STORM resolution (20-30nm), which therefore confirms its presence during *B. subtilis* WT growth. Such a banding pattern is reminiscent of the PG architecture revealed by AFM where cabled

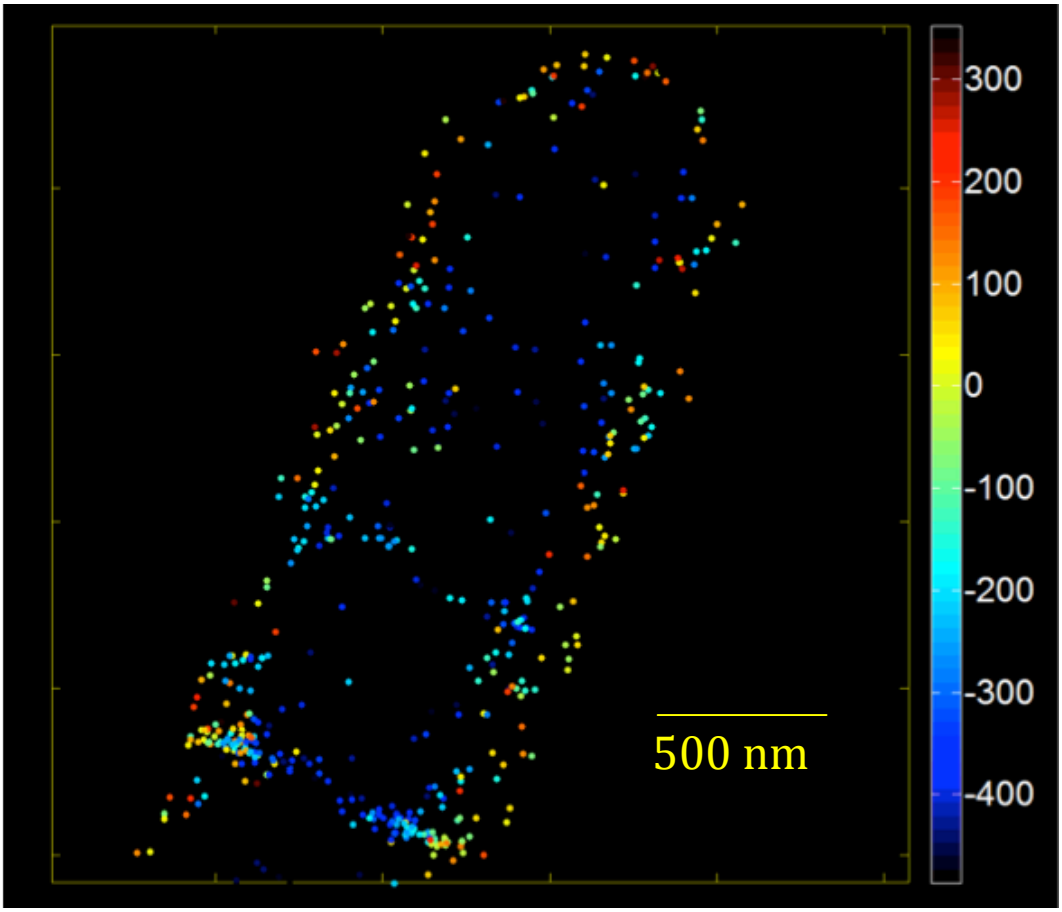

Figure 4.9. WT *B. subtilis* labelled with clickable amino acid and examined by STORM. Cell walls are labelled with clickable amino acid that was incorporated into cell PG and fluoresced following the addition of a fluorophore during the click reaction. The vertical scale represents the height/depth of the Z-axis in nm. Image in collaboration with R.D. Turner and V.A. Lund.

of material have been shown to be running across the short axis of the *B. subtilis* cylinder (Hayhurst et al., 2008)

4.2.4 AFM analysis of *B. subtilis* WT peptidoglycan architecture

Atomic Force Microscopy (AFM) was previously utilised as a method of examining the architectural features of the bacterial cell wall PG (Hayhurst et al., 2008; Turner et al., 2010, 2013; Wheeler et al., 2011).

In this study, *B. subtilis* WT PG sacculi were examined by AFM. *B. subtilis* WT cells were mechanically broken and purified by boiling in SDS, pronase treatment and incubation in HF to remove all non-covalently and covalently bound wall polymers including teichoic acids. The only remaining material was therefore PG sacculi. Sacculi were air-dried onto a clean mica-sheet and imaged by AFM in tapping-mode under ambient conditions. A typical field of sacculi is shown in **Figure 4.10**.

4.2.4.1 Gross architectural features of *B. subtilis* WT peptidoglycan

The topographical information provided by examination of purified PG sacculi of *B. subtilis* WT using AFM revealed interesting details about its gross architecture (**Figure 4.10**). The cell sacculi were broken across their short axes, as previously found by Hayhurst et al. (2008). This indicated that the orientation of PG architectural features run in a manner that is perpendicular to the longitudinal axis of the cell. The rod-shaped cylindrical morphology,

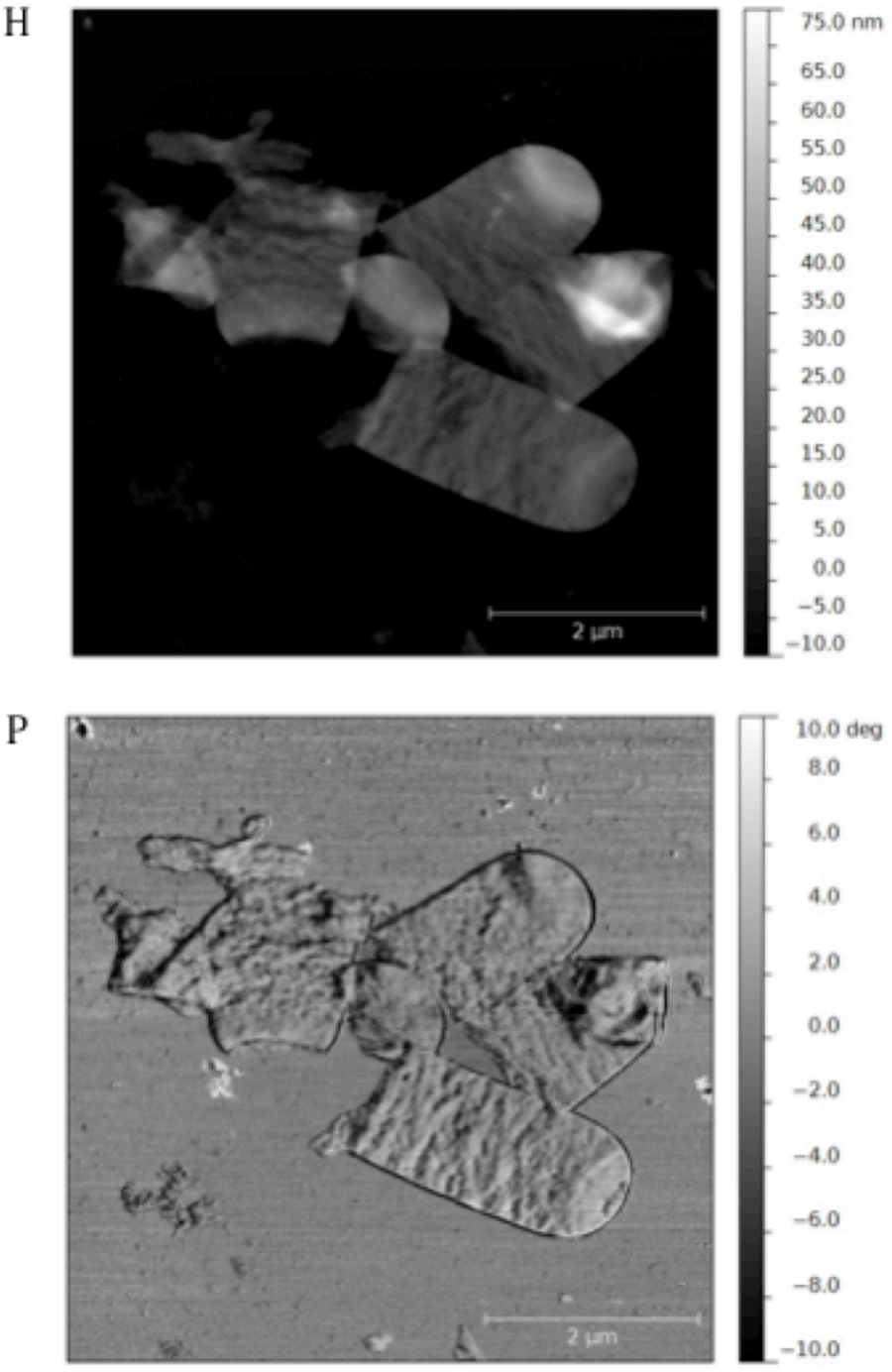

Figure 4.10. AFM analysis of purified WT *B. subtilis* PG sacculi. Height (H) and phase (P) images showing a typical field of broken *B. subtilis* sacculi dried onto a mica surface. The Z-axis scales on each image indicate the topographical height of the sample; the height image in nm and the phase image in relative degrees. Image in collaboration with E. Ratcliffe.

which is characteristic to *B. subtilis* WT, was retained by the sacculi. This indicated that PG architecture was the true provider of cell shape maintenance, as the cell morphology was preserved when only the PG itself was examined as purified sacculi. **Figure 4.11** shows an AFM image of two fragments of *B. subtilis* WT sacculi. Cross-striations of PG material are observed across the short axes of these PG fragments. This provides further evidence that PG is synthesized to create an architecture that is perpendicular to the longitudinal axis of the *B. subtilis* WT cell. Furthermore, the rough topographical texture of the sacculi was of varying thickness and heterogeneous, despite being composed of a single type of macromolecule, PG.

The data provided by this analysis supported the work carried out by Hayhurst et al.,(2008) that *B. subtilis* has a complicated PG architecture.

4.2.5 Analysis of the role of PG hydrolases in cell wall growth and architecture

In order to understand the dynamics of PG synthesis in *B. subtilis*, experiments were undertaken using the *B. subtilis* mutant strain BP115, provided by Kevin Devine. In this strain (P_{xyl}*yvcE*Δ*lytE*::*cm*^{r}), *yvcE* expression is inducible by xylose in a *lytE* null mutant background (Bisicchia et al., 2007). These two genes (*lytE* and *yvcE*) encode endopeptidase-type PG hydrolases. Whilst neither gene is essential alone, *B. subtilis* cells must have one or the other. If both proteins are absent, lateral cell wall synthesis and cell elongation are curtailed and cells cannot grow (Bisicchia et al., 2007).

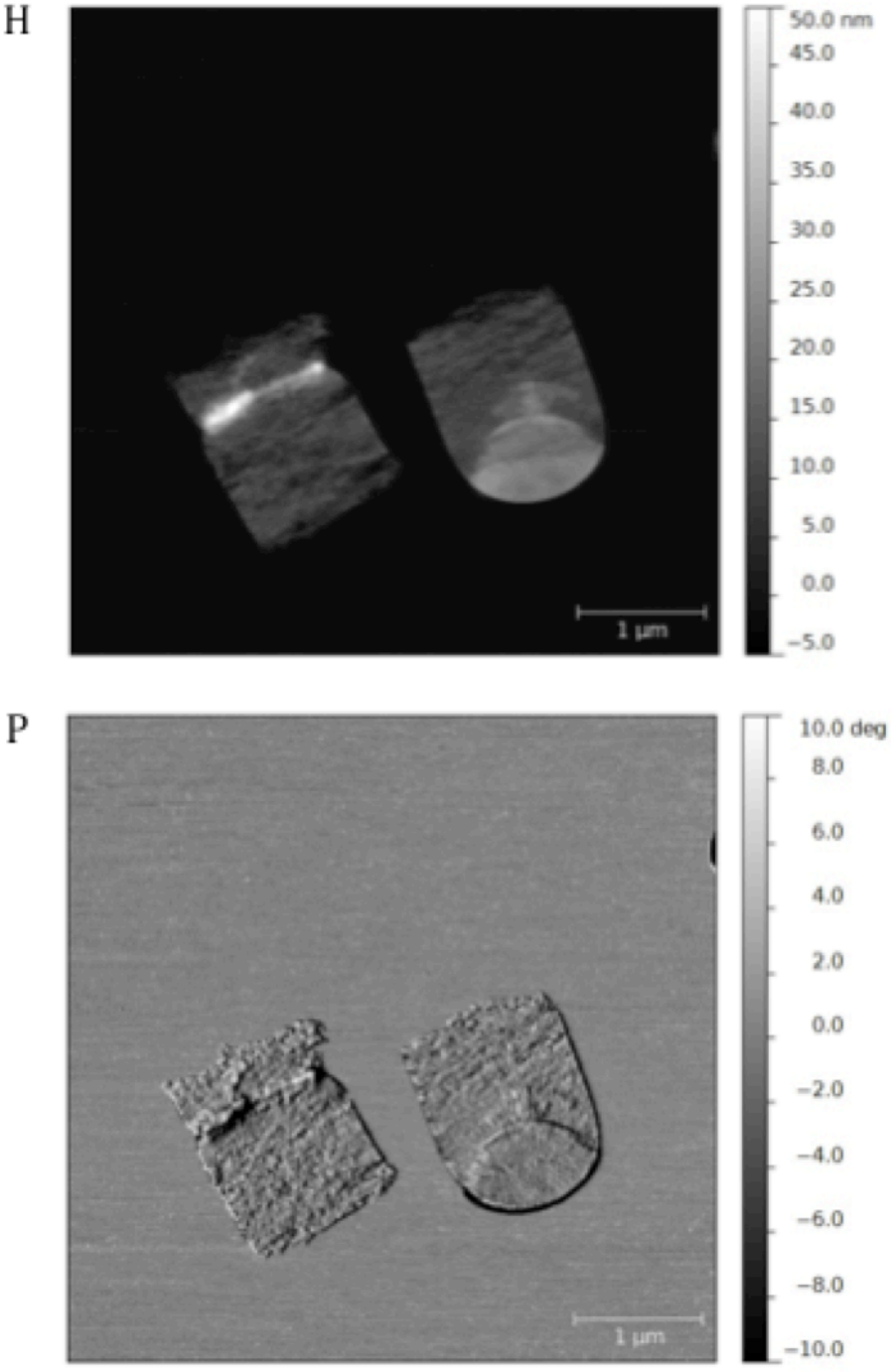

Figure 4.11. AFM analysis of purified WT *B. subtilis* PG sacculi. Height (H) and phase (P) images showing two separate fragments of broken *B. subtilis* PG sacculi dried onto a mica surface. The Z-axis scales on each image indicate the topographical height of the sample; the height image in nm and the phase image in relative degrees. Image in collaboration with E. Ratcliffe.

In order to determine the role of *lytE* and *yvcE* in cell wall dynamics, the effect of their loss on growth kinetics was first established by the growth of *B. subtilis* BP115 with and without 1% (w/v) xylose inducer. BP115 was grown in the presence of its inducer (1% (w/v) xylose) as a starter culture for 2 hours. This starter culture was then divided in two, harvested and each half resuspended to an OD of 0.05 and incubated for a further 2 hours; one with 1% (w/v) xylose and one without. Cell growth (OD_{600}) was monitored every hour (**Figure 4.12**). The blue starter culture plot showed exponential growth, indicating that the BP115 cells were growing normally in the presence of 1% (w/v) xylose. This growth was repeated by cells that were resuspended in the presence of 1% (w/v) xylose, as shown by the red plot. The xylose-induced cells' growth increased exponentially over 2 hours. This indicated that the growth of BP115 was unaffected if *yvcE* expression was induced. The cells from the starter culture that were resuspended without xylose grew initially for the first hour of incubation (denoted by the green plot). However, the xylose-starved cells' growth for the second hour of the incubation decreased, and in fact the yield declined. Therefore expression of *yvcE* is essential for cell growth in the absence of LytE.

Samples of the secondary culture, both xylose-induced and xylose-starved, were taken for use in further imaging experimentation.

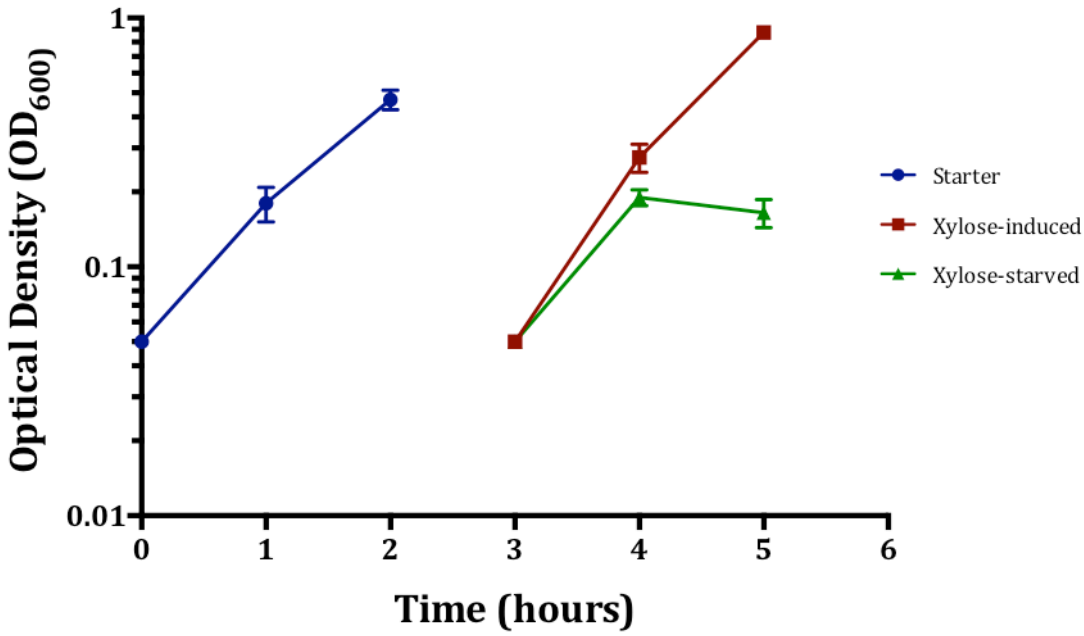

Figure 4.12. **Growth of *B. subtilis* BP115 in NB**. Changes to optical density were assessed by measuring the OD_{600} of the cell culture at hourly intervals. The growth of a starter culture grown in the presence of 1% xylose in NB is shown (blue plot). The starter culture was split and resuspended in NB with and without 1% (w/v) xylose (red and green plots, respectively). The error bars denote Standard Error.

4.2.6 Epifluorescence imaging of *B. subtilis* BP115 cells

The aim of this study was to determine the role of LytE and YvcE in PG dynamics. This would establish a potential link between alterations in cell wall morphology and the loss of endopeptidase activity. Samples were taken during mid-exponential growth, both with and without xylose induction. These samples were labelled using a variety of different fluorescent dyes/probes and approaches. These samples were then examined using epifluorescence microscopy. In addition, all *B. subtilis* BP115 cells examined during fluorescent imaging experiments were used in live cell microscopy, in order to directly observe PG *in vivo*.

4.2.6.1 Labelling of *B. subtilis* BP115 with fluorescent Vancomycin

B. subtilis BP115 cells with and without xylose induction were labelled with fluorescent Vancomycin for 5 minutes. Fluorescent Vancomycin binds to D-Ala D-Ala residues in the peptide side chain of PG, and thus binding is primarily associated with sites of nascent PG synthesis.

The Vancomycin-labelled samples were imaged using epifluorescence microscopy (**Figure 4.13**). The images of xylose-induced cells concur with those of *B. subtilis* WT previously discussed. The typical uniform rod-shape of *B. subtilis* cells is evident following xylose-induction of *yvcE*, with the cells measuring approximately 4μm in length and 1μm in width, despite the

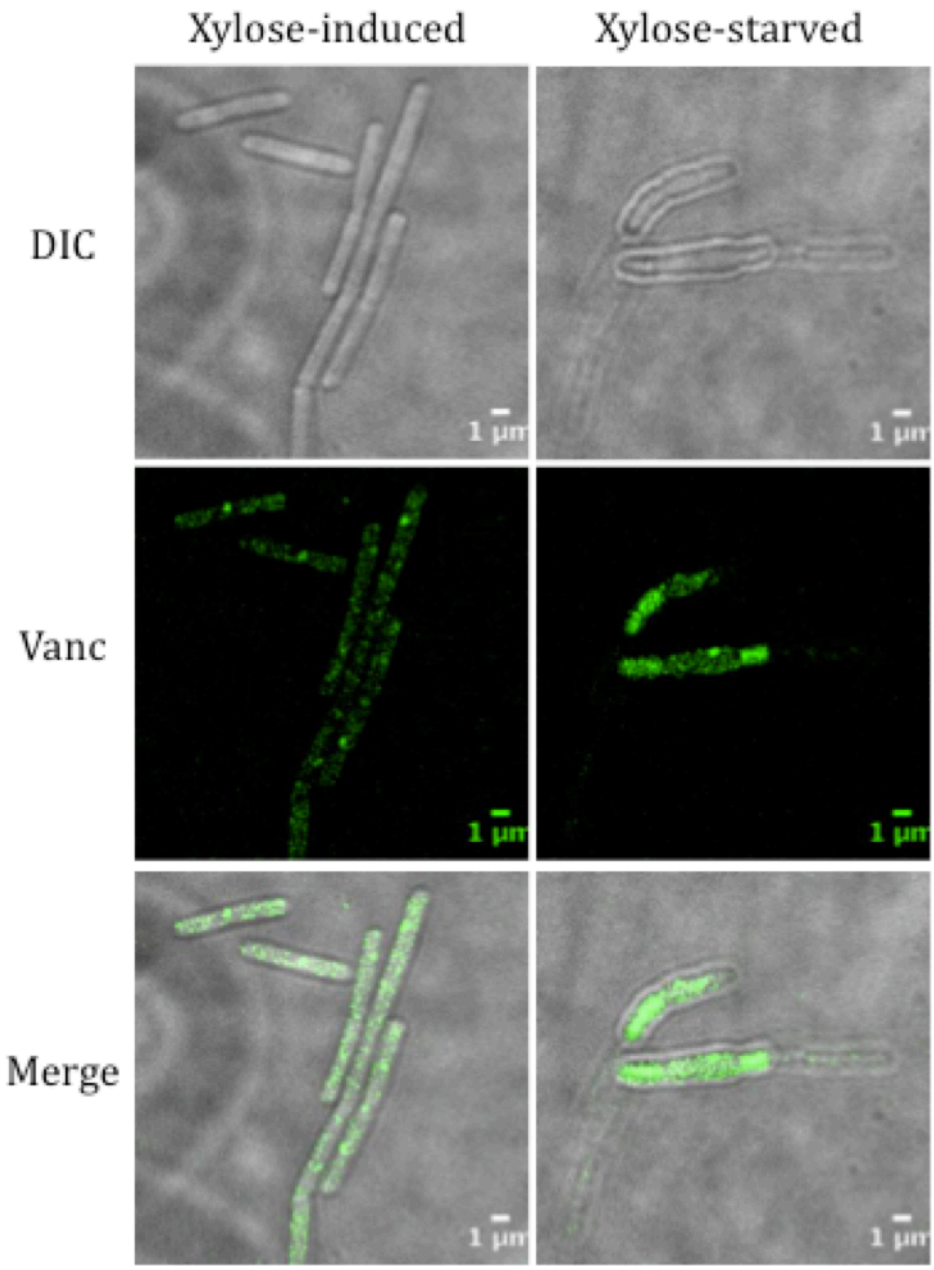

Figure 4.13. *B. subtilis* BP115 cells labelled with fluorescent vancomycin and examined by epifluorescence microscopy. BP115 was grown in the presence or absence of xylose for 90mins prior to fluorescent vancomycin labelling. These samples were examined by epifluorescence microscopy. Cell walls are labelled green with Vancomycin BODIPY-FL (Vanc), which binds D-Ala D-Ala residues in the PG.

absence of LytE. The pattern of Vancomycin labelling in xylose-induced BP115 cells was less reminiscent of the pattern exhibited by WT cells; the Vancomycin bound throughout the BP115 cells, showing no apparent specificity for the cell wall. However, some foci of Vancomycin binding were observed, possibly at septal sites, but these binding sites were not strongly fluorescent. Examination of the xylose-starved BP115 cells revealed an interesting morphology. Xylose-starved cells no longer had a constant rod-shape. The outermost layer of the xylose-starved cells appeared to be puckered in places and some areas of the cell appeared constricted across the short axis; this gave the cells a 'maggot-like' morphology. Furthermore, these possible belts of constriction gave the cells a 'blistered' appearance. The Vancomycin labelling of the xylose-starved cells was equally as unusual. Of the 3 cells shown in focus, only two showed any detectable Vancomycin binding at all. This occurred over repeats of this experiment, i.e. not all xylose-starved cells actually bound any fluorescent Vancomycin (images not shown). This is a direct contrast to the xylose-induced BP115 cells where all cells showed Vancomycin binding. Of the xylose-starved cells that did exhibit Vancomycin binding, the binding pattern itself also differed from that of the xylose-induced cells. The xylose-starved cells did not show uniform fluorescence, i.e. the Vancomycin bound to some areas of the cells more strongly than others. However, there seemed to be no clear pattern for this binding. It appeared as if the sites of nascent PG synthesis in xylose-starved BP115 cells were occurring randomly.

4.2.6.2 Incorporation of fluorescent amino acids into *B. subtilis* BP115 cell walls

The next step in the characterisation of *B. subtilis* BP115 morphology was the utilisation of FDAAs in imaging experiments, as used previously with *B. subtilis* WT cells. FDAAs were used in this study on both xylose-induced and xylose-starved BP115 cells.

B. subtilis BP115 cells were sampled following xylose-induction and xylose starvation. These samples were incubated with HADA and imaged by epifluorescence microscopy (**Figure 4.14**). All xylose-induced BP115 cells were uniformly rod-shaped and the cell measurements were generally as for WT cells; approximately 3-4μm in length and 1μm in width. (histograms of total cell measuremnts were not produced for this experiment). The xylose-induced cells showed a HADA incorporation pattern and morphology similar to *B. subtilis* WT cells. HADA incorporation was distinct, so much so that the characteristic rod-shape of *B. subtilis* was clear, even when only viewing the cells using fluorescent light. In contrast, the xylose-starved BP115 cells showed a markedly different morphology. The characteristic rod-shape observed in the xylose-induced cells had been lost, replaced by a more stunted and curved shape. As observed in the Vancomycin labelling experiment, the xylose-starved cells' outermost layer also appeared puckered and uneven in some areas. The possible constriction of the cells across their short axes was also evident. The incorporation of HADA into the xylose-starved cells' nascent PG was particularly unusual. The HADA showed

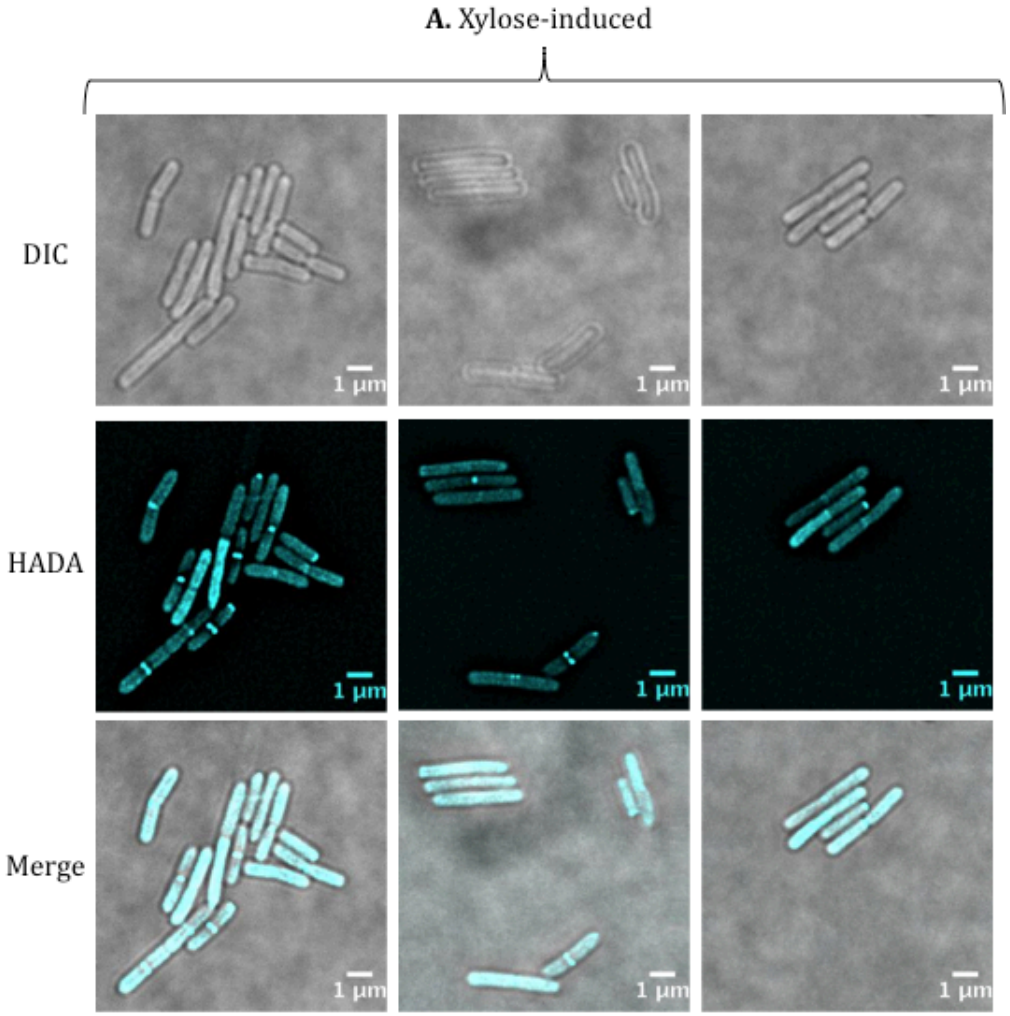
A. Xylose-induced
DIC
HADA
Merge
1 µm

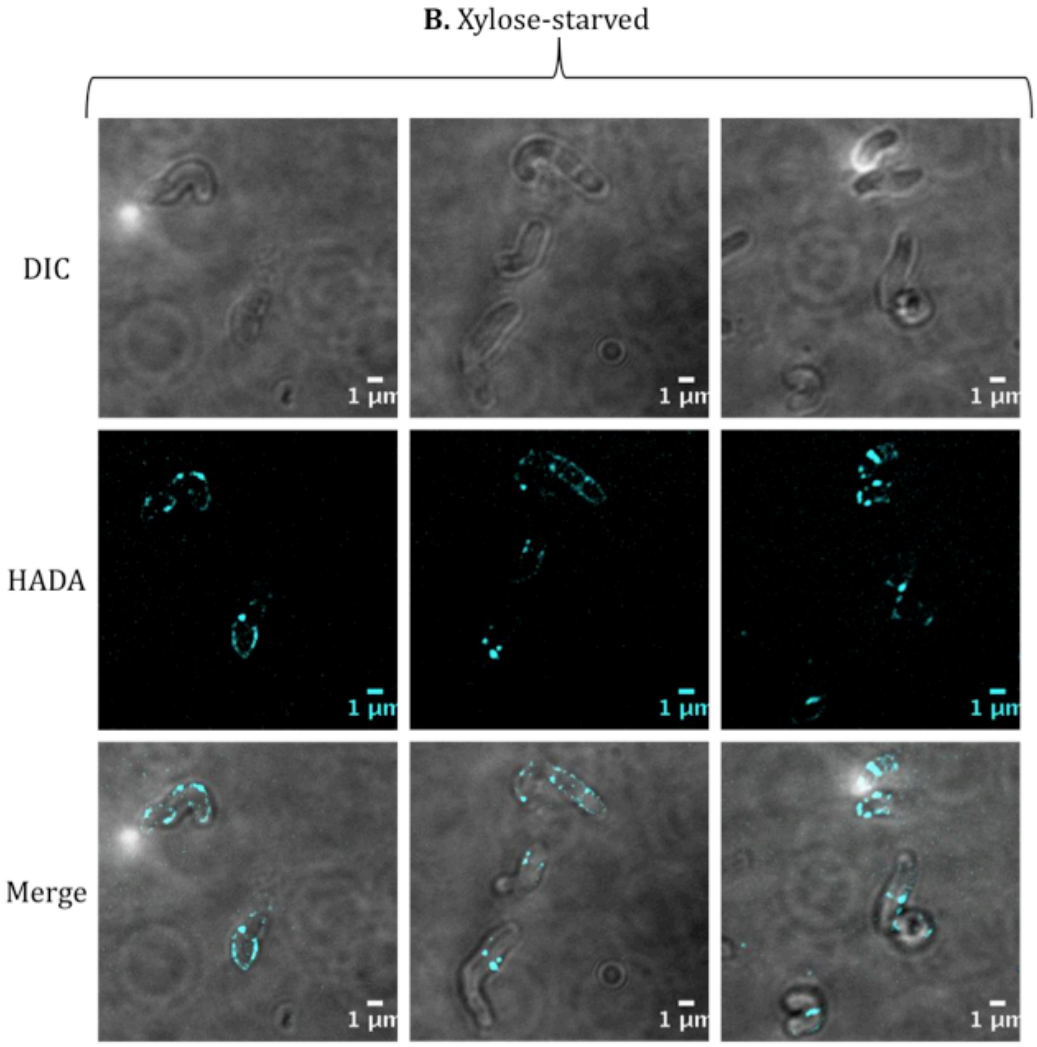

Figure 4.14. *B. subtilis* BP115 labelled with HADA (following xylose induction and starvation) and examined by epifluorescence microscopy. Panel **A** shows xylose-induced cells and Panel **B** shows xylose-starved cells. Cell walls were labelled cyan with HADA, a fluorescent D-amino acid which is incorporated into cell PG.

binding at some distinct areas of these cells, but never throughout the whole cell envelope. As HADA incorporates into sites of nascent PG synthesis, it is therefore likely that there are fewer sites of nascent PG occurring in xylose-starved cells than in xylose-induced cells. The HADA showed a preferential incorporation across the short axes of these cells, particularly in areas where a pronounced curvature of the cells morphology was also observed. It is possible that the HADA was incorporated into sites of septal placement, inaccurately prescribed by the cells themselves due to the lack of LytE and YvcE. These results demonstrate the correlation between *lytE* and *yvcE* expression and morphological changes to the cell. In addition, the incorporation of HADA into sites of nascent PG synthesis indicate that very little nascent PG synthesis occurs in cells where *lytE* and *yvcE* expression have been depleted.

The next step in the examination of BP115 cell morphology and PG synthesis was to utilise FDAAs in a pulse-chase imaging experiment to visually assess the effect of depletion of LytE and YvcE had on cell growth and subsequent PG synthesis. In this experiment, a small starter culture of *B. subtilis* BP115 cells was grown in the presence of 1% (w/v) xylose. All cells in this culture were labelled with NADA i.e. the cells were 'pulsed' with fluorescence. This culture was then halved, harvested and resuspended; one half was resuspended and incubated in the presence of 1% xylose and the other half was resuspended in the absence of xylose. Both samples were incubated for a further 90 minutes and then labelled with HADA i.e. the cells were 'chased' with another round of fluorescent labelling. The different fluorophores of

NADA and HADA allowed visual differentiation between the existing nascent PG and the effect of xylose induction and starvation on nascent PG synthesis after 90 minutes' incubation. These pulsed-chased- BP115 samples were examined using epifluorescence microscopy (**Figure 4.15**). The image showing the pre-split starter culture sample showed NADA incorporation throughout the cells' nascent PG, with increased binding at the cell walls and septa. The previously described rod shape of *B. subtilis* cells was also observed. The xylose-induced and xylose-starved cells retained the 'pulse' of NADA labelling. The xylose-induced cells in particular show the same pattern of NADA incorporation after 90 minutes of incubation, as well as the original rod-shaped morphology. In contrast, while the xylose-starved cells retained their NADA incorporation, the pattern of incorporation at the cell walls was lost and the cell morphology had changed. The xylose-starved cells had lost their original morphology and had become shorter, with a more curved shape (as seen in previous experiments). After 90 minutes' further incubation, the pulse of HADA labelling in the xylose-induced cells showed further incorporation of the second FDAA throughout the cell envelope. The HADA was incorporated at sites of nascent PG synthesis where the NADA pulse had previously bound. This was indicated by the merged purple fluorescence, created by the overlay of the magenta NADA and cyan HADA. The HADA was particularly visible alone at cell septa in the merged images where only the cyan fluorescence of the HADA chase was detected. This indicated that the nascent PG at the septa was associated with new sites of synthesis. The HADA labelling in xylose-starved cells showed a completely

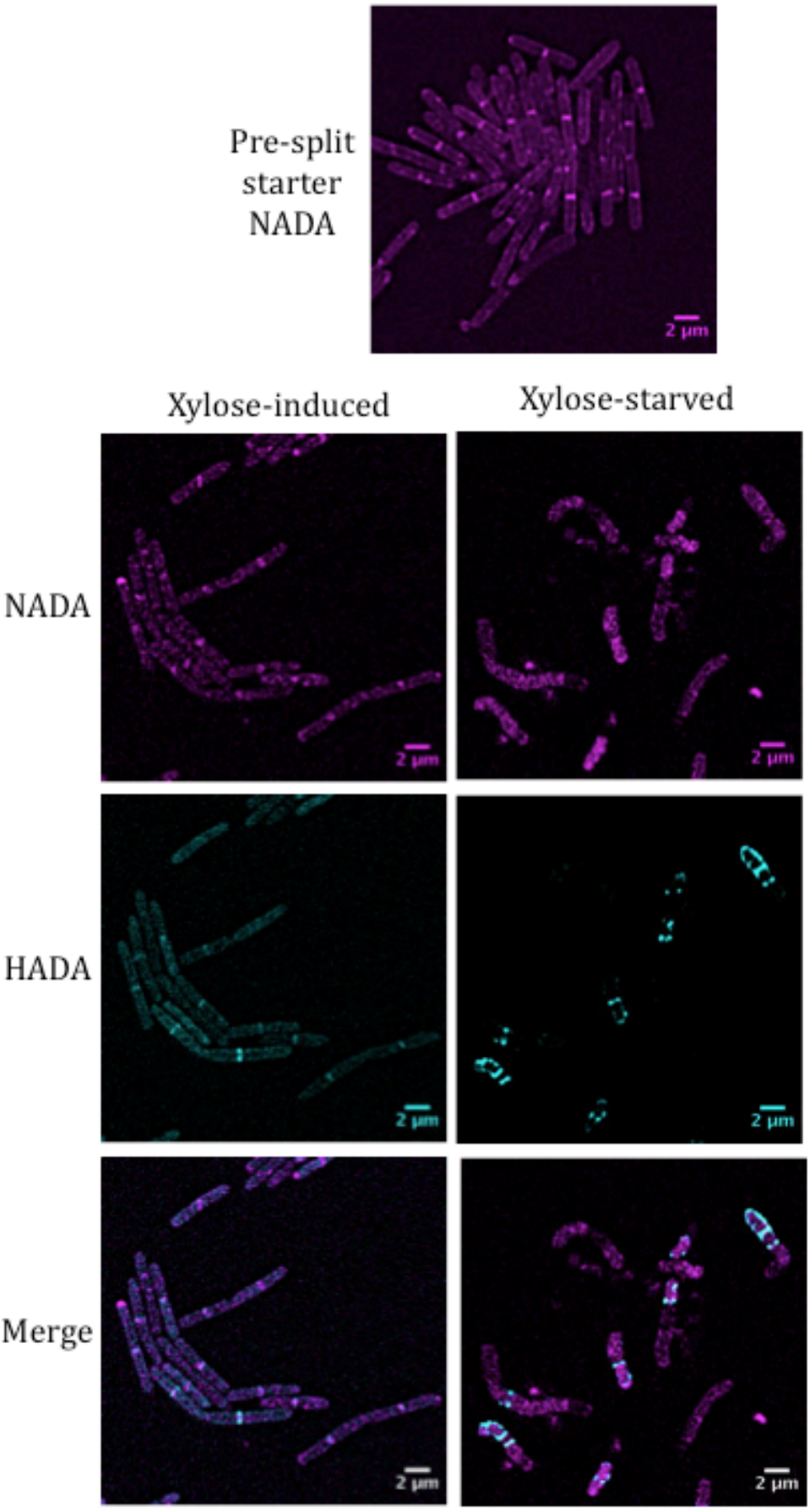
Pre-split starter NADA
Xylose-induced
Xylose-starved
NADA
HADA
Merge
2 µm

Figure 4.15 *B. subtilis* BP115 cells labelled with NADA and HADA in a pulse-chase experiment imaged using epifluorescence microscopy. A BP115 starter culture grown in the presence of 1% (w/v) xylose was labelled with NADA. An image of these pre-split starter culture cells labelled with NADA is shown. This NADA-labelled starter culture was split into two; one half grown in the presence of 1% (w/v) xylose and the other grown in the absence of xylose, both for 90 minutes incubation. Both cultures were then labelled with HADA and imaged using epifluorescence microscopy. BP115 cells were labelled with NADA and HADA (the pulse and chase), shown in magenta and cyan respectively.

different pattern of incorporation. The HADA pattern was patchy and only occurred at a few places. The HADA binding also occurred primarily at sites not previously labelled by NADA, as indicated by their cyan fluorescence in the merged image. Finally, as observed in the previous FDAA experiment using BP115 xylose-starved cells, bands of HADA incorporation were detected across the short axis of the cell. This experiment revealed even further details about this phenomenon; that some xylose-starved cells exhibited multiple bands of PG synthesis across the short axes of their cell cylinders.

These experiments ultimately demonstrated that *lytE* and *yvcE* expression in BP115 cells is essential for phenotypic control of the cell wall morphology. The absence of these proteins, as exhibited by the xylose-starved cells, results in very limited nascent PG synthesis throughout the cells as well as an abnormal cell morphology.

4.2.7 AFM analysis of *B. subtilis* BP115 xylose-starved peptidoglycan architecture

In this study, *B. subtilis* BP115 xylose-starved PG sacculi were subjected to examination by AFM to determine any correlation between abnormal cell morphology and PG architecture.

The cells were mechanically broken and purified by boiling in SDS, pronase treatment and incubation in HF to remove all non-covalently and covalently bound wall polymers including teichoic acids. The only remaining material was therefore PG sacculi. Sacculi were air-dried onto a clean mica-sheet and

imaged by AFM in tapping-mode under ambient conditions. A typical field of sacculi is shown in **Figure 4.16**. The BP115 xylose-starved

sacculi shown in this image fields were also frequently fragmented which was a potential indication of their weakened PG as a result of *lytE* and *yvcE* depletion.

The data provided by AFM examination showed that BP115 xylose-starved cell sacculi were much shorter and rounder than those of *B. subtilis* WT. This agreed with the information on these cells provided earlier in the study during epifluorescence microscopy. The previous experiments showed that the BP115 cells were distinctly shorter and more curved when starved of xylose and therefore depleted of *lytE* and *yvcE* expression. It is thus likely that it is the alteration of sacculus shape that gives the xylose-depleted cells their morphological defect.

In **Figure 4.17**, another image of BP115 xylose-starved cell sacculi examined using AFM show bands of constriction across the short axis with a bowed 'maggot-like' PG structure. These ridges of constricted PG were concentrated perpendicular to the longitudinal axis of the sacculi. The results of this AFM analysis showed that it was the PG itself that was affected by the lack of LytE and YvcE. Their loss leads to abnormalities in PG synthesis and architecture.

4.3 Discussion

This study aimed to further elucidate the complex PG architecture of *B. subtilis* and how it is maintained. This has given new insights into the role of

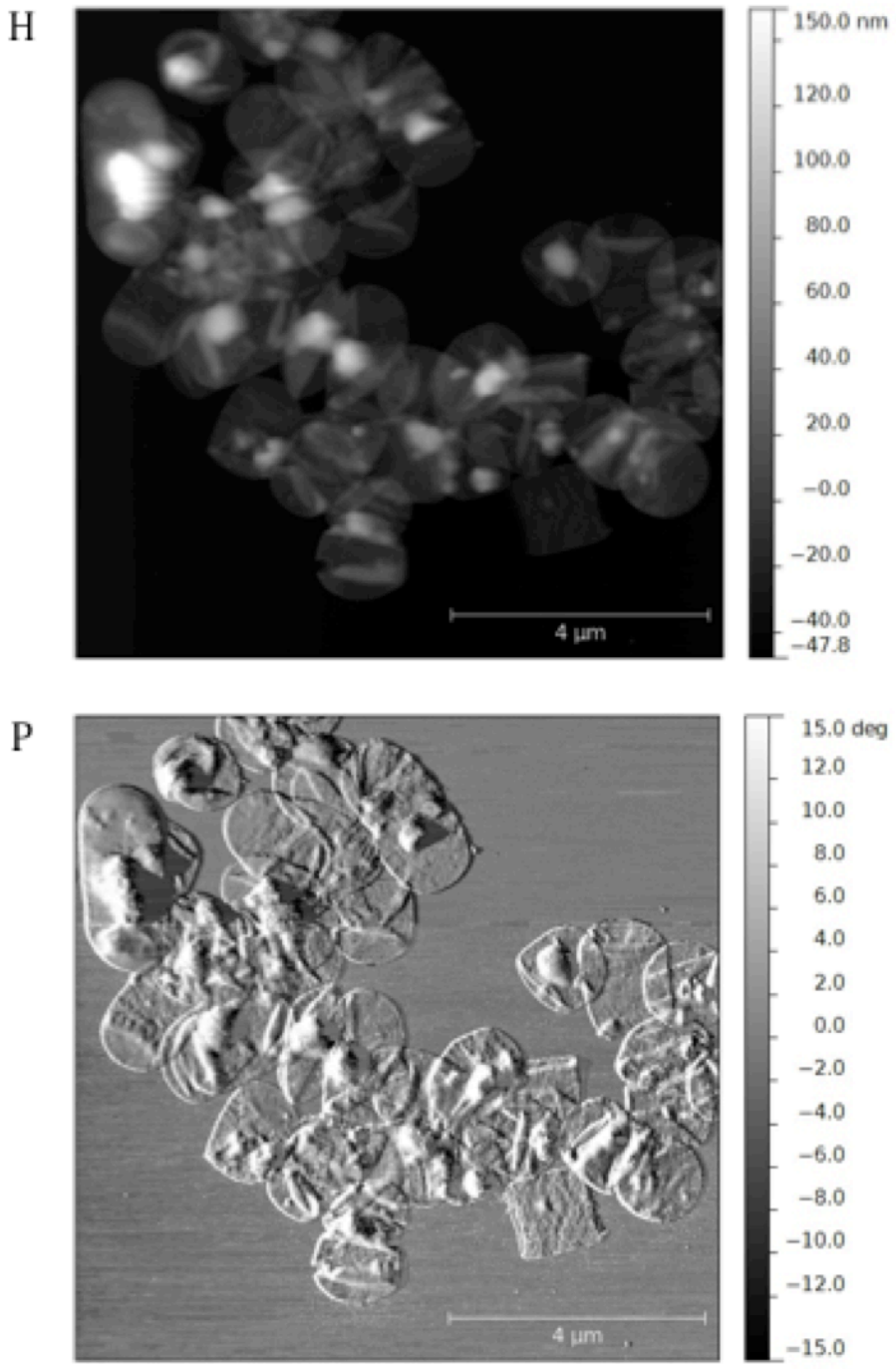

Figure 4.16 AFM analysis of purified *B. subtilis* BP115 sacculi derived from xylose-starved cells. Height (H) and phase (P) images showing a typical field of broken *B. subtilis* BP115 xylose-starved sacculi dried onto a mica surface. The Z-axis scales on each image indicate the topographical height of the sample; the height image in nm and the phase image in relative degrees.

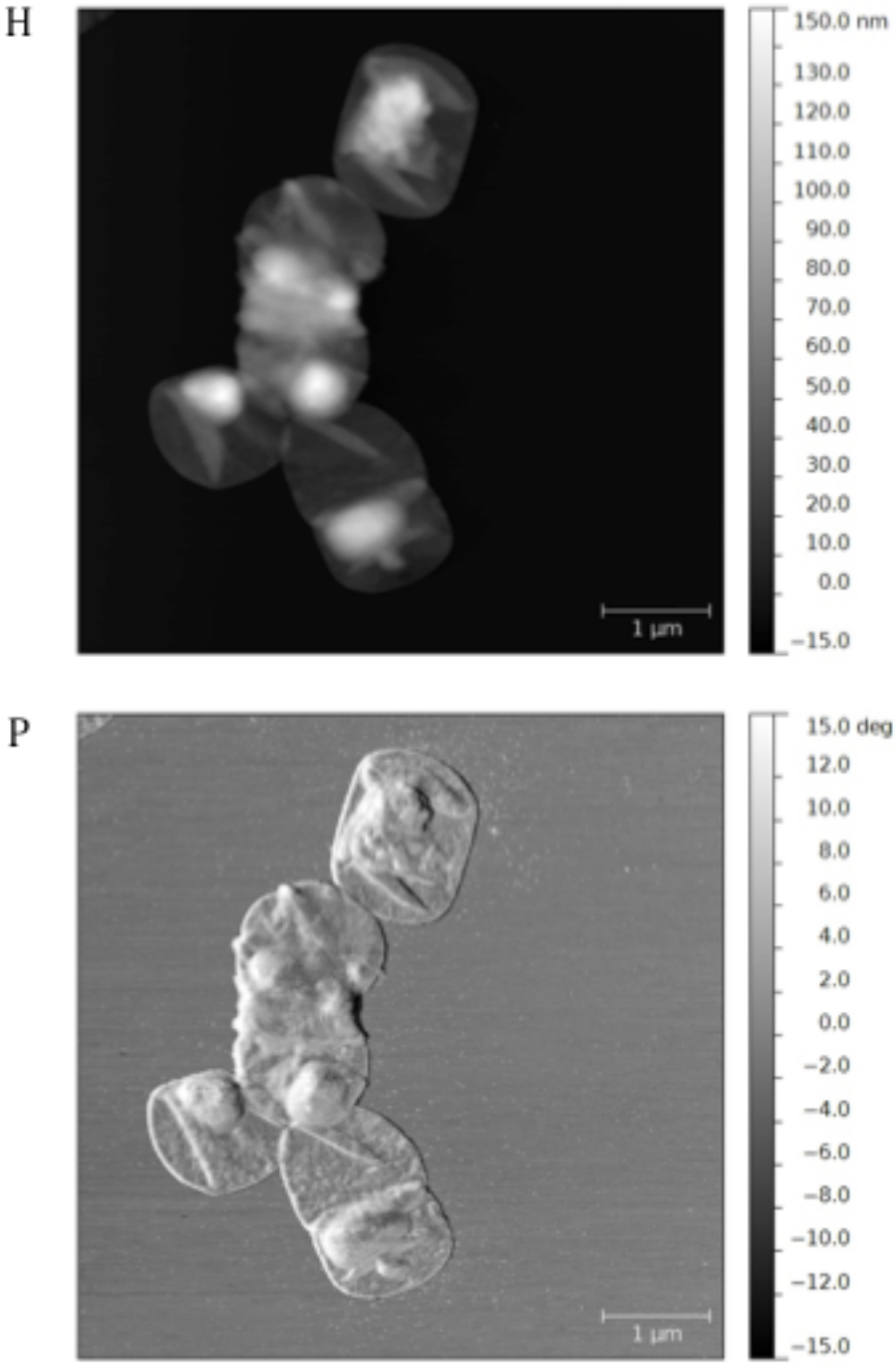

Figure 4.17. AFM analysis of purified *B. subtilis* BP115 sacculi derived from xylose-starved cells. Height (H) and phase (P) images showing a few broken *B. subtilis* BP115 xylose-starved sacculi dried onto a mica surface in closer detail. The Z-axis scales on each image indicate the topographical height of the sample; the height image in nm and the phase image in relative degrees.

PG as a macromolecule and how it provides the structural framework for the *B. subtilis* cell wall.

4.3.1 *B. subtilis* WT PG architecture and dynamics

Epifluorescence microscopy detection of fluorescent Vancomycin and FDAA labelling of *B. subtilis* revealed the easily detectable and reproducible rod-shaped morphology that is typical of the species. These results confirmed that PG is located at the outermost layer of the cell periphery. The experiments also showed that the nascent PG synthesis is concentrated at the cell septa and also along the cylinder. This was to be expected as septa form prior to cell division and become poles of the subsequent daughter cells post division.

This study also generated a temporal framework from the cell cycle in that it takes approximately 30 minutes for *B. subtilis* WT septa to form. This was revealed using a pulse-chase experiment where FDAAs were incorporated into sites of nascent PG synthesis and detected using epifluorescence microscopy *in vivo*. While the epifluorescence microscopy has long been used to study PG dynamics, the use of FDAAs in this study is novel. As well as providing a new insight into the dynamics of PG synthesis in *B. subtilis* WT, this approach also highlights the versatility of FDAA incorporation into PG as a tool for studying cell wall synthesis. This versatility has also been seen in other work, where FDAAs have been used to elucidate the incorporation pattern of amino acids into PG in *B. subtilis* as well as other bacterial species (Kuru et al., 2012; Liechti et al., 2014; Shieh et al., 2014; Siegrist et al., 2013).

These approaches complement the earlier work which established understanding of *B. subtiilis* PG dynamics and architecture (Atrih et al., 1999; Hayhurst et al., 2008). This was achieved through the use of epifluorescence microscopy, particularly when combined with the utilization of FDAAs.

4.3.2 Role of *lytE* and *yvcE* in control of *B. subtilis* PG architecture

The unusual morphological images generated from examination of *B. subtilis* BP115 cells depleted of LytE and YvcE provided an interesting insight into the control of PG dynamics. As demonstrated using a variety of different imaging approaches, the loss of these proteins from BP115 cells results in an uneven, bowed and 'maggot-like' phenotype. This phenotype was shown to be divergent from the characteristic wild-type *B. subtilis* rod-shaped cell, being both wider and shorter. Furthermore, bands of constricted PG were observed across the short axes of cells that were deficient in *lytE* and *yvcE* expression. This ultimately proved that the loss of endopeptidase function has a direct influence on the retention of cell straightness and uniformity. This raises the question of how this happens. It is arguable that the lack of endopeptidase function results in an asymmetrical PG sacculus. This is likely to be caused by the uneven peptide chain length that results from the lack of peptide bond cleavage provided by endopeptidases. In contrast, when *lytE* is deleted and *yvcE* is the major autolysin available, *B. subtilis* cells become thinner and longer (Domínguez-Cuevas et al., 2013).

The findings generated by this study are supported by published works that investigated the role that *lytE* and/or *yvcE* (sometimes called *cwlO*) play(s) in

the governance of *B. subtilis* PG architecture. Hashimoto et al. (2012) stated that LytE and YvcE (CwlO) activity is essential for cell proliferation and these genes may participate in the loosening of the *B. subtilis* sacculus during growth. This was supported by the AFM analyses of xylose-starved BP115 cells, showing an uneven, constricted PG sacculus. Domínguez-Cuevas et al. (2013) suggest that *lytE* is synthesized and migrates to the outer cell wall as a stress response when the cell wall expansion is compromised. This paper also showed that the loss of *yvcE* i.e. when *lytE* is the only functional endopeptidase available causes *B. subtilis* cells to lose control over cell width and the loss of the ability to maintain a consistent longitudinal axis of growth. The data in this study correlates with this as any xylose-starved BP115 cells exhibited a curved/bowed phenotype. In contrast, when *lytE* is deleted and YvcE is the major endopeptidase available *B. subtilis* cells become thinner and longer (Domínguez-Cuevas et al., 2013).

4.3.2.1. The effect of endopeptidase activity on *B. subtilis* PG architecture

Endopeptidases in *B. subtilis* hydrolyse the amide bond between two amino acids in peptidoglycan. This breaking of peptide bonds allows expansion of the sacculus during cell growth (Vollmer et al., 2008b). The data generated by this study was developed into a model of how LytE and YvcE activity influence PG architecture and subsequently cell elongation in *B. subtilis* (**Figure 4.18**). This model builds upon the 'coiled-coil' model of PG

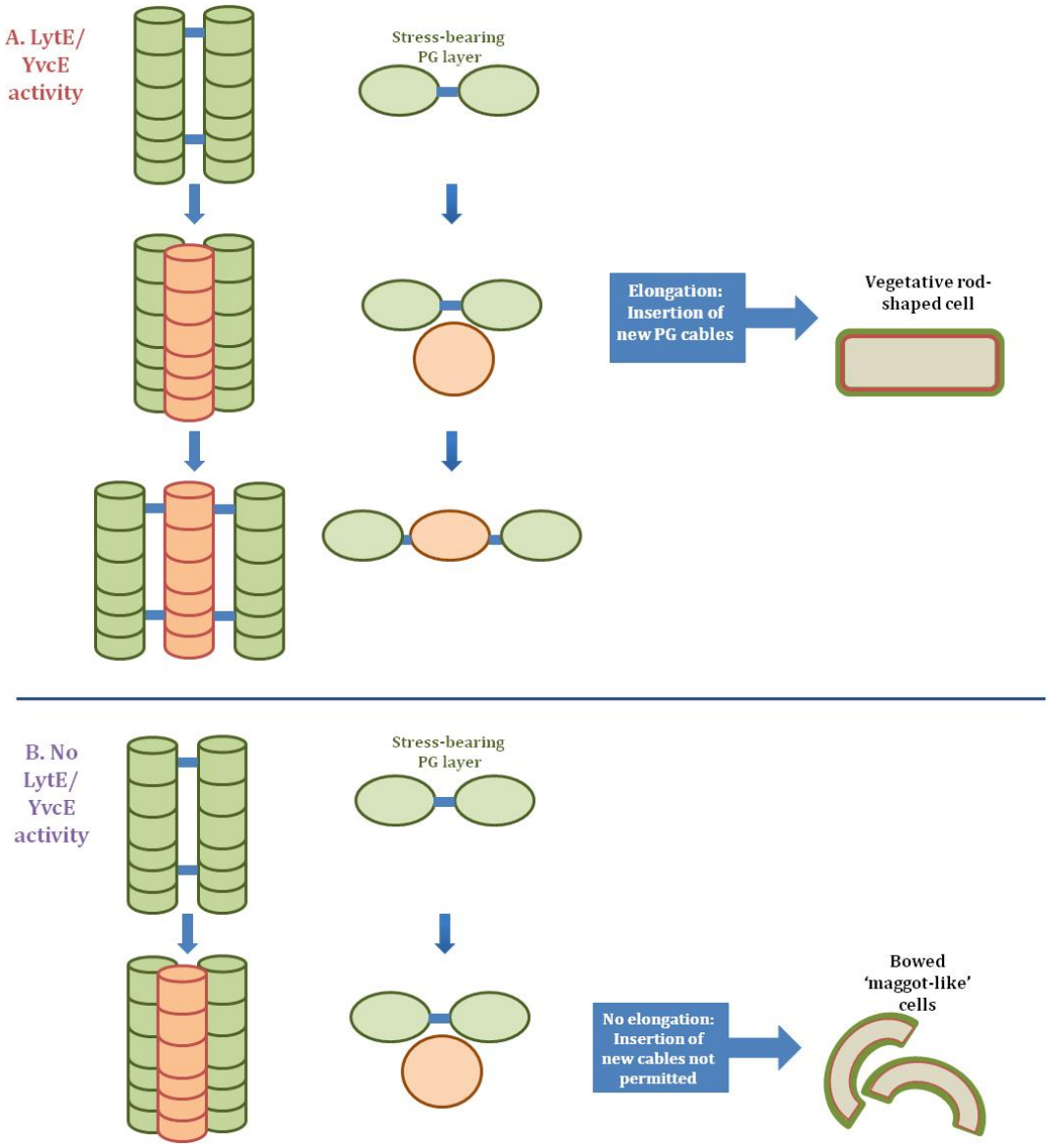

Figure 4.18. Model of how LytE/YvcE endopeptidase activity affects *B. subtilis* PG sacculus morphology. LytE and/or YvcE endopeptidases cleave the peptide side chains between the architectural PG cables in the *B. subtilis* sacculus, allowing the insertion of new PG cables into the stress-bearing layer of PG during cell elongation. Without LytE or YvcE, the peptide side chains remain intact and elongation cannot occur as no space is created for the new cable. Therefore, cables of PG material accumulate. This leads to the observed bowed 'maggot-like' cell morphology.

architecture proposed by Hayhurst et al. (2008), whereby PG coils into cables that run perpendicularly to the long axis of the cell cylinder. Here, we propose that the loss of LytE and YvcE endopeptidase activity prevents insertion of new PG cables and thus elongation of the cylinder, as the peptide side chains linking the PG cables are not cleaved to make room for new cell wall material. Therefore, newly synthesized cables of PG accumulate. This effect on PG architecture creates a differentiation from vegetative *B. subtilis* rod-shaped morphology to produce a bowed 'maggot-like' morphology.

4.3.3 Use of STORM as a new imaging technique

The final point of discussion raised by this chapter concerns the use of STORM as an imaging technique. This study reported the use of STORM imaging to study PG architecture in *B. subtilis* WT; both fluorescent Vancomycin and click-labelled FDAAs were used (separately) to label sites of nascent PG synthesis in the cells. STORM is capable of detecting individual fluorophores with a 20nm resolution (Rust et al., 2006). This resolution makes STORM a pioneering new technique to the field of imaging-based research, with huge potential impact and data generation with regard to PG architecture and dynamics research.

At the time of writing, this study detailed the first reported use of STORM to image *B. subtilis* cells. Turner et al. (2013) utilised STORM to reveal the nanoscale insertion pattern of PG in *E. coli* and *Caulobacter crescentus*. Examination of *B. subtilis* WT cells revealed the incorporation of D-amino acids across the short axis of the cell, reminiscent of the sacculus architectural features discovered by Hayhurst et al. (2008).

STORM detection of fluorescent D-amino acid incorporation was first reported in this study, this was concentrated to *B. subtilis* cell septa indicating a site of nascent PG synthesis. The merits of using STORM as an imaging technique are immediately obvious. The incredible resolution provided by this technique i.e. being able to individually resolve individual fluorophores in cell dyes, was demonstrated when used to examine *B. subtilis* cells. To further utilize this technique, subjecting *B. subtilis* mutants with a PG morphology defect e.g. BP115 to STORM investigation using PG-specific STORM-compatible dyes is likely to reveal even more information about PG dynamics. A slight disadvantage encountered when using STORM was that it was not yet compatible with live cell imaging as with epifluorescence microscopy. This meant that none of the STORM imaging of nascent PG synthesis in *B. subtilis* was performed *in vivo*, which is a desirable experimental approach when dealing with a complex and dynamic macromolecule such as PG.

A limitation to the utilization of STORM is that the technique has only been available for a short while and its reliability and reproducibility is not yet established with regard to imaging PG. Furthermore, there is new scope for combining the increased resolution provided by STORM with other more established microscopy techniques e.g. AFM. It should therefore be an aim of further study to optimize and advance the use of STORM in imaging cell walls. In future, this has huge potential to further expand and consolidate understanding of PG dynamics and architecture in *B. subtilis* and other species.

Chapter 5

B. subtilis cell wall peptidoglycan dynamics during sporulation and germination

5.1 Introduction

5.1.1 Sporulation in *Bacillus subtilis*

Sporulation is one of the most well understood examples of cellular differentiation and development (Errington, 2003). Spores can endure environmental stress and ensure their continued survival by retaining their chromosomal genetic information.

Bacillus subtilis (*B. subtilis*) is the best known and most characterised Gram-positive bacterium. In addition to this, *B. subtilis* is also able to undergo sporulation and germination. The dormant spore is resistant to a wide range of stresses. The morphological changes associated with sporulation rely on the dynamic nature of the main Gram-positive cell wall polymer, peptidoglycan (PG).

5.1.1.1 Advantages of sporulation to *B. subtilis*

As a result of their differentiated structure, *B. subtilis* spores can survive environmental conditions that would otherwise harm vegetative cells. *B. subtilis* spores are able to survive damage by dessication, chemical solvents,

detergents, radiation, hydrolytic enzymes and extremes of temperatures as high as 100°C (Nicholson et al., 2000).

5.1.1.2 Key stages of *B. subtilis* sporulation cycle

As part of differentiation, *B. subtilis* undergoes several morphological stages (**Figure 5.1**). Prior to sporulation morphological dynamics, the cell reorganises its genetic material by duplication and segregation of its chromosome, (Errington, 2003).

The first morphologically recognised stage of sporulation is the formation of an asymmetric septum, which differs from vegetative cell septa that centrally bisect *B. subtilis* cells during division (Beall and Lutkenhaus, 1991; Errington, 2003, 2001; Scheffers and Errington, 2004). The formation of the asymmetric septum creates a compartment at one cell pole containing one of the two chromosomes. This compartment is known as the prespore. The prespore is then engulfed by the mother cell PG to form the spore precursor, the forespore. At this point, spore PG is deposited to form a spore cortex. The spore cortex provides the main mechanism of maintenance of heat resistance for the spore (Popham and Setlow, 1993). The cortex then matures and a spore coat is formed. The spore coat is composed of over 25 polypeptide components, organized into several morphologically distinct layers and acts as a subsequent final barrier to the external environment upon mother cell lysis (Driks, 1999). The final stage of sporulation is the lysis of the mother cell by *B. subtilis* autolysins, which release the fully formed spore (Smith et al., 2000).

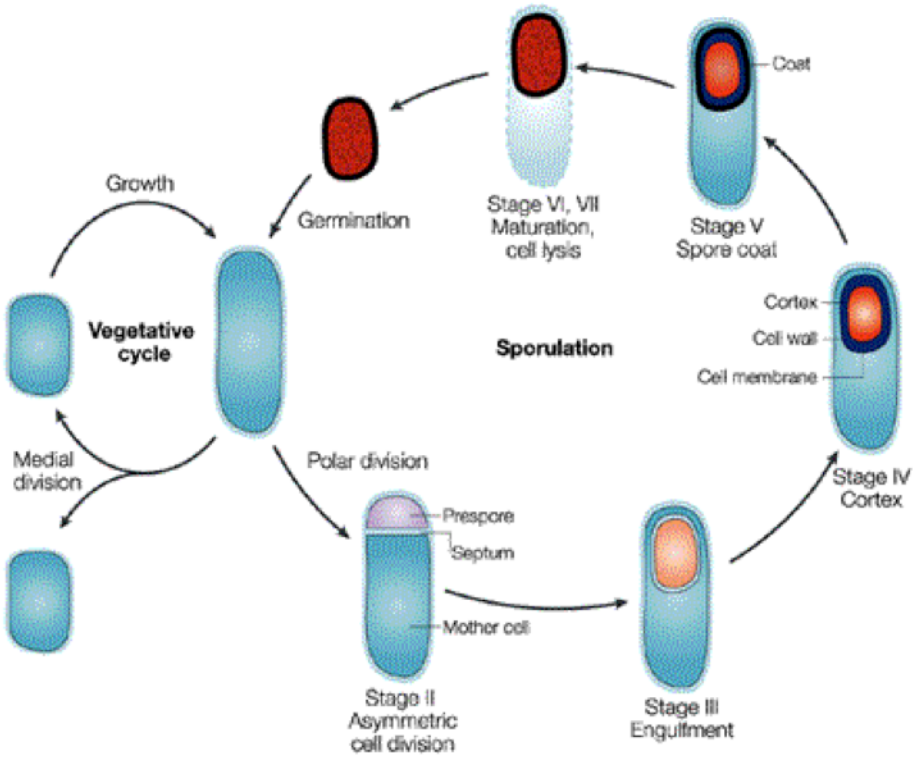

Figure 5.1. Schematic showing sporulation and germination stages in *B. subtilis.* Each differential stage exhibits its own distinct morphology. Events during sporulation and germination occur in a precise, genetically controlled order. Roman numerals refer to the stages of sporulation. Adapted from Errington (2003).

While these processes are well characterized in terms of their genetic initiation and control, very little is understood about PG dynamics. Therefore, one of the main aims of this chapter was to elucidate a greater understanding of the dynamics and architecture of PG during sporulation morphogenesis.

5.1.2 Spore germination in *B. subtilis*

In favourable environmental conditions, germination of spores allows regeneration and outgrowth of a new vegetative cell.

5.1.2.1 Key stages of *B. subtilis* spore germination

Initiation of spore germination can occur when the *B. subtilis* germinant receptor protein GerA responds to L-alanine in the extracellular environment (Moir and Smith, 1990). After germination initiation, there are two main stages of *B. subtilis* germination; Stage I and Stage II (Setlow, 2003).

Stage I of germination is as follows: first, release of spore H^+ and monovalent cations from the spore core (Jedrzejas and Setlow, 2001); second, release of the spore core's large deposit of pyridine-2, 6-dicarboxylic acid (dipicolinic acid [DPA]) and its associated divalent cations, predominantly Ca^{2+}; third, replacement of DPA by water, resulting in an increase in core hydration and causing some decrease in spore wet-heat resistance. Stage II of germination is as follows: first, hydrolysis of the spore's PG spore cortex by autolysins (Popham et al., 1996; Smith et al., 2000). The two crucial cortex lytic enzymes in *B. subtilis* spore germination are CwlJ and SleB (Moir, 2006) and it is believed that these proteins recognize the muramic δ-lactam structure, which is unique to the spore cortex (Atrih et al., 1998; Fukushima et al., 2002). Secondly, the spore core swells through further water uptake and

expansion of the germ cell wall (Setlow et al., 2001). Only after this further increase in core hydration does protein mobility in the core return, facilitating the action of cytosolic enzymes (Setlow, 2003). The initiation of enzyme action in the spore core after completion of stage II allows initiation of spore metabolism (Cowan et al., 2003) and hydrolysis of the large depot of small, acid-soluble spore proteins (Setlow, 2003). This is followed by the macromolecular synthesis that converts the germinated spore into a growing cell, escaping the spore coat; a stage named spore outgrowth (Setlow, 2003).

The initiation and control of spore germination and outgrowth in *B. subtilis* is well characterised. However, the architecture and dynamics of the PG that occur during this form of cell morphogenesis are not well understood, despite the involvement of PG differentiation in this phenomenon. Therefore, investigation of PG dynamics during *B. subtilis* spore germination was investigated.

5.1.3 Aims of this study

The experimental aims and objectives for this study are as follows:

1. Characterise PG dynamics during *B. subtilis* sporulation.
    a. Establish time course of morphological changes during early sporulation.
    b. Investigate PG architecture during asymmetric septation.
2. Characterise PG dynamics during *B. subtilis* germination.

5.2 Results

5.2.1 *B. subtilis* sporulation in 2xSG media

B. subtilis WT sporulating cells were generated by inoculating 2xSG media and incubating this culture for 12 hours at 37°C. Samples of this culture were taken every 2 hours and their cell density measured using a spectrophotometer (**Figure 5.2**). The graph generated shows that the *B. subtilis* grew at an exponential rate for the first 6 hours of the experiment. During the final 6 hours of the experiment, the optical density of the *B. subtilis* culture decreased with every sample. Free spores were not detected after 12 hours' incubation.

5.2.2 *B. subtilis* sporulation morphology time-course

The *B. subtilis* 12-hour sporulation experiment described previously (**Chapter 5.2.1**) was repeated and separate samples were taken every 2 hours. These samples were then subjected to visual analysis using epifluorescence microscopy. This approach was utilised to monitor the morphological changes that occur during *B. subtilis* sporulation. This approach was combined with the chronological mapping of the *B. subtilis* sporulation changes resulting in the establishment of a morphological time-course, attributing a sporulation stage with an interval of elapsed time.

The six *B. subtilis* sporulation samples were labelled *in vivo* with NADA for 5 min. NADA is a fluorescent D-amino acid (FDAA), which is incorporated into sites of nascent PG synthesis. FDAAs have small fluorophores attached to

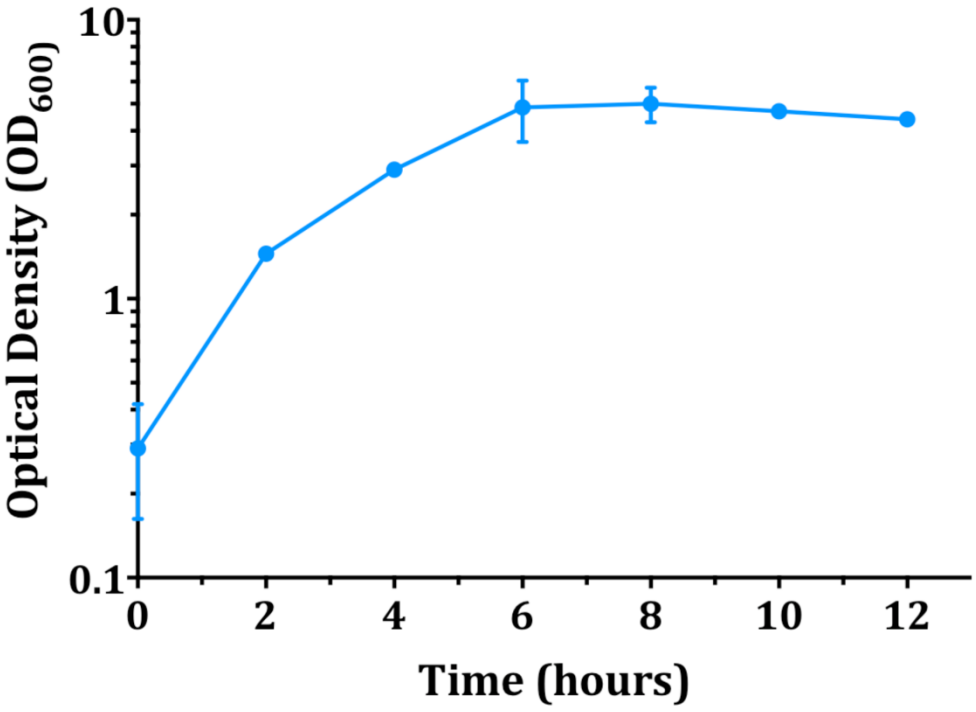

Figure 5.2. ***B. subtilis*** **growth and sporulation in 2xSG media over 12 hours**. Change in optical density was assessed by measuring the OD_{600} of the cell culture every 2 hours over 12 hours. The error bars indicate Standard Error over 2 culture repeats.

DAA backbones. When added during growth, these are incorporated into the cell PG (Kuru et al., 2012).

The sporulation timecourse samples were examined using epifluorescence microscopy, shown in **Figure 5.3** and at higher magnification in **Figure 5.4**. The images generated from the first three samples, i.e. between hours 2 and 6 of the culture (T_2, T_4 and T_6), showed that the *B. subtilis* cells exhibited expected vegetative morphology. The rod-shaped cell morphology characteristic to the species was observed in all three samples; the cells measured approximately 2-4μm in length and 0.5μm in width. However, there was no detection of sporulation events in any of these three samples, i.e. no sporulation and therefore differentiation of cell wall PG had occurred in the first 6 hours of the assay. NADA was incorporated into these three samples in the same manner as described in **Chapter 4**; the NADA incorporated into the outermost layer of the *B. subtilis* cell walls, as well as depositing as foci in the cell septa and poles. This incorporation pattern indicated the areas of nascent PG synthesis in the growing vegetative cells. This provided a useful basis of comparison for examining nascent PG synthesis patterns sporulating cell morphology in the later assay samples.

The results generated from the second half of assay (T_8, T_{10} and T_{12}) showed differentiation of the *B. subtilis* PG during sporulation. The image generated

$T_{2\ hours}$

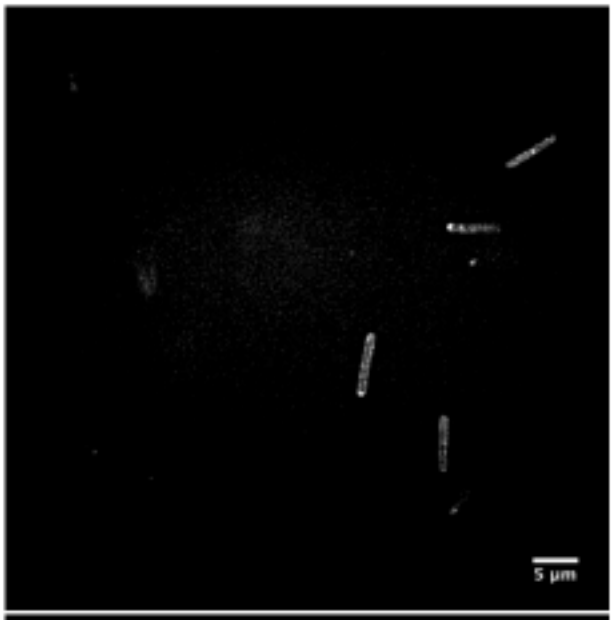

$T_{4\ hours}$

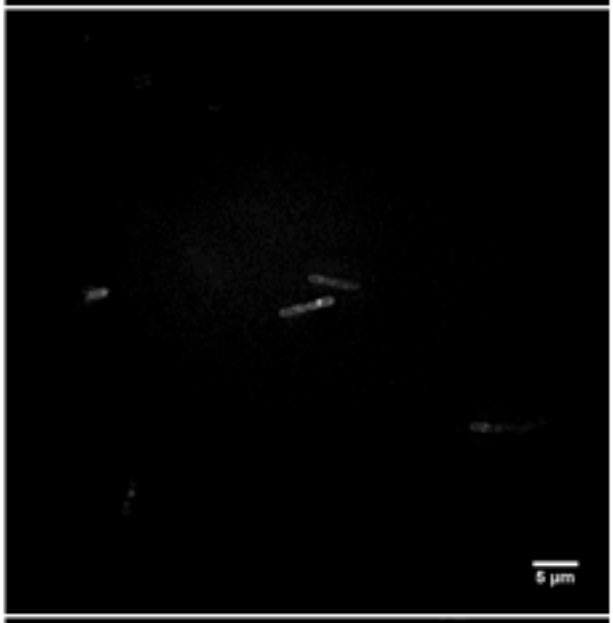

$T_{6\ hours}$

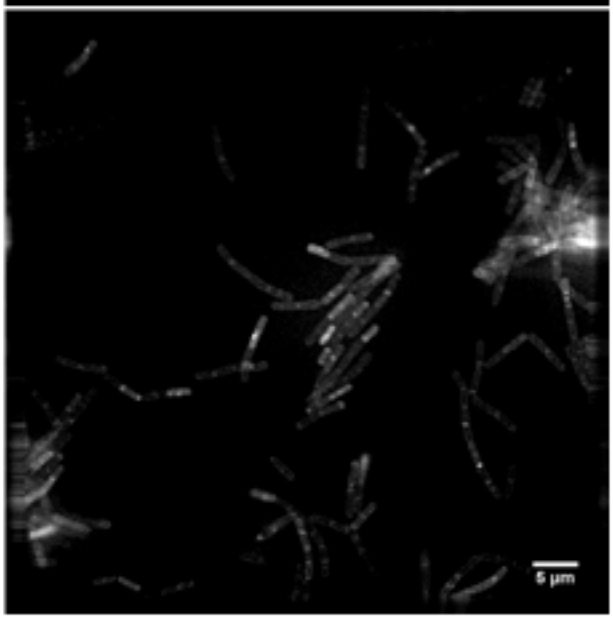

$T_{8\ hours}$

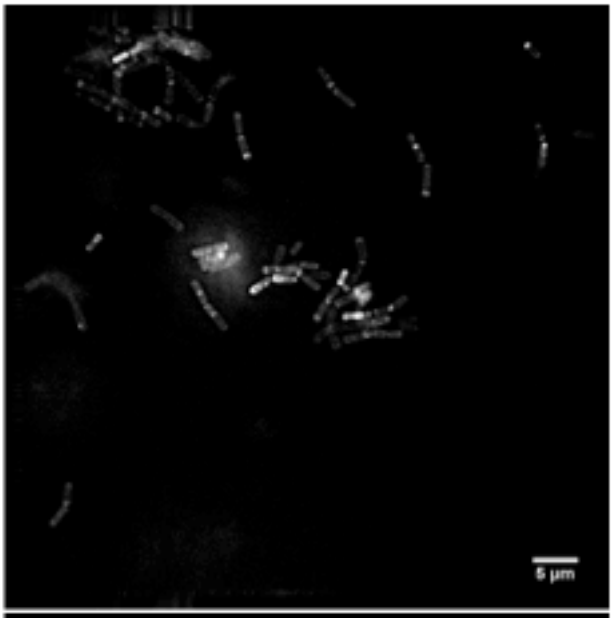

$T_{10\ hours}$

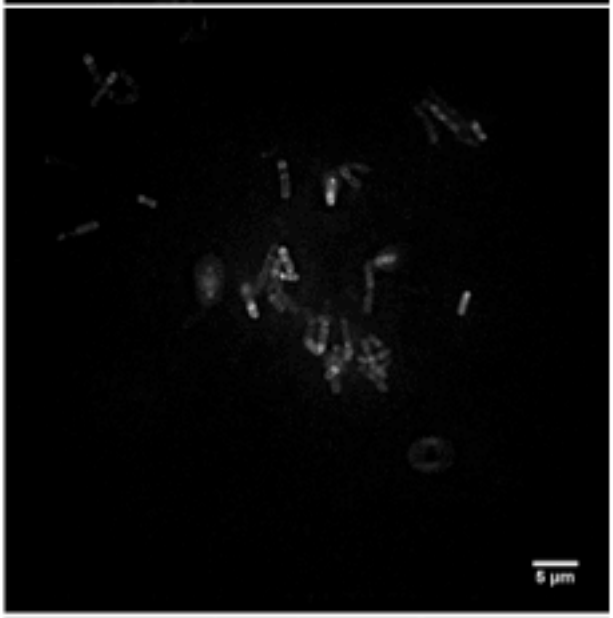

$T_{12\ hours}$

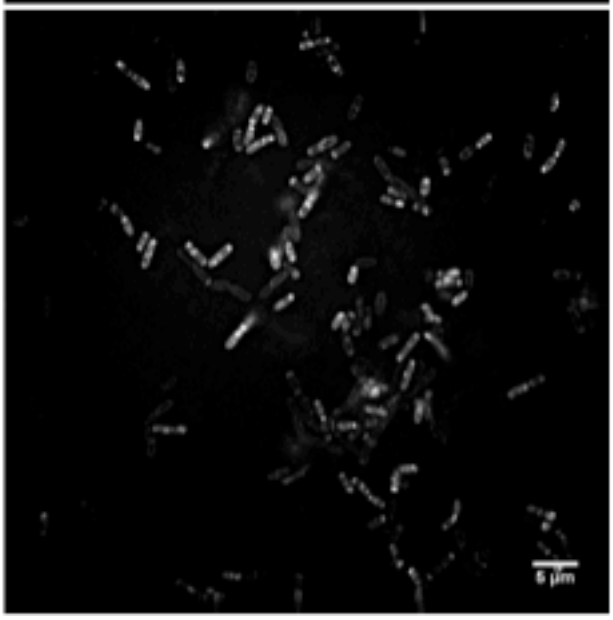

Figure 5.3. *B. subtilis* vegetative cells over a 12 hour sporulation time course: stained with NADA and examined by fluorescence microscopy. Cell walls were stained white with NADA, a fluorescent D-amino acid that incorporated into cell PG. Cells were sampled every 2 hours over 12 hours in sporulation media (2xSG) to produce 6 samples; T_2, T_4, T_6, T_8, T_{10} and T_{12}.

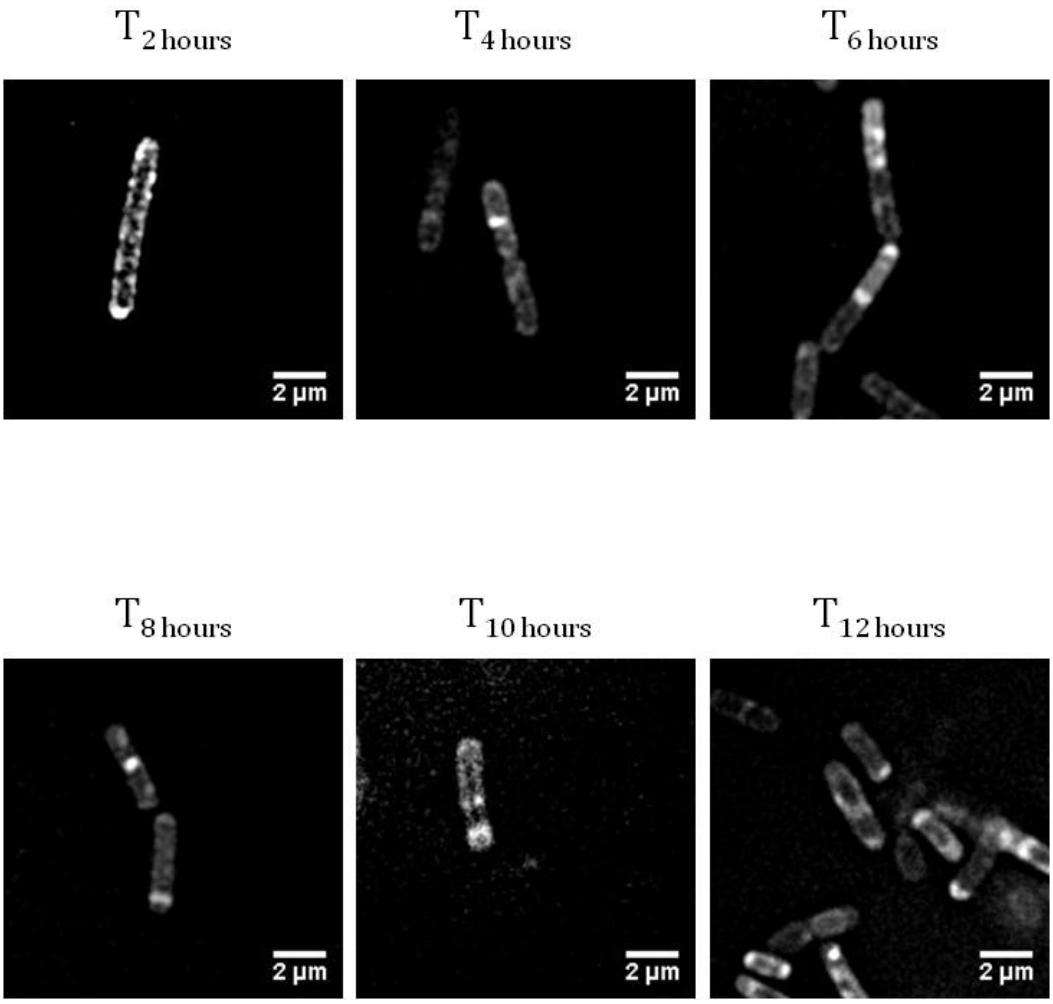

Figure 5.4. High magnification of *B. subtilis* morphology during a 12 hour sporulation time course: labelled with NADA and examined by fluorescence microscopy. Cell walls were labelled white with NADA, a fluorescent D-amino acid that incorporates into cell PG. Cells were sampled every 2 hours over 12 hours in sporulation media (2xSG) to produce 6 samples; T_2, T_4, T_6, T_8, T_{10} and T_{12}. Cells were not fixed prior to viewing.

for T_8 revealed cells that had septated asymmetrically, thus indicating that *B. subtilis* had begun sporulating (discussed in more depth in **Chapter 5.2.4.**). This was evident due to the targeting of these new asymmetric septa by NADA, which was incorporated and therefore detected at these new sites of nascent PG synthesis. The observed asymmetric septa were still present in T_{10}. In addition, what appeared to be potential forespores inside the mother cells were observed in this sample; indicated by the incorporation of NADA into their ovoid-shaped outermost layer.

5.2.3. Analysis of *B. subtilis* after 12 hours' incubation in 2xSG

5.2.3.1 TEM analysis of *B. subtilis* after 12 hours' incubation in 2xSG

The *B. subtilis* sporulation experiment, cultured in 2xSG, was sampled at the end of its 12-hour incubation. This sample was processed and subjected to analysis by Transmission Electron Microscopy (TEM); **Figure 5.5**. The image shows the characteristic rod-shaped morphology of *B. subtilis* (when imaged along their longitudinal axes). These typical *B. subtilis* cells exhibit cell lengths of approximately 2μm and short axis widths of approximately 0.5μm. It must be noted that due to TEM processing, some cells are shown as a cross-section across the short axis of the cell cylinder. This accounts for the seemingly spherical cells in the image field. Most importantly, ovoid shapes were observed at one pole of some cells, showing darker labelling than the rest of the cell envelope; these ovoids were the *B. subtilis* forespores. The forespores were observed at cell poles when said cells were imaged along

their longitudinal axes. In addition, the forespores were observed when seen in the cross section across the short axis of a cell cylinder. To provide greater architectural details a sporulating *B. subtilis* cell of the same sample was examined at a higher magnification using TEM (**Figure 5.6**).

At increased magnification a forespore formed after 12 hours' incubation is visible inside the mother cell (**Figure 5.6**). The periphery of the potential forespore showed distinct layers. The forespore cell membrane encloses the spore cytoplasm. A fibrillar layer outside of this was noted which was presumed to be the spore cortex, not yet electron transparent. The outer forespore membrane defines the outer limit of the cortex.

5.2.3.2 Fluorescent labelling of *B. subtilis* after 12 hours' sporulation

In order to confirm the PG synthesis in *B. subtilis* sporulating cells formed after 12 hours in 2xSG, this sample was labelled with a PG precursor analogue; HADA, another type of FDAA. The detection of HADA fluorescent binding sites therefore indicated the presence of nascent PG in the cell. This sample was then examined using epifluorescence microscopy (**Figure 5.7**). The DIC channel of the sample (which only detects visible light) shows the positioning of the forespores at the poles of the *B. subtilis* cell cylinders; indicated by the

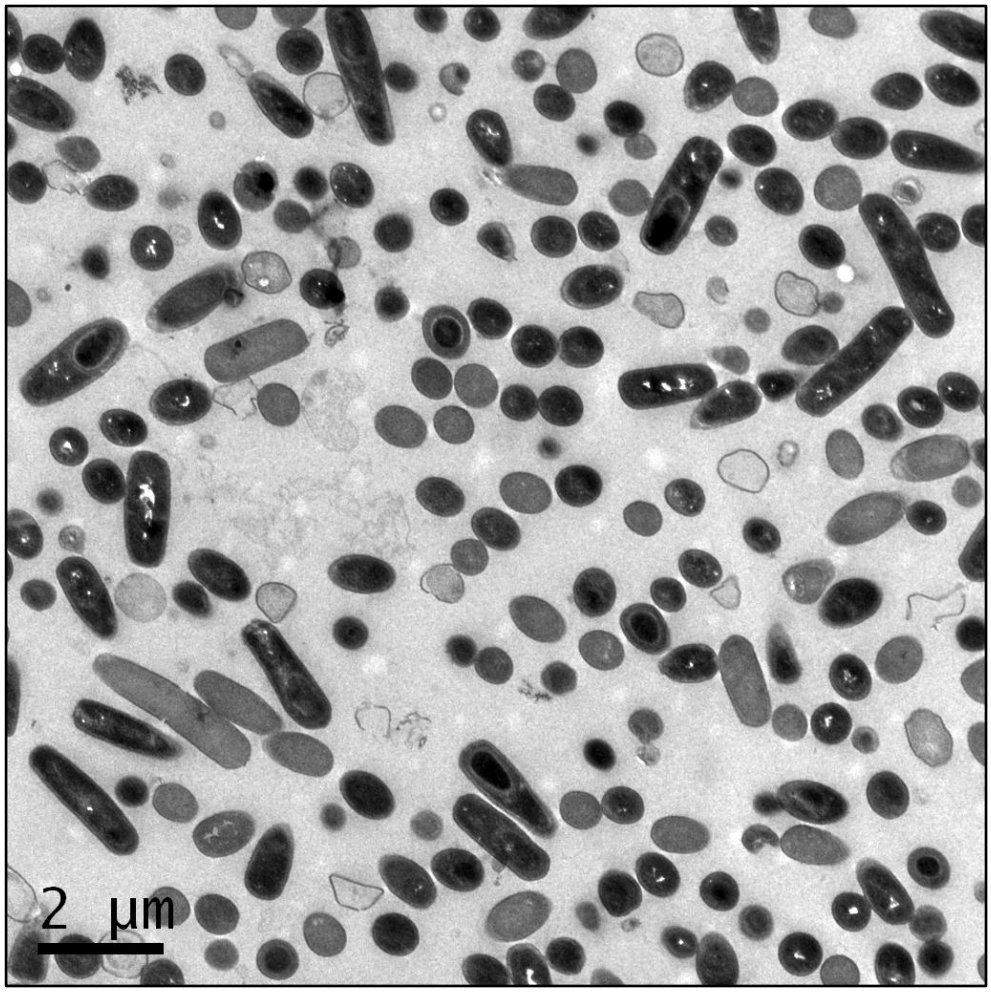

Figure 5.5. WT *B. subtilis* cells after 12 hours of sporulation: examined by TEM. Cells were sampled after 12 hours in sporulation media (2xSG), then fixed and processed for TEM. The image shows a full field of cells.

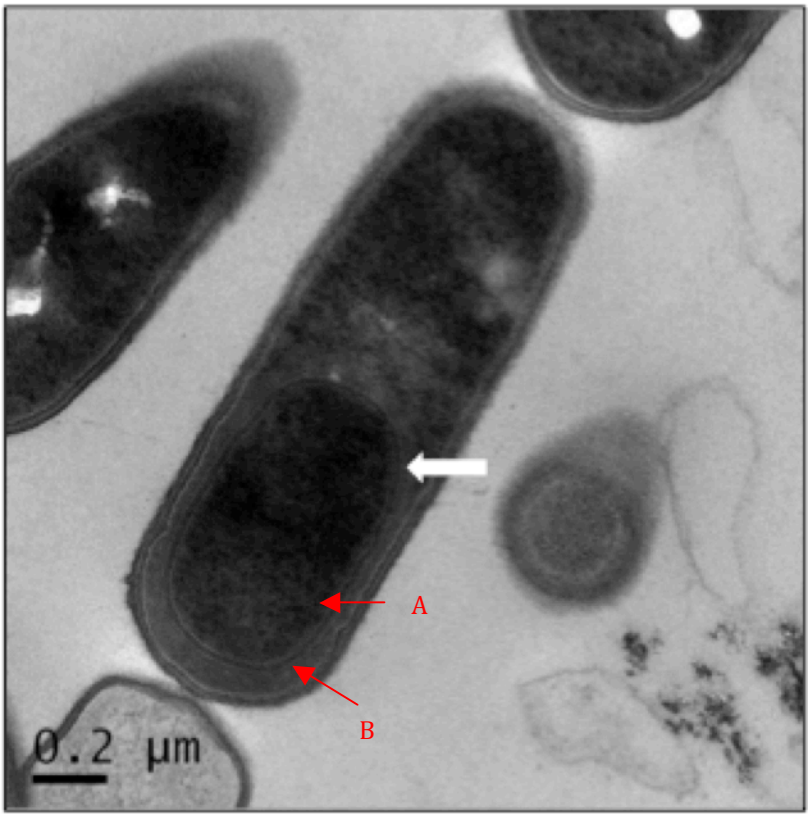

Figure 5.6. WT *B. subtilis* cell after 12 hours of sporulation: examined by TEM at high magnification. Cells were sampled after 12 hours in sporulation media (2xSG), then fixed and processed for TEM. The image field shows a single sporulating *B. subtilis* cell. The white arrow indicates the prespore. The red arrows, labelled A and B indicate the forespore membrane and the primordial cell wall respectively.

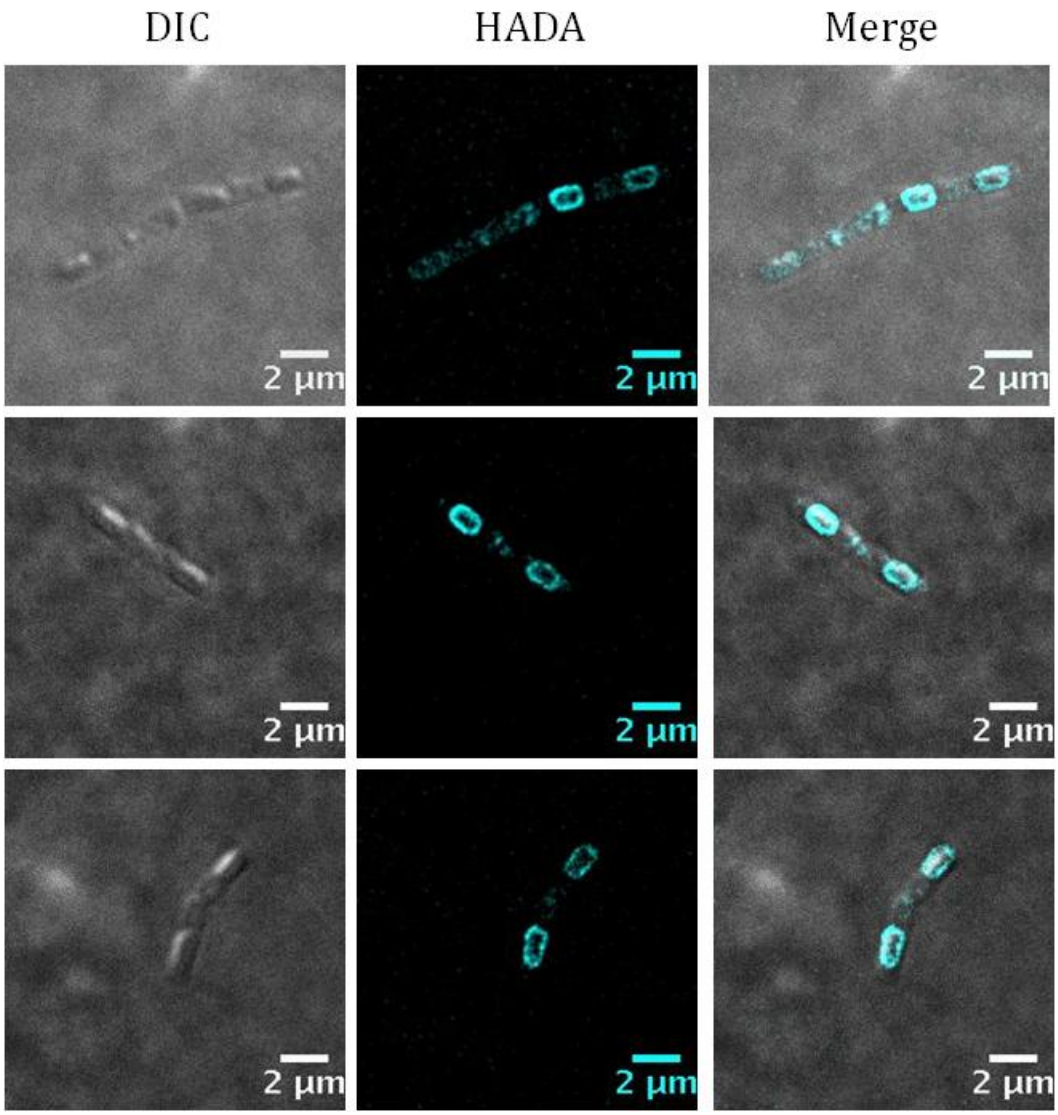

Figure 5.7. WT *B. subtilis* cells after 12 hours of sporulation: labelled with HADA and examined by epifluorescence microscopy. Formation of the forespores (prior to mother cell lysis) is observed. Cell walls are labelled cyan with HADA, a fluorescent D-amino acid which is incorporated into cell PG. Cells were sampled after 12 hours in sporulation media (2xSG). Cells were not fixed prior to viewing.

raised, bulged foci of the cells. These spores measured approximately 1μm in length and approximately 0.4μm in width. This data was correlated with the size and positioning of the spore structures detected using TEM analysis of the same sample. The binding of HADA to the sporulating *B. subtilis* cells shows a clear predilection for the peripheral ovoid-shaped layer of the spores. This binding was correlated with the position of the spores seen at the cell poles in the DIC images i.e. the HADA bound where the spores were located. The strong binding of HADA to the spores likely confirms that sites of nascent PG synthesis are present. This experiment verified that one of the outermost layers of the spore was indeed composed of PG. The labelling of PG in the complete outermost ovoid layer of the spore indicated that complete engulfment of the spore had occurred after 12 hours' incubation in 2xSG media.

5.2.4 Asymmetric septation during *B. subtilis* sporulation

Asymmetric septa are formed in the first morphological stage of sporulation. The information generated from the epifluorescence microscopy analysis of *B. subtilis* 12-hour sporulation time course revealed that the T_8 sample was the first time-point at which the cells had formed asymmetric septa. Therefore, T_8 samples were taken and subjected to further microscopic analysis.

5.2.4.1 Study of *B. subtilis* asymmetric septation using NADA

Cell samples were taken from an 8-hour *B. subtilis* sporulation culture. The cells were then labelled with NADA and imaged using epifluorescence

microscopy (**Figure 5.8**). The asymmetric septa, which have formed at Stage II of the sporulation process, were immediately obvious as a result of the NADA labelling. These asymmetric septa were located approximately ¾ along the longitudinal axes of the *B. subtilis* cylinders. This was easily distinguishable from previously observed vegetative *B. subtilis* septa, which bisect *B. subtilis* cell cylinders centrally. The NADA incorporated very strongly directly into the asymmetric septa and this binding was more concentrated in comparison to the *B. subtilis* cell wall. Because of NADA's incorporation into sides of nascent PG synthesis, this suggested that more nascent PG synthesis was occurring at the asymmetric septa than at the peripheral cell wall. However, analysis of the *B. subtilis* asymmetric septa using epifluorescence microscopy did not reveal any information regarding the PG architecture of these structures.

5.2.4.2 AFM analysis of *B. subtilis* PG sacculi during asymmetric septation

In order to examine the architecture of *B. subtilis* asymmetric septa during sporulation, purified PG sacculi were analysed using Atomic Force Microscopy (AFM). A cell sample was taken 8 hours into a *B. subtilis* sporulation assay. The cells were mechanically broken and purified by boiling in SDS, pronase treatment and incubation in HF, to remove all non-covalently and covalently bound cell wall polymers including teichoic acids.

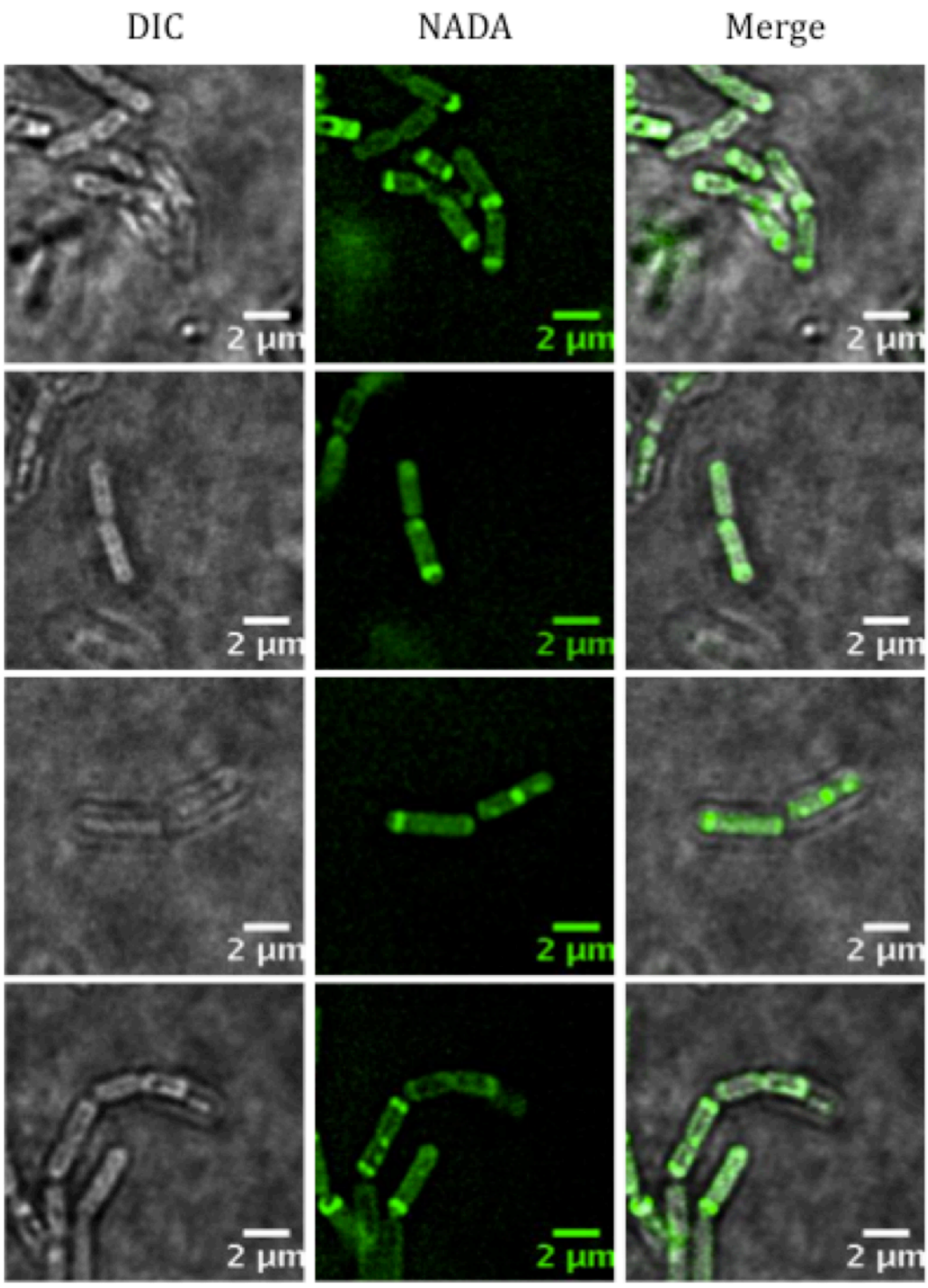

Figure 5.8. WT *B. subtilis* cells after 8 hours of sporulation: labelled with NADA and examined by epifluorescence microscopy. Cell walls were labelled green with NADA, a fluorescent D-amino acid that is incorporated into cell PG. Cells were sampled after 8 hours in sporulation media (2xSG). Cells were not fixed prior to viewing

The only remaining cell wall material was therefore purified PG sacculi. Sacculi were air-dried onto a clean mica-sheet and imaged by AFM in tapping-mode under ambient conditions. A typical field of sacculi is shown in **Figure 5.9**.

The images of early-sporulating *B. subtilis* PG sacculi (**Figure 5.9**) showed some features never previously reported. In all three of these full field images, *B. subtilis* sacculi can be seen which appear to be broken ¾ of the way along their longitudinal axes, leaving an open-ended sacculus. This was suggestive of an asymmetric septal placement and the sacculus breakage occurring as a result of AFM processing. The sacculi were also broken across their short axis, suggesting that PG architecture runs transversely across *B. subtilis* cylinders even during sporulation. This correlated with Hayhurst et al. (2008) who showed this short-axis breakage of PG sacculi in *B. subtilis* vegetative cells.

In some 8-hour sporulating *B. subtilis* sacculi, a circular ring-like PG structure was observed at the closed end of the sacculus in question, as indicated by the white arrows in **Figure 5.9**. It is arguable that these PG discs could be the internal component of the asymmetric septa that had fallen through and deposited at the closed end of the sacculi. These septal discs were different in appearance to folding of vegetative sacculi onto the mica sheet. In support of this, folding of the closed end of some sacculi was often seen in conjunction with these septal discs so the observations cannot be attributed to a simple fold. Furthermore, an isolated septum of PG was also observed, indicated by the red arrow in Panel C, **Figure 5.9**. This septum was presumed to be

A

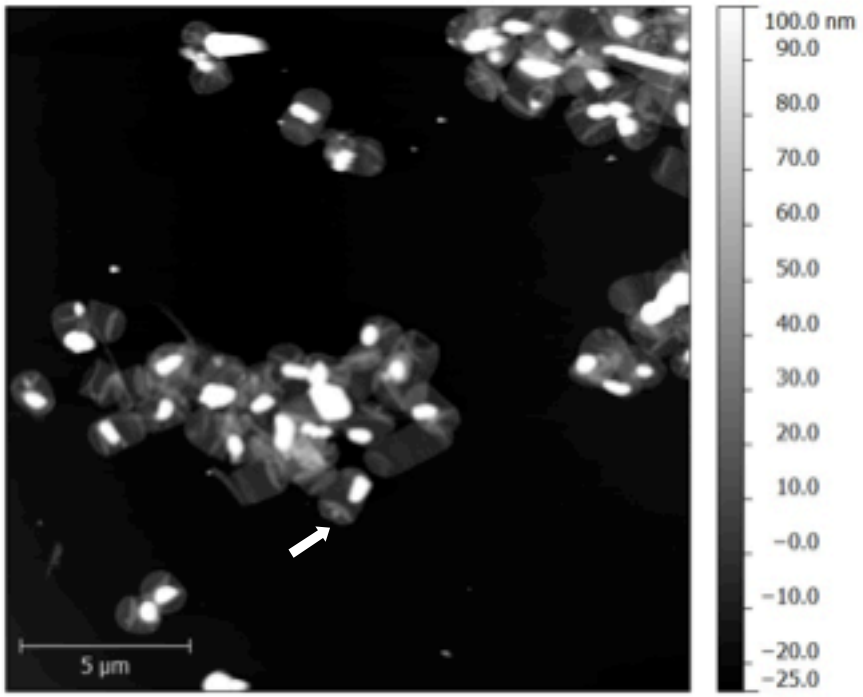
100.0 nm
90.0
80.0
70.0
60.0
50.0
40.0
30.0
20.0
10.0
−0.0
−10.0
−20.0
−25.0
5 µm

B

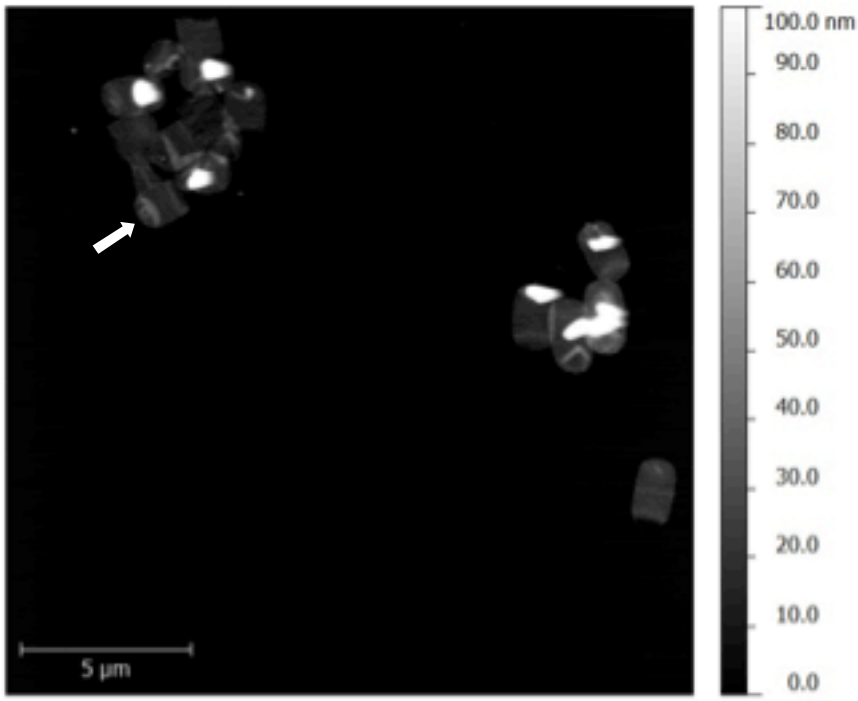
100.0 nm
90.0
80.0
70.0
60.0
50.0
40.0
30.0
20.0
10.0
0.0
5 µm

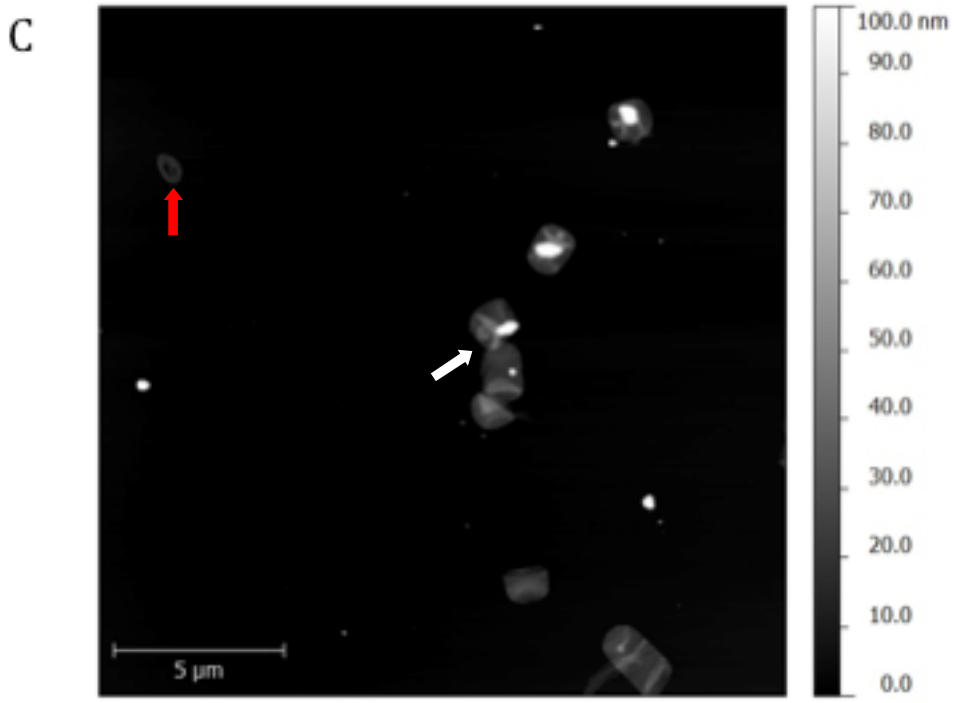

Figure 5.9. AFM analysis of purified WT *B. subtilis* PG sacculi, sampled after 8 hours of sporulation. The AFM height images show a typical field of multiple broken *B. subtilis* sacculi dried onto a mica surface. Panels A, B and C show separate fields taken from the same sample. White arrows indicate the presence of a ring-like structure observed at the closed end of some sacculi. The red arrow on Panel C indicates a possible whole asymmetric septum. The Z-axis scales on each image indicate the topographical height of the sample, measured in nm.

mechanically separated from a whole sporulating sacculus and was therefore a possible asymmetric septum.

AFM analysis of sporulating *B. subtilis* PG sacculi was also carried out at higher magnification (**Figure 5.10**). In this image, the formation of an asymmetric septum during *B. subtilis* sporulation is evident. A thicker, ridged band of PG material crossed the short axis of the sacculus and approximately ¾ along the longitudinal axis of the sacculus is indicated by the white arrow label in **Figure 5.10**. This can be attributed to the formation and presence of an asymmetric septum during sporulation. For comparison, a typical sacculi fold created during AFM processing is also shown (Red bracket, **Figure 5.10**). The ridged quality and increased thickness of the asymmetric septal PG were likely caused by the differentiation and increased deposition of PG in its formation. The PG sacculus structure (including the asymmetric septal PG) architecture matches the nascent PG synthesis pattern previously highlighted by NADA labelling, where a clear band of septal PG was observed across the short axes of the *B. subtilis* cell cylinders in an asymmetric fashion (**Figure 5.8**).

5.2.5 *B. subtilis* spore germination and outgrowth

As mentioned previously, *B. subtilis* spore germination permits outgrowth and required turnover of PG. Therefore, the next step after investigating PG dynamics during *B. subtilis* sporulation was to examine *B. subtilis* spore germination.

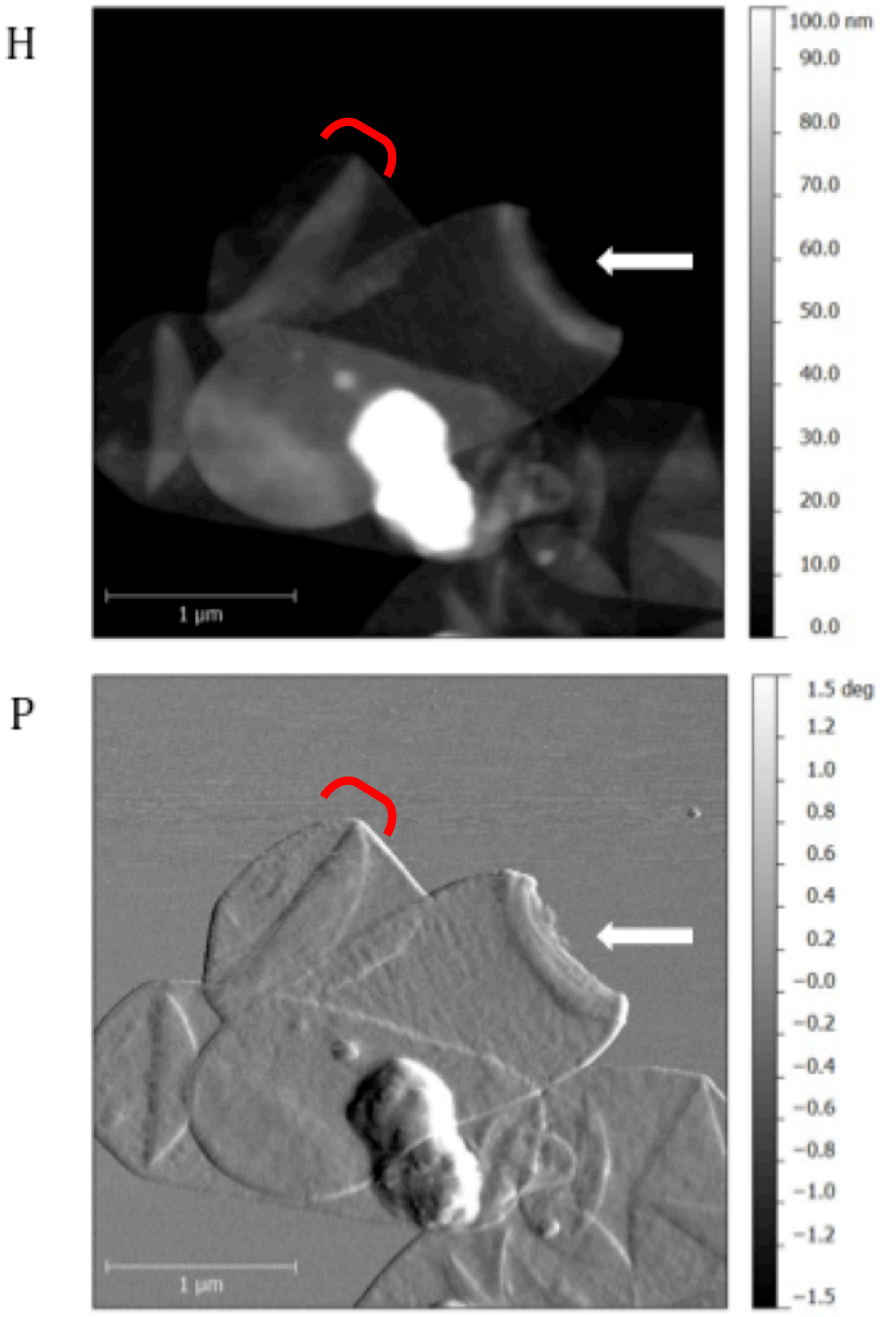

Figure 5.10. AFM analysis of purified WT *B. subtilis* PG sacculi, sampled after 8 hours of sporulation. The AFM height (H) and phase (P) images show a typical field of multiple broken *B. subtilis* sacculi dried onto a mica surface. The images show the same field of sacculi as in **Figure 5.6** at higher magnification. An asymmetric septum was observed on one sacculus, indicated by the white arrow on both panels. Both images show a typical folding of the *B. subtilis* sacculus, highlighted by red brackets. The Z-axis scales on each image indicate the topographical height of the sample; the height image in nm and the phase image in relative degrees.

5.2.5.1 *B. subtilis* spore germination assay

Spores generated from a previous *B. subtilis* sporulation experiment were heat shocked and incubated in NB media supplemented with 1mM L-alanine for 2 hours. Samples were taken every 30 minutes and germination monitored by measuring the culture's optical density (OD_{600}) (**Figure 5.11**).

The graph in **Figure 5.11** shows an initial decrease in optical density for the first 30 minutes of the experiment. A decrease in optical density has been indicates that spore germination has started (Boschwitz et al., 1991; McCormick, 1965; Popham et al., 1996). Therefore, this data indicated that the germination of the *B. subtilis* spores took place between $T_{0\ min}$ and $T_{30\ min}$. Following this, the optical density of the culture showed an increase for the next 90 minutes of the incubation, indicating the outgrowth of the germinating *B. subtilis* spores. This data was supported by previous work suggesting that the germination and outgrowth events occur in the first 90 minutes of spore germination assays (Harry, 2001; Santo and Doi, 1974). Therefore, these four samples ($T_{0\ min}$, T_{30min}, $T_{60\ min}$ and $T_{90\ min}$) were taken for use in further imaging experimentation.

5.2.5.2 Labelling of *B. subtilis* germination timecourse using NADA

To create a morphological timecourse, the four *B. subtilis* germination assay samples were labelled with NADA for 5 min, as NADA is incorporated into sites of nascent PG biosynthesis and examined using epifluorescence microscopy (**Figure 5.12**).

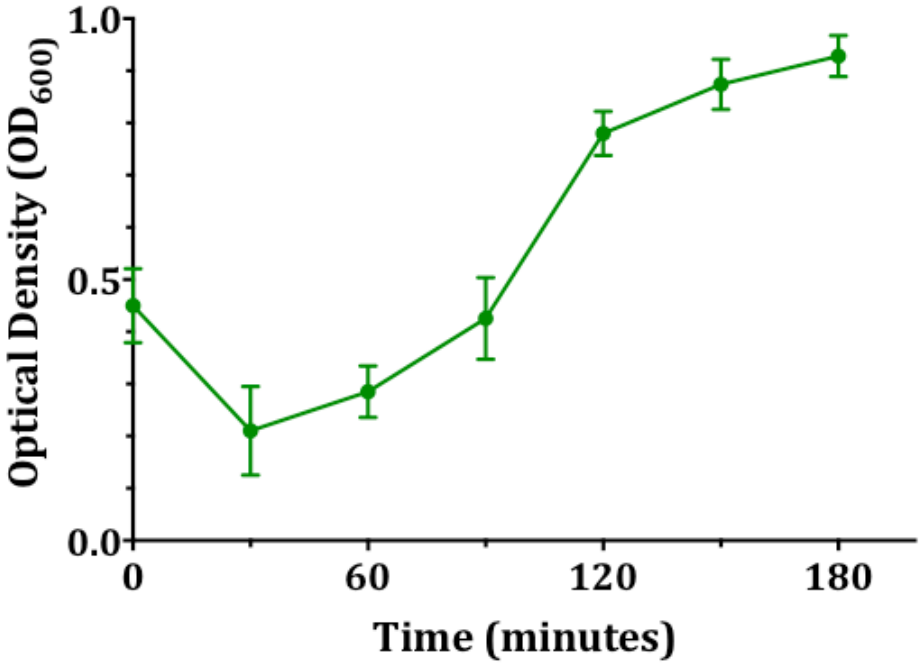

Figure 5.11. ***B. subtilis*** **germination and outgrowth in NB + 1mM L-Alanine media over 2 hours**.. Change in optical density was assessed by measuring the OD_{600} of the cell culture every 30 minutes over 3 hours, as denoted by the plot in green. The error bars show Standard Error for 2 culture repeats.

$T_{0\,min}$

DIC

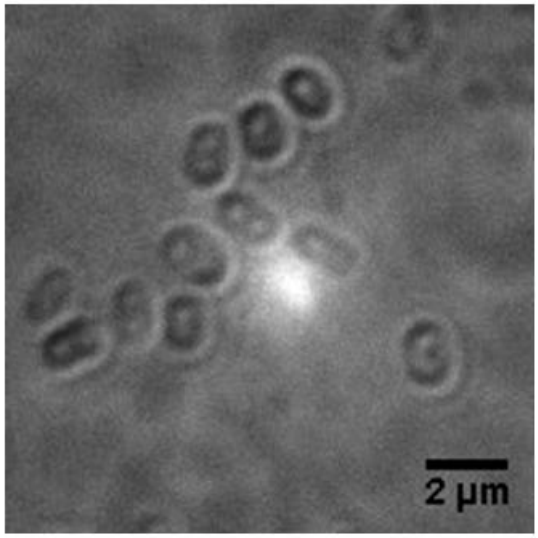

NADA

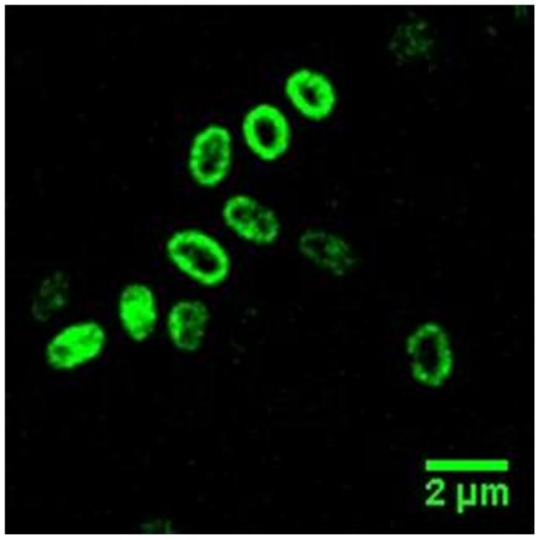

Merge

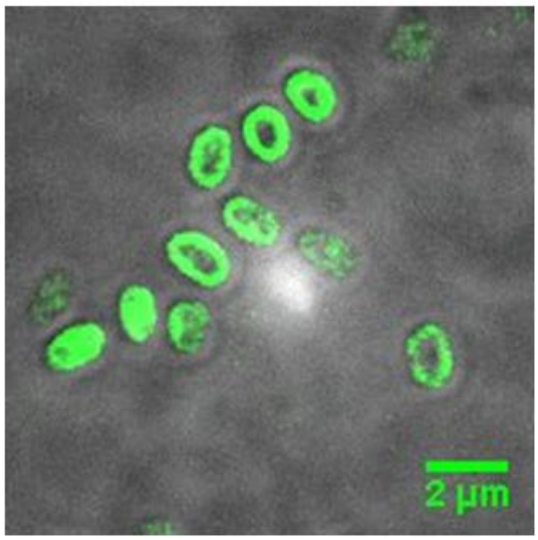

$T_{30\ min}$

DIC

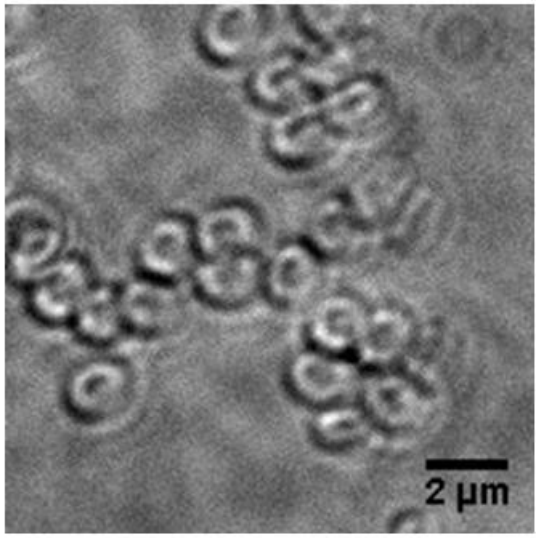

NADA

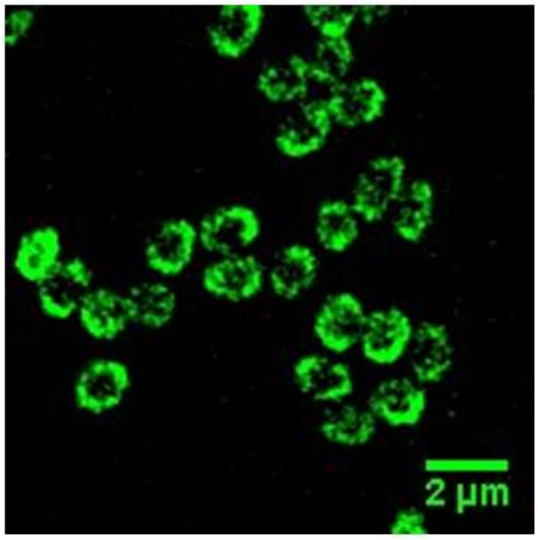

Merge

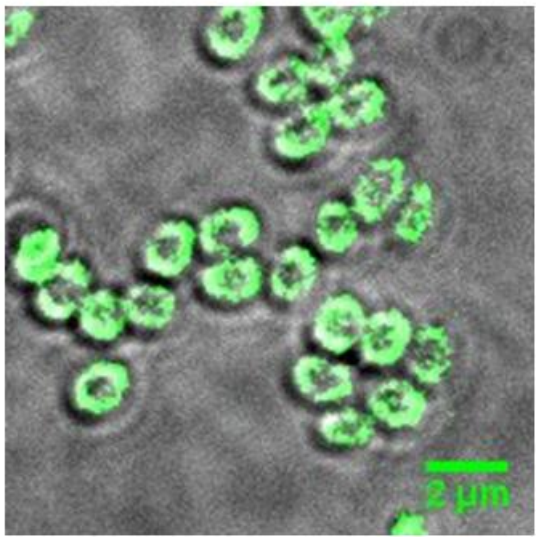

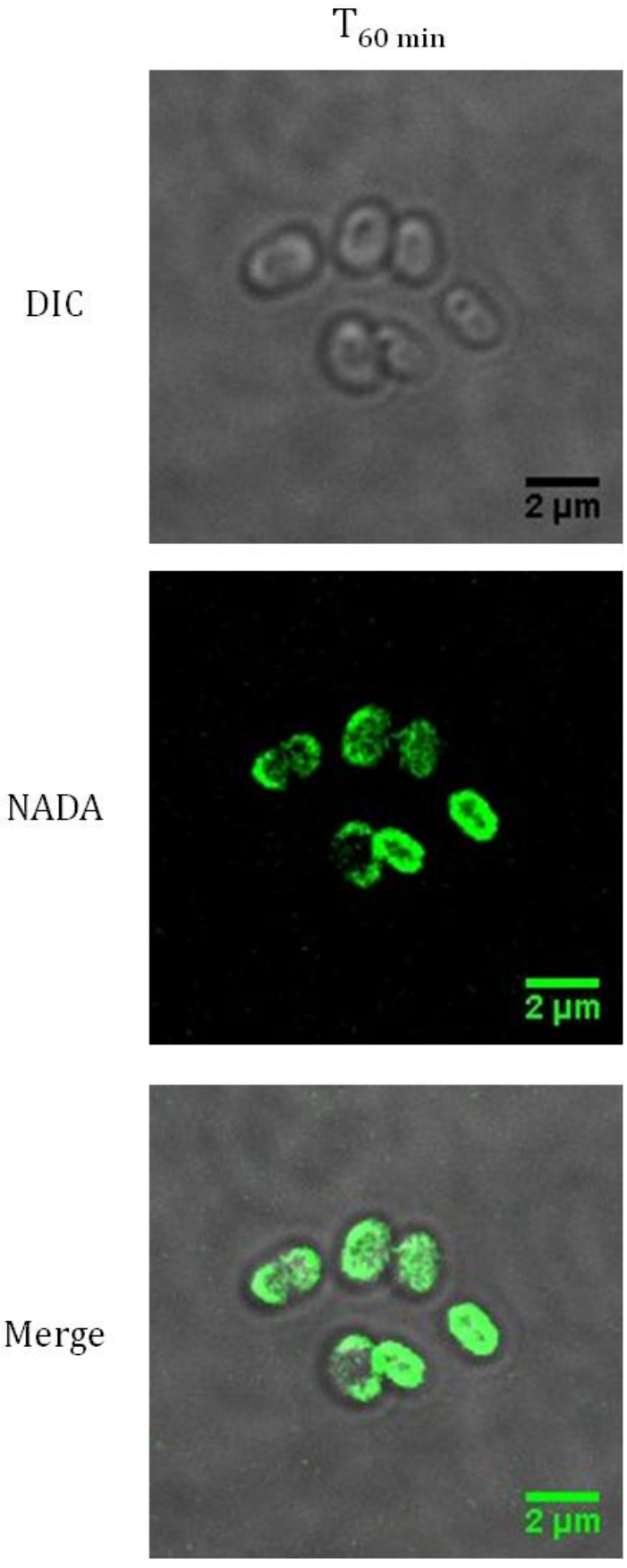
T60 min
DIC
2 µm
NADA
2 µm
Merge
2 µm

$T_{90\ min}$

DIC

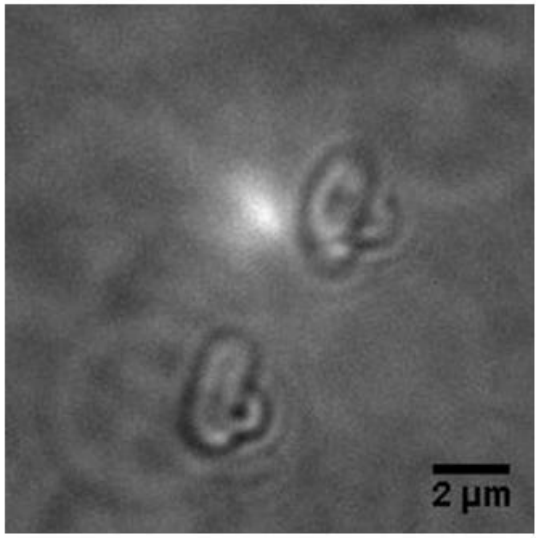

NADA

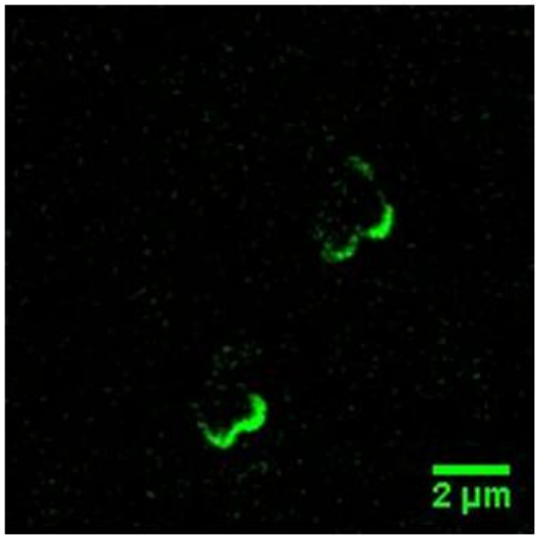

Merge

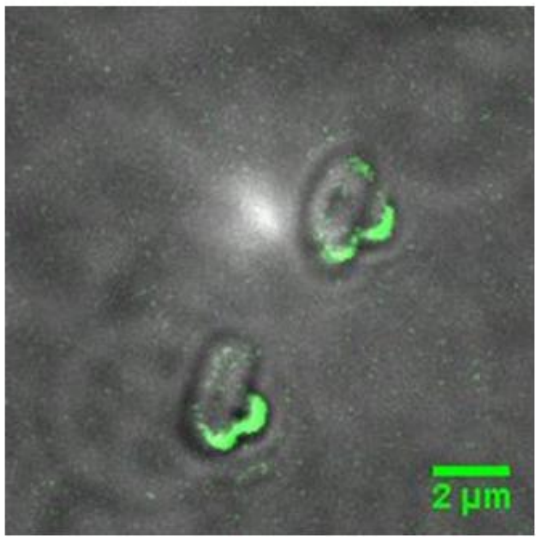

Figure 5.12. Timecourse of *B. subtilis* spore germination: labelled with NADA and examined using epifluorescence microscopy. Cell walls were labelled green with NADA, a fluorescent D-amino acid that incorporated into cell PG. Cells were sampled every 30 minutes over 90 minutes' incubation in NB containing 1mM L-Alanine. The four samples are shown sequentially; T_{0min}, T_{30min}, T_{60min} and T_{90min}.

At T_0, ovoid spore structures were observed using visible light in the DIC channel. NADA was incorporated into the entirety of the outer spore layers i.e. the coat. This was verified by the merged image where the fluorescent NADA binding to the spore coat completely overlapped the visible light DIC image. The incorporation of NADA into the spore coats of this sample was non-specific, as germination had not yet begun. The NADA labelling throughout the remainder of the experiment was therefore also considered to be non-specific. At T_{30}, the non-specific binding of NADA to the spore coats was again observed. However, outgrowth was not yet observed in this sample.

The images of germinating spores after 60 minutes showed that germination and subsequent outgrowth had already begun at this timepoint. The DIC image showed that the spores had partially elongated, measuring approximately 1.5μm along their longitudinal axes. The NADA was primarily incorporated into two 'crescents' of material at both ends of germinating spores. This was again likely to be two separated fragments of previous spore coat, created by the elongation of the cell during outgrowth that had split the coat.

Finally, after 90 minutes in germination media, the *B. subtilis* spores appeared to have completely germinated. This was shown most obviously when combining the DIC and fluorescence channels in the merged image. The fluorescence image again shows incorporation of NADA into two crescents of spore coat material; two crescents per cell. However, in the merged image there were cell features detected by DIC that were not

detected by the fluorescence channel due to their apparent lack of NADA incorporation. Closer inspection of the DIC channel image revealed cylinder-like structures emerging out of the crescents of what was previously spore coat. This was likely to be complete outgrowth of the germinated *B. subtilis* spores undergoing a change in morphology to return to a vegetative cell state. Interestingly, the level of NADA incorporation in the nascent vegetative PG was significantly less than that bound to the remaining spore coat material.

5.3 Discussion

5.3.1 PG dynamics during *B. subtilis* sporulation

The results of this study demonstrated the dynamic nature of PG and its architecture during sporulation in *B. subtilis*.

The initial experiment, studying spores after 12 hours' incubation in sporulation media using TEM, reiterated previous findings that *B. subtilis* sporangia exhibit a complex, layered internal spore structure (McPherson et al., 2005). Furthermore, additional microscopic analysis of *B. subtilis* after 12 hours' sporulation proved that nascent PG synthesis was occurring at the spore cortex inside the sporangium. This is in agreement with previously published work that showed PG was synthesized at the spore cortex, following from germ cell wall PG synthesis (Meador-Parton and Popham, 2000).

The timecourse created using NADA labelling was particularly useful in highlighting active sites of nascent PG synthesis during the different stages of *B. subtilis* sporulation. Using NADA to probe PG allowed the highlighting of the spores inside the sporangia and thus revealed that key sporulation events occur 8-12 hours during incubation in sporulation media. This replicated the original experimental timescale generated when using 2xSG media to induce sporulation in *B. subtilis* (Leighton and Doi, 1971). Further information elucidated by this experiment indicated that PG synthesis occurs throughout the remainder of the sporangia during all sporulation events. During sporulation, *B. subtilis* cells are not elongating and dividing as vegetative cells. Therefore, the evidence of PG synthesis sites throughout the original cell walls of sporangia indicates that PG modification and maintenance of the *B. subtilis* cylinder still occurs during sporulation.

One of the main conclusions from the NADA sporulation timecourse was that Stage IIa of sporulation begins between 6-8 hours after incubation in 2xSG sporulation media. This stage of sporulation therefore included asymmetric septation of *B. subtilis* cells, a phenomenon particularly interesting to the study of PG dynamics.

5.3.1.1 PG dynamics during asymmetric septation

B. subtilis forms an asymmetric septum at an early stage in sporulation. This form of septation is a modified version of the cell division process (Errington, 2003). A recent paper by Tocheva et al. (2013) suggested that *B. subtilis* can synthesize thin, Gram-negative-like PG layers during the early stages of sporulation, particularly asymmetric septation and engulfment, as well as its

thick, archetypal Gram-positive cell wall (**Figure 5.13**). Tocheva et al. (2013) suggest that this hypothesis refutes the coiled-coil model of *B. subtilis* PG architecture suggested by Hayhurst et al. (2008). Tocheva et al. (2013) argue that 50 nm coils, as described by Hayhurst et al. (2008), could not be 'thinned' by hydrolysis to just ~2nm thick without jeopardizing the integrity of the cable.

The data elucidated by this study, provided by epifluorescence microscopy and AFM, indicated that nascent PG synthesis was occurring, i.e. new cell wall material is created to form the asymmetric septa. This however doe not contradict the idea that the asymmetric septa is formed of a thin, Gram-negative-like PG layer derived from the original mother cell wall PG, as the architecture cannot be inferred from epifluorescence microscopy. The AFM analysis of purified PG sacculi exhibit evidence of asymmetric septation, derived from *B. subtilis* cells undergoing sporulation, also contradicts Tocheva et al., (2013). The topographic analysis of asymmetric septa revealed that the PG in the region where the septum meets the mother cell wall forms a thicker, ridged architecture.

The experimental approaches in this study were purely concerned with the qualitative visual examination of sporulating *B. subtilis* PG during asymmetric septation. The initiation and control of asymmetric septation is a complex interplay between several proteins (FtsZ, PBP1, SpoIIE and the Min system) (Beall and Lutkenhaus, 1991; Errington, 2003, 2001; Scheffers and Errington, 2004). However, the relationship between these proteins and their effect on the gross architecture of asymmetric septa has not yet been examined. In

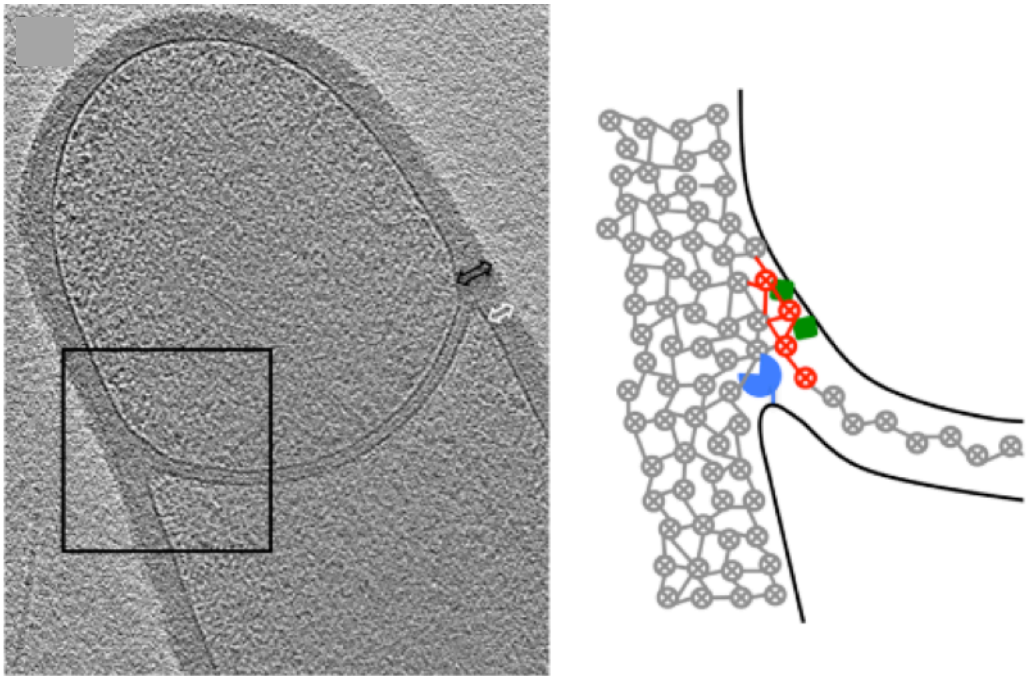

Figure 5.13. A model for PG hydrolysis and synthesis during spore engulfment as suggested by Tocheva et al. (2013). Schematics represent the boxed areas in the tomographic cryo-EM slices. Membranes are shown in black, glycan strands are viewed end-on (circled X's) interconnected by peptide bonds (lines). Older glycan strands and cross-links are shown in grey, new glycan strands and cross-links are shown in red, PG synthases are green and PG hydrolases are blue.

Tocheva et al. (2013) propose that during engulfment, co-ordinated PG synthesis at the 'front' and hydrolysis at the 'back' of the septal junction may drive membrane migration towards the pole. Black arrow indicates PG synthesis, white arrow points to average thickness of vegetative cell wall.

Adapted from Tocheva et al. (2013).

order to produce a greater understanding of *B. subtilis* PG architecture during asymmetric septating, future work should attempt to ally the data generated in this study with the function of the proteins mentioned.

5.3.2 PG dynamics during *B. subtilis* spore germination

The incorporation of NADA into the spore cortex/coats indicated that this binding was non-specific, as PG synthesis does not occur during dormancy prior to spore germination. In comparison, the level of NADA incorporation into the new material emerging from the spore cortex upon germinaton was much lower, which was unexpected. This was possibly due to a short exposure time during imaging of the cells combined with deconvolution of the images, which masked the NADA incorporation into the outgrowing vegetative cell PG. Thus, the method of labelling PG synthesis during germination will require some refinement.

Chapter 6

General Discussion

6.1 Analysis of *B. subtilis* morphology

In their vegetative state, *B. subtilis* cells are rod-shaped cylinders. The results of this study highlighted and utilised *B. subtilis*' morphogenesis from its vegetative rod-shape to alternative morphologies, depending on the experimental conditions. It was also observed that the *B. subtilis* rod-shape could be re-established.

Peptidoglycan (PG) is essential for cell viability, growth and division of *B. subtilis*. Three aspects of PG structure and dynamics were studied - protoplast generation and regeneration, the role of PG hydrolases, and sporulation and germination. All of these processes led to alterations to the cell morphology. A diagram summarising these processes in *B. subtilis* is shown in **Figure 6.1**.

6.1.1 Generation and regeneration of *B. subtilis* protoplasts

In this study, cell walls of *B. subtilis* WT cells were stripped of their PG using lysozyme to generate protoplasts. Protoplasts are spherical structures formed from the remaining cell lipid bi-layer membrane, which contains the cytoplasm, maintained in osmotically stabilising media. The loss of cell wall PG

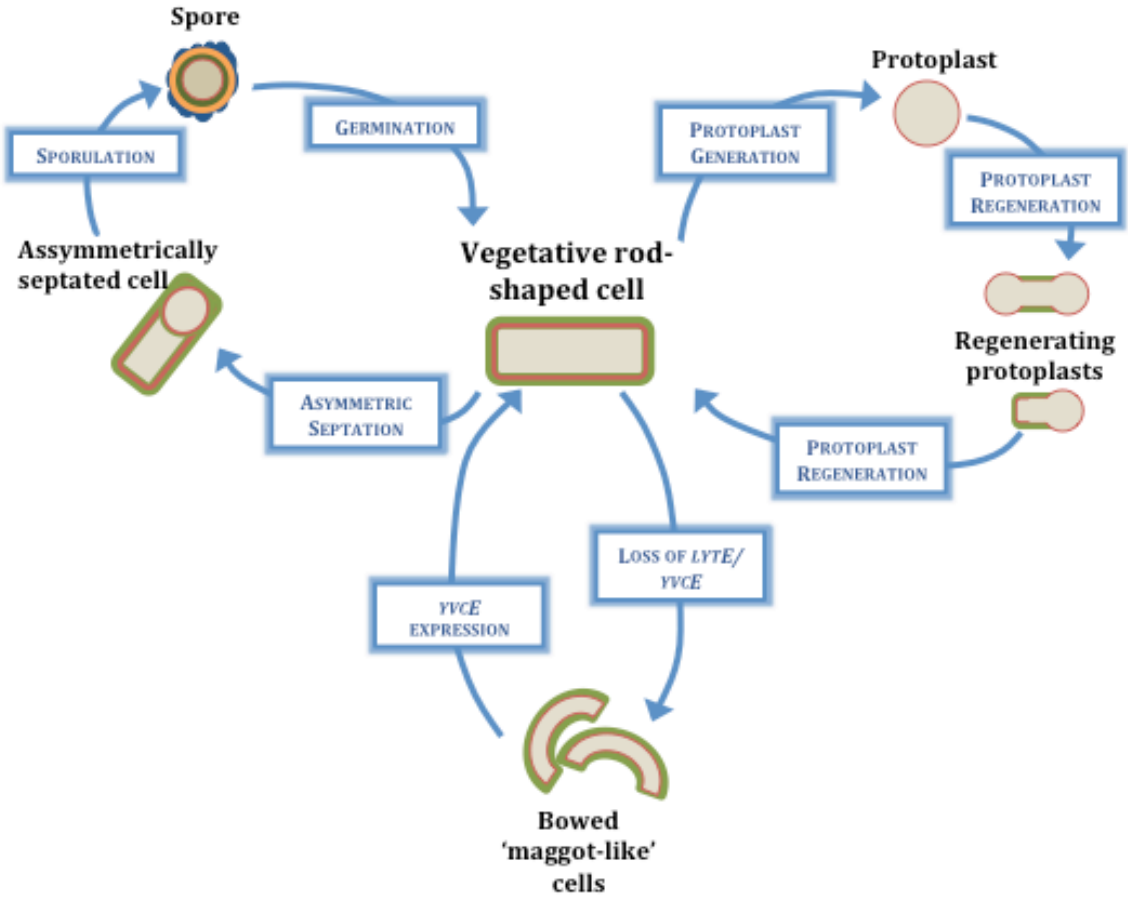

Figure 6.1. Model of *B. subtilis* morphological differentiation from vegetative rod-shaped cells. Three cell differentiation processes are shown; protoplast generation and regeneration, PG hydrolase depletion and expression, and sporulation/germination. Schematics for each type of cell morphology are shown and PG is represented in green. The representative schematics are not shown to scale.

and the subsequent conversion to a spherical shape indicates that PG provides the structural framework for vegetative cell morphology.

Protoplasts were able to regenerate their cell walls to re-establish their rod-shaped morphology. A model was developed for this phenomenon, where cell wall regeneration occurred through a series of morphological division intermediates. These division intermediates (known as 'dumbbells' and 'lollipops') will eventually produce vegetative *B. subtilis* cells. This mode of cell wall regeneration echoes spheroplast regeneration as studied in *Eshcerichia coli* (Ranjit and Young, 2013).

Sites of nascent PG synthesis were detected on the *B. subtilis* regeneration intermediates, indicating the active regeneration of cell wall material after its removal. These sites formed 'cuffs' of PG, similar in structure to the *B. subtilis* cell wall cylinder. From this, 'dumbbells' divide into two 'lollipops'. This raises some questions of how PG regeneration is initiated and controlled:

i. Are the protoplasts able to measure their diameters to specify where to synthesise new PG material to form 'cuffs'?
ii. Does the PG 'cuff' constrict the protoplast to form a 'dumbbell'?
iii. Does FtsZ specify the division site in a 'dumbbell's' PG 'cuff' to divide into two 'lollipops'?

6.1.2 Depletion and expression of PG hydrolases in *B. subtilis*

PG hydrolases form a diverse group of bacterial enzymes that cleave specific bonds within the peptidoglycan network (Ghuysen, 1968). Loss of certain PG hydrolases has a clear effect on the morphology of *B. subtilis* vegetative cells.

B. subtilis mutant cells lacking LytE and depleted for YvcE exhibit defects in lateral cell wall synthesis and cell elongation (Bisicchia et al., 2007). These LytE/YvcE depleted cells exhibited a bowed, 'maggot-like' phenotype (**Figure 6.1**). The bowed 'maggot-like' phenotype was also exhibited by the purified PG sacculus of the same cells, indicating that it was the PG itself providing this differentiated morphology. Furthermore, bands of constricted PG were observed across the short axes of cells that were deficient in *lytE* and *yvcE* expression. This ultimately proved that the loss of endopeptidase function has a direct influence on the retention of cell straightness and uniformity. We hypothesise that this is a result of the lack of hydrolysis between the cables of PG suggested by Hayhurst et al. (2008). This indicates that the metastructure of sacculus architecture in *B. subtilis* is influenced on a molecular level.

In future, it would be interesting to study the effect that depletion of other growth and division machineries has on *B. subtilis* sacculi. LytE and YvcE are part of a larger group of PG hydrolases (Smith et al., 2000). The single and collective role of all PG hydrolases in PG dynamics is yet to be established.

Another study suggested that in *B. subtilis* cells depleted of both YvcE (CwlO) and LytE, the PG synthetic machinery continues moving circumferentially until cell lysis, suggesting that cross-link cleavage is not required for glycan strand polymerization (Meisner et al., 2013). Conversely, *B. subtilis* cells with induced *yvcE* expression (yet still lacking LytE) exhibited the normal *B. subtilis* rod-shaped phenotype (**Figure 6.1**).

6.1.3 Sporulation and germination in *B. subtilis*

6.1.3.1 Sporulation

Sporulation and germination in *B. subtilis* were studied to elucidate their effects on PG architecture and dynamics. Both of these are complex differentiation processes involving morphogenesis of *B. subtilis* cells.

The formation of asymmetric septa and prespore engulfment was observed during sporulation. Further investigation into asymmetric septation revealed sites of nascent PG synthesis. Sites of nascent PG synthesis were also detected surrounding the prespore during engulfment. The topographic AFM analysis of asymmetric septa revealed that the PG in the region where the septum meets the mother cell wall forms a thicker, ridged architecture.. These findings may disprove a recent paper by Tocheva et al. (2013) who suggested that *B. subtilis* synthesises thinner 'Gram-negative like' layer of PG, ~2nm thick, which forms the asymmetric septum prior to engulfment during sporulation. Tocheva et al. (2013) suggest that this hypothesis refutes the coiled-coil model of PG architecture suggested by Hayhurst et al. (2008). Tocheva et al. (2013) argue that 50 nm coils could not be 'thinned' by hydrolysis to just ~2nm thick without jeopardizing the integrity of the cable. By disproving this, these findings therefore also further support the 'coiled-coil' model of PG architecture.

6.1.3.2 Germination

Less was elucidated about PG dynamics and architecture during *B. subtilis* spore germination. The non-specific binding of NADA to the spore coat prior

to germination meant that this line of investigation was halted. However, the imaging of PG dynamics during germination could be continued if a probe is developed with specific binding for PG synthesis during this process.

6.2 Use of new imaging techniques on *B. subtilis* cells

One of the main questions raised in the study of cell walls is how to establish a link between PG biochemistry and PG architecture. Therefore, it is imperative to be able to dissect PG dynamics with specific probes at molecular resolution. Recently, this has become possible with the advent of fluorescent D-amino acids as cell wall probes, Stochastic Optical Resolution Microscopy and the combination of these two approaches. My study has demonstrated the potential use of these recent techniques in the examination of *B. subtilis* PG dynamics and architecture.

6.2.1 Fluorescent D-amino acids as cell wall probes

A recent paper by Kuru et al. (2012) demonstrated the use of fluorescent D-amino acids (FDAAs) as cell wall probes for *B. subtilis*. FDAAs are incorporated into the peptide side chain of growing cell wall PG and detected using fluorescence microscopy. The use of this technique in my study therefore provided a unique opportunity to image nascent PG synthesis in the *B. subtilis* cell wall. Furthermore, the availability of FDAAs that fluoresce at different wavelengths meant that a pulse-chase experiment could be developed, allowing the mapping of nascent PG synthesis over time. This approach would be useful in future experiments in studying *B. subtilis*

sporulation and germination; to map the loss or gain of PG during these processes.

6.2.2 Stochastic Optical Resolution Microscopy

Super-resolution fluorescence microscopy provides the spatial resolution to examine cell features. Stochastic Optical Resolution Microscopy (STORM) has a 20nm resolution range (Rust et al., 2006). My study has highlighted its potential to be able to elucidate further information regarding PG organization and dynamics in *B. subtilis*. Examination of *B. subtilis* cells using fluorescent PG probes revealed a banded organization pattern across the short axis of the cylinder, similar to the architecture of the PG sacculus described by Hayhurst et al. (2008). Thus, FDAA incorporation can be used in conjunction with STORM's super-resolution to further elucidate PG dynamics.

This approach expanded on previously published work from our lab which used STORM to reveal the nanoscale insertion pattern of PG in *E. coli* and *Caulobacter crescentus* (Turner et al., 2013). This approach is also potentially incredibly useful in the mapping of regenerating *B. subtilis* protoplasts; an interesting future prospect.

6.3 Future perspectives

This study has focussed on the differentiation of *B. subtilis* morphology and the role PG dynamics and architecture play in these processes. The work presented in this study contributes to the growing evidence for an elegant PG

architecture, which is complex and dynamic; adapting and changing to comply with different external environments.

However, there are still many avenues of investigation left to pursue. In particular, harnessing *B. subtilis* protoplast regeneration is an exciting new investigative approach to understanding PG dynamics and architecture. In future, it would be interesting to build upon the work in this study and further dissect how the rod-shape architecture of PG of *B. subtilis* is re-established. Future experiments could include a live cell time-course of *B. subtilis* protoplast regeneration; tracking a single cell's morphological changes and PG dynamics/architecture in real time.

The advent of super resolution microscopy allows imaging of PG synthesis and hydrolysis at a molecular level. This exciting new technology for PG imaging can be further developed. This could build upon the utilisation of STORM in this study and involve the use of newer STORM-compatible probes. It could also expand to include the use of other super-resolution microscopy techniques e.g. stimulated-emission depletion (STED) or structured-illumination microscopy (SIM) (Coltharp and Xiao, 2012). These approaches will allow us to continue to bridge the gap between PG chemistry and architecture by observing single molecules of PG-specific probes.

REFERENCES

Adams, D.W., and Errington, J. (2009). Bacterial cell division: assembly, maintenance and disassembly of the Z ring. Nat. Rev. Microbiol. *7*, 642–653.

Akamatsu, T., and Taguchi, H. (2001). A simple and rapid method for intra- and interspecific transformation of Bacillus subtilis on solid media by DNA in protoplast lysates. Biosci. Biotechnol. Biochem. *65*, 446–448.

Akamatsu, T., and Taguchi, H. (2012). Plasmid transformation of competent Bacillus subtilis by lysed protoplast DNA. J. Biosci. Bioeng. *114*, 138–143.

Allan, E.J., Hoischen, C., and Gumpert, J. (2009). Bacterial L-forms. Adv. Appl. Microbiol. *68*, 1–39.

Archibald, A., Hancock, I., and Harwood, C. (1993). Cell wall structure, synthesis and turnover. In Bacillus Subtilis and Other Gram-Positive Bacteria: Biochemistry, Physiology and Molecular Genetics, A. Sonenshein, J. Hoch, and R. Losick, eds. (Washington DC: American Society for Microbiology), pp. 381–410.

Atrih, A., Zöllner, P., Allmaier, G., Williamson, M.P., and Foster, S.J. (1998). Peptidoglycan Structural Dynamics during Germination of Bacillus subtilis 168 Endospores. J. Bacteriol. *180*, 4603–4612.

Atrih, A., Bacher, G., Allmaier, G., Williamson, M.P., and Foster, S.J. (1999). Analysis of peptidoglycan structure from vegetative cells of Bacillus subtilis 168 and role of PBP 5 in peptidoglycan maturation. J. Bacteriol. *181*, 3956–3966.

Betzig, E., Patterson, G.H., Sougrat, R., Lindwasser, O.W., Olenych, S., Bonifacino, J.S., Davidson, M.W., Lippincott-Schwartz, J., and Hess, H.F. (2006). Imaging intracellular fluorescent proteins at nanometer resolution. Science *313*, 1642–1645.

Beveridge, T.J., and Graham, L.L. (1991). Surface layers of bacteria. Microbiol. Rev. *55*, 684–705.

Bisicchia, P., Noone, D., Lioliou, E., Howell, A., Quigley, S., Jensen, T., Jarmer, H., and Devine, K.M. (2007). The essential YycFG two-component system controls cell wall metabolism in Bacillus subtilis. Mol. Microbiol. *65*, 180–200.

Bisicchia, P., Lioliou, E., Noone, D., Salzberg, L.I., Botella, E., Hübner, S., and Devine, K.M. (2010). Peptidoglycan metabolism is controlled by the WalRK (YycFG) and PhoPR two-component systems in phosphate-limited Bacillus subtilis cells. Mol. Microbiol. *75*, 972–989.

Blackman, S.A., Smith, T.J., and Foster, S.J. (1998). The role of autolysins during vegetative growth of Bacillus subtilis 168. Microbiology *144*, 73–82.

Boneca, I.G., Huang, Z.H., Gage, D.A., and Tomasz, A. (2000). Characterization of Staphylococcus aureus cell wall glycan strands, evidence for a new beta-N-acetylglucosaminidase activity. J. Biol. Chem. *275*, 9910–9918.

Boschwitz, H., Gofshtein-Gandman, L., Halvorson, H.O., Keynan, A., and Milner, Y. (1991). The possible involvement of trypsin-like enzymes in germination of spores of Bacillus cereus T and Bacillus subtilis 168. J Gen Microbiol *137*, 1145–1153.

Carballido-López, R., Formstone, A., Li, Y., Ehrlich, S.D., Noirot, P., and Errington, J. (2006). Actin Homolog MreBH Governs Cell Morphogenesis by Localization of the Cell Wall Hydrolase LytE. Developmental Cell *11*, 399–409.

Chang, S., and Cohen, S.N. (1979). High frequency transformation of Bacillus subtilis protoplasts by plasmid DNA. Mol. Gen. Genet. *168*, 111–115.

Coltharp, C., and Xiao, J. (2012). Superresolution microscopy for microbiology. Cell. Microbiol. *14*, 1808–1818.

Cowan, A.E., Koppel, D.E., Setlow, B., and Setlow, P. (2003). A soluble protein is immobile in dormant spores of Bacillus subtilis but is mobile in germinated spores: implications for spore dormancy. Proc. Natl. Acad. Sci. U.S.A. *100*, 4209–4214.

Daniel, R.A., and Errington, J. (2003). Control of cell morphogenesis in bacteria: two distinct ways to make a rod-shaped cell. Cell *113*, 767–776.

Daniel, R.A., Harry, E.J., and Errington, J. (2000). Role of penicillin-binding protein PBP 2B in assembly and functioning of the division machinery of Bacillus subtilis. Molecular Microbiology *35*, 299–311.

Daniel, R.A., Noirot-Gros, M.-F., Noirot, P., and Errington, J. (2006). Multiple interactions between the transmembrane division proteins of Bacillus subtilis and the role of FtsL instability in divisome assembly. J. Bacteriol. *188*, 7396–7404.

Dempwolff, F., Reimold, C., Reth, M., and Graumann, P.L. (2011). Bacillus subtilis MreB orthologs self-organize into filamentous structures underneath the cell membrane in a heterologous cell system. PLoS ONE *6*, e27035.

Devine, K.M. (2012). Bacterial L-forms on tap: an improved methodology to generate Bacillus subtilis L-forms heralds a new era of research. Mol. Microbiol. *83*, 10–13.

Dmitriev, B.A., Toukach, F.V., Schaper, K.-J., Holst, O., Rietschel, E.T., and Ehlers, S. (2003). Tertiary structure of bacterial murein: the scaffold model. J. Bacteriol. *185*, 3458–3468.

Domínguez-Cuevas, P., Mercier, R., Leaver, M., Kawai, Y., and Errington, J. (2012). The rod to L-form transition of Bacillus subtilis is limited by a requirement for the protoplast to escape from the cell wall sacculus. Molecular Microbiology *83*, 52–66.

Domínguez-Escobar, J., Chastanet, A., Crevenna, A.H., Fromion, V., Wedlich-Söldner, R., and Carballido-López, R. (2011). Processive movement of MreB-associated cell wall biosynthetic complexes in bacteria. Science *333*, 225–228.

Dworkin, J. (2010). Form equals function? Bacterial shape and its consequences for pathogenesis. Mol. Microbiol. *78*, 792–795.

Elliott, T.S., Ward, J.B., and Rogers, H.J. (1975a). Formation of cell wall polymers by reverting protoplasts of Bacillus licheniformis. J. Bacteriol. *124*, 623–632.

Elliott, T.S., Ward, J.B., Wyrick, P.B., and Rogers, H.J. (1975b). Ultrastructural study of the reversion of protoplasts of Bacillus licheniformis to bacilli. J. Bacteriol. *124*, 905–917.

Erickson, H.P., Anderson, D.E., and Osawa, M. (2010). FtsZ in bacterial cytokinesis: cytoskeleton and force generator all in one. Microbiol. Mol. Biol. Rev. *74*, 504–528.

Errington, J. (2003). Regulation of endospore formation in Bacillus subtilis. Nat Rev Micro *1*, 117–126.

Errington, J., Daniel, R.A., and Scheffers, D.-J. (2003). Cytokinesis in bacteria. Microbiol. Mol. Biol. Rev. *67*, 52–65, table of contents.

Fuchs-Cleveland, E., and Gilvarg, C. (1976). Oligomeric intermediate in peptidoglycan biosynthesis in Bacillus megaterium. PNAS *73*, 4200–4204.

Fukushima, T., Yamamoto, H., Atrih, A., Foster, S.J., and Sekiguchi, J. (2002). A Polysaccharide Deacetylase Gene (pdaA) Is Required for Germination and for Production of Muramic δ-Lactam Residues in the Spore Cortex of Bacillus subtilis. J. Bacteriol. *184*, 6007–6015.

Fukushima, T., Afkham, A., Kurosawa, S.-I., Tanabe, T., Yamamoto, H., and Sekiguchi, J. (2006). A new D,L-endopeptidase gene product, YojL (renamed CwlS), plays a role in cell separation with LytE and LytF in Bacillus subtilis. J. Bacteriol. *188*, 5541–5550.

Fukushima, T., Szurmant, H., Kim, E.-J., Perego, M., and Hoch, J.A. (2008). A sensor histidine kinase co-ordinates cell wall architecture with cell division in Bacillus subtilis. Mol. Microbiol. *69*, 621–632.

Gabor, M.H., and Hotchkiss, R.D. (1979). Parameters governing bacterial regeneration and genetic recombination after fusion of Bacillus subtilis protoplasts. J. Bacteriol. *137*, 1346–1353.

Ghuysen, J.M. (1968). Use of bacteriolytic enzymes in determination of wall structure and their role in cell metabolism. Bacteriol Rev *32*, 425–464.

Goffin, C., and Ghuysen, J.M. (1998). Multimodular penicillin-binding proteins: an enigmatic family of orthologs and paralogs. Microbiol. Mol. Biol. Rev. *62*, 1079–1093.

Habuchi, S. (2014). Super-Resolution Molecular and Functional Imaging of Nanoscale Architectures in Life and Materials Science. Front Bioeng Biotechnol *2*.

Harry, E.J. (2001a). Bacterial cell division: regulating Z-ring formation. Molecular Microbiology *40*, 795–803.

Harry, E.J. (2001b). Coordinating DNA replication with cell division:Lessons from outgrowing spores. Biochimie *83*, 75–81.

Hayhurst, E.J., Kailas, L., Hobbs, J.K., and Foster, S.J. (2008). Cell wall peptidoglycan architecture in Bacillus subtilis. Proc Natl Acad Sci U S A *105*, 14603–14608.

Heijenoort, J. van (2001). Formation of the glycan chains in the synthesis of bacterial peptidoglycan. Glycobiology *11*, 25R – 36R.

Heijenoort, J. van (2007). Lipid Intermediates in the Biosynthesis of Bacterial Peptidoglycan. Microbiol. Mol. Biol. Rev. *71*, 620–635.

Higgins, D., and Dworkin, J. (2012). Recent progress in Bacillus subtilis sporulation. FEMS Microbiol. Rev. *36*, 131–148.

Hoffmann, T., Troup, B., Szabo, A., Hungerer, C., and Jahn, D. (1995). The anaerobic life of Bacillus subtilis: cloning of the genes encoding the respiratory nitrate reductase system. FEMS Microbiol. Lett. *131*, 219–225.

Höltje, J.V. (1995). From growth to autolysis: the murein hydrolases in Escherichia coli. Arch. Microbiol. *164*, 243–254.

Höltje, J.V. (1998). Growth of the stress-bearing and shape-maintaining murein sacculus of Escherichia coli. Microbiol. Mol. Biol. Rev. *62*, 181–203.

Höltje, J.V., and Heidrich, C. (2001). Enzymology of elongation and constriction of the murein sacculus of Escherichia coli. Biochimie *83*, 103–108.

Höltje, J.V., Mirelman, D., Sharon, N., and Schwarz, U. (1975). Novel type of murein transglycosylase in Escherichia coli. J. Bacteriol. *124*, 1067–1076.

Hopwood, D.A. (1981). Genetic studies with bacterial protoplasts. Annu. Rev. Microbiol. *35*, 237–272.

Horsburgh, G.J., Atrih, A., and Foster, S.J. (2003). Characterization of LytH, a differentiation-associated peptidoglycan hydrolase of Bacillus subtilis involved in endospore cortex maturation. J. Bacteriol. *185*, 3813–3820.

Huang, B., Wang, W., Bates, M., and Zhuang, X. (2008). Three-dimensional super-resolution imaging by stochastic optical reconstruction microscopy. Science *319*, 810–813.

Iber, D., Clarkson, J., Yudkin, M.D., and Campbell, I.D. (2006). The mechanism of cell differentiation in Bacillus subtilis. Nature *441*, 371–374.

Ishikawa, S., Yamane, K., and Sekiguchi, J. (1998). Regulation and Characterization of a Newly Deduced Cell Wall Hydrolase Gene (cwlJ) Which Affects Germination of Bacillus subtilis Spores. J. Bacteriol. *180*, 1375–1380.

Jedrzejas, M.J., and Setlow, P. (2001). Comparison of the binuclear metalloenzymes diphosphoglycerate-independent phosphoglycerate mutase and alkaline phosphatase: their mechanism of catalysis via a phosphoserine intermediate. Chem. Rev. *101*, 607–618.

Kawai, Y., Daniel, R.A., and Errington, J. (2009). Regulation of cell wall morphogenesis in Bacillus subtilis by recruitment of PBP1 to the MreB helix. Mol. Microbiol. *71*, 1131–1144.

Koch, A.L. (1998). Orientation of the peptidoglycan chains in the sacculus of Escherichia coli. Res. Microbiol. *149*, 689–701.

Koch, A.L., and Doyle, R.J. (1985). Inside-to-outside growth and turnover of the wall of gram-positive rods. Journal of Theoretical Biology *117*, 137–157.

Kruse, T., Bork-Jensen, J., and Gerdes, K. (2005). The morphogenetic MreBCD proteins of Escherichia coli form an essential membrane-bound complex. Mol. Microbiol. *55*, 78–89.

Kuru, E., Hughes, H.V., Brown, P.J., Hall, E., Tekkam, S., Cava, F., de Pedro, M.A., Brun, Y.V., and VanNieuwenhze, M.S. (2012). In Situ Probing of Newly Synthesized Peptidoglycan in Live Bacteria with Fluorescent D-Amino Acids. Angew. Chem. Int. Ed. *51*, 12519–12523.

Lawrence, P.J., and Strominger, J.L. (1970). Biosynthesis of the peptidoglycan of bacterial cell walls. XVI. The reversible fixation of radioactive penicillin G to the D-alanine carboxypeptidase of Bacillus subtilis. J. Biol. Chem. *245*, 3660–3666.

Leaver, M., Domínguez-Cuevas, P., Coxhead, J.M., Daniel, R.A., and Errington, J. (2009). Life without a wall or division machine in Bacillus subtilis. Nature *457*, 849–853.

Li, K., Lee, L.A., Lu, X., and Wang, Q. (2010). Fluorogenic “click” reaction for labeling and detection of DNA in proliferating cells. BioTechniques *49*, 525–527.

Liechti, G.W., Kuru, E., Hall, E., Kalinda, A., Brun, Y.V., VanNieuwenhze, M., and Maurelli, A.T. (2014). A new metabolic cell-wall labelling method reveals peptidoglycan in Chlamydia trachomatis. Nature *506*, 507–510.

Madigan, M.T., and Martinko, J.M. (2006). Brock Biology of Microorganisms (Pearson Prentice Hall).

Marston, A.L., Thomaides, H.B., Edwards, D.H., Sharpe, M.E., and Errington, J. (1998). Polar localization of the MinD protein of Bacillus subtilis and its role in selection of the mid-cell division site. Genes Dev. *12*, 3419–3430.

Matias, V.R.F., and Beveridge, T.J. (2005). Cryo-electron microscopy reveals native polymeric cell wall structure in Bacillus subtilis 168 and the existence of a periplasmic space. Mol. Microbiol. *56*, 240–251.

Matias, V.R.F., and Beveridge, T.J. (2008). Lipoteichoic acid is a major component of the Bacillus subtilis periplasm. J. Bacteriol. *190*, 7414–7418.

Matteï, P.-J., Neves, D., and Dessen, A. (2010). Bridging cell wall biosynthesis and bacterial morphogenesis. Curr. Opin. Struct. Biol. *20*, 749–755.

McCormick, N.G. (1965). Kinetics of Spore Germination. J Bacteriol *89*, 1180–1185.

McPherson, D.C., Driks, A., and Popham, D.L. (2001). Two class A high-molecular-weight penicillin-binding proteins of Bacillus subtilis play redundant roles in sporulation. J. Bacteriol. *183*, 6046–6053.

Meisner, J., Montero Llopis, P., Sham, L.-T., Garner, E., Bernhardt, T.G., and Rudner, D.Z. (2013). FtsEX is required for CwlO peptidoglycan hydrolase activity during cell wall elongation in Bacillus subtilis. Mol. Microbiol. *89*, 1069–1083.

Merchante, R., Pooley, H.M., and Karamata, D. (1995). A periplasm in Bacillus subtilis. J. Bacteriol. *177*, 6176–6183.

Mercier, R., Domínguez-Cuevas, P., and Errington, J. (2012). Crucial role for membrane fluidity in proliferation of primitive cells. Cell Rep *1*, 417–423.

Mercier, R., Kawai, Y., and Errington, J. (2013). Excess membrane synthesis drives a primitive mode of cell proliferation. Cell *152*, 997–1007.

Misra, G., Rojas, E.R., Gopinathan, A., and Huang, K.C. (2013). Mechanical Consequences of Cell-Wall Turnover in the Elongation of a Gram-Positive Bacterium. Biophysical Journal *104*, 2342–2352.

Moir, A. (2006). How do spores germinate? Journal of Applied Microbiology *101*, 526–530.

Muchová, K., Wilkinson, A.J., and Barák, I. (2011). Changes of lipid domains in Bacillus subtilis cells with disrupted cell wall peptidoglycan. FEMS Microbiol. Lett. *325*, 92–98.

Murray, T., Popham, D.L., and Setlow, P. (1996). Identification and characterization of pbpC, the gene encoding Bacillus subtilis penicillin-binding protein 3. J. Bacteriol. *178*, 6001–6005.

Murray, T., Popham, D.L., Pearson, C.B., Hand, A.R., and Setlow, P. (1998). Analysis of outgrowth of Bacillus subtilis spores lacking penicillin-binding protein 2a. J. Bacteriol. *180*, 6493–6502.

Nelson, D.E., and Young, K.D. (2001). Contributions of PBP 5 and DD-carboxypeptidase penicillin binding proteins to maintenance of cell shape in Escherichia coli. J. Bacteriol. *183*, 3055–3064.

Ohnishi, R., Ishikawa, S., and Sekiguchi, J. (1999). Peptidoglycan hydrolase LytF plays a role in cell separation with CwlF during vegetative growth of Bacillus subtilis. J. Bacteriol. *181*, 3178–3184.

Popham, D.L., and Setlow, P. (1993). Cloning, nucleotide sequence, and regulation of the Bacillus subtilis pbpE operon, which codes for penicillin-binding protein 4* and an apparent amino acid racemase. J. Bacteriol. *175*, 2917–2925.

Popham, D.L., Illades-Aguiar, B., and Setlow, P. (1995). The Bacillus subtilis dacB gene, encoding penicillin-binding protein 5*, is part of a three-gene operon required for proper spore cortex synthesis and spore core dehydration. J. Bacteriol. *177*, 4721–4729.

Popham, D.L., Helin, J., Costello, C.E., and Setlow, P. (1996). Muramic lactam in peptidoglycan of Bacillus subtilis spores is required for spore outgrowth but not for spore dehydration or heat resistance. Proc Natl Acad Sci U S A *93*, 15405–15410.

Popham, D.L., Gilmore, M.E., and Setlow, P. (1999). Roles of low-molecular-weight penicillin-binding proteins in Bacillus subtilis spore peptidoglycan synthesis and spore properties. J. Bacteriol. *181*, 126–132.

Ranjit, D.K., and Young, K.D. (2013). The Rcs stress response and accessory envelope proteins are required for de novo generation of cell shape in Escherichia coli. J. Bacteriol. *195*, 2452–2462.

Reith, J., and Mayer, C. (2011). Peptidoglycan turnover and recycling in Gram-positive bacteria. Appl. Microbiol. Biotechnol. *92*, 1–11.

Rust, M.J., Bates, M., and Zhuang, X. (2006). Stochastic optical reconstruction microscopy (STORM) provides sub-diffraction-limit image resolution. Nat Methods *3*, 793–795.

Sauvage, E., Kerff, F., Terrak, M., Ayala, J.A., and Charlier, P. (2008). The penicillin-binding proteins: structure and role in peptidoglycan biosynthesis. FEMS Microbiol. Rev. *32*, 234–258.

Scheffers, D.-J., and Errington, J. (2004). PBP1 is a component of the Bacillus subtilis cell division machinery. J. Bacteriol. *186*, 5153–5156.

Scheffers, D.-J., and Pinho, M.G. (2005). Bacterial cell wall synthesis: new insights from localization studies. Microbiol. Mol. Biol. Rev. *69*, 585–607.

Scheffers, D.-J., Jones, L.J.F., and Errington, J. (2004). Several distinct localization patterns for penicillin-binding proteins in Bacillus subtilis. Molecular Microbiology *51*, 749–764.

Schleifer, K.H., and Kandler, O. (1972). Peptidoglycan types of bacterial cell walls and their taxonomic implications. Bacteriol Rev *36*, 407–477.

Setlow, P. (2003). Spore germination. Curr. Opin. Microbiol. *6*, 550–556.

Setlow, B., Melly, E., and Setlow, P. (2001). Properties of Spores of Bacillus subtilis Blocked at an Intermediate Stage in Spore Germination. J. Bacteriol. *183*, 4894–4899.

Shieh, P., Siegrist, M.S., Cullen, A.J., and Bertozzi, C.R. (2014). Imaging bacterial peptidoglycan with near-infrared fluorogenic azide probes. Proc. Natl. Acad. Sci. U.S.A. *111*, 5456–5461.

Siegrist, M.S., Whiteside, S., Jewett, J.C., Aditham, A., Cava, F., and Bertozzi, C.R. (2013). d-Amino Acid Chemical Reporters Reveal Peptidoglycan Dynamics of an Intracellular Pathogen. ACS Chem. Biol. *8*, 500–505.

Silhavy, T.J., Kahne, D., and Walker, S. (2010). The Bacterial Cell Envelope. Cold Spring Harb Perspect Biol *2*.

Smith, T.J., Blackman, S.A., and Foster, S.J. (2000). Autolysins of Bacillus subtilis: multiple enzymes with multiple functions. Microbiology (Reading, Engl.) *146 (Pt 2)*, 249–262.

Smith, T.J., Blackman, S.A., and Foster, S.J. Autolysins of Bacillus subtilis: multiple enzymes with multiple functions.

Snowden, M.A., and Perkins, H.R. (1990). Peptidoglycan cross-linking in Staphylococcus aureus. An apparent random polymerisation process. Eur. J. Biochem. *191*, 373–377.

Stock, A.M., Robinson, V.L., and Goudreau, P.N. (2000). Two-component signal transduction. Annu. Rev. Biochem. *69*, 183–215.

Swoboda, J.G., Campbell, J., Meredith, T.C., and Walker, S. (2010). Wall Teichoic Acid Function, Biosynthesis, and Inhibition. Chembiochem *11*, 35–45.

Tocheva, E.I., López-Garrido, J., Hughes, H.V., Fredlund, J., Kuru, E., Vannieuwenhze, M.S., Brun, Y.V., Pogliano, K., and Jensen, G.J. (2013). Peptidoglycan transformations during Bacillus subtilis sporulation. Mol. Microbiol. *88*, 673–686.

Tseng, C.-L., Chen, J.-T., Lin, J.-H., Huang, W.-Z., and Shaw, G.-C. (2011). Genetic evidence for involvement of the alternative sigma factor SigI in controlling expression of the cell wall hydrolase gene lytE and contribution of LytE to heat survival of Bacillus subtilis. Arch. Microbiol. *193*, 677–685.

Turner, R.D., Ratcliffe, E.C., Wheeler, R., Golestanian, R., Hobbs, J.K., and Foster, S.J. (2010). Peptidoglycan architecture can specify division planes in Staphylococcus aureus. Nat Commun *1*, 26.

Turner, R.D., Hurd, A.F., Cadby, A., Hobbs, J.K., and Foster, S.J. (2013). Cell wall elongation mode in Gram-negative bacteria is determined by peptidoglycan architecture. Nat Commun *4*, 1496.

Typas, A., Banzhaf, M., Gross, C.A., and Vollmer, W. (2012). From the regulation of peptidoglycan synthesis to bacterial growth and morphology. Nat. Rev. Microbiol. *10*, 123–136.

Vollmer, W., and Seligman, S.J. (2010). Architecture of peptidoglycan: more data and more models. Trends Microbiol. *18*, 59–66.

Vollmer, W., Blanot, D., and de Pedro, M.A. (2008). Peptidoglycan structure and architecture. FEMS Microbiol. Rev. *32*, 149–167.

Wang, T.-S.A., Manning, S.A., Walker, S., and Kahne, D. (2008). Isolated peptidoglycan glycosyltransferases from different organisms produce different glycan chain lengths. J. Am. Chem. Soc. *130*, 14068–14069.

Ward, J.B. (1973). The chain length of the glycans in bacterial cell walls. Biochem. J. *133*, 395–398.

Ward, J.B., and Perkins, H.R. (1973). The direction of glycan synthesis in a bacterial peptidoglycan. Biochem. J. *135*, 721–728.

Wei, Y., Havasy, T., McPherson, D.C., and Popham, D.L. (2003). Rod shape determination by the Bacillus subtilis class B penicillin-binding proteins encoded by pbpA and pbpH. J. Bacteriol. *185*, 4717–4726.

Wei, Y., McPherson, D.C., and Popham, D.L. (2004). A mother cell-specific class B penicillin-binding protein, PBP4b, in Bacillus subtilis. J. Bacteriol. *186*, 258–261.

Yamamoto, H., Kurosawa, S., and Sekiguchi, J. (2003). Localization of the vegetative cell wall hydrolases LytC, LytE, and LytF on the Bacillus subtilis cell surface and stability of these enzymes to cell wall-bound or extracellular proteases. J. Bacteriol. *185*, 6666–6677.